ISSN 1980-9743

Soils and Rocks

Soils and Rocks

An International Journal of Geotechnical and Geoenvironmental Engineering

Volume 38, N. 1
January-April 2015

Soils and Rocks Volume 38, N. 1 2015

Soils and Rocks is an International Journal of Geotechnical and Geoenvironmental Engineering published by

ABMS - Brazilian Association for Soil Mechanics and Geotechnical Engineering
Av. Queiroz Filho, 1700 – Torre A Sky, Sala 106 – Vila Hamburguesa
05319-000, São Paulo, SP
Brazil

SPG – Portuguese Geotechnical Society
LNEC, Avenida do Brasil, 101
1700-066 Lisboa
Portugal

Issue Date: *April 2015*

Issue: *400 copies and 800 online-distributed copies*

Manuscript Submission: *For review criteria and manuscript submission information, see Instructions for Authors at the end.*

SOILS and ROCKS

An International Journal of Geotechnical and Geoenvironmental Engineering

Editor Waldemar Coelho Hachich - University of São Paulo, Brazil

Co-editor Manuel Matos Fernandes - University of Porto, Portugal

"Ad hoc" Reviewers (2014-2015)

Ana Cristina Sieira
UERJ, Brazil

André Luís Brasil Cavalcante
UnB, Brazil

Antonio Airton Bortolucci
USP-S. Carlos, Brazil

Arsenio Negro Jr.
Bureau, Brazil

Bernadete Ragoni Danziger
UERJ, Brazil

Carlos Medeiros Silva
Embre, Brazil

Claudio Fernando Mahler
UFRJ, Brazil

Claudio Michael Wolle
USP-Poli, Brazil

David Martins Geraldo Taborda
Imperial College, UK

Denise Gerscovich
UERJ, Brazil

Eda Quadros
BGTECH, Brazil

Edgar Odebrecht
Geoforma, Brazil

Edgard Poiate
Petrobrás, Brazil

Edmundo Rogério Esquível
USP-S. Carlos, Brazil

Eurípedes Vargas
PUC-RJ, Brazil

Fernando Antonio Medeiros Marinho
USP-Poli, Brazil

Fernando Olavo Franciss
Progeo, Brazil

Francisco Chagas da Silva Filho
UFC, Brazil

Francisco de Rezende Lopes
UFRJ, Brazil

Frederico Falconi
ZF, Brazil

Isabel Lopes
IST, Portugal

João Manuel Marcelino Mateus da Silva
LNEC, Portugal

José Camapum de Carvalho
UnB, Brazil

José Renato Baptista de Lima
USP-Poli

Kátia Bicalho
UFES, Brazil

Leonardo Becker
UFRJ, Brazil

Luís Valenzuela
Arcadis, Chile

Marc Vinches
Ecole des Mines d'Alès, France

Marcia Maria dos Anjos Mascarenhas
UFG, Brazil

Maria Cláudia Barbosa
UFRJ, Brazil

Maurício Ehrlich
UFRJ, Brazil

Nelson Aoki
USP-S.Carlos, Brazil

Paulo Scarano Hemsi
ITA, Brazil

Renato Pinto da Cunha
UnB, Brazil

Sussumu Niyama
Tecnum, Brazil

Tácio Campos
PUC-RJ, Brazil

Tiago Miranda
Univ. do Minho, Portugal

Waldyr Lopes de Oliveira Filho
UFOP, Brazil

Soils and Rocks publishes papers in English in the broad fields of Geotechnical Engineering, Engineering Geology and Geo-environmental Engineering. The Journal is published in April, August and December. Subscription price is US$ 90.00 per year. The journal, with the name "Solos e Rochas", was first published in 1978 by the Graduate School of Engineering, Federal University of Rio de Janeiro (COPPE-UFRJ). In 1980 it became the official magazine of the Brazilian Association for Soil Mechanics and Geotechnical Engineering (ABMS), acquiring the national character that had been the intention of its founders. In 1986 it also became the official Journal of the Brazilian Association for Engineering Geology and the Environment (ABGE) and in 1999 became the Latin American Geotechnical Journal, following the support of Latin-American representatives gathered for the Pan-American Conference of Guadalajara (1996). In 2007 the journal acquired the status of an international journal under the name of Soils and Rocks, published by the Brazilian Association for Soil Mechanics and Geotechnical Engineering (ABMS), Brazilian Association for Engineering Geology and the Environment (ABGE) and Portuguese Geotechnical Society (SPG). In 2010, ABGE decided to publish its own journal and left the partnership.

Soils and Rocks

1978,	1 (1, 2)
1979,	1 (3), 2 (1,2)
1980-1983,	3-6 (1, 2, 3)
1984,	7 (single number)
1985-1987,	8-10 (1, 2, 3)
1988-1990,	11-13 (single number)
1991-1992,	14-15 (1, 2)
1993,	16 (1, 2, 3, 4)
1994-2010,	17-33 (1, 2, 3)
2011,	34 (1, 2, 3, 4)
2012-2014,	35-37 (1, 2, 3)
2015,	**38 (1,**

ISSN 1980-9743 CDU 624.131.1

ISSN 1980-9743

SOILS and ROCKS

An International Journal of Geotechnical and Geoenvironmental Engineering

Publication of

ABMS - Brazilian Association for Soil Mechanics and Geotechnical Engineering

SPG - Portuguese Geotechnical Society

Volume 38, N. 1, January-April 2015

Table of Contents

Articles

K_0 Measurement in a Sand Using Back Volume Change

T. Santana, M. Candeias

Abstract. An experimental technique, using a computer controlled triaxial test to evaluate the coefficient of earth pressure at rest, K_0, is presented. The method does not require the use of any radial measurement transducers and is free from any side friction effects, typical of oedometer testing. It uses commercial software (GDSlab) which applies ramps of radial stress with back volume measurement, ensuring that the diameter change remains zero. The method is applicable only to saturated specimens in drained conditions. The equipment used is briefly described, as well as the testing procedure. Results of a laboratory test, on a granular material, applying a loading-unloading-reloading condition, are presented, and the relation of K_0 with OCR (overconsolidation ratio) is investigated. The experimental results are compared with empirical equations given by other publications, suggesting the adequacy of this test method to determine K_0 either in normally consolidated or overconsolidated stress paths.

Keywords: coefficient of earth pressure at rest, overconsolidation ratio, Toyoura sand, triaxial system.

1. Introduction

The deposition of soils has a history of one-dimensional deformation in the vertical direction with zero lateral strains. When the soil gets unloaded, due to erosion of overlying strata, it follows also a one dimensional path. The coefficient of earth pressure at rest, K_0, where there has been no lateral strain within the ground, refers to effective stresses, as:

$$K_0 = \frac{\sigma'_3}{\sigma'_1} \tag{1}$$

where: σ'_3 is the effective radial stress; σ'_1 is the effective axial stress.

In fact, each state of deformation of a soil, during one dimensional normal compression, is essentially similar to all the preceding states and, if the soil is normally consolidated, the effective stress states have the same similarity. The value of K_0 is then found to be a constant (Wood, 1990). Therefore, in normally consolidated soils at any stress state not smaller than in situ one, the undisturbed initial stress state can be known measuring K_0 (Lirer *et al.*, 2011).

The importance of estimating K_0 for predicting the initial conditions for soil/water coupled finite element analysis of geotechnical structures has been emphasized by a number of researchers that used either analytical correlations or experimental evidence to measure K_0. They recognized that the K_0-values of normally consolidated soils (K_0^{NC}) could be well estimated from the Jaky's equation:

$$K_0^{NC} = 1 - \sin\phi' \tag{2}$$

where ϕ' is the effective angle of internal friction.

Some of them also studied the coefficient of earth pressure at rest in overconsolidated soils and, based on experimental evidence, they found that K_0 is typically represented as a function of OCR (overconsolidation ratio), by an empirical relationship in the form:

$$K_0^{OC} = K_0^{NC} \times OCR^{\alpha} \tag{3}$$

where α is an exponent ($\alpha \leq 1$) proposed in previous publications, as follows. Mayne and Kulhawy (1982) suggested, for granular materials, that usually $\alpha = \sin\phi'$. Meyerhoff (1976), cited by Hanna *et al.* (2008), suggested that α should be equal to 0.5. Hanna *et al.* (2008) suggested $\alpha = \sin\phi' - 0.18$. Lirer *et al.* (2011) tested two coarse grained materials and, in an over consolidated stress path, they found $\alpha = 0.6$.

K_0 can be determined by either laboratory or in-situ tests. The in-situ methods gave some variations due to many uncertainties related to the sensitivity of K_0 value to the small disturbance caused by inserting the probe into the ground. Laboratory test methods that have been published fall into two distinct classes (Teerachaikulpanich *et al.*, 2007): rigid lateral boundary and flexible lateral boundary. The first one allows the required zero lateral strain but also allows undefined friction between the wall and the soil. The second has no side friction but requires a feedback system to control the soil specimen to achieve zero lateral strain.

This paper focuses on a laboratory test for determination of K_0 by means of a triaxial cell (flexible lateral boundary) with back volume change control ensuring that the cross section area remains constant.

Teresa Santana, PhD, Departamento de Engenharia Civil, Faculdade de Ciências e Tecnologia, Universidade Nova de Lisboa, Campus Universitário, 2829-516 Caparica, Lisboa, Portugal. e-mail: mtgs@fct.unl.pt.
Mariline Candeias, MSc, Departamento de Engenharia Civil, Faculdade de Ciências e Tecnologia, Universidade Nova de Lisboa, Campus Universitário,2829-516 Caparica, Lisboa, Portugal. e-mial: mt.candeias@campus.fct.unl.pt.
Submitted on April 24, 2013; Final Acceptance on August 26, 2014; Discussion open until December 31, 2015.

K_0 consolidation tests were performed in a consecutive loading-unloading-reloading cycle and it was clarified the influence of OCR on the K_0-values.

2. Experimentals

2.1. Testing equipment

The most conventional and simple laboratory test to measure K_0 is the method where a specimen is confined in an oedometer ring, with a rigid boundary, instrumented in order to measure the lateral stresses. In these methods, the wall friction of the ring may induce some effects on measured K_0-values (Okochi and Tatsuoka, 1984). In order to avoid such effects, many previous publications refer the use of a triaxial cell with its flexible lateral boundary around the specimen. This method uses a feedback system to maintain the boundary in position in a condition of null radial strain (Teerachaikulpanich *et al.*, 2007). The most popular method of measuring K_0 by this technique is loading axially a sample in a triaxial cell and continuously adjusting the cell pressure with an automated system, in order to maintain the zero lateral strain condition. This requires accurate strain measurements, with local radial strain measurement devices, provided that the sample is saturated and is deforming uniformly (Lo and Chu, 1991; Piriyakul and Haegeman, 2005).

But there are alternative methods of determining K_0 in a triaxial test, without the need of radial measurement transducers. These require controlling the incremental ratio between volumetric and axial strain, in order to obtain $\varepsilon_v/\varepsilon_1 = 1$ (where ε_v and ε_1 are, respectively, the volumetric and axial strains). This can be accomplished by strain path (Menzies, 1988; Lo and Chu, 1991; Eliadorani *et al.*, 2005), provided that the volume change in the pore water duct be always equal to the volume of axial deformation times the original average cross-sectional area.

This paper presents a method of determining K_0 in a common triaxial system, with back volume measurement, without the requirement of any special local instrumentation to give feedback on lateral strain, based on a stress path test.

The equipment used to perform K_0 triaxial tests is a computer controlled system, which controls two GDS digital pressure/volume controllers, a submersible internal load cell and a 50 kN servo-hydraulic load frame, as shown in Fig. 1. Each pressure/volume controller regulates accurately both pressure and volume change of de-aired water supplied either to the triaxial cell or to the interior of the specimen. The submersible load cell measures the axial load acting on the specimen and has a capacity of 16 kN. Pore water pressure is measured with a pressure transducer and the axial displacement is also monitored externally with an LVDT.

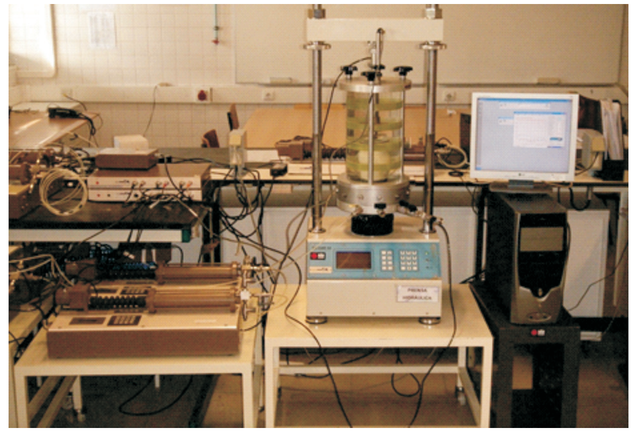

Figure 1 - Equipment: triaxial cell, pressure/volume controllers and loading frame.

It is used a commercial software, GDSLAB, to control the K_0 stress path tests, using a ramp of radial stress with back volume change measurement. On a saturated specimen, the test begins with an imposed radial stress ramp, with a certain loading rate chosen to ensure drained conditions. The volume change of the sample is extracted out of the back-pressure controller and, in order to guarantee zero radial strain increment ($\varepsilon_1 = \varepsilon_v$), each axial displacement (ΔH) is calculated, as follows:

$$\Delta H = H_0 \varepsilon_v \tag{4}$$

where H_0 is the initial height of the sample and ε_v is the volumetric strain.

To ensure the new required specimen height, the system applies the necessary velocity to the load frame inducing a new axial stress on the load cell. As shown in Fig. 2, during the test, radial stress is a perfect ramp, while axial stress and axial strain have to adjust automatically during the test.

Several continuous plots given by the software, during the test, enable the detection of any slight out of control. The loading rate of the radial stress ramp had to be deter-

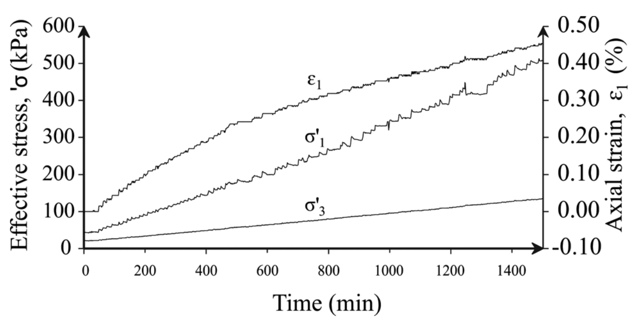

Figure 2 - Ramps of radial and axial stresses and axial strain.

mined by trial, so that only negligible excess pore water pressures develop in the specimen. This was accomplished subjecting a specimen to successively faster rates of loading, until an excess of pore water pressure began to develop in the specimen. This was taken as the satisfactory loading rate for the ramp of radial stress.

An over-consolidated condition can be simulated by loading the sample to a pre-consolidation axial stress and then unload (and reload if it is the case) along a stress-path to the target radial stress.

2.2. Material and testing procedures

The material used in this study is the Toyoura sand, which is an uniform, clean and fine sand having an uniformity coefficient, $C_u = 1.46$, a specific gravity, $G = 2.65$ and a maximum and minimum void ratios, $e_{max} = 0.977$ and $e_{min} = 0.597$, respectively.

Triaxial specimens of Toyoura sand, having 70 mm of nominal diameter and 134 mm of height, were reconstituted by tamping. The sand was compacted in four layers in a mold, by tamping manually with a rod which has a foot with a 66 mm of diameter. The tamping was adjusted to the desired target density. The void ratio achieved was $e_0 = 0.7$.

Following the reconstitution, a vacuum of 10 kPa was applied to the specimen when removing the mold. Saturation was accomplished, firstly by flushing the specimen with carbon dioxide for approximately 15 min, after which de-aired water was added to the bottom of the specimen to circulate through the drainage line. Afterwards, a linear increase of the cell and back pressures was applied till it was reached a B-value of 96%. The sample was considered fully saturated and reached an equilibrium state when, after consolidation, there was no excess of pore water pressures. The effective stress state, prior to initiating K_0 test, was hydrostatic, that is, $p'_0 = 20$ kPa.

After setting up the triaxial cell in the loading frame, a K_0 test was conducted as explained above. The radial stress ramps tested are shown in Table 1, all of them performed at a stress rate of 6 kPa/h. The sample was loaded, then unloaded and reloaded again, along stress-paths targeting the radial stresses. Because of this system requirement, it is only possible to obtain the exact value of OCR, after the test is complete. The value of OCR is given by σ'_1 / σ'_p, being σ'_p the effective axial stress at which unloading initiates (Table 1).

3. Test Results

3.1. Validation

The applied radial stresses and the correspondent vertical effective stresses are shown in Fig. 3 for the entire test. It can be seen that radial stress-paths performed perfect ramps, while axial stress-paths have adjusted their values, not only during loading, but during unloading and reloading.

Figure 4 shows the evolution of the ratio $\varepsilon_3/\varepsilon_1$ during the K_0 test, where ε_3 is the radial strain. It may be noted that, as soon as this strain ratio falls below about 2%, the approach to the K_0 state appears virtually complete.

Other verifications of the K_0 condition with this technique are shown in Figs. 5 and 6. In Fig. 5, the area change is not greater than 0.2% during whole test. Figure 6 shows the pore water pressure developed during the test, which indicates that the test was clearly drained.

The plot of the void ratio against the effective vertical stress is shown in Fig. 7. It presents typical stress paths for both normally consolidated and over consolidated conditions. It clearly shows that after an unload-reload cycle (after $\sigma'_1 = 520$ kPa), the reload stress path merges back on to the normal consolidated path.

3.2. K_0 values

With the technique used validated, it can be seen from the results presented in Fig. 8 that the stress path followed a more or less linear pattern during normally consolidated conditions and followed a curve during overconsolidated

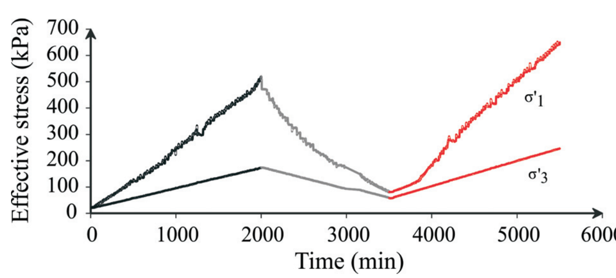

Figure 3 - Effective stress paths during the test.

Table 1 - Experimental data.

Cycle	Target values			Reached values		OCR
	σ_3 (kPa)	Back pressure, BP (kPa)	Test duration (min)	σ'_3 (kPa)	σ'_1 (kPa)	
Loading	739		2000	174	520	
Unloading	589	539	1500	59	67	7.76
Reloading	789		2000	246	650	-

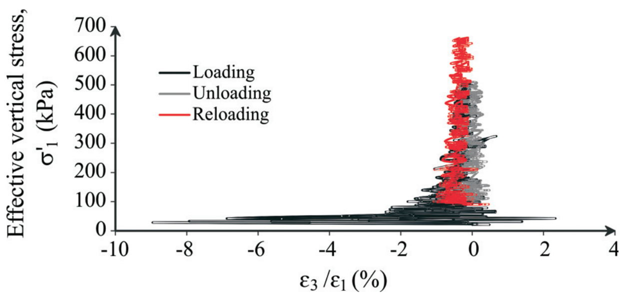

Figure 4 - Evolution of the ratio $\varepsilon_3/\varepsilon_1$ with σ'_1 during the K_0 test.

conditions. The ratio σ'_3/σ'_1 is the value of K_0, which is independent of σ'_1, during the first load. This is more clearly shown in Fig. 9, where the variation of K_0 *vs.* σ'_1 is presented. Initially, K_0 is significantly affected by isotropic consolidation but it reduces rapidly from its initial value of 1.0, to a constant value of 0.38. During unload and reload the soil is in an over-consolidated condition where K_0 depends on the effective vertical stress. However, during reloading, K_0 seems to be again independent of σ'_1 for values of σ'_1 greater than 520 kPa, the pre-consolidation pressure (σ'_p), following a straight line.

In Fig. 9 it can be also seen that the maximum value of K_0 reached in the test is about 0.9.

In Fig. 10 it is possible to observe the trend of K_0 in relation to different values of OCR for unloading and reloading test data.

It appears that exists a unique K_0-OCR relationship for unloading and reloading, at least for the values of OCR tested.

The relationship obtained is of the type:

$$K_0^{OC} = K_0^{NC} \times OCR^a \tag{5}$$

As it can be seen in the same Fig. 10, the value obtained for the exponent α is about 0.4.

3.3. Comparison of the test results with previous publications

During first loading the coefficient of earth pressure at rest of 0.38 is in agreement with the theoretical values given by the Jaky's equation. In fact, a drained triaxial com-

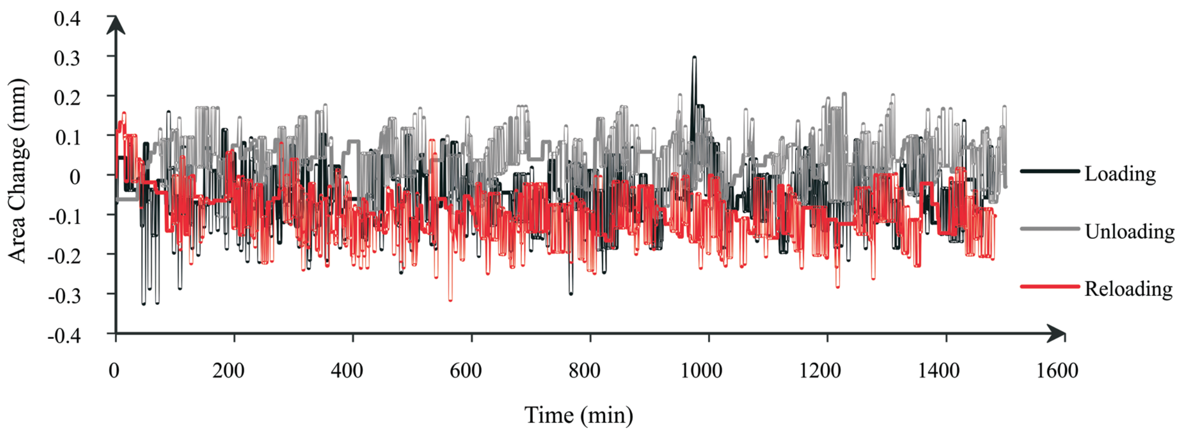

Figure 5 - Variation the area of the specimen during the K_0 test.

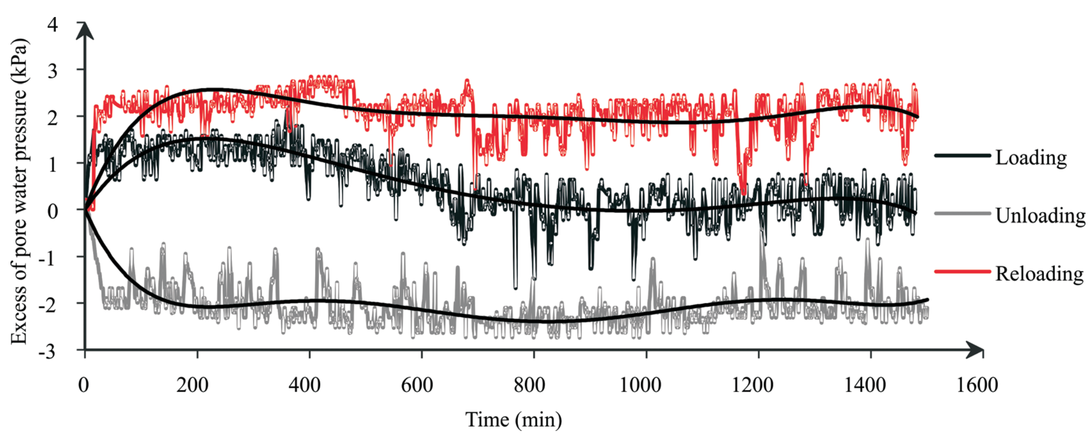

Figure 6 - Excess of pore water pressure developed during the K_0 test.

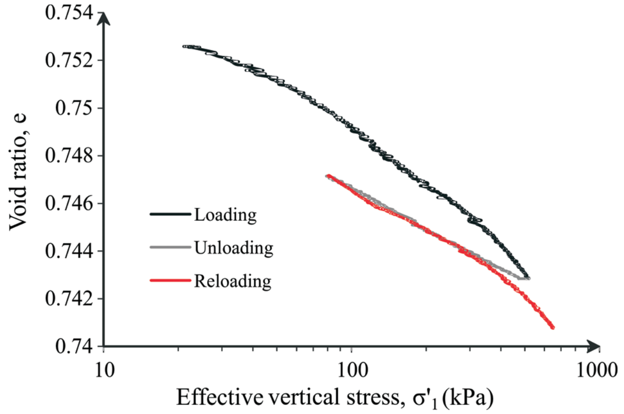

Figure 7 - Relation between axial strain and axial effective stress during all stages of K_0 test.

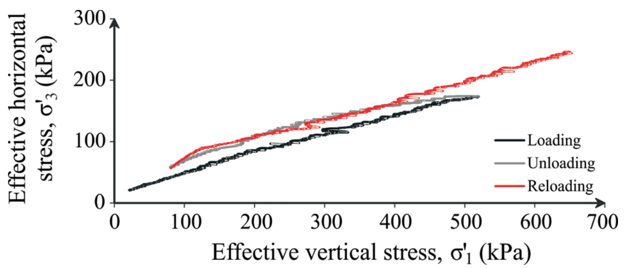

Figure 8 - Stress paths for load-unload-reload.

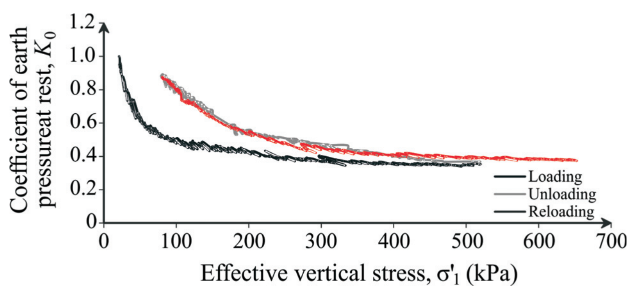

Figure 9 - K_0 *vs.* σ'_1 for all stress paths: load-unload-reload.

pression test, carried out after the anisotropic consolidation, gave a ϕ' value near 38°.

During unloading and reloading, as already seen in Fig. 10, the equation is similar to the one obtained by other publications.

Figure 11 has a comparison with previous proposals referred in item 1, for different values of α, for overconsolidated soils. These correlations, for $K_0^{NC} = 0.38$, gave K_0 values higher than the experimental study where the trend resembles the most with the empirical correlation presented by Hanna *et al.* (2008).

4. Conclusions

The K_0 laboratory test carried out in this study, using a triaxial stress path test, with back volume measurement to constantly adjusting the axial stress, showed that this method can be used to determine K_0 value in normally consolidated and overconsolidated conditions.

K_0 value is estimated with an anisotropic consolidation, keeping a constant ramp of radial stress and constantly adjusting the axial stress on the load frame by means of a computer control.

Before starting K_0 test, the specimen must be in equilibrium, *i.e.*, fully saturated and consolidated with no excess of pore water pressures.

During the K_0 test, the maximum radial strain of the sample was kept into acceptable values, with $\varepsilon_3/\varepsilon_1 < 2\%$. Also the negligible excess of pore water pressures developed indicated that the test was clearly drained.

The relation between radial effective stresses and axial effective stresses gave a straight line during the first load. The estimated K_0 value was 0.38, clearly similar to the one obtained from Jacky's formula for this soil.

The K_0 values during unload and reload increased with the increase of OCR. For the stress state tested, it was found an empirical correlation similar to the one found in previous publications, Eq. (3) with α = 0.447.

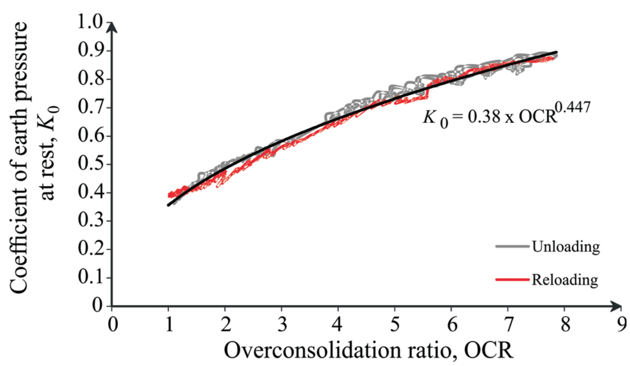

Figure 10 - K_0 *vs.* OCR for the stress paths: unload-reload.

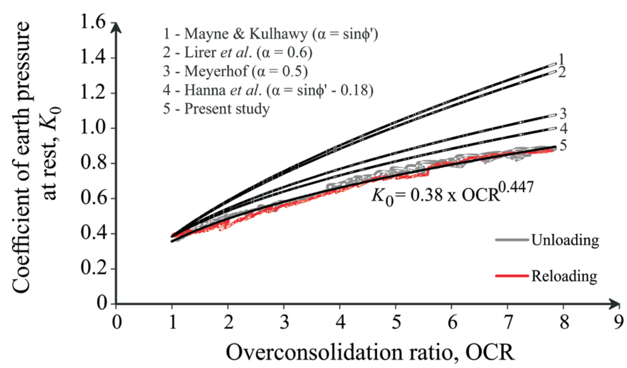

Figure 11 - Comparison of K_0 values with other publications.

From the test results it can be concluded that the method used in this work to determine K_0 is practical enough for both normally and overconsolidated soils.

Acknowledgments

The authors are grateful to the technical assistant, Jorge Silvério, for the preparation of specimens.

References

Eliadorani, A.A. & Vaid, Y.P. (2005). The measurement of K_0, the coefficient of earth pressure at rest by strain path loading technique. Proc. 16th Int. Conf. on Soil Mech. and Geotechnical Engineering, ICSMGE, Osaka, vol. 2, pp. 345-348. (CD-ROM).

Hanna, A. & Al-Romhein, R. (2008). At-rest earth pressure of overconsolidated cohesionless soil. Journal of Geotechnical and Geoenvironmental Engineering, 134(3):408-412.

Lirer, S.; Flora, A. & Nicotera, V. (2011). Some remarks on the coefficient of earth pressure at rest in compacted sandy gravel. Acta Geotechnica, 6(1):1-12.

Lo, R. & Chu, J. (1991). The measurement of K_0 by triaxial strain path testing. Soils and Foundations, 31(2):181-187.

Mayne, P.W. & Kulhawy, F.H. (1982). K_0-OCR relationships in soil. Journal of Geotechnical Engineering Division, ASCE, 108(GT6):851-872.

Menzies, B.K. (1988). A computer controlled hydraulic triaxial testing system. Advanced Triaxial Testing of Soil and Rock. ASTM STP 977, Philadelphia, pp. 82-94.

Meyerhof, G.G. (1976). Bearing capacity and settlement of pile foundations. Journal of Geotechnical Engineering Division, 102(3):195-228.

Michalowski, R. (2005). Coefficient of earth pressure at rest. Journal of Geotechnical and Geoenvironmental Engineering, 131(11):1429-1433.

Okochi, Y. & Tatsuoka, F. (1984). Some factors affecting K_0-values of sand measured in triaxial cell. Soils and Foundations, 24(3):52-68.

Piriyakul, K. & Haegeman, W. (2005). Automated K_0 consolidation in stress path cell. Proc. 16th Int. Conf. on Soil Mech. and Geotechnical Engineering, ICSMGE, Osaka, vol. 2, pp. 575-578. (CD-ROM).

Teerachaikulpanich, N.; Okumura, S.; Matsunaga, K. & Ohta, H. (2007). Estimation of coefficient of earth pressure at rest using modified oedometer test. Soils and Foundations, 47(2):349-360.

Wood, D.M. (1990). Soil Behavior and Critical State Soil Mechanics. Cambridge University Press, Cambridge, 462 pp.

Influence of Physicochemical Interactions on the Mechanical Behavior of Tropical Residual Gneiss Soils

M.M. Futai, W.A. Lacerda, A.P.S. Martins

Abstract. When soils are inundated with liquids other than water, a physicochemical interaction takes place and can alter the soil behavior. Depending on the type of soil and on the solution, the soil can become more compressible and lose strength (or the contrary). In this paper, tropical residual gneiss soils are used, namely lateritic and saprolitic soils. The solution used are a mixture of sodium hexametaphosphate and sodium carbonate. Solutions were prepared with different concentrations such that the pH value remained at 10.5. Sodium concentration was used to interpret the results. Oedometer and triaxial compression tests were carried out with samples permeated with these solutions. The lateritic soil behavior was found to be quite distinct from the saprolitic one. While the lateritic soil becomes much more compressible upon the increase in the concentration of sodium, the saprolitic soil swells progressively. However, the compression curve converges at more elevated stress levels. The stress-strain curve also alters in relation to the concentration. The lateritic soil loses strength and its stiffness is greatly reduced with the increase in concentration.
Keywords: physicochemical, tropical soil, lateritic soil, saprolitic soil.

1. Introduction

Physicochemical interactions often have a damaging impact on natural soils, such as excessive settlements and expansion, failures due to piping associated with dispersive clay soils, the contamination of underground water by the migration of contaminants, etc. Furthermore, in these situations, the knowledge of physicochemical properties constitutes an important tool for diagnosing and for solving problems. Physicochemical interaction can turn soils not previously presenting engineering problems into problematic soils. For example, non-expansive soils can swell or non-collapsible soils can be deformed through collapses caused by the infiltration of liquids that alter the soil structure.

Tropical soils have quite a different chemical and mineralogical composition as compared to temperate soils, as they have a dominance of minerals with a variable charge as well as distinct electro-chemical behavior. Consequently, research is needed to expand the knowledge of the mechanisms and factors related to physical and chemical interaction processes and their impacts in terms of structural changes and geo-mechanical behavior.

In the literature, various experimental works were found referring to the physicochemical interaction of different liquids (salt, acid, base, organic) with the soil. The studies in question investigated permeability, (Anandarajah, 2003), compressibility (Bolt, 1956; Abdullah *et al.*, 1997; Alawaji, 1999; Chen *et al.*, 2000; Brancucci *et al.*, 2003 and Sivapullaiah & Manju, 2006) and shear strength (Moore, 1991; Anandarajah & Zao, 2000 and Brancucci *et al.*, 2003). The works cited used predominantly clayey or pure clay soils and a mineralogical composition consisting of illite, kaolinite, montmorillonite or mixtures of these minerals. The samples were prepared through remolding or compaction. Chen *et al.* (2000) studied the influence of different liquids on the compression of soils and used the dielectric constant to compare the influence of different fluids. Anandarajah & Zao (2000) did the same with triaxial tests. Sivapullaiah & Manju (2006) used sodium hydroxide (NaOH) in different concentrations to study the compressibility of kaolinite. The pH of a solution with NaOH is known to vary according to the concentration, while Sivapullaiah & Manju (2006) also found that NaOH transforms kaolinite into zeolite; in other words, it attacks the clay chemically.

Our aim is to verify the physicochemical interaction in the behavior of tropical soils with a base solution containing sodium. The chemical and mining industries frequently use sodium hydroxide (NaOH) and, as a result, produce Na concentration effluent. NaOH significantly increases pH and, for this reason, the dispersion of clay is attributed to the increase in the basic pH. We used a combined solution of sodium hexametaphosphate and sodium carbonate which has a physicochemical interaction similar to that of NaOH. The proportion of this mixture allows the pH to be controlled so that even when the concentration of sodium varies, the pH remains constant. Therefore, the aim is to investigate the mechanical and physicochemical interaction of the sodium concentration in a basic environment with a principal content. Whenever the influence of the

Marcos Massao Futai, DSc, Associate Professor, School of Engineering, Department of Structures and Geotechnical Engineering, University of São Paulo, São Paulo, Brazil. e-mail: futai@usp.br.
Willy A. Lacerda, Ph. D., Full Professor, Graduate School of Engineering, Federal University of Rio de Janeiro, Rio de Janeiro, Brazil. e-mail: willyl@globo.com.
Adriana P.S. Martins, MSc, Research Engineer, Federal University of Rio de Janeiro, Rio de Janeiro, Brazil. e-mail: adrianapsmartins@infolink.com.br.
Submitted on August 7, 2013; Final Acceptance on March 26, 2015; Discussion open until December 31, 2015.

concentration of Na is mentioned in the text, it should be understood that this refers to a basic environment of pH = 10.5.

Physicochemical interactions influence various properties of clayey soils, including Atterberg limits, compressibility, permeability and shear strength (Mitchell, 1976). To understand the mechanical behavior of clayey soils, the nature of antiparticle forces must be examined. The most important antiparticle forces are Born's repulsion force, Van Der Waals' forces of attraction and the double layer repulsion force. Most studies involving the influence of physicochemical interactions in the behavior of clayey soils concern sedimentary soils and take into account only double layer repulsion forces, due to the complexity of the quantification of the other forces (Mitchell, 1976). The theory of the electrical double layer (EDL), first developed by Gouy (1910) and Chapman (1913) and later improved by Stern (1924), describes, from both the qualitative and quantitative viewpoints, physicochemical phenomena on surfaces with electrical charges. Although this theory is still commonly used and is still unanimously accepted, it should be noted that in real soils there are fractions with different grain sizes, hindering the effects of the electrical double layer. In common soils, this theory functions for soils which have clay minerals as their predominant fraction.

The repulsion created by the double layer and the electromagnetic attractions resulting from Van Der Waals' connections combined result in the force that defines the tendency towards approximation or distancing of soil particles. Repulsion energy is sensitive to changes in electrolytic concentration, cation valence, dielectric constant, and pH, while attractive energy is only sensitive to changes in the dielectric constant and temperature (Mitchell, 1976).

2. Material and Methods

The tests were performed with tropical gneiss lateritic and saprolitic soil. A chemical solution was used to understand its influence on mechanic behavior. This item describes the characteristics of solutions and of the soil, the methodology used in the oedometer and triaxial tests. All the tests were carried out in a room kept at 20 °C.

2.1. Characteristics of solutions

To simulate real situations in laboratory, in which the soil is percolated with different chemical substances, the interstitial fluid was replaced with a solution used on a daily basis in soil laboratories, with a simple stable chemical composition that can be dissolved in water capable of inducing structural changes without dissolving the clay minerals in the soil. Solutions containing sodium hexametaphosphate $(NaPO_3)_n$ and sodium carbonate (Na_2CO_3), with predefined concentrations and pH = 10.5, were selected. The pH value was adopted to guarantee chemical stability, avoiding the reversal of sodium hexametaphosphate to sodium orthophosphate. The dissolution of the sodium hexametaphosphate in distilled water provided a solution with pH of around 6, with the addition of sodium carbonate (Na_2CO_3), making it necessary to raise the pH to 10.5. The characteristics of the solutions used in the tests are given in Table 1.

The solutions herein will always be identified by the total concentration of sodium ions (Na^+) expressed in g/L. In addition, the solutions chosen to interact with the soil were verified not to corrode the aluminum and latex components used in the tests. In the case of the triaxial tests, the possibility of the interstitial fluid ions in the test samples flowing to the water chamber through molecular diffusion was investigated. A diffusion test was carried out by Martins (2005), and this type of flow was found not to occur.

The treatment of the soils studied with sodium hexametaphosphate $(NaPO_3)_n$ provides sodium cations (Na^+) for the double layer on the larger side of the clay minerals. The phosphate anion $(PO_3)^-$ is absorbed by the smaller side (the edge), while the effect of this adsorption is the transformation of the edge, through the coverage of a mono phosphate -layer, from a positive charge to a negative one. Side-edge and edge-edge interactions are destroyed, and the soil structure becomes more disperse (Santos, 1975). Equation 1 presents the chemical reaction associated with the addition of $(NaPO_3)_n$:

Table 1 - Characteristics of the solutions used in the tests.

Concentration $(NaPO_3)_n$	Concentration (g/L)				Total concentration Na^+(g/L)	pH
	$(NaPO_3)_n$	Na^+(*)	(Na_2CO_3)	Na^+(**)		
0.001 N	0.102	0.023	1.52	0.66	0.68	10.5
0.01 N	1.02	0.23	1.38	0.60	0.83	10.5
0.1 N	10.2	2.29	12.4	5.38	7.67	10.5
1 N	102	22.95	74.7	32.42	55.37	10.5

Note: N - normal state.
Na^+(*) - concentration of sodium in $(NaPO_3)_n$.
Na^+(**) - concentration of sodium in (Na_2CO_3).

$$(NaPO_3)_n \xrightarrow{H_2O} nNa^+ + nPO_3^- \quad (1)$$

The addition of sodium carbonate (Na_2CO_3) can be better understood through the main associated chemical reactions (2) and (3):

$$Na_2CO_3 + 2H_2O \rightarrow 2NaOH + H_2CO_3 \quad (2)$$

$$H_2CO_3 \rightarrow CO_2 + H_2O \quad (3)$$

The hydrolysis of sodium carbonate generates a strong base (NaOH) and a weak acid (H_2CO_3). The presence of hydroxyls in the pore solution, associated with the formulation of sodium hydroxide (NaOH), causes the dissociation of hydrogen (H^+) from the SiOH, AlOH and FeOH groups existing on the edges of the clay minerals, resulting in an increase of negative surface charge of particles and the consequent increase in the repulsion forces of the clay-water system (dispersive effect). Concomitantly, the sodium added by the treatment dislocates the hydrogen and/or aluminum adsorbed by the soil, which go to the pore solution to neutralize the hydroxyls, resulting in a stabilizing effect on pH (buffer effect). At elevated pH conditions, the tendency for dissociation of the hydroxyl (OH) exposed on the sides and edges of the clay minerals is increased. The higher the pH, the greater the tendency of H^+ to go to the pore solution, the greater the negative charge of the particle, the greater the repulsion force associated with the double layer.

2.2. Characterization of soils

The specimens were collected in the municipality of Ouro Preto in the southeast of Brazil. The geotechnical profile is typical of a residual gneiss soil in a tropical environment. Futai *et al.* (2004) summarize the conventional data of the physical index and the granulometric composition of this location (Fig. 1). The surface layer is a lateritic soil, while the lower layer is a saprolitic soil. The soil samples were collected at 1 m and 5 m depths to represent both types of soil. In this paper, results of geotechnical tests with chemical solutions will be presented and only conventional tests were performed by Futai *et al.* (2004).

The physical index, the Atterberg limits and the grain size analysis results are given in Table 2. The 1 m soil depth is more weathered than the 5 m soil depth, with a lower natural specific weight and a greater void ratio due to the weathering process to which it was submitted. The difference in the specific gravity of soil solids is associated with differences in the mineralogical composition. The level of

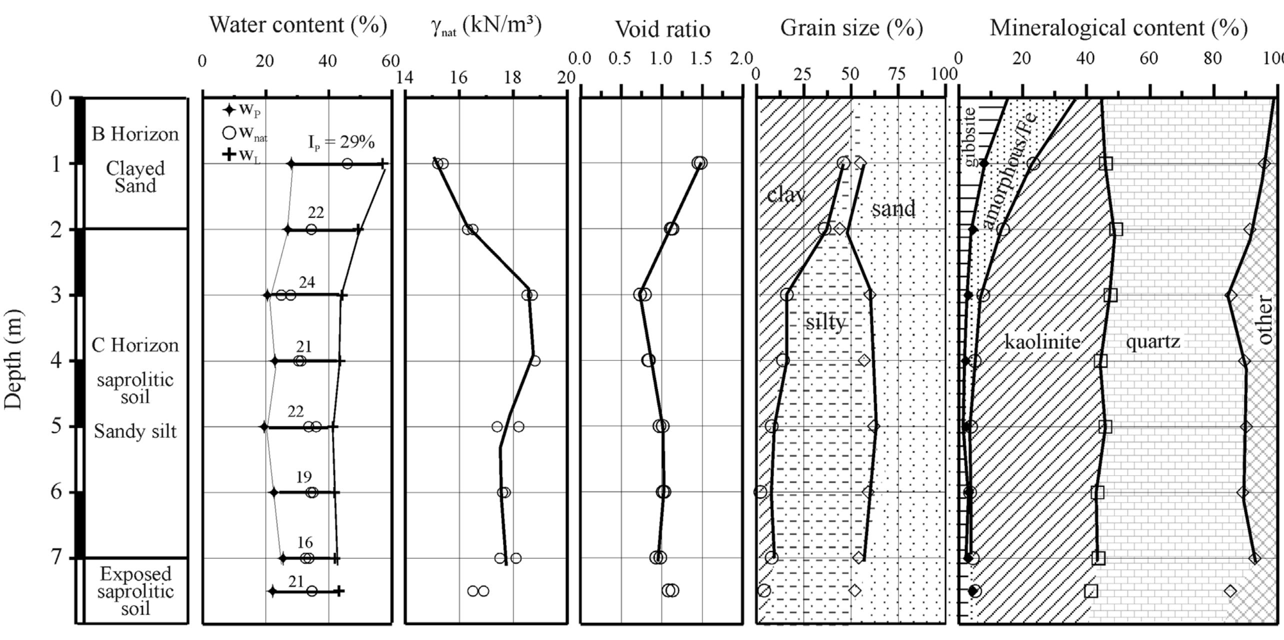

Figure 1 - Site characteristics (Futai *et al.*, 2004).

Table 2 - Physical indices, consistency limits and grain size analysis of the soils studied.

Depth (m)	γ_{nat} (kN/m^3)	w_{nat} (%)	E	G_s	S (%)	w_L (%)	w_P (%)	I_P (%)	Clay (%)	Silt (%)	Sand (%)
1	15.4	45.9	1.45	2.635	83.4	57.1	28.1	29.0	50* (0)	9* (37)	41* (63)
5	17.4	33.6	1.01	2.675	89.0	41.3	19.5	21.8	6 (0)	60 (64)	34 (34)

*according to the Brazilian standard and in brackets: (without deflocculant and without mechanical dispersion).

clay is greater in horizon B, resulting in higher Atterberg limits due to higher clay and oxide content. The degree of saturation demonstrated the unsaturated condition of the profile. The study of the unsaturated behavior of these soils was presented by Futai & Almeida (2005).

The X-ray diffraction (DRX) results are presented in Fig. 2. The soil was sifted in sieve #200. The sample preparation technique was the orientation of the particles of the glass plate method. Apart from natural soil, samples treated with the solutions were also prepared.

The mineralogical composition is essentially constituted of quartz and kaolinite (around 40%), although there is also an important presence of iron oxides and hydroxides and aluminum for the 1 m soil and illite and mica for the 5 m soil. The granulometric composition of saprolitic soil is silt, yet the largest part of this fraction is kaolinite. These data and oxides content explain the plasticity of a soil with a low level of clay. The cationic exchange capacity is less than 2.9 meq/100 g, a low value compatible with the dominant clay mineral (kaolinite). The pH of the soils in water is acid, with a value of approximately 5. The mineralogical composition of the soils determined by DRX (Fig. 2) confirms that 1 m soil depth is more weathered than 5 m soil depth.

The treatment of soils with solutions of sodium hexametaphosphate $(NaPO_3)_n$ and sodium carbonate (Na_2CO_3) did not dissolve the constituent minerals. DRX tests carried out on the fine fraction of the soil treated with the solutions showed (Fig. 2) that there is no change in the mineralogical composition when soils interact with the solutions. Cation exchange capacity tests (Table 3) and selective chemical analyses for sulfuric attack (Table 4) showed that the chemical composition changed little when the results for the natural soil are compared to soil treated with solutions. Thus, the solution used has the same effect as NaOH, although it allows the pH to be kept constant in relation to variations in the Na concentration in the solution.

Scanning Electron Microscopic, SEM, sweep tests show that the intact microstructure of the lateritic soil (1 m depth) is characterized by the aggregation of clay particles caused by the presence of cementing materials (iron oxides and hydroxides and aluminum) with significant porosity (Figs. 3a and 3b). The SEM micrographs of the intact saprolitic soil (5 m depth) showed an interlocking arrangement of the constituent minerals with kaolinite, mica plates (silt size) interwoven with quartz grains and a small amount of clay aggregate. (Figs. 4a and 4b).

Samples were prepared, remolded and treated with a solution corresponding to 7.67 g/L of Na to observe the structure in SEM. The treated body was molded into a ring and was submerged in a solution for twenty-four hours. The remolding of the lateritic soil (1 m) broke the aggregations of connectors, while the rounding and corners disappeared (Figs. 3c and 3d). There was a change in the form and distribution of the pores, which became more uniform. The treatment of the lateritic soil with the solution altered the struc-

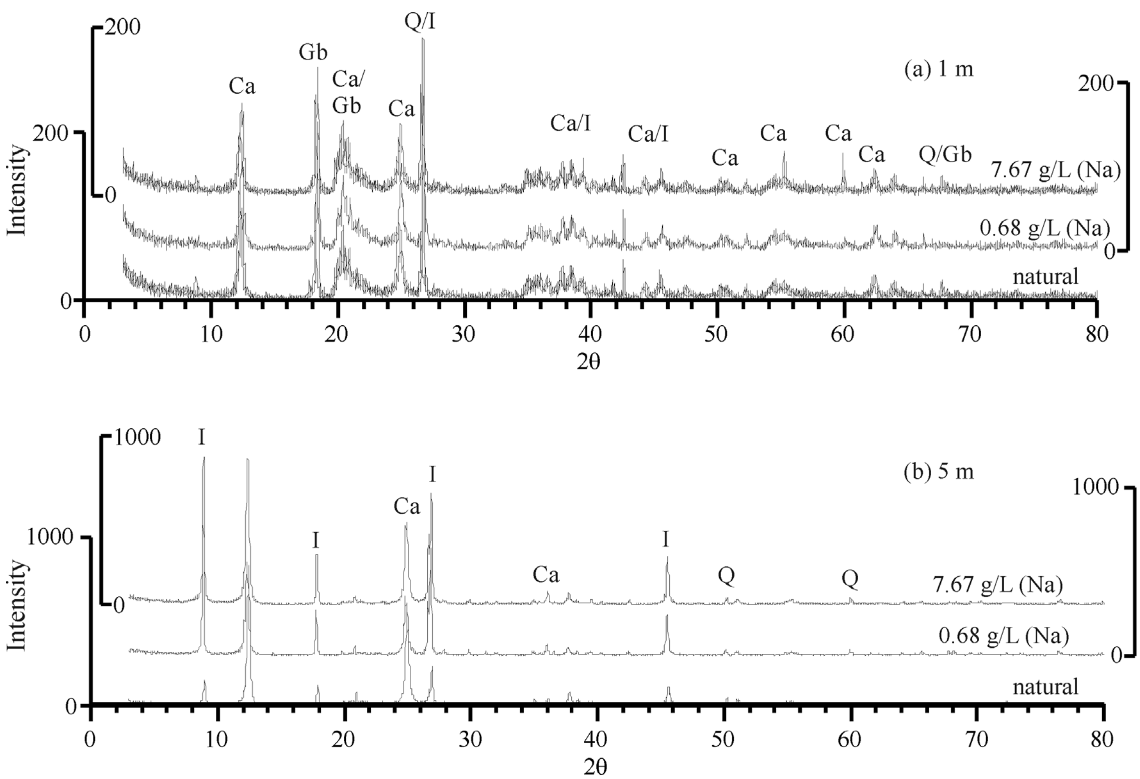

Figure 2 - X-Ray analysis: (a) 1 m depth and (b) 5 m depth.

ture (Figs. 3e and 3f) without any mechanical action taking place. The cementation was broken, making the soil more homogenous and more similar to the remolded soil. However, there was a difference in relation to the form of dispersion, since the physicochemical action is more effective than the mechanical remolding.

In the saprolitic soil (5 m), the remolding destroyed the kaolinite silt particle piles, stimulated the homogeniza-

Table 3 - Cation exchange capacity tests.

Depth (m)	Concentration Na (g/L)	Cation exchange capacity (cmol/kg)						
		$Ca^{2+} + Mg^{2+}$	K^+	Na^+	S*	Al^{3+}	H^+	T**
1	0	0.7	0.04	0.05	0.8	0.0	1.8	2.6
	0.68	0.6	0.01	1.22	1.8	0.0	0.0	1.8
	7.67	0.6	0.06	5,6	6.3	0.0	0.0	6.3
5	0	0.8	0.01	0.01	0.8	1.4	0.7	2.9
	0.68	0.7	0.03	1.36	2.1	0.0	0.0	2.1
	7.67	0.7	0.06	0.82	1.6	0.0	0.0	1.6

*S = ($Ca^{2+} + Mg^{2+} + K^+ + Na^+$). **T = ($S + Al^{3+} + H^+$).

Table 4 - Selective chemical analysis for sulfuric attack.

Depth (m)	Concentration Na (g/L)	Selective chemical (%)						
		SiO_2	Al_2O_3	Fe_2O_3	TiO_2	K_2O	Ki	Kr
1	0	13.8	22.8	3.7	0.40	0.17	1.03	0.93
	0.68	13.5	23.4	5.3	0.21	0.15		
	7.67	13.3	25.1	5.5	0.44	0.14		
5	0	22.3	18.2	2.7	0.30	1.22	2.08	1.9
	0.68	18	21.7	6	0.07	0.82		
	7.67	27.5	16.3	3.9	0.39	1.45		

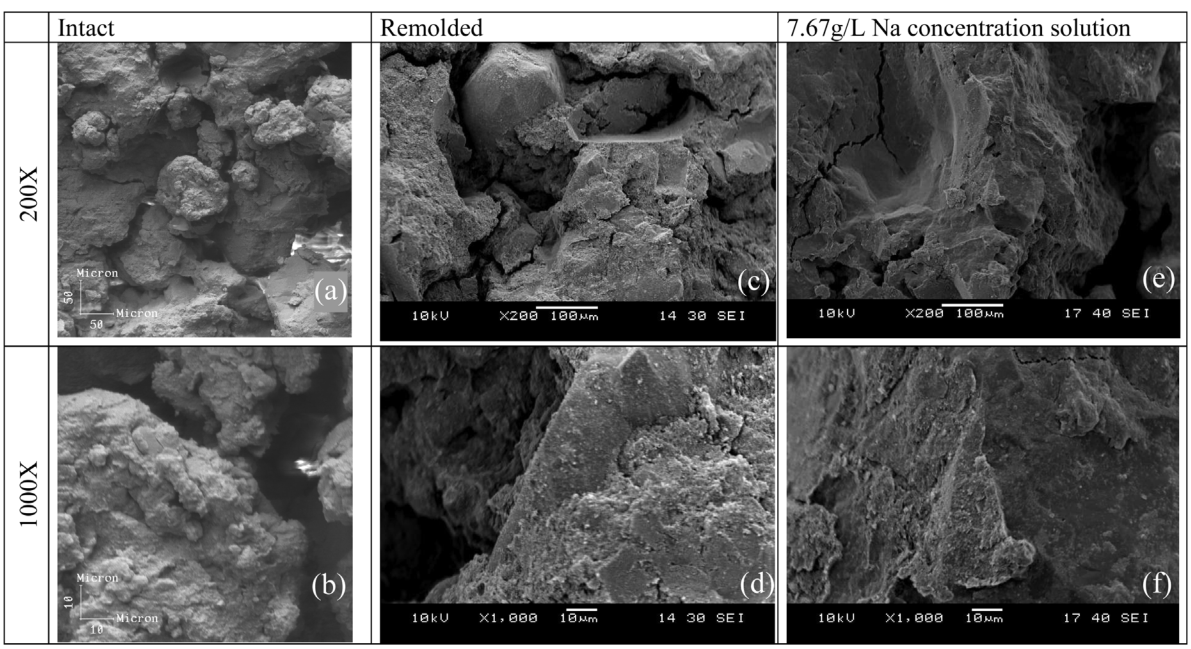

Figure 3 - SEM image of lateritic soil.

tion of voids and a small content of clay remained aggregated (Figs. 4c and d). The reorientation of particles could also be seen due to remolding. Compared with Fig. 4e (or Fig. 4f), in which the sample was treated with the solution, the alteration of the structure was verified not to be as striking as that of remolding.

The Atterberg limits and grain size analyses of both types of soil were obtained using the solutions detailed in Table 1, with the results presented in Figs. 5 and 6. Atterberg-limit values decreased with the increase of the concentration for the 1 m depth (Fig. 5). For kaolinite clays, sodium reduces the rigidity of the adsorbed water, reducing the connection force exercised by this layer, thus facilitating interparticle movement. Consequently, it reduces the water content necessary to reach the limits. Sodium may tend to displace molecules that otherwise satisfy the net negative charge of the clay particles. For the saprolitic soil (Fig. 5), the results did not indicate an influence of concentration. The accuracy of the method did not permit effective conclusions. The low clay fraction influences these observations. Additionally, the soil structure can be compared to explain the difference between two soils due to chemical interaction: the micropores of the 1 m soil depth retain more water than the 5 m soil depth; however, the disaggregation has more influence on the 1.0 m soil depth and the plasticity decreases. The conventional grain size analyses were performed according the Brazilian Standard (NBR 7181) and the tests with solutions (or water) were performed without mechanical dispersion. The results of the grain size analysis for the lateritic soil (Fig. 6a) showed a significant increase in the clay content with an increase in the total concentration of sodium, and the consequent reduction in the sand and silt fractions to compensate this increase. The saprolitic soil (Fig. 6b) presented different behavior in relation to the grain size analysis, with the clay, silt and sand fractions varying little with the increase in the total concentration of sodium. This is because the clay aggregation content is low, but it remains after treatment. When the soils were tested without deflocculant and without mechanical dispersion, the clay fraction was null. After the comparison with the results of the methodologies with and without chemical deflocculant, it indicated that the clay fraction is flocculated in the *in situ* condition.

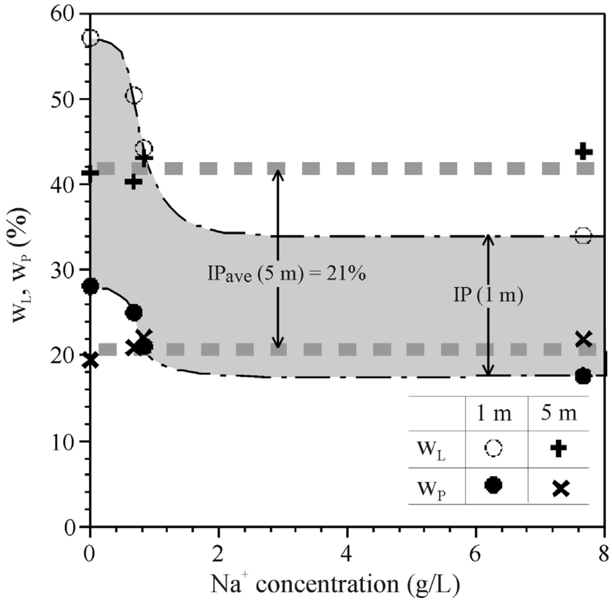

Figure 5 - Atterberg Limits using solutions, 1.0 and 5.0 m depths.

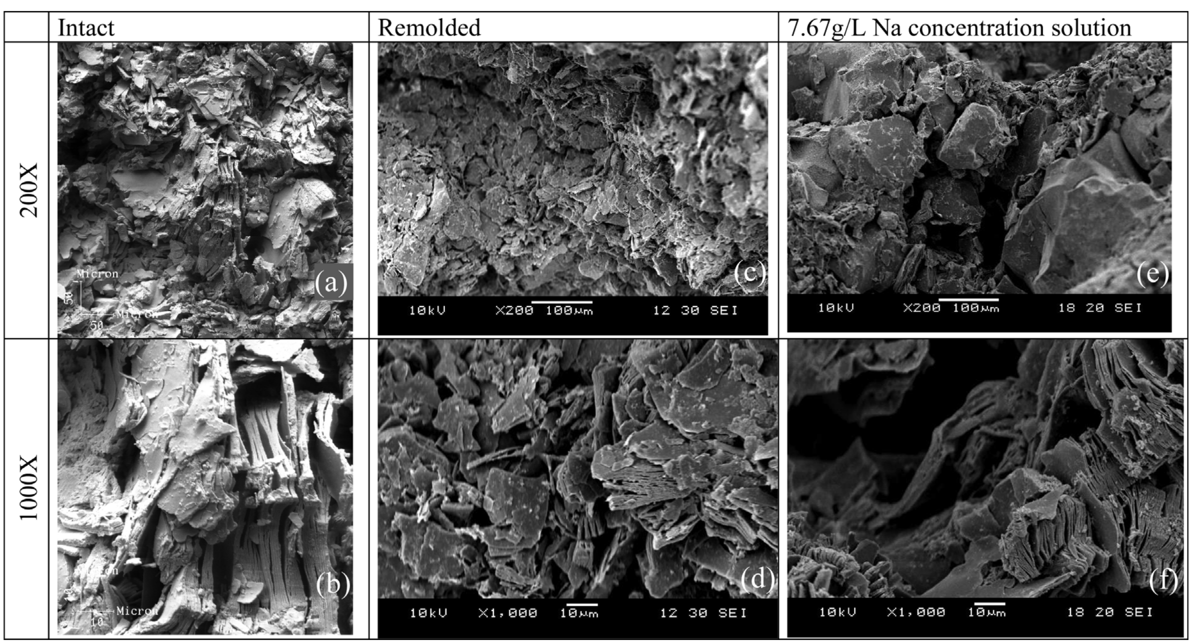

Figure 4 - SEM image of saprolitic soil.

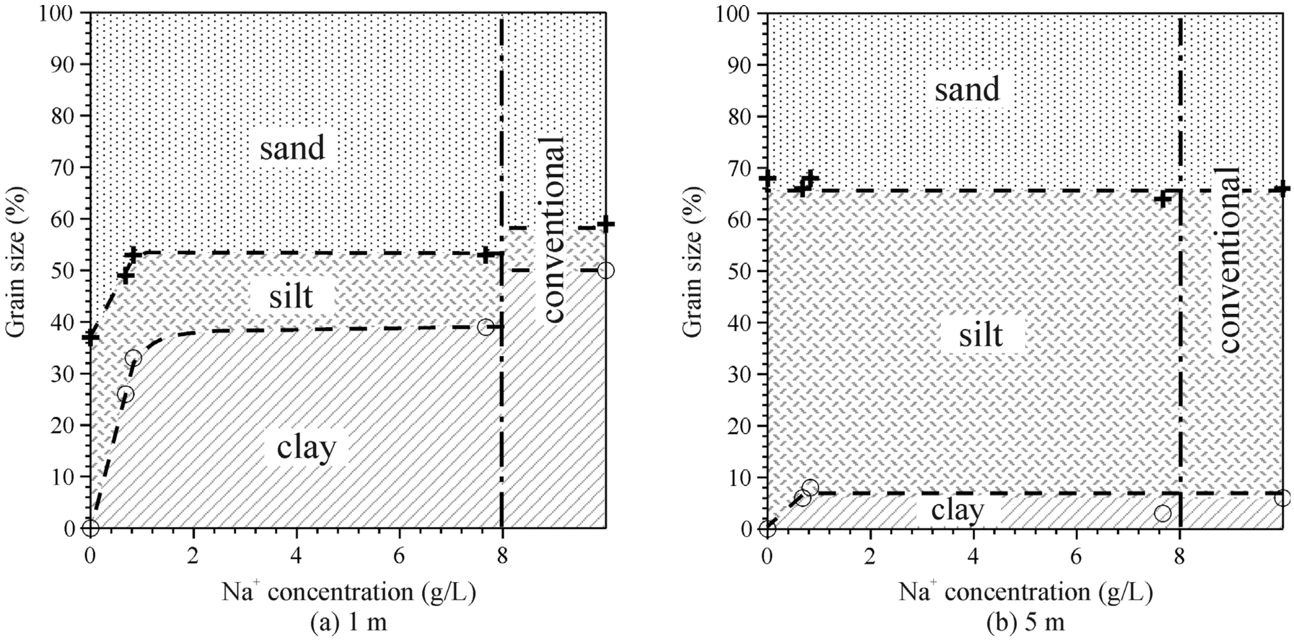

Figure 6 - Grain size analysis using solutions, 1 and 5 m depths.

2.3. Oedometer compression tests

Conventional oedometer tests were carried out on inundated samples of lateritic and saprolitic soils, which were intact, remolded and permeated with solutions containing sodium at concentrations of 0.68 g/L; 0.83 g/L; 7.67 g/L and 55.37 g/L. The samples were inundated with distilled water or with solutions after the stabilization of the settlement corresponding to the 3.125 kPa stage (settlement load). The increases in load stages maintained the ratio $\Delta\sigma_v/\sigma_v = 1$. In the tests with the solutions, after the stabilization of the deformations corresponding to the inundation with solution, the samples were percolated with a volume of the solution equal to twice their void ratio. The duration of each loading stage was sufficient to allow for the stabilization of deformations.

The soil parameters were obtained using conventional methods. The pre-consolidation stress was determined by the Casagrande method and was called vertical yield stress, σ_{vy}.

2.4. Triaxial tests

The objective of the triaxial tests was to study the influence of physicochemical interactions on the stress-strain behavior and on the shear strength for the lateritic soil sample. Tests were carried out in the saturated condition, both drained and undrained, using remolded soil at approximately the liquid-limit, and permeated with solutions with total sodium concentrations of 0.68 g/L and 7.67 g/L. The results of these tests were compared with those of the intact soil. The test samples (diameter 50 mm; height 100 mm) were saturated by back-pressure saturation, and the B coefficient was considered to be satisfactory when greater than 0.96. The strain rates of tests were determined in accordance to Head (1986). For the 1 m depth, they were 0.011 and 0.04 mm/min for the drained and undrained tests, respectively. The strain rate adopted in the drained tests was justified by the relatively elevated permeability of the soil, resulting from its aggregated microstructure, and from the fact that primary consolidation occurred almost instantaneously. In the test with the solutions, before the saturation stage, a volume of the solution was percolated through the sample equal to twice the void ratio of the samples (approximately 220 mL). The percolation was carried out with an upwards flow, applying back-pressure of 10 kPa at one extremity of the test sample and collecting the percolated solution at the other extremity, open to atmospheric pressure. Simultaneously to the application of the back-pressure, a confining pressure of 15 kPa was applied to the cell to guarantee the integrity of the sample. The percolation required extremely variable times from 30 min to around 12 h, while these times were not related to the sodium concentrations in the solutions. This heterogeneous behavior may be associated with the dispersed effect of the percolating fluid, causing the dragging of fine particles and the blocking/unblocking of flow paths.

3. Results and Discussion

This item will presented results of the oedometer test for 1 m end 5 m depth with solutions described in the methodology. The results of the triaxial test carried out for 1.0 m depth are provided.

3.1. Oedometer tests with the lateritic (1 m depth)

The void ratio of the lateritic soil varies a lot due to its heterogeneity. Various tests were carried out with the same solutions, as shown in Fig. 7, and the compressibility parameters are presented in Table 5. The vertical deformation could not normalize the compression curves. For the samples with the highest void ratio and in the same test conditions, the greater the void ratio, the lower the vertical yield stress was observed.

To facilitate the interpretation of the influence of the solutions used in the compressibility, the results were organized according to the void ratio intervals, as shown in Fig. 8.

The results of the alteration in structure are shown in Fig. 3 and the dispersion of clay in Fig. 6 can also be seen in the compressibility of the lateritic soil. The greater the concentration, the more compressible the soil becomes. In Fig. 8c (samples with the highest void ratio), the tests with concentrations of 7.67 g/L and 55.37 g/L of Na present high compression with the first load.

The compression curve of the remolding soil depends on the initial water content (or void ratio) in which the sample was prepared. Three tests were carried out with different initial water content (Figs. 8b and 8c). It was not possible to prepare remolded samples with e = 1.0, since at

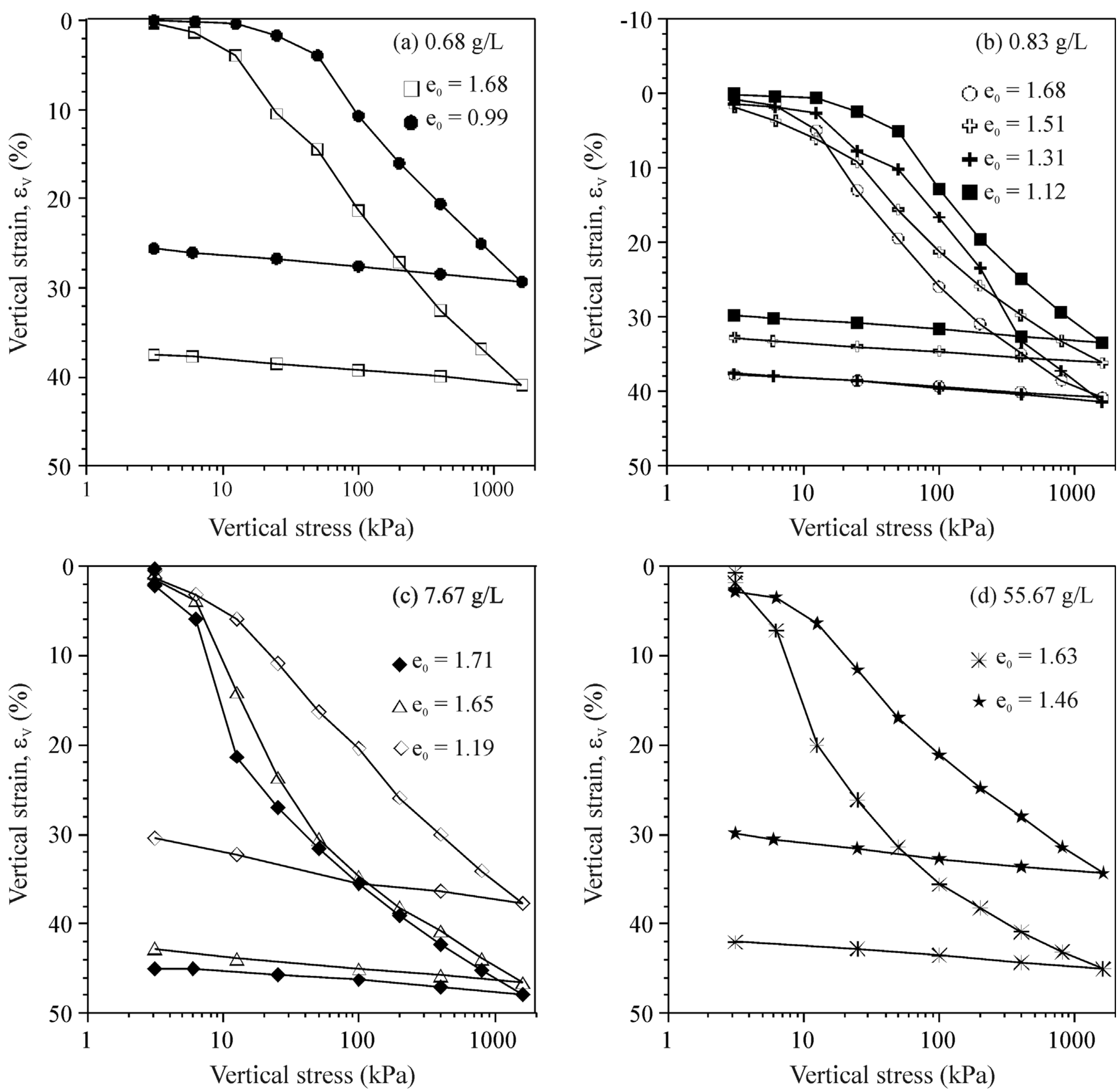

Figure 7 - Compressions curves of lateritic soil (1 m depth): void ratio influence.

this level there was too much water content below the liquid limit.

Figures 8b and 8c allow verifying that the compression curve of the intact soil is positioned above the curve of the remolded soil, a behavior typical of structured soil, in accordance with the models proposed by Vargas (1953) and Vaughan (1988 and 1992). The presence of cementation due to iron oxides and hydroxides and aluminum allows the intact soil to maintain void ratios higher than the remolded soil.

3.2. Oedometer tests with the saprolitic soil (5 m-depth)

Figure 9 shows the results of the oedometer compression tests for the saprolitic soil, while the compressibility curves were also obtained (Table 6). Some tests were carried out in duplicate (Figs. 9a, 9b and 9c) to investigate the heterogeneity of the soil and the repeatability of the tests. The compression curve of the intact soil is positioned below the curve for the remolded soil at the liquid limit, a characteristic that is typical of soils that are not structured by cementation (Vaughan, 1988 and 1992). The 5 m-depth has this structure due to the interlocking arrangement of its constituent materials, and is similar to a highly over-consolidated soil. This aspect was visualized with SEM sweep tests (Fig. 2), as reported above, in relation to the soil description. In Fig. 9d, compression tests were selected with initial vacuum levels between 0.9 and 1 in order to compare the results without the interference of heterogeneity. When the soil was tested with solutions, the results were in an intermediate position between those of intact soils and remolded soils. The greater the concentration, the greater the initial swelling; for higher stresses, the curves are convergent (Fig. 9d). The parameter C_c for $\sigma_v > 500$ kPa is practically the same; *i.e.*, concentration and remolding do not exert an influence, as shown in the detail of Fig. 9. This was limited to a vertical stress equal to 30 kPa and included the volumetric strain due to swell. The intact soil did not swell when inundated with distilled water, while inundation with the solutions caused significant expansions of up to 5% (Fig. 10). The vertical yield stress σ_{vy} is reduced with the increased concentration of Na. This occurs due to the initial swelling which raises the initial part of the curve. The data in Table 6 show that the recompression index did not practically vary for the different conditions tested, while remolding caused the breaking of the mineral arrangement, resulting in destructured soil.

3.3. Comparison of oedometer-testing parameters

The variation in the compressibility parameters with concentration can be seen in Fig. 11. In this figure, the parameters referring to the tests presented in Figs. 8c and 9d were used.

There is a rapid reduction in the vertical yield stress with the increase in the concentration of Na both for the lateritic and the saprolitic soil (Fig. 11a). This behavior is

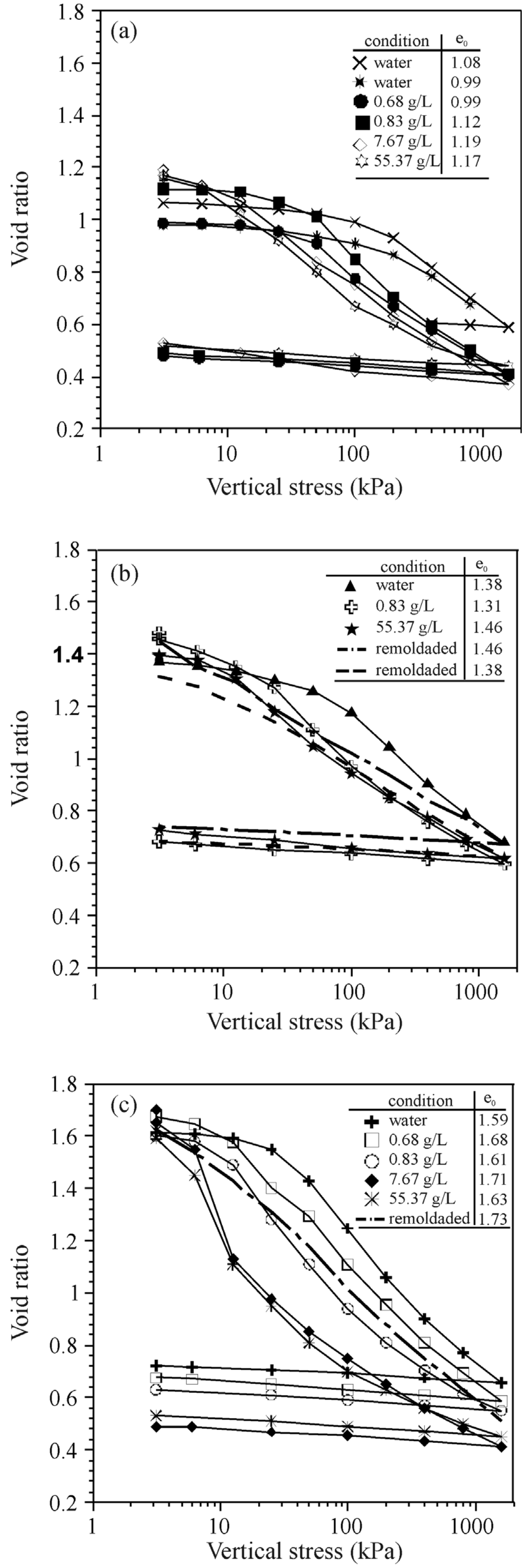

Figure 8 - Compressions curves of lateritic soil (1 m depth): Na concentration influence.

Table 5 - Oedometric compression parameters and initial void ratios, lateritic soil.

Soil condition	Pore fluid	Conc. Na (g/L)	e_o	σ'_{vy} (kPa)	C_c	C_s	C_r
Intact	Water	0	1.62	65	0.51	0.02	0.03
		0	1.38	75	0.42	0.02	0.03
		0	1.08	180	0.37	0.02	0.03
		0	0.98	260	0.35	0.02	0.03
	Solution	0.68	1.68	19	0.47	0.02	0.03
		0.68	0.99	38	0.32	0.02	0.03
		0.83	1.61	9	0.46	0.02	0.05
		0.83	1.50	30	0.41	0.02	0.16
		0.83	1.31	22	0.48	0.02	0.05
		0.83	1.12	45	0.39	0.02	0.03
		7.67	1.71	5	1.36 (5 kPa < σ_v < 15 kPa)	0.02	0.18
					0.29 (50 kPa < σ_v < 1600 kPa)		
		55.37	1.63	4	0.49 (5 kPa < σ_v < 15 kPa)	0.02	0.45
					0.23 (50 kPa < σ_v < 1600 kPa)		
		55.37	1.46	9	0.29	0.02	0.05
Remolded	Water	0	1.38	-	0.29	0.02	-
		0	1.46	-	0.32	0.02	-
		0	1.74	-	0.42	0.02	-

not repeated for the compression index. In the lateritic soil, C_c is reduced with the increase in the concentration of Na; however, it practically does not influence the values of C_c in the saprolitic soil (Fig. 11b). The recompression index, C_r, of the lateritic soil is significantly affected by the concentration of Na. In the highest concentrations (7.67 g/L and 55.37 g/L of Na), the values of C_r were greater than C_c (Fig. 11c). This is the result of the occurrence of an abrupt change in the structure under a low load level. Figures 11b and 11c contain a schematic drawing that illustrates this behavior. On the other hand, the values of C_r for the saprolitic soil vary little with the concentration.

Figure 10 shows that the saprolitic soil is significantly influenced by the initial swelling and this is also confirmed in the swelling index, C_s (Fig. 11d). The tendency of C_s increases with the concentration of sodium in the case of the saprolitic soil, but there is practically no influence on the lateritic soil. Figures 7c and 8d show that the compression curves of the lateritic soil are located more to the left as the concentration of Na increases. Conversely, the compression curve for saprolitic soil is found more and more above and to the right according to the increase in the concentration of Na.

Table 6 - Oedometric compression parameters and initial void ratios, saprolitic soil.

Soil condition	Pore fluid	Concentration Na (g/L)	e_o	$e_{after\ swell}$	σ'_{vy} (kPa)	C_c	C_s	C_r
Intact	Water	0	0.92	0.92	280	0.35		0.07
		0	0.87	0.87	320	0.35	0.04	0.12
	Solution	0.68	0.91	0.96	200	0.35	0.07	0.09
		0.68	0.77	0.80	350	0.35	0.07	0.05
		0.83	1.00	1.06	85	0.37	0.1	0.1
		0.83	0.98	1.03	100	0.35	0.1	0.07
		7.67	0.94	1.03	120	0.36	0.12	0.1
		55.37	0.92	0.99	170	0.35	0.1	0.09
Remolded	Water	0	1.22	1.22	0	0.37	0.09	-

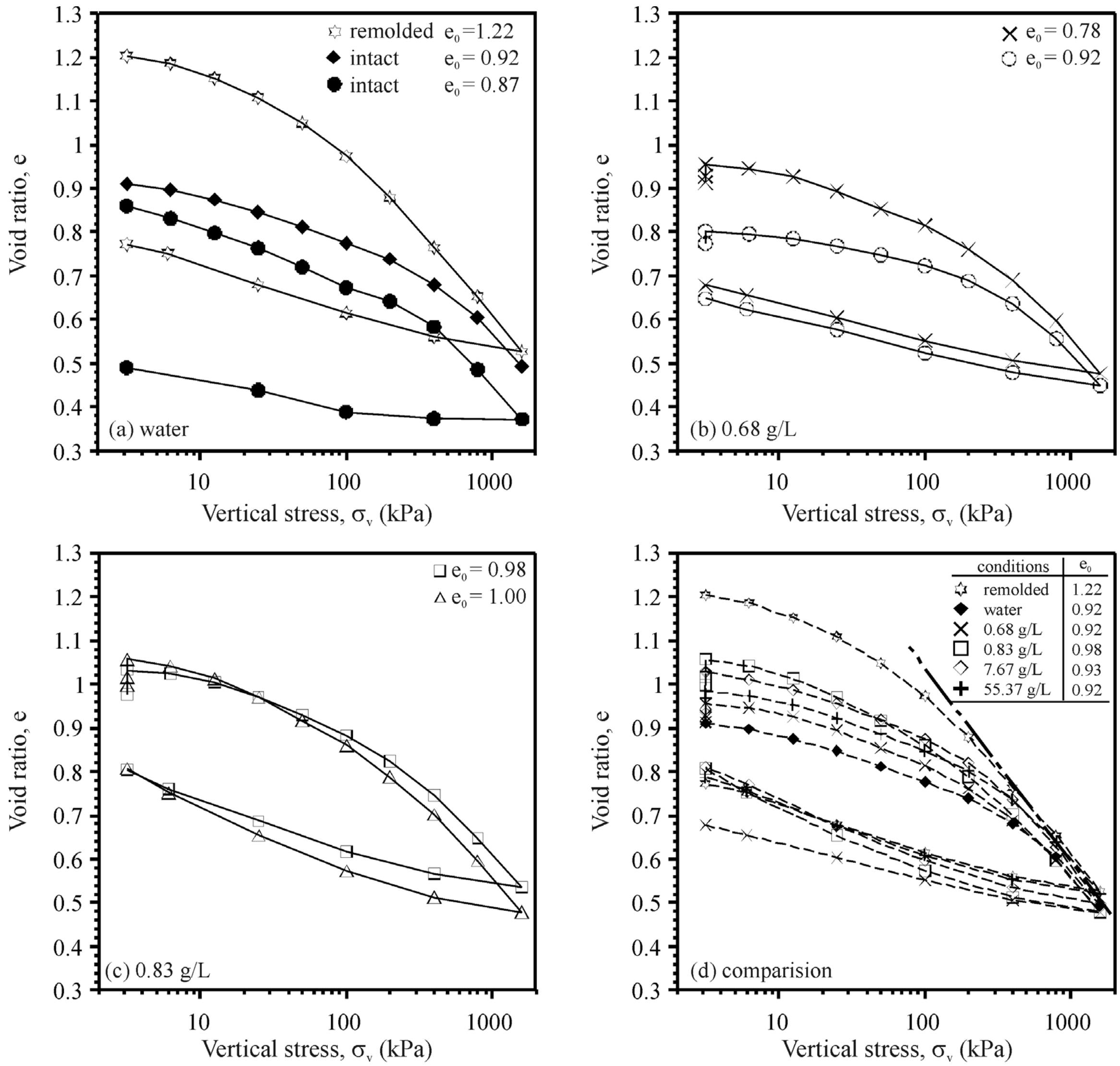

Figure 9 - Compressions curves of saprolitic soil (5 m depth).

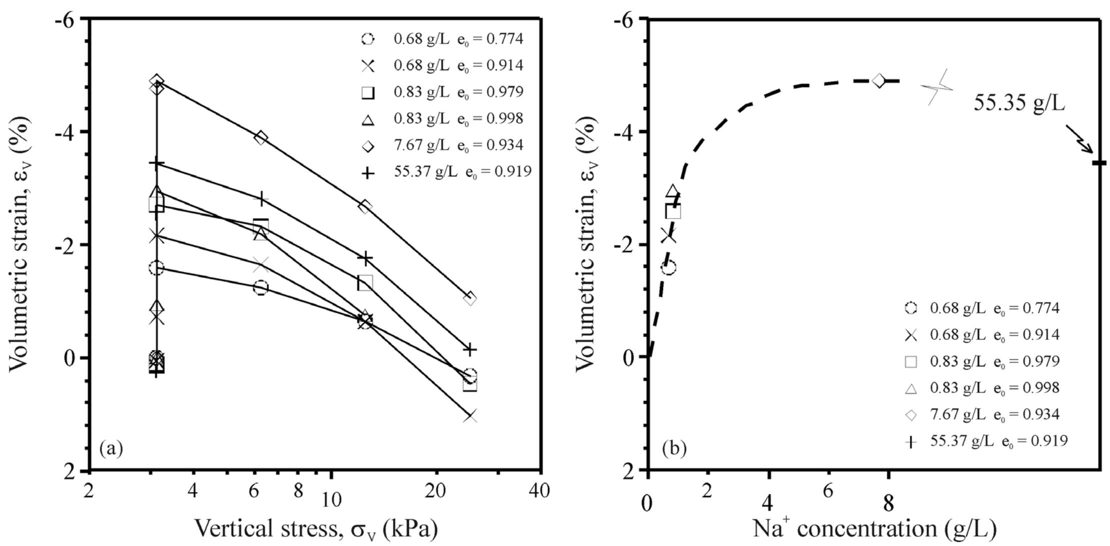

Figure 10 - Initial swelling of saprolitic soil.

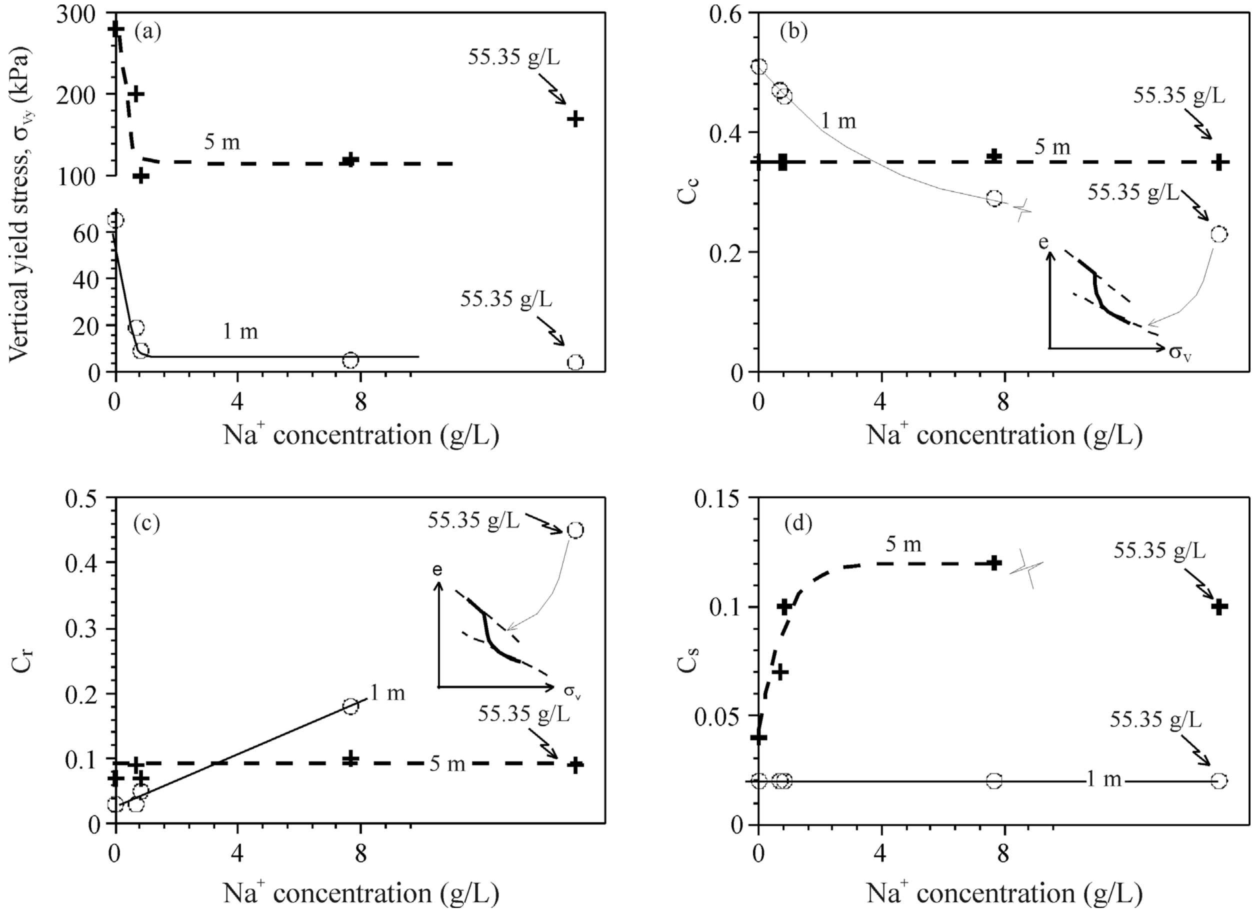

Figure 11 - Compressibility parameters.

The difference in behavior can be explained by the granulometric composition (the lateritic soil is more clayey and the saprolitic soil is more silty), degree of weathering, mineralogy and by the structure seen in SEM (lateritic soil with weakly cemented aggregations of clay and a saprolitic soil organized by the piling of kaolinite particles).

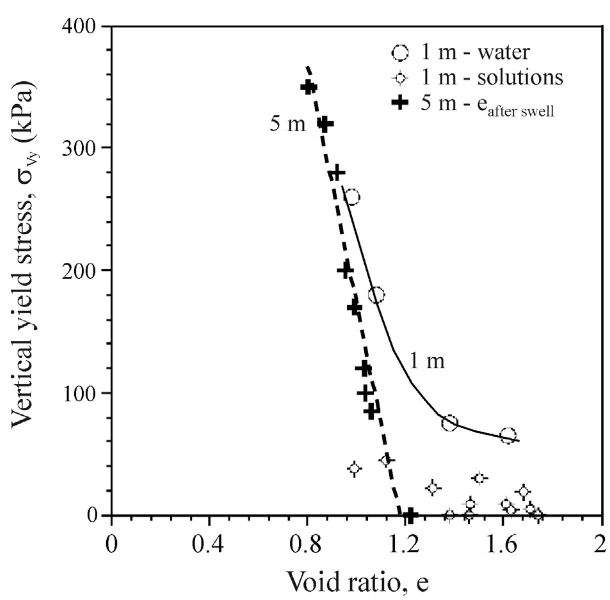

Figure 12 - Vertical yield stress and void ratio relationship.

Putting e: σ_{vy} into a graph (Fig. 12), some differences between the lateritic soil tested with distilled water and the soil tested with solutions with different concentrations can be verified, the data of which are shown in Table 6. It can also be observed that there is a relationship between e and σ_{vy} in the lateritic soil tested with distilled water; the same cannot be said for the other tests carried out using solutions.

The void ratio for the saprolitic soil used in Fig. 12 contains values after the initial swelling. There is a direct relationship between the void ratio and the vertical stress yield. Therefore, the saprolitic yield stress depends on the initial swelling.

Bolt (1956), Abdullah *et al.* (1997), Alawaji (1999), Chen *et al.* (2000), Brancucci *et al.* (2003) and Sivapullaiah & Manju (2006) tested compacted soils. It is difficult define a general aspect of physicochemical influence on natural soil such as presented in this paper, because it will depend on the soil, on the solution and on their interaction.

3.4 Triaxial tests

The results of the triaxial tests carried out on the lateritic soil sample and the low confining stress (σ'_c = 25 kPa) can be seen in Fig. 13. Based on the results presented in Figs. 13(a) and (b), the maximum deviator stress was verified not to be well defined in the drained tests, except for the test with intact soil, which presented a discrete peak obtained by an axial deformation (5%). The peak formation demonstrates the influence of cementing on the intact soil when tested with confining stress lower than the vertical yield stress obtained in the oedometer test, σ'_{vy} = 60 kPa. The remolded soil obtained a maximum deviator stress close to that of the intact soil, yet it required a greater level of axial deformation, *i.e.*, approximately 20% greater. The interaction of the soil with the solutions caused its dispersion, with a reduction in soil strength regarding the intact soil. This reduction was approximately 30% for the most diluted solution and of approximately 60% for the most concentrated solution. All the test specimens exhibited compressive behavior during the drained shearing. Futai (2002) explained this soil does not dilate because the porous structure is maintained by lateritic processes. Taking an axial deformation level of around 20%, volumetric deformations of around 1.5%, 11.5% and 7% were obtained for sodium concentrations equal to zero (intact soil), 0.68 g/L and 7.67 g/L, respectively. The volumetric strains at the consolidated stage were 0.5%, 1.1% and 10.5% were obtained for sodium concentrations equal to zero (intact soil), 0.68 g/L and 7.67 g/L, respectively, these results explain why the 0.68 g/L presented lower volumetric strain than 7.67 g/L at the compression stage.

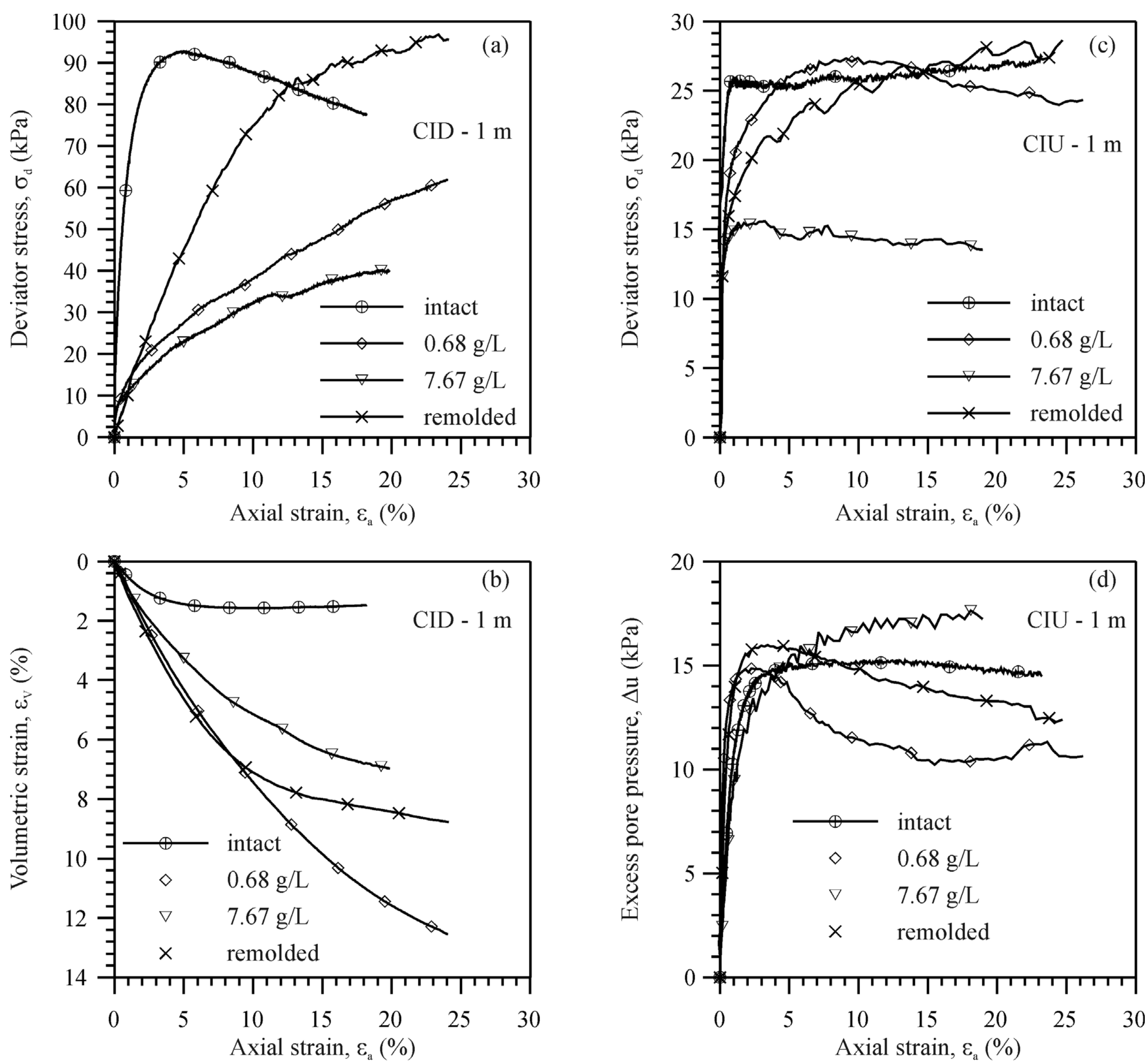

Figure 13 - Results of triaxial tests σ'_c = 25 kPa.

The stress strain behavior of the soil under undrained-testing conditions can be seen in Figs. 13(c) and 13(d). For the 7.67 g/L sodium concentration solution, there was a reduction of peak strength of approximately 45% regarding the intact soil. Positive excess pore-water pressures were generated during the undrained test. When the most diluted solution was employed, excess pore-water pressures generated increased up to 2% of the axial deformation, after which it decreased. This behavior was different from that obtained in the test with the most concentrated solution in which the excess pore pressure always increased.

The 1 m depth was also tested with a higher confining stress (σ'_c = 400 kPa), the results of which are presented in Fig. 14. Analyzing the curves presented in Figs. 9(a) and (b), the increase in the confining stress was found to reduce the differences in the stress-deformation behavior. There was a tendency towards the stabilization of the deviator stress associated with the stabilization of volumetric deformations, while approximately 20-25% of the axial deformations resulted in rupture.

The remolded soil had greater strength and stiffness than the intact soil. For all the confining stresses tested, the remolded soil terminated the hydrostatic consolidation and achieved failure with lower void ratios than the intact soil, resulting in greater strength at the shear stage. The most accentuated effect of the soil solution interactions occurred with the sodium concentration solution of 7.67 g/L, with a reduction of peak strength of around 30% being found in relation to the intact soil. All the samples became elongated during shearing, while the remolded soil on which solutions had been used became deformed to a lesser extent than in the intact condition.

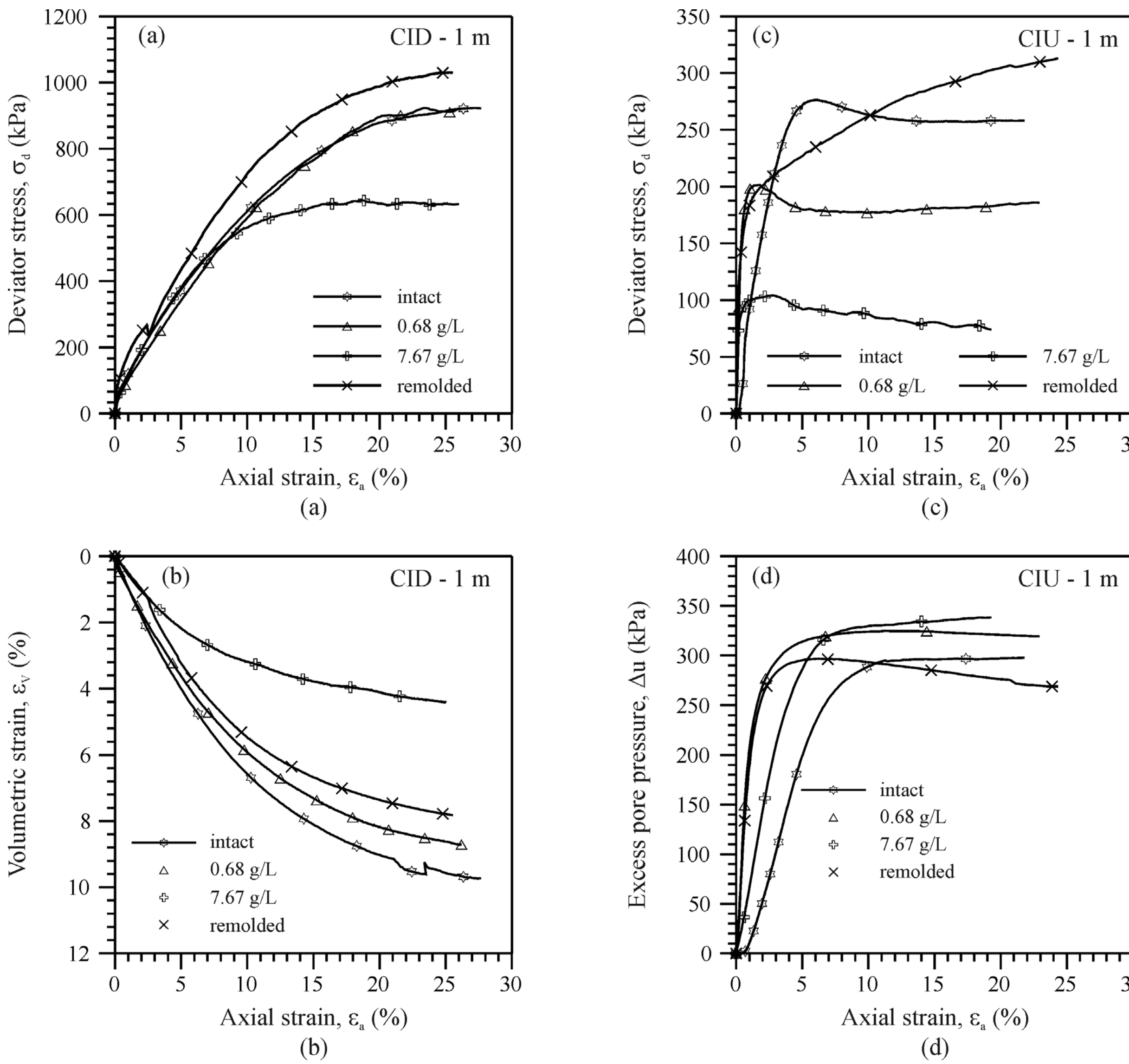

Figure 14 - Results of triaxial tests with σ'_c = 400 kPa.

Figures 14(c) and 14(d) indicate that, in the undrained tests, the intact soil and the soil with solutions had increasing deviator stress until their failure, followed by a decrease in resistance with the formation of a post-peak level, associated with the stabilization of the excess pore-water pressure. The peaks are not associated with the fall in the excess pore pressure generated. The remolded soil always had a rising deviator stress, while the maximum deviator stress adopted was 25% for axial deformation. The interaction with the solutions caused a reduction in resistance of around 30% to 60% for the sodium concentrations equal to 0.68 g/L and 7.67 g/L, respectively. All the test specimens developed excess positive pore pressure during shearing. In the intact conditions and with solutions, the standard stress-deformation behavior differed, although the responses in terms of excess pore pressure were similar. The remolded soil presented increasing excess pore pressure up to approximately 5% of axial deformation, which afterwards declined until the significant deformation condition was reached.

The physicochemical interaction changed the shear strength of the soil, as shown by Moore (1991), Anandarajah & Zao (2000) and Brancucci *et al.* (2003). The result could be increased or decreased of shear strength depending on the soil being flocculate, deflocculate, attacking the minerals or cement. However, the results presented herein only show the results of the tested soil with the used solution.

The effective stress paths and those around the undrained test peaks can be seen in Fig. 15(a), with the details for low confining stress also being presented in Fig. 15(b). The stress paths for the intact soil (Fig. 15) tend towards the left, and generally have an accentuated development of excess pore pressure. When the soil is tested with solutions (Fig. 15), the paths tend to curve towards the left, even though they are more constrained than the intact soil paths. The stress paths of the remolded soil (Fig. 15) are 'S'-shaped. Initially, they follow an approximately 45° direction, before bending to the left until they reach the envelope, which corresponds to the section in which the excess pore pressure is declining.

The peak envelope of the intact soil is a curve for lower confining stress than the oedometer vertical yield stress, σ'_{vy} = 60 kPa (Futai, 2002), even though a linear adjustment was used in order to obtain the strength parameters. The peak resistance parameters for the intact and remolded soil and the soil on which solutions were used are given in Fig. 15(a). When the soil is remolded or tested with solutions, the cementing is broken and the intergranular mechanical contacts are diminished; consequently, the cohesion intercept vanishes and the friction angle tends toward lower values. For sodium concentrations equal to zero (intact soil), 0.68 g/L and 7.67 g/L, the friction angle presents declining values, as shown in Fig. 16. Despite the large difference around the peak, all the trajectories follow the same direction for the critical states. The same occurs for the drained tests that reach the same line of critical states without a peak of strength and with large axial deformations.

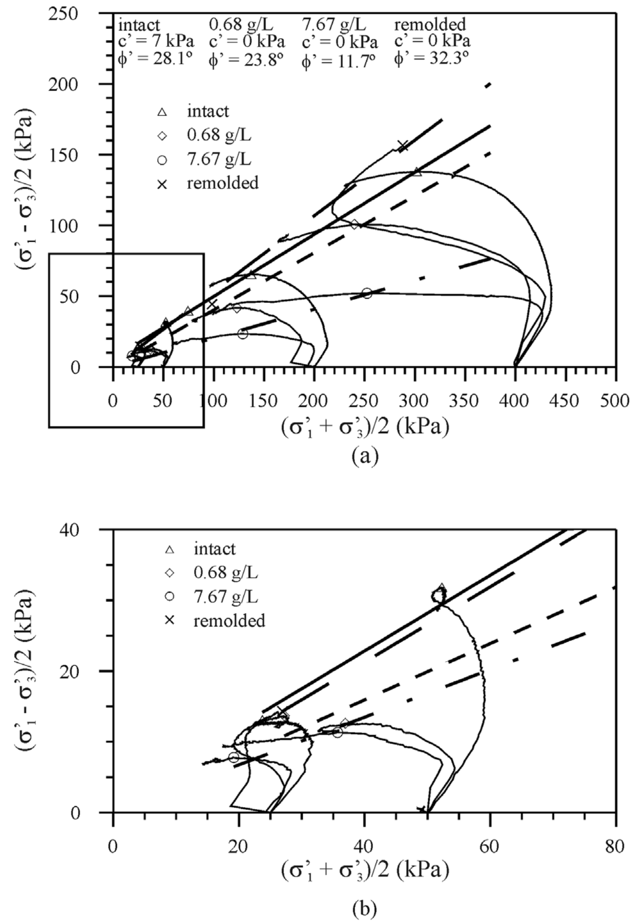

Figure 15 - Effective stress paths and peak envelopes, CIU tests, 1 m soil depth.

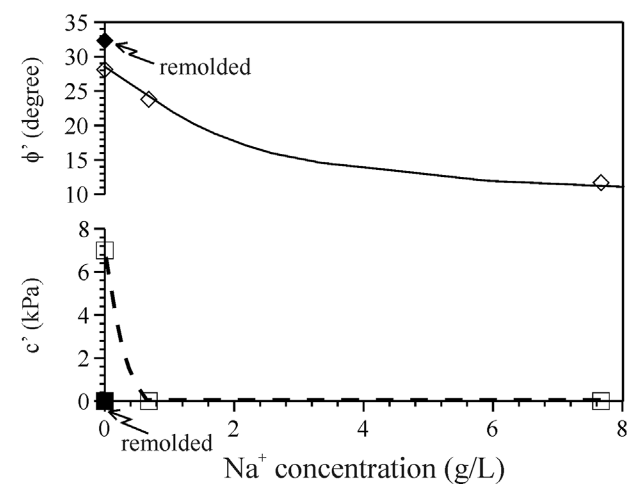

Figure 16 - Influence of the sodium concentration on strength parameters.

4. Conclusions

1) The dispersion of soils was the result of chemical reactions associated with salts $(NaPO_3)_n$ and (Na_2CO_3), and the pH value adopted (pH = 10.5), with an increase in the negative charge of clay mineral particles and the consequent increase in the repulsive particles associated with the electrical double layer. Since the pH value was kept constant, the influence of the concentration of sodium void ratio, mineralogy and degree of weathering on the mechanical behavior of the soil was analyzed.
2) The effect of the physicochemical interactions observed in the Atterberg limits, grain size analysis, oedometer and triaxial tests was more accentuated for the 1 m depth due to the higher level of clay it contained than for the 5 m depth (around tenfold). The physicochemical interaction changed the fabric and microstructure of lateritic soil. The aggregation was destroyed and the plasticity index reduced as the concentration of the solution increased.
3) Specimens formed intact at 1 m-depth (lateritic soil) and 5 m (saprolitic soil), despite the same weathering environment, presented different behavior in the oedometer compression tests due to their (chemical and mineralogical) composition and microstructure peculiarities, associated with the degree of alteration of each soil. The behavior of the 1-meter intact soil reflects the existence of the cementing of iron and aluminum sesquioxides, while the behavior of saprolitic soil reflects the influence of the arrangement of the constituent minerals. The cementing (lateritic soil) and the mineral arrangements (saprolitic soil) were gradually broken, while for the highest vertical stress, the behavior of the intact soil was closer to the behavior of the remolded soil.
4) The physico-chemical interaction between the solution and the lateritic soil increased the compressibility of the soil. There was a reduction in the vertical yield stress and the compression index with the increase in the concentration of Na, maintaining pH = 10.5. The recompression index for the lateritic soil obtained in the initial part of the load increased with concentration.
5) The intact saprolitic soil did not swell when being inundated with water (oedometric tests) although it expanded significantly when inundated with solutions containing sodium. These expansions were probably caused by structural changes and the rupture of connections that inhibit the expansion of the intact state when inundated with water. Electronic microscope sweep tests using soil treated with the solution allowed the visualization of these structural changes. The mechanical behavior of the saprolitic soil was verified to be associated with the initial expansion (unlike the lateritic soil). There is a direct relationship between the void ratio after swelling and the vertical yield stress. The interaction was found not to significantly influence C_c or C_r, even though C_s rose according to the increase in the concentration of Na, maintaining the pH constant and equal to 10.5. The compression curves for the saprolitic soil tend to converge in the 'normally condensed' band, which does not occur with the lateritic soils.

The study confirmed that the mechanical and physicochemical interaction when the pH is kept constant and elevated also depends on the concentration. This can be important in monitoring the dispersion of solutions such as NaOH. It was shown that not only pH is important but also the concentration of specific chemical elements.

Acknowledgments

The study was financially support by CNPq (Brazilian National Council of Scientific and Technological Development - Ministry of Science and Technology).

References

Abdullah, W.S.; Al-Zou'bi, M.S. & Alshibli, K.A. (1997). On the physicochemical aspects of compacted clay compressibility. Canadian Geotechnical Journal, 34:551-559.

Alawaji, H.A. (1999). Swell and compressibility characteristics of sand-bentonite mixtures inundated with liquids. Applied Clay Science, 15:411-430.

Anandarajah, A. (2003). Mechanism controlling permeability change in clays due to changes in pore fluid. Journal of Geotechnical and Geoenvironmental Engineering, 129(2):163-172.

Anandarajah, A. & Zhao, D. (2000). Triaxial behavior of kaolinite in different pore fluids. Journal of Geotechnical and Geoenvironmental Engineering, 126(2):148-156.

Bolt, G.H. (1956). Physical-chemical analysis of the compressibility of pure clay. Géotechnique, 6(2):86-93.

Brancucci, A.; Covielho, R & Di Maio, C. (2003). Influence of fluid constant dieletric on clay soil behavior. Annual Geotechnical Symposium, Potenza, pp. 18-20.

Chapman, D.L. (1913). A contribution to the theory of electrocapillarity. Philosophical Magazine, 25(6):475-481.

Chen, J.; Anandarajah, A. & Inyang, H. (2000). Pore fluid properties and compressibility of kaolinite. Journal of Geotechnical and Geoenvironmental Engineering, 126(9):798-807.

Futai, M.M. (2002). Theoretical and Experimental Study of Unsaturated Tropical Soil Behavior: Applied a Gully Case. PhD Thesis, COPPE, Federal University of Rio de Janeiro, 559 p (in Portuguese).

Futai, M.M. & Almeida, M.S.S. (2005). An experimental investigation of the mechanical behaviour of an unsaturated gneiss residual soil. Geotechnique, 55(3):201-213.

Futai, M.M.; Almeida, M.S.S. & Lacerda, W.A. (2004). Yield, strength, and critical state behavior of a tropical saturated soil. Journal of Geotechnical and Geoenvironmental Engineering, 130(11):1169-1179.

Gouy, G. (1910). Sur la constitution de la charge electrique a la surface d'un electrolyte. Anniue Physique, 9(4):457-468.

Head, K.H. (1986). Manual of Soil Laboratory Testing. First Edition. Vol. 3. Ele International Limited, London, 416 p.

Martins, A.P.S. (2005). Influence of Physico-Chemical Interaction on Two Tropical Soil Behavior. Masters' Thesis, COPPE/UFRJ, Rio de Janeiro, 321 p. (in Portuguese).

Mitchell, J.K. (1976). Fundamentals of Soil Behaviour. John Wiley and Sons., Inc., New York, 592 p.

Moore, R. (1991). The chemical and mineralogical controls upon the residual strength of pure and natural clays. Géotechnique, 41(1):35-47.

Santos, P.S. (1975). Clay Technology Applied to Brazilian Clays. Ed. Edgard Blucher, São Paulo, v. 1, 340 p.

Sivapullaiah, P.V. & Manju, M. (2006). Effect of zeortization on the volume-change behavior of kaolinitic soils. Canadian Geotechnical Journal, 43:969-978.

Stern, O. (1924). Zur Theorie der Elektrolytischen Doppelschriht. Zietschrift Electrochem, 30:508-516.

Vargas, M. (1953). Some engineering properties of residual clay soils occurring in Southern Brazil. Proc. 3rd Int. Conf. On Soil Mechanics and Foundation Engineering, Zurich, v. 1, pp. 67-71.

Vaughan, P.R. (1988). Characterising the mechanical properties of *in-situ* residual soil. Proc. II International Conference on Geomechanics in Tropical Soils, Singapore, v. 2, pp. 469-487.

Vaughan, P.R. (1992). Contribution to the study of residual and other structured soils. US/Brazil Geotechnical Workshop on Applicability of Classical Soil Mechanics Principle to Structured Soils, Belo Horizonte, pp. 338-345.

List of Symbols

c: cohesion

ϕ: friction angle

e: void ratio

G_s: specific gravity of soil grains

I_P: plasticity Index

S: degree of saturation

w: gravimetric water content

w_L: liquid limit

w_P: plastic limit

C_c: compression index

C_s: swelling index

C_r: recompression index

σ'_v: vertical effective stress

σ_c: confining pressure

σ_d: deviator stress (σ_1 - σ_3)

σ_{vy}: vertical yield stress

γ: unit weight

Critical Rainfall Parameters: Proposed Landslide Warning System for the Metropolitan Region of Recife, PE, Brazil

A.P.N. Bandeira, R.Q. Coutinho

Abstract. In the Metropolitan Region of Recife, Northeast Brazil, landslides caused a total of 214 deaths between 1984 and 2012. Efforts have been made, but there is still need to improve the risk area management by discovering the correlations between the rainfall and landslides and by implementing a disaster warning and prevention system in order to reduce the number of accidents and fatalities. The purpose of this study is to propose rainfall parameters likely to trigger mass movements, as a contribution to risk management in this region. It specifically addresses the study undertaken in three municipalities: Recife, Camaragibe and Jaboatão dos Guararapes, which have disorganized occupation in high and very high risk areas. In order to achieve the prime objective, rainfall and landslides were tracked during 2009 to obtain correlations between them. After the data was logged, the rainfall accumulation associated with landslides was checked. According to each area with civil defense action of the municipalities involved in the study, critical values of the cumulative rainfall in 72 h ($I_{72\,h}$), in the long term (P_{ac}) and the parameter R_{crit} resulting from the product of $I_{72\,h}$ by P_{ac}, are suggested herein to be recommended for operations of the Warning and Alert states. By achieving these critical values, they increase the probability of landslide events, and are important for taking decisions and instructions on Civil Defense actions.
Keywords: risk management, landslides, preventive plan, critical rainfall, civil defense.

1. Introduction

Natural disasters are increasingly frequent in large cities both at home and abroad. Recently, a number of catastrophes worldwide were due to landslides and flooding, these processes being associated with severe atmospheric instabilities. In recent decades research has evidenced that there has been a sharp increase not only in the frequency of natural disasters but also in intensity, due to the occurrence of extreme rainfall, causing serious damage and socioeconomic losses.

The world's worst landslide-related disaster ever was in the Soviet Union in 1949, when around 12,000 people died. In the last ten years, other serious disasters occurred, for example in China in August 2010, when more than 1,700 people lost their lives; in the Philippines in February 2006, with around 1,126 fatal victims (EM-DAT, 2013); and in third place, the landslides in the mountain region in the state of Rio de Janeiro, Brazil, in January 2011, when around 1000 people died.

The main factor for the disaster in the mountains in Rio de Janeiro State was the extreme rainfall events. Accumulated rainfall of 280.8 mm in 48 h, the highest recorded in the last 45 years in the region, caused several landslides and flooding. This event was classified as one of the ten worst disasters caused by landslides in the world in the last 10 years according to the UN, and the worst ever in the history of Brazil. This catastrophe exceeded the number of victims recorded in 1967 in the municipality of Caraguatatuba, São Paulo State, when 436 people lost their lives in landslides and around 3,000 were made homeless.

EM-DAT (2012) has calculated in Brazil, for the period 1900-2012, the occurrence of 202 major natural disasters, with 12,235 fatal victims and damage worth approximately 14.6 billion dollars. These disasters include flooding, landslides, drought, epidemics and so on. According to the database of the São Paulo Technological Research Institute (IPT-SP) for the period 1988-2012, a total of 3,288 people were victims of landslides in the country, 1,240 in 2010 and 2011 alone, including records from the mountainous region outside Rio de Janeiro.

Although the Recife Metropolitan Region in Northeast Brazil has not recorded a large number of fatalities from a single rainfall event, the region has a history of disasters over the years. A total of 214 deaths from landslides in this region were calculated between 1984 and 2012. In 2011, nine fatal victims were registered after rainfall of 120.3 mm in 24 h in July (within the region's wet season). In the region, that month had a total rainfall of 535 mm, corresponding to 39% above historic average for the month, which is 386 mm according to the National Meteorology Institute. A total of 2,749 mm of cumulative rainfall had fallen between January and July, exceeding the historic average of 2,243 mm. In those cases, good risk management by implementing a disaster prevention and alert system would reduce the consequences and number of fatalities.

Ana Patrícia Nunes Bandeira, DSc, Associate Professor, Federal University of Cariri, Ceará, CE, Brazil. e-mail: anabandeira@cariri.ufc.br.
Roberto Quental Coutinho, DSc, Associate Professor, Federal University of Pernambuco, Recife, PE, Brazil. e-mail: rqc@ufpe.br.
Submitted on November 5, 2013; Final Acceptance on December 19, 2014; Discussion open until December 31, 2015.

The aforementioned data show that the management activities in risk areas in Brazil need to be upgraded (structural and non-structural actions). Many people are living in a risk situation on hillsides and it is impossible to eliminate this risk in the short term. In this case, it is also necessary to take non-structural preventive actions by means of a good alert system and to restrict further occupation. An effective risk area management program is the main tool that the municipal administration should have at hand. The concept of a preventive plan is to take steps prior to the outbreak of accidents, based on preventing conditions potentially susceptible to their occurrence. In the case, for example, of an alert system accompanied by some parameters, such as: rainfall, weather forecast and knowledge of the critical rainfall accumulation, together with onsite follow-up, it would increase identifying possible landslide events. Fell *et al.* (2008) provide a guide to prepare risk maps, and comment that landslide frequency can be related to rainfall, in which the correlations indicate areas of possible landslide processes.

An early warning system is defined by UNISDR (2009) as "the set of capacities needed to generate and disseminate timely and meaningful warning information to enable individuals, communities and organizations threatened by a hazard to prepare and to act appropriately and in sufficient time to reduce the possibility of harm or loss". A people-centered early warning system necessarily comprises four key elements: (i) knowledge of the risks; (ii) monitoring, analysis and forecasting of the hazards; (iii) communication or dissemination of alerts and warnings; (iv) local capabilities to respond to the warnings received. (UNISDR, 2009).

Intrieri *et al.* (2013) define and present a practical guideline in the design of a landslide Early Warning System. The authors describe the EWS as the balanced combination of four main activities: design (geological knowledge, risk scenarios, design criteria, and choice of geo-indicators), monitoring (instruments, installation, data collection, data transmission and data elaboration), forecasting (data interpretation, comparison with thresholds, foresting methods, and warning) and education (risk perception, safe behaviors, response to warning and population involvement). A toolbox is presented that can help end-users (such as civil protection agencies and administrations) to create an Early Warning System for every landslide requirement.

Calvello (2014) presents "components" of a regional rainfall-induced landslide Early Warning System: a correlation model between rainfall events and landslide events; warning levels and alert phases; decision-making to activate the alerts; monitoring and warning strategy; emergency plan and communication strategy; all steps are connected to the risk perception. An efficient model (regional warning) and an efficient system are necessary, with three players: people, scientist and managers. Table 1 shows world examples of an alert system with some information, including rainfall thresholds.

The knowledge that cumulative rainfall could cause large numbers of slope instability processes associated with the weather forecast is key information for civil defense actions, such as, for example, triggering the state of alert. Although alerts would not prevent the occurrence of the processes, they may reduce the number of fatal victims caused by disasters, since the population living in risk areas can be informed beforehand about the need or not to leave their homes before landslides occur.

In this sense the purpose of this study is to submit a proposal of technical parameters of cumulative rainfall, which indicate the probability of landslides occurring in the areas of the Metropolitan Region of Recife, thereby providing support for the civil defense teams to raise Warning and Alert states. The subject of this article is part of the research line "Analysis and Risk Management for Erosion and Landslides", included in the CNPq PRONEX Project, which was developed by GEGEP (Geotechnical Engineering Group on Hillsides, Plains and Disasters) of the Civil Engineering Department of the Federal University of Pernambuco (UFPE), coordinated by Prof. Roberto Quental Coutinho. Bandeira (2010) did his PhD research on this project and some of his results are presented herein below.

2. Risk Area Management

Risk area management is a decision-making process involving the definition of requirements, recognizing acceptable options and choosing appropriate strategies to reduce risks. In the 1990s, the Office of the United Nations Disaster Relief Coordinator (UNDRO) contributed significantly to the risk area management process at an international level and suggested four stages of management: a) Risk identification and analysis; b) Structural preventive measures; c) Non-structural measures; d) Public information and capacity building for self-defense. Several countries have adopted these stages, namely: Hong Kong (China), Australia, USA and Brazil (Coutinho & Bandeira, 2012a). Internationally, a framework has also been set up consisting of three steps presented by Fell & Hartford (1997) and Fell *et al.* (2005), which are: i) Risk Analysis; ii) Risk Assessment; iii) Risk Management.

In Brazil, a risk area management system takes into account international suggestions, involving joint actions at three government levels (federal, state and municipal); it also receives support from higher education and research institutions. As an example of work done by those institutions, it is worth mentioning Coutinho (2013), who presents a technical report from a national technical commission study of processes involving mass movements, guidelines for intervention, urban planning and parameters for geotechnical mapping for the areas susceptible to these natural disasters.

Table 1 - Examples of alert systems - rainfall thresholds to trigger landslides (Calvello, 2014).

Where	Managers	Period of activity	Alert levels	Landslide types	Slopes	Area	Rainfall thresholds	Other variables
Hong Kong (China)	CEDD-GEO	Since 1977	2	4	Manmade	1100 km^2	24 h	
Rio de Janeiro (Brazil)	GEO-Rio	Since 1996	4	13	Natural and manmade	1260 km^2	1 h 24 h 96 h	
Seattle (USA)	USGS	Since 2003	4	Shallow slides & debris flows	Natural	370 km^2	I [mm/h] = aD^b 3 day-15 day	Water content index
Campania (Italy)	Regional Civil Protection	Since 2005	4	Shallow slides & debris flows	Natural	13595 km2	1 day 2 day 3 day	

For accident prevention municipal governments take structural actions (slope retention work) and non-structural actions (follow-up system, community talks and creating volunteer civil defense centers), the latter being directly adopted in the communities, called Proximity Management in Recife. This grassroots educational and interactive work is essential, since potential landslides are directly influenced by unsuitable anthropic actions, such as: badly executed cuts and fills, precarious drainage systems, wastewater discharge and removal of the slope surface protection (Coutinho & Bandeira, 2012a). The population's wastewater discharge and inflow throughout the year increase the moisture in the ground, weakening it, even on dry days, thereby increasing the probability of landslides during short showers (Coutinho & Severo, 2009). The population is often given instructions on this kind of problem but stricter structural actions are necessary to reduce these problems.

At a state level, specific programs have managed the work of the municipal governments, seeking the best way to counter the practices of emergency and specific actions, offering an interdisciplinary and differentiated methodology, and giving communities better living and housing conditions.

At a federal level, the government has created risk area management programs, providing financial conditions to prepare risk maps and downsizing plans, as well as offering capacity-building courses on risk area management and preparing engineering designs (based on Coutinho & Bandeira, 2012b). An important improvement in the disaster legislation in Brazil was the Federal Law - 12,608 of April 10, 2012.

Although the actions are being taken at the three government levels, every year rainfall causes dozens of landslides, some fatal, evidencing the need to have more in-depth knowledge of the correlations between rainfall and slope instability processes, as well as to improve forecasts of rainfall indices in the risk areas.

In relation to civil defense actions in the Recife Metropolitan Region (MR) and the other Brazilian cities, the main cities adopt three levels of operation, as follows: Observation, Warning and Alert. The Recife-MR civil defense teams take actions based on the follow-up of weather forecasts and site inspections. Hence, this study proposes values of rainfall parameters for civil defense actions, contributing to the local government alert system.

By analyzing the frequencies of mass movements and flooding in a number of areas in Brazil, some researchers have presented critical rainfall accumulations based on which they increase the number of occurrences of these processes.

Tavares *et al.* (2004), on analyzing the variability of time and space of the rainfall associated with the movements along the coastline of the State of São Paulo, concluded that there is a predominance of mass movements when there is 72-h cumulative rainfall of over 120 mm. These authors state that landslides with rainfall accumulation below this figure may be correlated to anthropic actions or heavy rain in a 24-h period.

Gonçalves (2003) found that 60 mm or more of heavy rain falls in 24 h in Salvador, Bahia State, with major spatial repercussion; with this intensity, flooding in the municipality as well as more serious slope failures occur from an intensity of 70 mm/24 h.

Macedo *et al.* (2004), studying the correlations between the landslides and 72-h cumulative rainfall for some regions in the State of São Paulo, confirmed that when the accumulated rainfall reaches 80 mm in 72 h, it is likely that mass movements would occur in the following places: Campos do Jordão, Campinas, ABC and Sorocaba. Now, in places in the Baixada Santista and Paraíba Valley the authors found rainfall accumulation of 100 mm in 72 h; and 120 mm for the northern coast of São Paulo.

Gusmão Filho *et al.* (1987), when examining the frequencies of mass movements on the hills of Olinda, Northeast Brazil, found that the instability of the slopes in this location, as a result of the rise in water level in the area, is the result of the joint action between the intensity of accumulated rainfall (P_{ac}), from January to the date under consideration, with occurrence of a daily rainfall of minimum intensity (I). So the authors defined a parameter $R_{crít}$, to the value of 60,000 mm^2, as the product of 24-hr rainfall (I) by the rainfall accumulation (P_{ac}) to the date of the event ($R_{crít} = P_{ac}$ x I), and countless situations could trigger landslides (Gusmão Filho, 2001). For example, when the accumulated rain is 800 mm, probably the ground is heavily saturated and a daily 75 mm rainfall would loosen the mass. This study shows how important the weather forecast is to identify the probable value of I and, consequently, the value of $R_{crít}$, which would help decide on accident prevention measures.

This kind of study is a valuable contribution to improving risk area management. The technical parameters suggested for the Warning and Alert states, associated with good weather forecasts and site inspections to identify the features of instability, can provide effective preventive measures and risk mitigation, also reducing loss of human lives, by adopting an alert system. The purpose of this system is to expedite the departure of people living in risk areas and prevent them from becoming victims of landslides, but this system is only effective if the technical parameters of critical cumulative rainfall are known. In addition to those parameters, it is necessary to have a good monitoring system of the climate and weather conditions, by means of, for example, weather radars, which can warn about the arrival of heavy rain. Radar can warn hours beforehand about the occurrence of heavy rain, and over a range of hundreds of miles. It is also essential to have an automatic permanent rain gauge network installed in risk areas (high and very high risk) with ongoing analysis of the results. In short, to ensure fewer fatalities caused by landslides it is necessary that the civil defense system draw up its preventive plan based on identifying the risk areas and on the critical rainfall parameters, It should also implement technologies and support of partner agencies in their taking preventive and emergency measures of risk management. The people in the communities need to be involved, trained and to feel co-responsible.

Some examples of alert systems could be the issue of property alerts and sirens, sending SMS messages or similar devices. In the city of Rio de Janeiro, for example, the Rio Alert System issues warnings based on weather reports, namely, the intensity of expected rainfall. When heavy rain is forecast, which may cause isolated landslides, property alerts to the population are issued (via the press and Alert Rio website: www.sistemaalerta-rio.com.br). The city of Rio de Janeiro also has *Community Heavy Rainfall Warning*, where the local inhabitants receive SMS alert warnings of rainfall. These warnings occur when heavy rain is forecast for the next few hours that may cause isolated landslides. The sirens installed in the most critical areas also issue warnings, and are sounded when very heavy rain is expected in the next few hours and might cause generalized landslides, in which case it would be a maximum alert situation.

3. Study Area Characteristics

The study area in this article covers the municipalities of Recife, Camaragibe and Jaboatão dos Guararapes, in the State of Pernambuco, Northeast Brazil. Together they occupy an area of around 530 km^2, and are between projections 265000 to 300000 East and 9085000 to 9125000 North, of the geographic coordinate system WGS-1984 zone 25S, according to the Universal Transverse Mercator (UTM) projection (Fig. 1).

In terms of climate, the study areas within the climate range type As', as wet tropical climate according to the W. Köppen classification, with a dry summer and a wet season, which begins in the fall. Figure 2 shows a historic series of the average rainfall logged in the city of Recife between 1910 and 1985, considered as a benchmark for the entire Metropolitan Region. Figure 2 shows that between March and August there is a concentrated wet season, with monthly averages of over 150 mm. This period is considered critical for the civil defense units in the Recife Metropolitan Region, where several landslides have been recorded. The monthly maximum rainfall is logged in May, June and July, with monthly averages of more than 300 mm rainfall. On average, the September-February period has a low monthly rainfall (less than 150 mm).

Specifically in the municipality of Recife, the annual average total rainfall is 2,243 mm. In recent years the maximum monthly rainfall recorded in June 2005 in the municipalities of the Metropolitan Region was 681.3 mm in Recife; 728.8 mm in Camaragibe, and 609.9 mm in Jaboatão

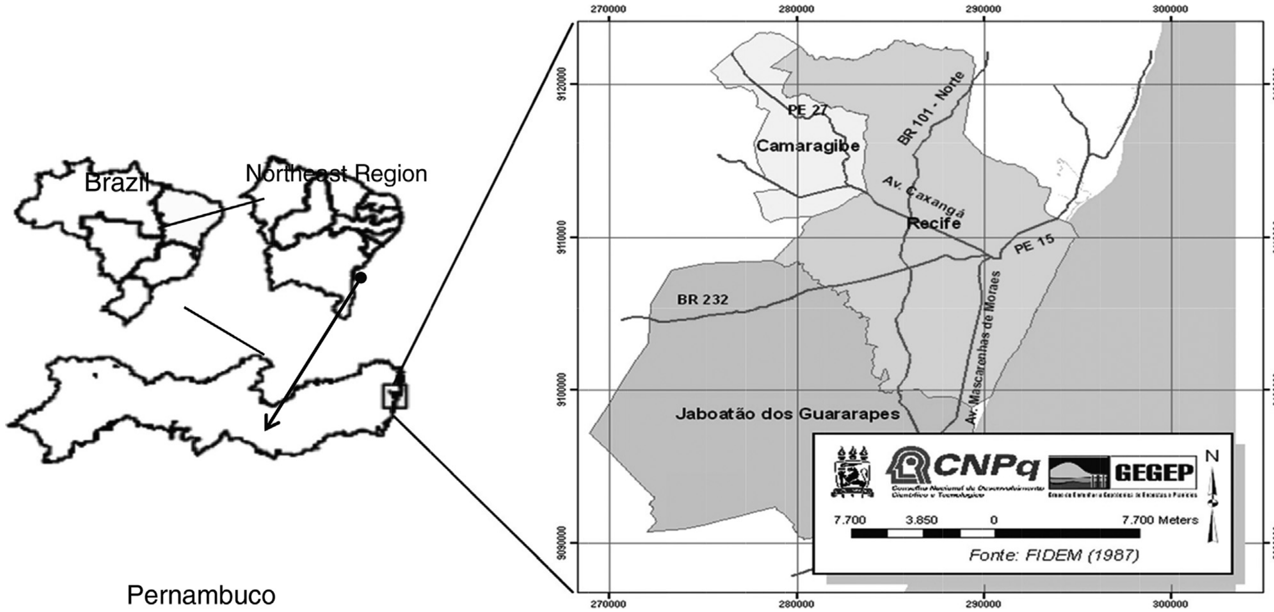

Figure 1 - Location of the Study Area - Cities of Camaragibe, Jaboatão and Recife - FIDEM (1987).

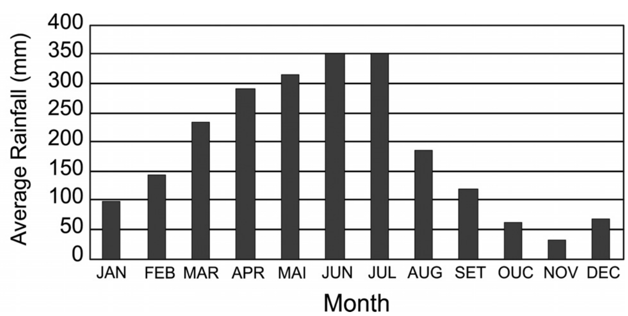

Figure 2 - Average Monthly Rainfall Readings in Recife (1910-1985) (Extract from Girão, 2007).

dos Guararapes. In 2011, the rainfall volumes logged for some months in Recife were also high, for example in April (635.7 mm), May (685.1 mm) and July (550.6 mm). The annual total rainfall recorded in the municipality of Recife in 2011 was 3,097.9 mm, higher than the annual average according to the Pernambuco State Water and Climate Agency.

The local climate is closely related to the soil formation of the soils and the latter with slope failure. The high humidity rates and temperature of Recife-MR affect the chemical weathering processes of the soils, breaking down weaker minerals, such as feldspars and micas. These minerals are quite common in the granitic rocks of the crystalline substratum and in the sedimentary overburden of the Barreiras Formation, present in large areas of Recife-MR (Alheiros *et al.*, 2003). According to Bandeira (2003), the action of chemical weathering in the region strongly impacts processes of mass movements, since the feldspar particles, initially in size of sand particles in the Barreiras Formation sediments, contribute to increasing the clay content, leading to slope failure.

The Barreiras Formation is commonly found in the hillside areas of Recife-MR. This deposit associated with Cenozoic events of a climate and/or tectonic nature, towards the end of the Tertiary period (Pliocene) widely covered the exposed surfaces of the substratum, filling a fairly disturbed relief. In general, this formation consists of clay-sand sediments, cream to reddish in color, depending on the intensity of the oxidation of the iron, and occurs through a vast sedimentary overburden (Alheiros *et al.*, 1988). This geological unit extends along the Brazilian coast from Rio de Janeiro (Southeast) to the State of Amapá (North), covering Mesozoic sedimentary deposits in several coastal basins (Bezerra *et al.*, 2006). In the study area herein, the Barreiras Formation sediments are located in two areas (Fig. 3): the first is farther North, covering the table l and to the North of Camaragibe and Recife; and the second, farther South, consists of table l and remnants and hills between the northern and southern municipal boundaries of Jaboatão dos Guararapes and Recife, respectively. The locations of the Barreiras Formation sediments coincide with the hillside areas, where landslides are frequent.

In some hillside areas of the municipality of Camaragibe and Jaboatão dos Guararapes residual soil of the crystalline substratum occurs, more widespread on the hillsides of the municipality of Jaboatão dos Guararapes (Bandeira, 2010). Here the residual soil of the gneiss-migmatite complex is predominant, with a clayey-sand texture, and consequently susceptible to a larger number of landslides in this type of soil.

The relief of the study area herein is characterized by a sharp division between the plain and the hills. On the

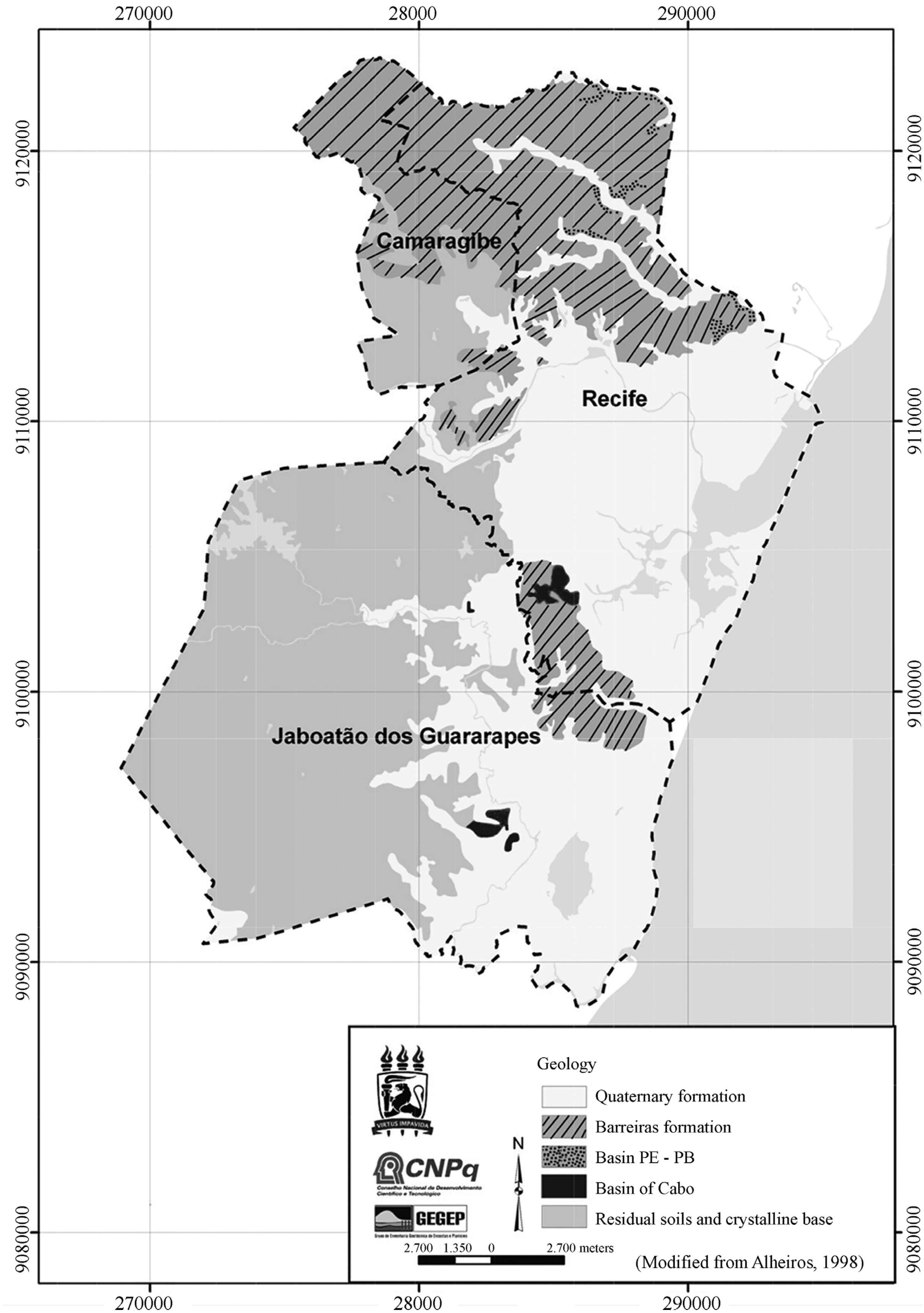

Figure 3 - Principal Geological Units in the Study Area (Bandeira *et al.*, 2009).

plain several places are below sea level, and flooding often occurs. In the hilly areas altitudes of up to 200 m above sea level can be encountered. Hilltop occupation is normally planned, but a low-income population in precarious conditions occupies the hillsides. Between 1996 and 2002 there was a sharp increase of 251,600 inhabitants in the hillside areas, to cause higher demographic density, covering a wider area in the municipalities. In 2004 the CONDEPE/FIDEM State Agency found that there were 345,714 homes built on hillsides and in areas prone to flooding in Recife-MR, representing 38% of all households existing in the region (FIDEM, 2006).

4. Methodological Aspects

Seven main work stages described below were set up to identify and develop a proposal for cumulative rainfall parameters, likely to cause landslides in the study area of this paper.

a) Expansion of the rain gauge network: the municipalities considered the rainfall to be similar in the areas; this is the reason for few rain gauges throughout the study area (530 km^2) - only five instruments. Under the GEGEP - CNPq/PRONEX and CNPq-Universal Project, another 17 instruments were installed, 11 of which were manual gauges (Ville de Paris) and six rainfall data loggers, in order to give a good correlation between the rainfall and landslides (see Figs. 4 and 5). The data loggers provide information about the intensity and duration of the rain, helping to understand the landslide events caused by rainfall concentrated in less than 24 h.

b) Defining the rain gauge collection points: the location of the risk zones (high or very high risk), the geological characteristics of interest and the areas of civil defense action determined the sites where the new rain gauges were to be installed. These risk zones, were obtained from pre-existing maps subsidized by federal government funds (Fig. 5). Figure 5 - Location of rain gauges in the 'High' and 'Very High Risk' areas, and the local rainfall indices during 24 h registered on April 13th, 2009 (Coutinho *et al.*, 2010).

c) With regard to geological aspects, the rain gauges were installed on sites where the soil had sedimentary characteristics of the Barreiras Formation and residual characteristics from the crystalline substratum, and where historically a larger number of landslides had occurred in the study area. In their working areas the civil defense teams operate on a decentralized basis (Coutinho & Bandeira, 2012b). In the municipality of Recife, for example, the territory is divided into Regionals: North, Northeast, West, Northwest and South. In Camaragibe the division is by Area: Area I, II, III, IV-Tabatinga and IV-Vera Cruz. In the municipality of Jaboatão dos Guararapes the Regionals are: Cavaleiro, Jaboatão Centro, Curado, Muribeca, Prazeres and Praias. So, for each working area of the civil defense teams, rain gauges were installed to accompany the rainfall and record the landslides.

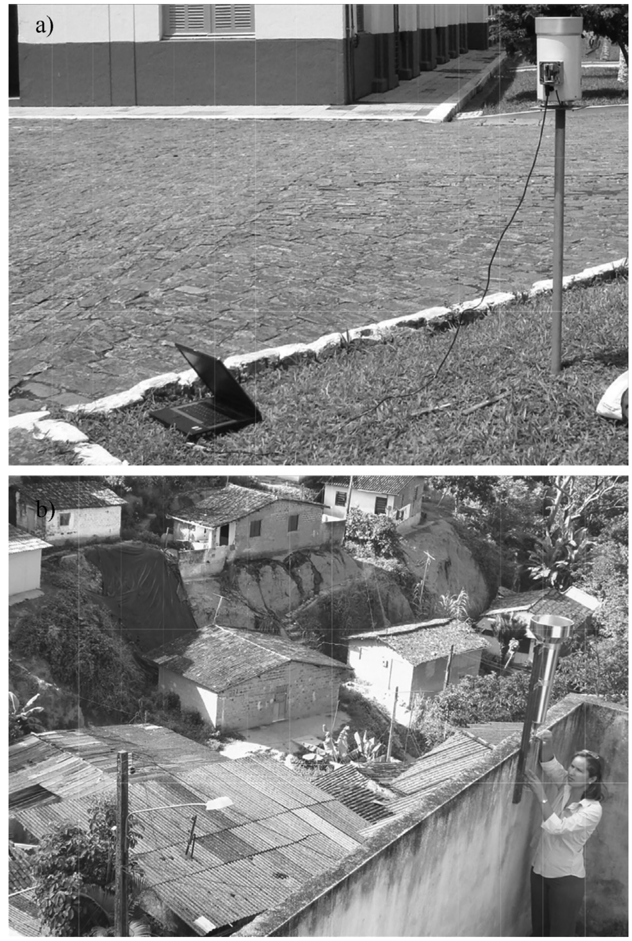

Figure 4 - Examples of rain gauges installed in the study area (Coutinho *et al.*, 2010). a) Recording style rain gauge ('Data Logger') in Jaboatão dos Guararapes. b) Manual rain gauge ('Ville de Paris') in Camaragibe.

d) Logging rainfall and landslides: throughout 2009 rainfall in the study was monitored on a daily basis using the rain gauges. Landslide data were obtained first in the civil defense units of the municipalities and from news coverage. These data were logged on electronic spreadsheet. Landslide information was logged as follows: place and date of occurrence; type of movement and geological-geotechnical characteristics.

e) Identification of accumulated rainfall associated with landslides: For information about landslide-related cumulative rainfall, the rainfall accumulation was recorded in 72 h or less before the date of the landslide and in the long term (from early in the year), collected from the data logged by the rain gauge closest to the event. From these data, histograms were drawn, showing the number of landslides as a result of certain intervals of cumulative rainfall for each working area of the civil defense teams.

f) Proposed rainfall parameters for civil defense actions: at this stage rainfall accumulations were proposed for the Warning and Alert states. The critical rainfall accumu-

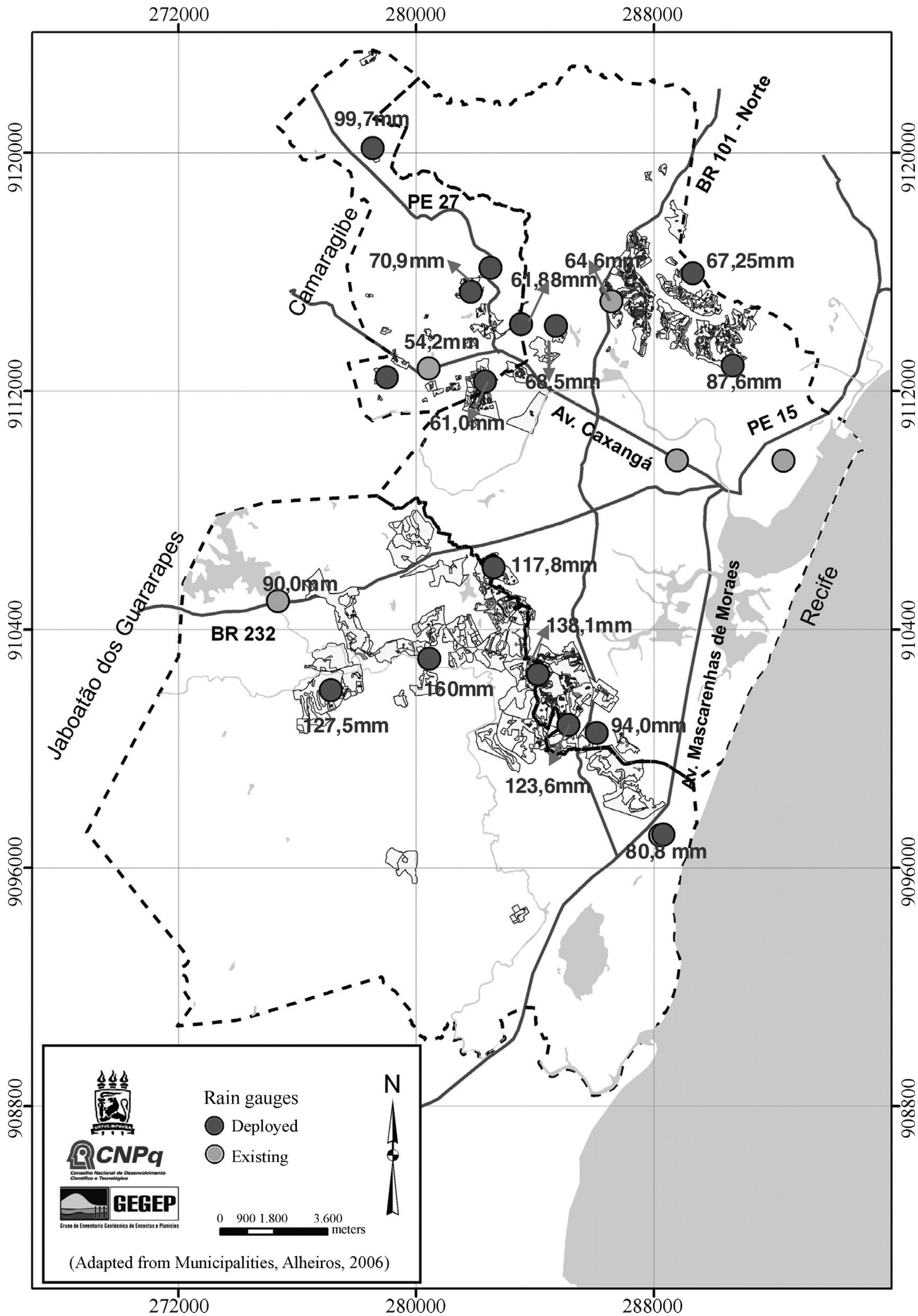

Figure 5 - Location of rain gauges in the 'High' and 'Very High Risk' areas, and the local rainfall indices during 24 h registered on April 13th, 2009 (Coutinho *et al.*, 2010).

lated in 72 h ($I_{72\,h}$), in the long term (P_{ac}) and R_{crit} values were proposed in each study area, the last obtained using the products of $I_{72\,h}$ by P_{ac}. These values were based on data from the graphs drawn during the previous stage.

g) Validation of the proposed alert systematics: through ROC analysis (Fawcett, 2006) the performance of the recommended rainfall parameters was assessed for civil defense actions. This stage was developed in all study areas in the municipality of Camaragibe.

5. Results Obtained and Discussions

Extending the rain gauge network in this study was necessary to obtain the rainfall accumulations that had caused the landslides in the areas. Positioning the instruments close to the most critical areas of risk helped to achieve a better correlation between the rainfall and processes of slope failure.

An example of this key step in the work is the rainfall logged on April 13, 2009, in the municipalities involved in the study. In Camaragibe, for example, rainfall was recorded as follows: 99.7 mm in Vera Cruz (using the instrument installed in this study) and 54.2 mm in Timbi (using the instrument previously existing in the municipal station) for the same 24 h. It should be mentioned that the latter instrument is used by the civil defense as a benchmark for its work; in other words, in Vera Cruz the civil defense would only act if there was an urgent call from the population, since the rainfall logged in the rain gauge that the civil defense team uses as a base (in Timbi) was around 50% of that logged in Vera Cruz. In the municipality of Recife, 123.6 mm of rain fell in 24 h in the South Regional, while in the North Regional the rainfall was 67.25 mm for the same period. In Jaboatão dos Guararapes 160 mm of rainfall was logged in the district of Socorro, while in Prazeres district the rain gauge used by the civil defense as a benchmark for its actions recorded rainfall of 80.75 mm during the same 24 h. This information shows how important it is to extend the rain gauge network for this study and for civil defense actions. Figure 5 illustrates the location of the rain gauges in the areas of high and very high risk and the rainfall data logged on April 13, 2009.

Throughout the base year of this study (2009), 1,367 cases of slope failure and 10 fatalities were recorded. Of this total, 827 occurred in the municipality of Recife, registering six deaths; 160 landslides in Camaragibe, with one death; and 380 landslides in Jaboatão dos Guararapes, with three fatalities. The majority of the landslides recorded in Recife occurred in the North Regional (32%) and South Regional (28%), which include areas of high landslide risks. In Camaragibe, 45% of landslides in 2009 occurred in Area II, concentrated in Tabatinga and Bairro dos Estados, which are considered to be the most problematic in the municipality. In Jaboatão dos Guararapes most of the landslides occurred in the Regionals of Jaboatão Centro and Cavaleiro (77% logs). In general the landslides in the municipalities involved in this study were closely related to high rainfall indices in February, April, June and July (Fig. 6).

After registering the 1,367 landslides, the accumulated rainfall was investigated to find which had triggered the processes. The following items describe the results found in each place.

5.1. Rainfall and landslides in the municipality of Recife

For each civil defense working area in the municipality of Recife (Regionals: South, Northeast, Northwest, West and North) the number of landslide events associated with cumulative rainfall in 72 h (Fig. 7) and in the long term, from January 1st (Fig. 8) were checked. Of the 827 landslide events in this municipality, 619 (75%) were directly related to rainfall and 208 (25%) landslides were not caused by rain as the main factor, with evidence of low rainfall indices. These landslides may have been aggravated by anthropic action and were not considered in the correlation analysis between the accumulated rainfall and slope failure processes.

Figure 7a shows that the rainfall caused 190 landslides in the South Regional. Of this total, 131 (69%) occurred when the 72-h cumulative rainfall was over 60 mm, with a higher concentration of rainfall accumulation of 120-150 mm. The 30 landslides (16%) occurring due to cumulative rainfall of 40-60 mm were caused by heavy rainfall in 24 h (> 40 mm). On the other hand, landslides occurring with accumulated rainfall of less than 40 mm/72 h (29 landslides) were related to the already saturated ground conditions, since slope failures were recorded after April, with accumulated indices higher than 600 mm from January 1st. Seventy-five percent (142) of all landslides in this Regional occurred in Lagoa Encantada. This Regional had the highest number of landslide processes in 2009.

In the Northeast Regional (Fig. 7b) 92 landslides occurred, 66 of them (72%) when the 72 h cumulative rainfall was more than 40 mm. In this Regional, the landslide was more evenly distributed in relation to the cumulative rainfall. When the accumulated rainfall was under 40 mm 26 (28%) landslides were registered; most of which occurred in May onward, when the ground was heavily saturated and the rain was concentrated during 24 h.

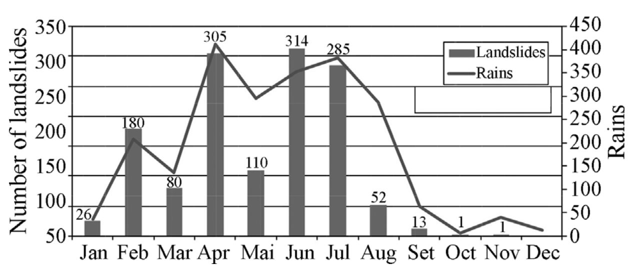

Figure 6 - Landslides and monthly rainfall during 2009 in the studied area.

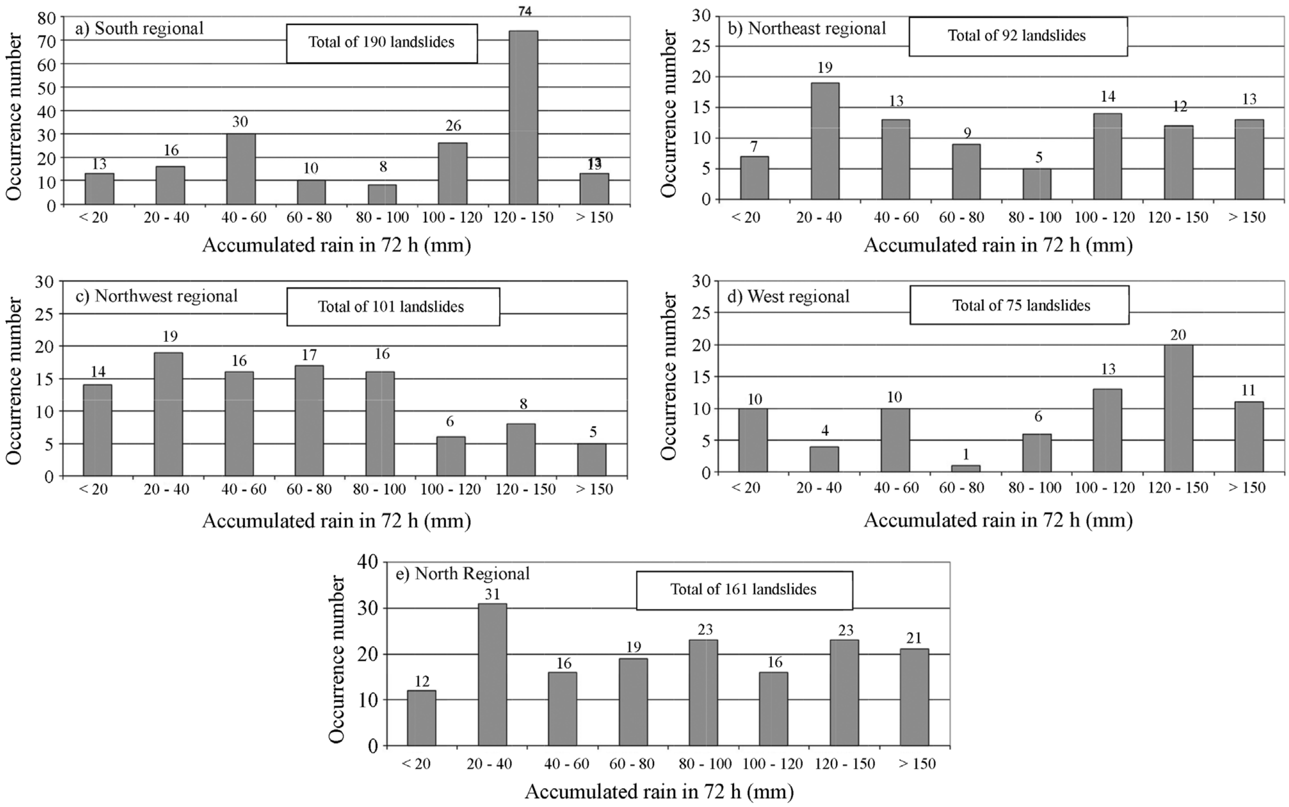

Figure 7 - Landslides per 72 h - accumulated rainfall in Recife Regionals - Total of 827 landslides.

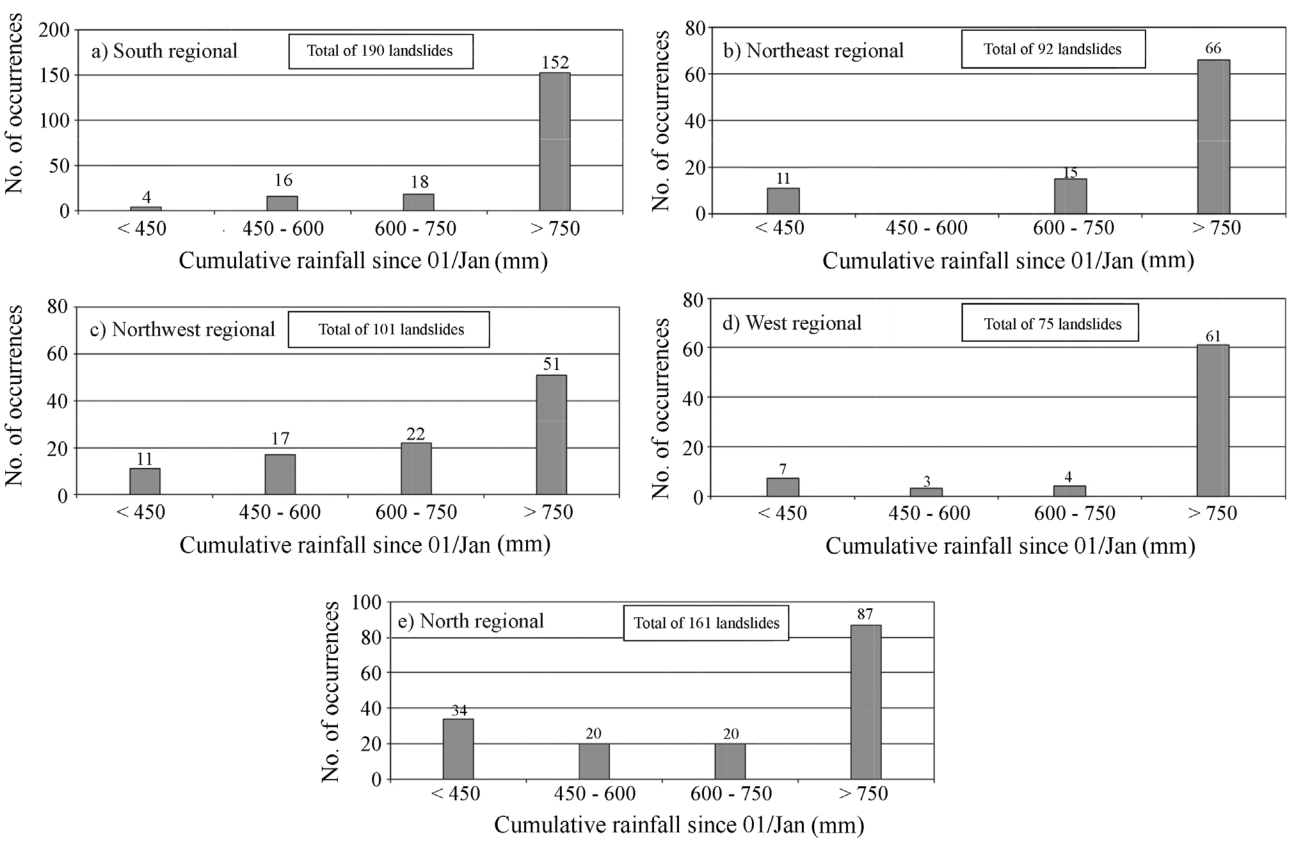

Figure 8 - Landslides due to accumulated rainfall from January 1st in Recife Regionals, Pernambuco - Total of 827 landslides.

In the Northwest Regional 101 landslides were recorded in 2009. Sixty-eight cases (67%) of this total occurred when the 72 hour accumulated rainfall was above 40 mm (Fig. 7c). In this area most cases were practically evenly distributed, with cumulative rainfall of 80-100 mm or less. When the accumulated rainfall was less than 20 mm/72 h 14 landslides were recorded, but all occurring after April, when the ground was heavily saturated. Around 84% (16 cases) of the 19 processes of slope failure with accumulated rain of 20-40 mm in 72 h also occurred after the high rate of ground saturation.

The West Regional suffered 75 landslides, 50 of which (67%) with cumulative rainfall of 80 mm or more in 72 h (Fig. 7d), with a slightly higher concentration for the 120-150 mm rainfall. The majority of landslide events, with accumulated rainfall below 80 mm in 72 h, occurred after the high degree of ground saturation.

In the North Regional with 161 recorded landslides ranked second with the highest number of processes than anywhere else in the study area. This area had a relatively even distribution of landslides between the ranges of cumulative rainfall. Of all the landslides, 118 (63%) were recorded when the 72-h rainfall accumulation was above 40 mm (Fig. 7e). Fourteen (45%) of the 31 landslides as a result of accumulated rainfall of 20-40 mm in 72 h occurred in May (after soil saturation); ten (32%) occurred in January and February, most of them related to the concentrated rainfall during 24 h; and seven (23%) in April, with the majority of landslides related to the average rainfall of 35 mm in 72 h . Eight (67%) of the 12 landslides with rainfall under 20 mm/72 h happened after the high saturation rate of the ground; and four (33%) in February and March showed signs of being more closely related to anthropic actions.

By analyzing the long days of accumulated rainfall in the municipality of Recife (Fig. 8), it is found that after 750 mm of cumulative rainfall several landslides occurred in all the Regionals, representing 51%-81% of the total, with major events in the South, Northeast and West Regionals. In the South, Northeast, Northwest and West Regionals there is a clear upward trend in the number of landslides with cumulative rainfall values. The North Regional had a significant number of landslides with cumulative rainfall below 450 mm. The registered landslides with accumulated rainfall below 450 mm were closely related to the rainfall concentrated in 72 h, as occurred in the Northeast (11 cases - Fig. 8b), Northwest (11 cases - Fig. 8c) and North (34 cases - Fig. 8e) Regionals. It should be stressed that in the Northwest and North Regionals, the landslides with cumulative rainfall of 450-600 mm were also related to the rainfall concentrated in 72 h, with logs above 70 mm.

These landslide records show how important it is to know the product between long days of accumulated rainfall and the 72 h rainfall. Considering these data, the critical accumulation in 72 h could be considered 40 mm for the Northeast, Northwest and North Regionals; 60 mm for the South Regional; 80 mm for the West Regional; and the long-term critical accumulation (P_{ac}) for all the Recife Regionals could be considered 750 mm.

In relation to the geological-geotechnical aspects, the sediments in the Barreiras Formation can be said to be characteristic of Recife hillsides studied, only differing in the predominant sizes of particles in each Regional. In the South Regional, for example, sandy sediments prevail; however, the soils in the Northeast and Northwest Regionals are sandy-clay. The West Regional presents pockets of soils interspersed with sands and clays, which could provide a preferential landslide route on the hillsides; and the North Regional has more clayey soils in this formation.

5.2. Rainfall and landslides in the municipality of Camaragibe

One hundred and forty-six (91%) of the 160 landslides that occurred in the municipality of Camaragibe were directly related to rainfall, and since the other 14 (9%) landslides were not triggered by rainfall, they were excluded from the critical rainfall analyses.

Figure 9 shows the distributions of landslide events due to cumulative rainfall in 72 h for the municipality of Camaragibe. This figure shows that in Areas I, III and IV (Vera Cruz), most of the processes had cumulative rainfall of more than 80 mm in 72 h. However, the four landslide events in Area I, recorded with accumulated rainfall of 80-100 mm/72 h, occurred after the ground was heavily saturated, as in the two logs below 80 mm/72 h. In Areas II and IV (Tabatinga), the majority of processes occurred with accumulated rainfall above 60 mm/72 h, recording in this condition 55 and 18 landslides, respectively. Two of the nine landslides registered in Area II, with cumulative rainfall below 60 mm/72 h, happened in March, due to heavy rainfall of 42-58 mm in 48 h; and six occurred after April when the ground was already saturated, with 30 mm of rainfall concentrated in 24 h.

The landslides associated with the long days of accumulated rainfall in the municipality of Camaragibe are illustrated in Fig. 10. Figure 10a, corresponding to Area I, shows that 81% of the landslides (25 cases) were recorded when the rainfall accumulation exceeded 750 mm. In Area II, when the accumulated rainfall exceeded 600 mm, 41 landslide events (62%) were logged in separate places in this area (Fig. 10b). The 22 landslides with accumulated rainfall below 450 mm were related to the previous days' heavy rainfall (60 mm/72 h). Area III also showed a number of landslides with accumulated rainfall of more than 600 mm (Fig. 10c), the main driving factor of 75% of the landslides (15 events), that is, the saturated state of the ground. In Area IV-Tab, when the long-term accumulated rainfall reached 750 mm, 14 landslides (74%) were registered of the total 19 events in the area (Fig. 10d). In this Area, the three slope failures, with a recorded rainfall of 600-750 mm, were due to the heavy rainfall the previous

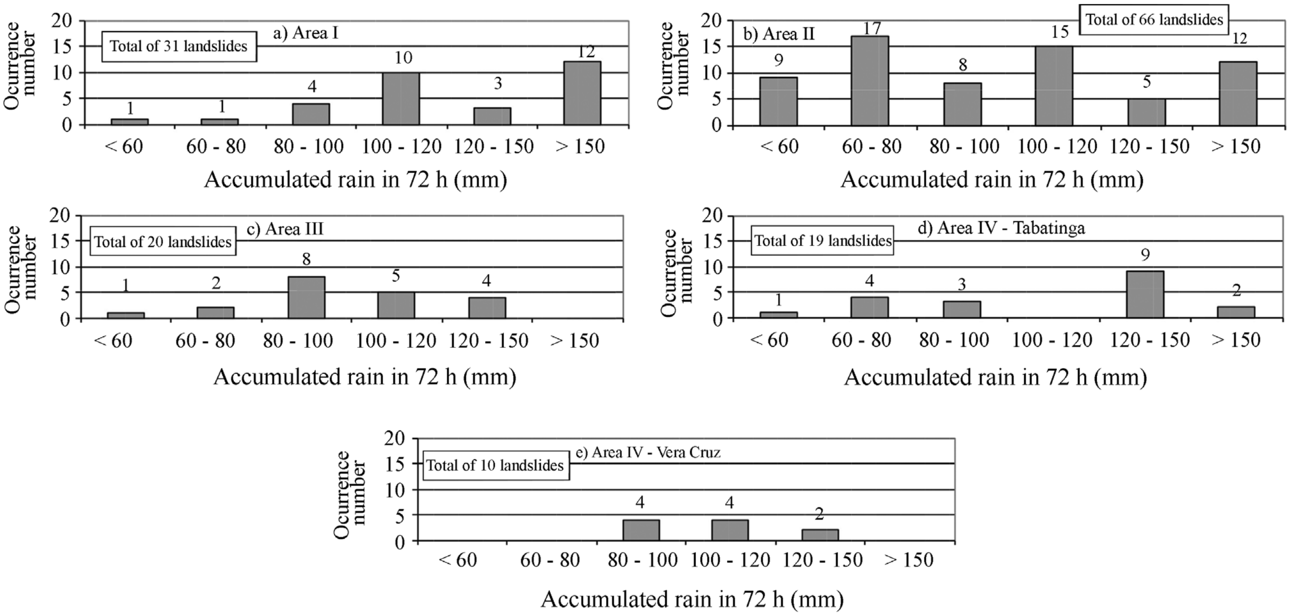

Figure 9 - Landslides per 72 h - accumulated rainfall in Camaragibe Regionals - Total of 160.

days (136 mm/72 h); and the two registered landslides with cumulative rainfall of less than 450 mm were due to the rainfall of 53 mm/24 h, on February 12, and of 98.5 mm/24 h, on February 27.

Area IV (Vera Cruz) had fewer landslides (10 cases), with eight (80%) registered with cumulative rainfall of less than 450 mm (Fig. 10e), in contrast to the other areas. These eight landslides occurred due to heavy rainfall every day during February; four of the landslides occurred with rainfall of 98.5 mm/24 h and four due to the concentrated rainfall of 88.5 mm/72 h, with no relation to the long days of rainfall. The other landslides in this Area (2 cases) that were correlated to the long-term cumulative rainfall occurred with rainfall of 600 mm or more. In short, in this area 80% of the cases were linked to rainfall concentrated in 24 h. This behavior may be due to the small size of the existing risk areas in that location. In general, except for Area IV (Vera Cruz), there was an increase in the number of landslides in Camaragibe with increased cumulative rainfall.

These data show that the 72 h-critical accumulation ($I_{72\ h}$) for Camaragibe could be considered as follows: 100 mm for Area I; 60 mm for Areas II and IV (Tabatinga), and 80 mm for Areas III and IV (Vera Cruz). On the other hand, the long-term critical accumulation (P_{ac}) can be considered to be 750 mm for Areas I and IV (Tabatinga) and 600 mm for Areas II, III and IV (Vera Cruz).

Concerning the geological-geotechnical characteristics, Area I consists of alternating sand and clay layers from the Barreiras Fm. Area II consists of sandy soils from this formation and residual silty soils of granite. The predominant characteristic of Area III, on the other hand, is clayey-sand residual soil of granite (Bandeira *et al.*, 2011). Tabatinga and Vera Cruz in Area IV reveal clayey-sand characteristics with pebble, of the Barreiras Formation.

5.3. Rainfall and landslides in the municipality of Jaboatão dos Guararapes

Figure 11 illustrates the distribution of landslide events due to 72 h-accumulated rainfall in each Regional of the municipality of Jaboatão dos Guararapes (Jaboatão Centro, Cavaleiro, Curado, Muribeca, Prazeres). In this municipality 380 landslides occurred, 324 (85%) of which were directly correlated with the rainfall. There are signs that the main factor for slope failure in the other landslides was anthropic action. Figure 11a shows that 80% of the landslide events (114) in Regional I (Jaboatão Centro) were due to accumulated rainfall of more than 80 mm/72 h, with a greater concentration of landslides with rainfall accumulation of more than 120 mm. The occurrence of 19 of the 22 landslides after rainfall accumulation of less than 80 mm/72 h was due to the high long-term rainfall accumulation (more than 600 mm). Most of the landslides (106) in Regional II (Cavaleiro), which were rainfall-related (130 cases), occurred with cumulative rainfall of 80 mm/72 h or more (Fig. 11b); and also with a larger concentration of landslides with accumulated rainfall of more than 120 mm. Ninety percent (90%) of the 24 cases that occurred with accumulation of less than 80 mm were correlated with the high degree of ground saturation, since they occurred after April when the long-day rainfall accumulation was already high.

In Regional III (Curado) there were 35 processes of slope failure concentrated in the District of Curado IV. Figure 11c shows that most of the landslides occurred after a rainfall accumulation of 100 mm/72 h (32 cases), with

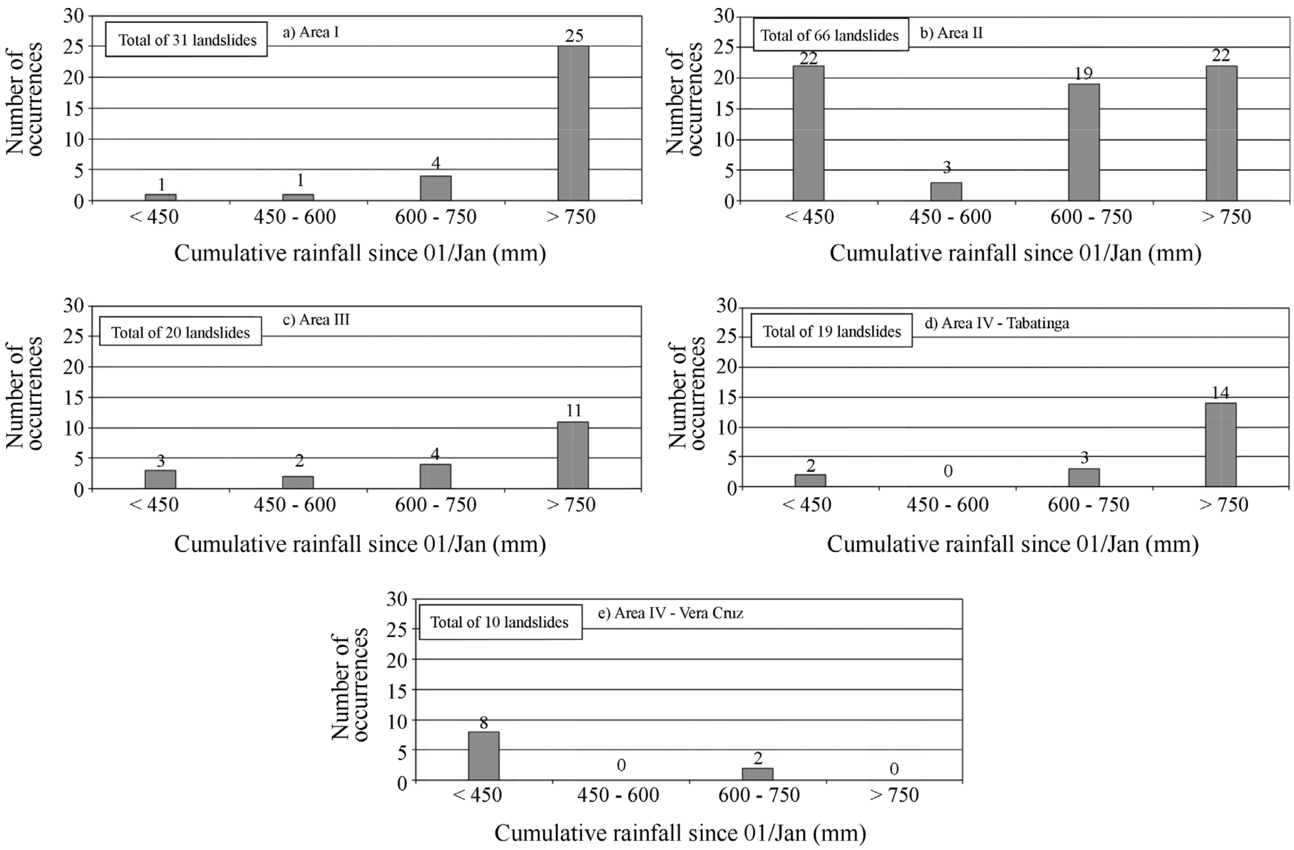

Figure 10 - Landslides due to accumulated rainfall from January 1st in Camaragibe Regionals, Pernambuco - Total of 160 landslides.

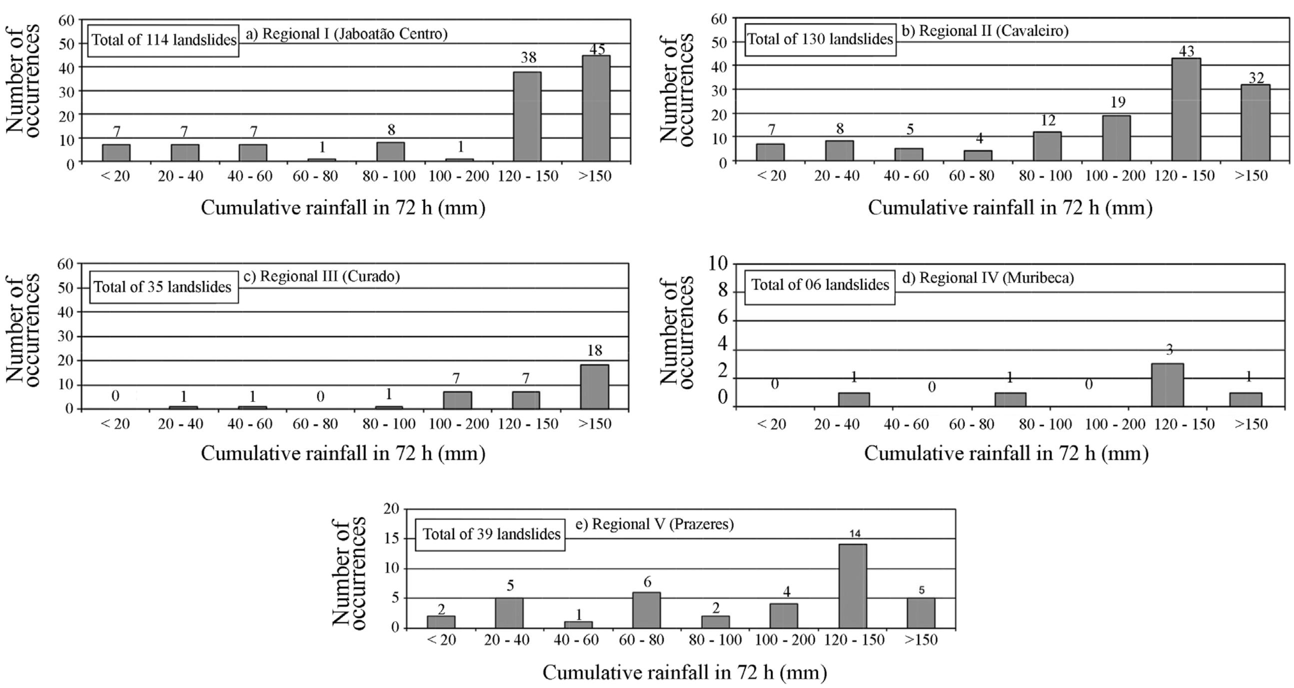

Figure 11 - Landslides per 72 h - accumulated rainfall in Jaboatão dos Guararapes Regionals - Total of 380 landslides.

higher concentration of landslides with cumulative rainfall of more than 150 mm. Around 50% of the landslide events (18 cases) in this Regional were in February, due to the heavy rainfall (115-137 mm/24 h) each day from the 22nd to 25th of that month. Regional IV (Muribeca) had six landslide events, four recorded with rainfall of more than 100 mm/72 h (Fig. 11d). All the landslides occurred after the long days of accumulated rainfall exceeding 600 mm. In this Regional there was a relatively even landslide distribution in the bands of accumulated rainfall in 72 h. It is worth mentioning that between January and April 2009 there was at least one record of rainfall above 100 mm/72 h, but there were no landslides due to these concentrated rains. All recorded landslides in this Regional occurred after the ground was saturated; in other words, after the beginning of April when the long-term accumulations exceeded 600 mm. Practical experiments in the Recife Metropolitan Region show that rainfall of 100 mm/72 h or more cause various landslides in the Region. The fact that no landslides occurred in the first four months of the year in this Regional can be explained by the small hillside areas to be found there, associated with low demographic density and, consequently, little influence of anthropic factors and interference in the original conditions of the relief.

In Regional V (Prazeres) 39 rainfall-related landslide occurred (Fig. 11e). When the rainfall accumulated above 60 mm/72 h, 31 landslides were recorded, corresponding to around 80% of all landslides in Regional V; generally, however, the number of landslides was relatively uniform in the distribution bands, except for the 120-150 mm band, which had the highest concentration. The two slope failures with rainfall of less than 20 mm/72 h were logged in February and July, the latter when the ground was already heavily saturated. Five landslides were recorded when the 72 h accumulation was 20-40 mm, after a large accumulation of long days of rain. When the accumulation was 40-60 mm/72 h, only one landslide in June was logged, after the long days of accumulation had exceeded the 600 mm. It is found that in Regionals II and V when more than 150 mm was accumulated there were fewer landslides compared to the processes associated with the 120-150 mm accumulation. This fact can be explained by the period of occurrence of landslides with higher accumulations between February and April, while the landslide events with accumulations of 120-150 mm occurred in June to August, when the ground had a higher saturation level. In Regional IV the same case was observed for a 120-150 mm accumulation compared to the landslides occurring with cumulative rainfall of 100-120 mm/72 h.

The correlations between the landslides and long days of cumulative rainfall are shown in Fig. 12. In Regional I, 90% of the cases had cumulative rainfall over 600 mm, corresponding to 103 of a total 114 landslides (Fig. 12a). Regional II, had around 70% (90 cases) of a total of 130 landslides, with accumulated rainfall above 750 mm (Fig. 12b). The slope instabilities had rainfall accumulations of less than 450 mm (23 cases) due to the concentrated rainfall in 72 h or less in February (14 landslides with rainfall of 113 mm/24 h; two with rainfall of 94 mm/48 h; and seven with cumulative rainfall of 164 mm/72 h). In Regional III, the same number of landslides (17) occurred with cumulative rainfall under 450 mm and over 750 mm (Fig. 12c). However, similar to the events in Regional II, slope failures with rainfall accumulation of less than 450 mm occurred due to the high rainfall during 72 h or less in February (15 landslides with rainfall of 113 mm/24 h; and two with accumulated rainfall of 164 mm/72 h), and were not directly related to the long days of accumulated rain. Figure 12d, referring to Regional IV shows that 100% of the landslides (6 cases) occurred when the cumulative rainfall was already over 600 mm. Regional V had a total of 39 landslides events (Fig. 12e), mostly (62%) with accumulated rainfall above 750 mm. The majority of logs of landslides with accumulated rainfall below 450 mm were due to the concentrated volumes of rain in 24 h, six occurring in January with rainfall of 118 mm/24 h; and three in February with concentrated rainfall of 91.3 mm/24 h.

With this information, estimated values of critical accumulations of rainfall in 72 h ($I_{72\ h}$) for the Regionals of Jaboatão dos Guararapes, are as follows: 80 mm for Regionals I and II - 80 mm; Regionals III and IV - 100 mm; and Regional V - 60 mm. The values relating to the critical accumulations of long-term rainfall (P_{ac}) are: Regionals I and IV - 600 mm, and Regionals II, III and V - 750 mm.

In relation to the geological formation, the hillsides of Regionals I, II and III have a predominantly clayey soil residual of mylonite. However, the Regionals IV and V hillsides are predominantly of sandy sedimentary soils of the Barreiras Formation.

6. Proposed Rainfall Parameters for Civil Defense Actions

In this section technical rainfall parameters are proposed, which increase the probability of triggering landslides in the study areas, creating support for the municipal civil defense teams to properly establish the levels of operation in four states: Observation, Warning, Alert and Maximum Alert. Tables 2, 3 and 4 summarize the data (rainfall parameters - $I_{72\ h}$, P_{ac} and R_{crit}) for the municipalities of Recife, Camaragibe and Jaboatão dos Guararapes, respectively.

It is recommended in all study areas to begin the state of Observation on December 1st, since the Region's monthly historic average is over 50 mm, which is a key value to start this operation. For the states of Warning, Alert and Maximum Alert parameters were proposed that are characteristic of each area in the municipalities. The references values were in general different for each area and between municipalities confirming the importance to have specific rainfall information.

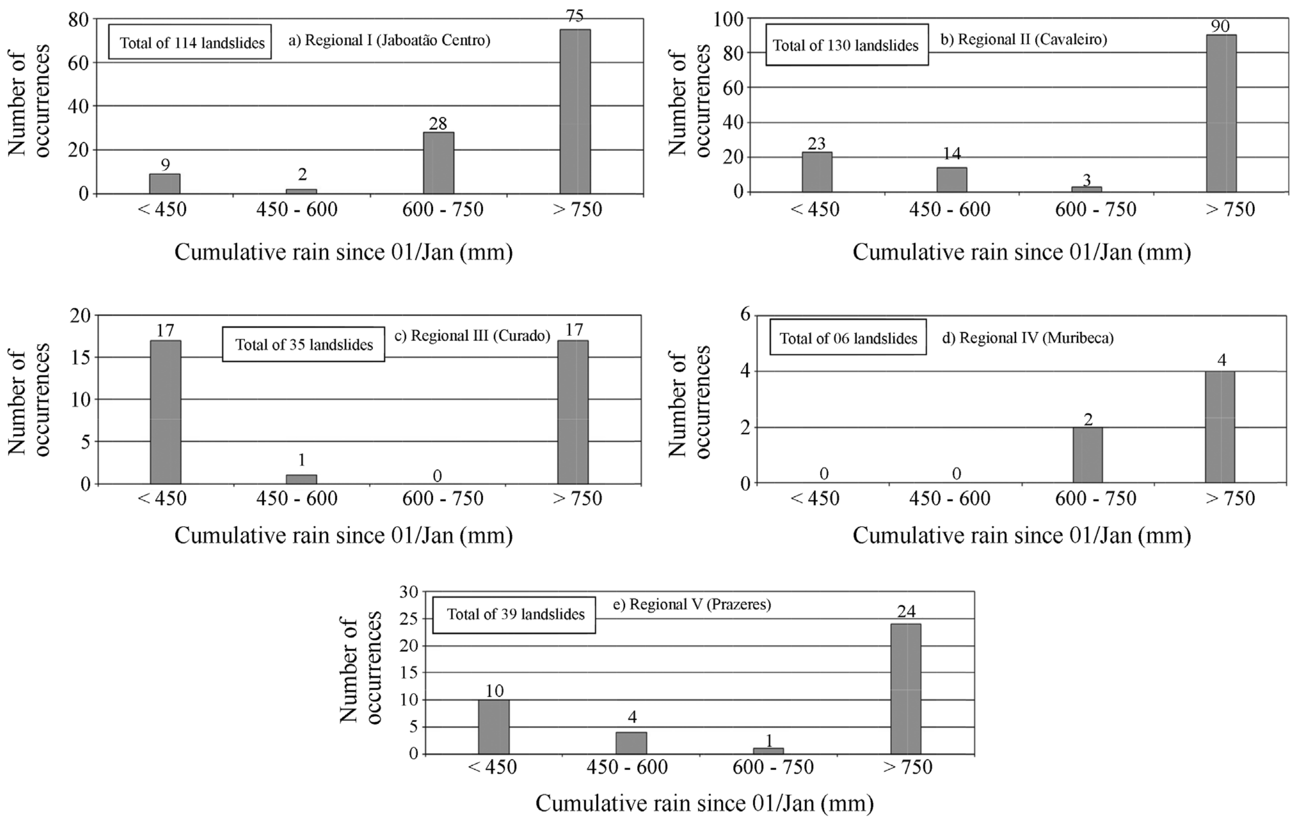

Figure 12 - Landslides due to accumulated rainfall from January 1st in Jaboatão dos Guararapes Regionals, Pernambuco - Total of 380 landslides.

It is worth mentioning that in any study area when the parameters P_{ac} and R_{crit} are reached during the rainy season (February to September) they will be valid for the Warning level; on the other hand, $I_{72\,h}$ is valid for any period of the year. It should be said that the Warning level could mean the occurrence of isolated landslides in the areas.

When establishing the Alert level in all study areas, it should be announced when $I_{72\,h}$ and R_{crit} are expected to be reached simultaneously and continuing rainfall is forecast. The Maximum Alert level should be announced when there is an Alert level in several areas in the municipality. Tables 2, 3 and 4 summarize the aforementioned data for the municipalities of Recife, Camaragibe and Jaboatão dos Guararapes, respectively.

The cumulative rainfall parameters suggested herein as support for Civil Defense actions in the study areas are limit values. At the start of the rain the Observation operating level is adopted (from December 1st), after what is considered the dry season (October-November). At this level there is no need for site visits, unless at the request of the local inhabitants. When the cumulative rainfall is predicted to reach the critical values within 72 h ($I_{72\,h}$), particularly in 24 h, or to reach the long-term critical rainfall figures (P_{ac}) or the R_{crit}, then the Warning level begins. This is the level in which the civil defense technical team begins its most active field inspections, to check the need for temporary or definitive removal of families living in the high risk and very high risk areas, considering the possibility of landslide events. When it is expected that R_{crit} and $I_{72\,h}$ reached at the same time, the Alert level is given, remaining at this level when weather forecasts indicate continuing heavy rainfall. At this operating level the civil defense may inform the population about the possible total evacuation from the highest risk areas; and this could be helped by implementing a sound system or other form of alert communication, informing the population about the strong possibility of generalized landslide events. At this level the need is assessed to evacuate the population living in the most critical risk areas and to set up a shift system for the civil defense teams, with technical personnel on call 24 h to provide assistance. The field inspections are also carried out at this stage.

Figure 13 presents the proposal in a follow-up graph of the rainfall parameters ($I_{72\,h}$ and R_{crit}) to establish the Observation, Warning and Alert levels for Area II of Camaragibe. The civil defense teams recommend drawing up a graph for the other study areas in the municipalities. Figure 13 shows that when the $I_{72\,h}$ and R_{crit} values were considerably higher, there was a major increase in the number of landslides and consequences. Continuing this study, different levels of alert associated with the gravity of the consequences could be established.

Table 2 - Proposed accumulated rainfall parameters for the Civil Defense operating levels in Recife.

Level/regional	South	Northeast	Northwest	West	North
Observation			From December 1st		
Warning*	$I_{72\,h}$ = 60 mm or P_{ac} = 750 mm or R_{crit} = 45,000 mm^2	$I_{72\,h}$ = 40 mm or P_{ac} = 750 mm or R_{crit} = 30,000 mm^2	$I_{72\,h}$ = 40 mm or P_{ac} = 750 mm or R_{crit} = 30,000 mm^2	$I_{72\,h}$ = 80 mm or P_{ac} = 750 mm or R_{crit} = 30.000 mm^2	$I_{72\,h}$ = 40 mm or P_{ac} = 750 mm or R_{crit} = 30,000 mm^2
Alert	$I_{72\,h}$ = 60 mm and R_{crit} = 45,000 mm^2	$I_{72\,h}$ = 40 mm and R_{crit} = 30,000 mm^2	$I_{72\,h}$ = 40 mm and R_{crit} = 30,000 mm^2	$I_{72\,h}$ = 80 mm and R_{crit} = 60,000 mm^2	$I_{72\,h}$ = 40 mm and R_{crit} = 30,000 mm^2
Maximum alert			When Alert occurs in all areas of the municipality		

*In this state isolated landslides may occur, particularly with heavy rainfall concentrated in 24 h.

R_{crit} must be monitored by following up the cumulative rainfall product since December 1st for the expected cumulative rainfall in 72 h. Continuing at the Alert level itis suggested that the rainfall indices are followed up daily and, if possible, at 60-min intervals. It is worth mentioning that the R_{crit} value proposed herein would only be valid when it is achieved during the wet season, which in Recife-MR is concentrated from February to September. If the location has some dry days, the critical cumulative rainfall may be reached after the wet season, when it will no longer be necessary to establish the state of Alert, but it is recommended to establish the Warning state, whenever necessary. Table 5 shows the criteria for the operating levels and their actions.

7. Validation of Rainfall Parameters Suggested for Actions in the Study Areas

In order to assess the performance of the rainfall parameters suggested herein for Alert level the rates of successfully predicted landslides were calculated using the ROC analysis (Fawcett, 2006). To do this the chosen pilot area was the municipality of Camaragibe. Table 6 gives the data used in this analysis and Tables 7 and 8 present a summary of the results. Figure 14 illustrates a ROC graph of the Camaragibe Areas.

Table 7 shows that the true positive classified rate of Alert days was higher than the number of days classified as false negative, in most areas, except in Area I and Area IV-VC. Nevertheless, the number of true positive days in Area I represents 68% of the landslide events in that area. In relation to Area IV-Vera Cruz, it should be mentioned that it has an atypical characteristic, showing relief in the form of a single valley, with disorganized occupation. The landslide events in this area are due to its peculiar characteristics, closely related to anthropic actions. On analyzing the entire municipality, the number of days said to be true positive (29 days) is 66% of total landslide occurrences (97 landslides of a total 146).

In Table 8 (ROC Analysis) the true positive rates of Areas II, III and IV-TAB are higher than 0.50, signifying a good result. In relation to the item Precision, Areas I, II and III are seen to have values of 0.37-0.47. Area IV-TAB had a precision of 0.28. It should again be mentioned that the atypical case is Area IV-Vera Cruz, which had the lowest value (0.08).

Figure 14 presents the ratio between the true and false positive rates. In this figure, when the points have ordered pairs close to 0-false positive rate, 1-true positive rate, they are more accurate as well as those located above the diagonal line. Figure 14 shows that points B, C and D, corresponding to Areas II, III and IV-TAB, respectively, have more satisfactory values, but no area has a point below the diagonal line (high false positive rate values), which demonstrates that the suggested parameters are satisfactory for alert system recommendations.

Table 3 - Proposed accumulated rainfall parameters for the Civil Defense operating levels in Camaragibe.

Level/area	Area I	Area II	Area III	Area IV - Tabatinga	Area IV-Vera Cruz
Observation			From December 1st		
Warning*	$I_{72\,h}$ = 100 mm or P_{ac} = 750 mm or R_{crit} = 75,000 mm²	$I_{72\,h}$ = 60 mm or P_{ac} = 600 mm or R_{crit} = 36,000 mm²	$I_{72\,h}$ = 80 mm or P_{ac} = 600 mm or R_{crit} = 48,000 mm²	$I_{72\,h}$ = 60 mm or P_{ac} = 750 mm or R_{crit} = 45,000 mm²	$I_{72\,h}$ = 80 mm or P_{ac} = 600 mm or R_{crit} = 48,000 mm²
Alert	$I_{72\,h}$ = 100 mm and R_{crit} = 75,000 mm²	$I_{72\,h}$ = 60 mm and R_{crit} = 36,000 mm²	$I_{72\,h}$ = 80 mm and R_{crit} = 48,000 mm²	$I_{72\,h}$ = 60 mm and R_{crit} = 45,000 mm²	$I_{72\,h}$ = 80 mm and R_{crit} = 48,000 mm²
Maximum alert			When Alert occurs in all areas of the municipality		

*In this state isolated landslides may occur, particularly with heavy rainfall concentrated in 24 h.

Table 4 - Proposed accumulated rainfall parameters for the Civil Defense operating levels in Jaboatão dos Guararapes.

Level/regional	Regional I (Jab. Centro)	Regional II (Cavaleiro)	Regional III (Curado)	Regional IV (Muribeca)	Regional V (Prazeres)
Observation			From December 1st		
Warning*	$I_{72\,h}$ = 80 mm or P_{ac} = 600 mm or R_{crit} = 48,000 mm²	$I_{72\,h}$ = 80 mm or P_{ac} = 750 mm or R_{crit} = 60,000 mm²	$I_{72\,h}$ = 100 mm or P_{ac} = 750 mm or R_{crit} = 75,000 mm²	$I_{72\,h}$ = 100 mm or P_{ac} = 600 mm or R_{crit} = 60,000 mm²	$I_{72\,h}$ = 60 mm or P_{ac} = 750 mm or R_{crit} = 45,000 mm²
Alert	$I_{72\,h}$ = 80 mm and R_{crit} = 48,000 mm²	$I_{72\,h}$ = 80 mm and R_{crit} = 60,000 mm²	$I_{72\,h}$ = 100 mm and R_{crit} = 75,000 mm²	$I_{72\,h}$ = 100 mm and R_{crit} = 60,000 mm²	$I_{72\,h}$ = 60 mm and R_{crit} = 45,000 mm²
Maximum alert			When Alert occurs in all areas of the municipality		

*At this level, isolated landslides may occur, particularly with heavy rainfall concentrated in 24 h.

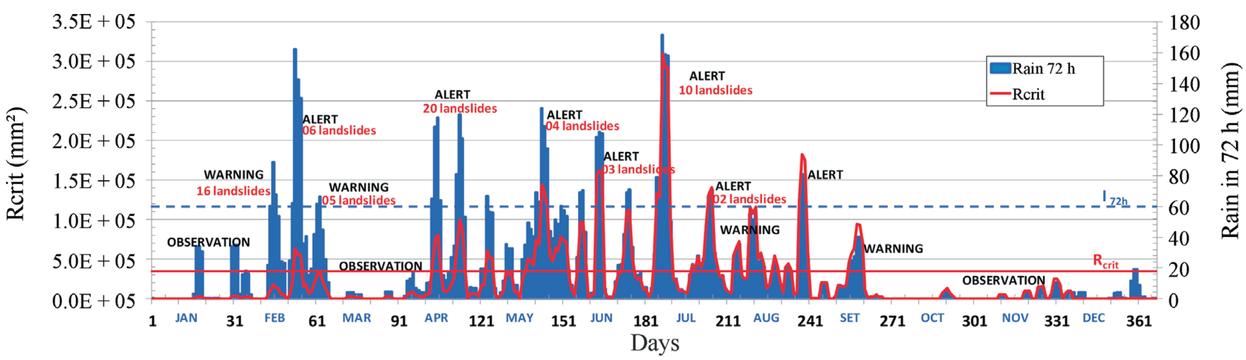

Figure 13 - Follow-up of rainfall parameters suggested for civil defense actions in Area II of Camaragibe.

Table 5 - Civil Defense operating levels and recommended actions for Recife-MR.

Operating level	Criteria	Actions
Observation	From December 1st	Follow up of rainfall indices and meteorology
Warning	When $I_{72\,h}$ is expected to occur at any time of the year; or when P_{ac} or R_{crit} is expected to occur within the wet season (Feb-Sep)	Inspections in the risk areas to check the possibility of isolated landslides
Alert	When $I_{72\,h}$ and R_{crit} are expected to occur at the same time within the wet season, with expected continuing rainfall	Inspections in the risk areas to check the possibility of generalized landslides, alert warning and preventive removal of families living in high and very high risk areas
Maximum alert	When R_{crit} and $I_{72\,h}$ are reached throughout the municipality within the wet season, with expected continuing rainfall	Warnings of general alert and mass removal of families living in the risk area

Table 6 - Landslides and Operating Levels in in Camaragibe.

Area	Date	Operating level	Number of landslides
Area I	13/Apr	Observation	1
	14/Apr	Warning	3
	22/Apr	Observation	1
	21/May	Warning	3
	23/May	Alert	3
	12/Jun	Alert	6
	06/Jul	Alert	12
	07/Aug	Warning	2
Area II	13/Feb	Warning	16
	22/Feb	Alert	5
	26/Feb	Observation	1
	01/Mar	Observation	2
	02/Mar	Warning	3
	14/Apr	Alert	13
	22/Apr	Alert	5
	23/Apr	Alert	2
	23/May	Alert	2
	30/May	Alert	2
	12/Jun	Alert	2
	22/Jun	Warning	1
	06/Jul	Alert	10
	22/Jul	Alert	1
	23/Jul	Alert	1
Area III	22/Feb	Warning	3
	23/Feb	Warning	1
	13/Apr	Alert	1
	14/Apr	Alert	4
	24/Apr	Alert	1
	23/May	Alert	1
	25/May	Alert	1
	12/Jun	Alert	3
	06/Jul	Alert	3
	22/Jul	Warning	2
Area IV-TAB	12/Feb	Observation	1
	14/Apr	Alert	3
	22/Apr	Alert	2
	21/May	Alert	1
	23/May	Alert	2
	25/May	Alert	1
	12/Jun	Alert	1
	06/Jul	Alert	5
	07/Aug	Alert	3
Area IV-VC	13/Feb	Warning	4
	22/Feb	Warning	4
	13/Apr	Alert	2

Table 7 - Performances of Alerts using ROC analysis in Camaragibe.

Area	Predictive Class for Alert	Number of days of the Alert	Actual class
Area I	if $I_{72\,h} \geq 100$ mm and $R_{crit} \geq 75{,}000$ mm^2	Yes/No	Landslide inventory for $I_{72\,h} \geq 100$ mm and $R_{crit} \geq 75{,}000$ mm^2
Landslide occurrence	No landslides		
Yes 07	True Positives (TP) 03	False Positives (FP) 04	
No 358	False Negatives (FN) 05	True Negatives (TN) 353	
Area II	if $I_{72\,h} \geq 60$ mm and $R_{crit} \geq 36{,}000$ mm^2	Yes/No	Landslide inventory for $I_{72\,h} \geq 60$ mm and $R_{crit} \geq 36{,}000$ mm^2
Landslide occurrence	No landslides		
Yes 27	True Positives 10	False Positives 17	
No 338	False Negatives 05	True Negatives 333	
Area III	if $I_{72\,h} \geq 80$ mm and $R_{crit} \geq 48{,}000$ mm^2	Yes/No	Landslide inventory for $I_{72\,h} \geq 80$ mm and $R_{crit} \geq 48{,}000$ mm^2
Landslide occurrence	No landslides		
Yes 15	True Positives 07	False Positives 08	
No 350	False Negatives 03	True Negatives 347	
Area IV-TAB	if $I_{72\,h} \geq 60$ mm and $R_{crit} \geq 45{,}000$ mm^2	Yes/No	Landslide inventory for $I_{72\,h} \geq 60$ mm and $R_{crit} \geq 45{,}000$ mm^2
Landslide occurrence	No landslides		
Yes 29	True Positives 08	False Positives 21	
No 336	False Negatives 01	True Negatives 335	
Area IV-VC	if $I_{72\,h} \geq 80$ mm and $R_{crit} \geq 48{,}000$ mm^2	Yes/No	Landslide inventory for $I_{72\,h} \geq 80$ mm and $R_{crit} \geq 48{,}000$ mm^2
Landslide occurrence	No landslides		
Yes 13	True Positives 01	False Positives 12	
No 352	False Negatives 02	True Negatives 350	

Table 8 - Performances of alerts using ROC analysis in Camaragibe.

Area	True positive rate (a)*	False positive rate (b)*	Specificity (c)*	Precision (d)*
I	0.38	0.01	0.99	0.43
II	0.67	0.05	0.95	0.37
III	0.70	0.02	0.98	0.47
IV-TAB	0.89	0.06	0.94	0.28
IV-VC	0.33	0.03	0.97	0.08

Note (*): (a) = TP/(TP+FN); (b) = FP/(FP+TN); (c) = TN/(TN+FP); (d) = TP/(TP+FP).

With regard to the isolated values of the critical cumulative rainfall in 72 h ($I_{72\,h}$), the 100 mm value suggested for the warning state in Area I of Camaragibe and Regionals III (Curado) and IV (Muribeca) of Jaboatão dos Guararapes (Tables 2 and 3), is similar to those proposed by Macedo *et al.* (2004) for the Baixada Santista and Paraíba Valley in São Paulo. The 80 mm value in 72 h or less for the warning state in the West Regional in the city of Recife (Table 1), for Areas III and IV (Vera Cruz) in Camaragibe (Table 2); and for Regionals I (Jaboatão Centro) and II (Cavaleiro) in Jaboatão dos Guararapes (Table 3), is similar to that proposed for the São Paulo Regions of Campos do Jordão, Campinas, ABC and Sorocaba. The critical cumulative rainfall value of 60 mm in 72 h recommended for the warning state in the South Regional of the city of Recife, and for Areas II and IV (Tabatinga) of Camaragibe and Regional V (Prazeres) of Jaboatão dos Guararapes, are lower than those found by Macedo *et al.* (1999) for the São Paulo

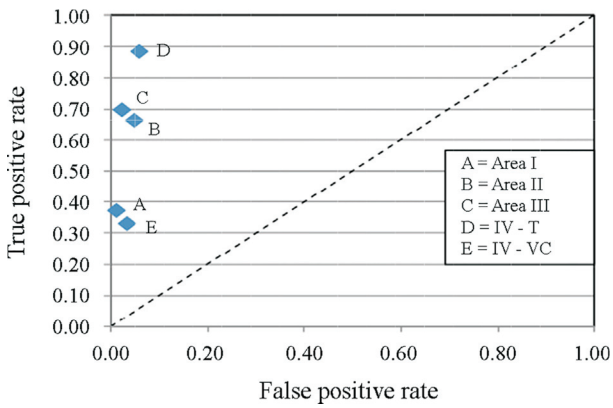

Figure 14 - ROC graph of the results in Camaragibe Areas.

Regions. The critical rainfall accumulated in 72 h for the Northeast, Northwest and North Regionals of Recife was 40 mm. This is the lowest critical value.

Figure 15 illustrates a landslide event on April 13, 2009, in the South Regional of Recife. This landslide, which destroyed a property, occurred after a concentrated rainfall of 123.6 mm/24 h and 137 mm/72 h, with long-term accumulation of 1,200 mm and an *R* parameter of 164,400 mm^2. It is thereby found that this landslide occurred with higher rainfall parameters than those suggested for the state of Warning and Alert in Recife-MR. Other landslides events recorded years after this study confirmed the critical rainfall parameters proposed herein, such as, for example, the landslides on March 23, 2010, where the cumulative rainfall of 104.2 mm/72 h and particularly 80 mm/24 h caused slope instabilities in a number of locations in the study area.

In 2009, the year when the rainfall and landslides were followed up in this study, 10 fatal victims were registered due to the landslides on hillsides: six deaths in Recife, one in Camaragibe and three in Jaboatão dos Guararapes. Table 9 shows the rainfall accumulation in 72 h, long days

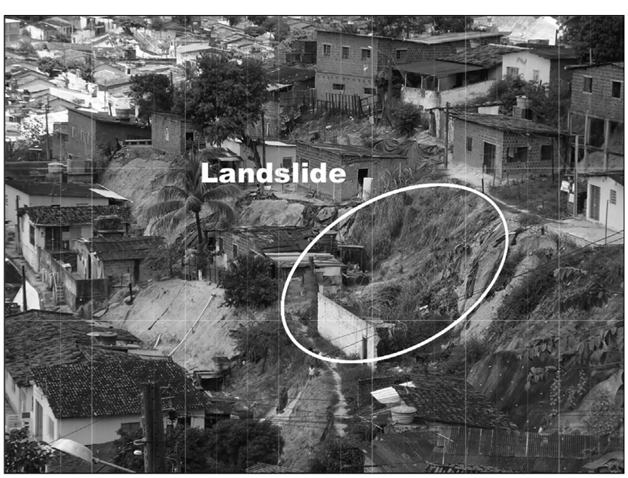

Figure 15 - Landslide showing destruction of buildings on June 13th, 2009 (Southern Regional Sector of Recife) (Bandeira, 2010).

Table 9 - Registration of rainfall-related fatalities in Recife-MR in 2009.

Date	Municipality/ Regional / District	No. of deaths	Rainfall logged in 72 h	Rainfall logged in long term (P_{ac})	R calculated (*Pac* x *I72* h)	Proposed parameters for Warning	Proposed parameters for Alert
Jan/14	Recife / South Regional / Ibura	5*	28.2 mm	31.2 mm	879.84 mm^2	$I_{72\,h}$ = 60 mm or P_{ac} = 750 mm or R_{crit} = 45,000 mm^2	$I_{72\,h}$ = 60 mm and R_{crit} = 45,000 mm^2
Feb/22	Camaragibe / Area IV / Tabatinga	1	120.7 mm	335 mm	40,451.0 mm^2	$I_{72\,h}$ = 60 mm or P_{ac} = 750 mm or R_{crit} = 45,000 mm^2	$I_{72\,h}$ = 60 mm and R_{crit} = 45,000 mm^2
Jun/12	Recife / South Regional / Ibura	1	130.8 mm	1,472 mm	192,537.6 mm^2	$I_{72\,h}$ = 60 mm or P_{ac} = 750 mm or R_{crit} = 45,000 mm^2	$I_{72\,h}$ = 60 mm and R_{crit} = 45,000 mm^2
Jun/12	Jaboatão / Regional 2 / Carneiros Dois	3	142.5 mm	1,502 mm	214,035 mm^2	$I_{72\,h}$ = 80 mm or P_{ac} = 750 mm or R_{crit} = 60,000 mm^2	$I_{72\,h}$ = 80 mm and R_{crit} = 60,000 mm^2

*Fatalities due to the burst water mains owned by the state company.

of accumulation and the Rs logged on the date of the landslide events. This table shows that the fatal landslides were directly correlated to the high cumulative rainfall indices in 72 h, and higher than the parameters suggested for the warning state. The exception was the accident with five fatalities that occurred in the South Regional of Recife on January 14, after cumulative rainfall of 28.2 mm/72 h, lower than that proposed in this study (60 mm/72 h).

In the accident in the South Regional of Recife on January 14, the main triggering factor of this landslide was anthropic action; a water mains belonging to the state company, without repair and with leakages, caused the landslide by a concentrated burst of water killing five people from the same family. However, the accidents on June 12, 2009, with four fatalities, were caused by high cumulative rainfall indices of 72-h, long-term and high Rs, all higher than suggested for the Alert levels.

8. Conclusion

This paper addressed the general concepts, fundamental components and examples of landslides and the early warning system. From the results in this study, it was found that in the Metropolitan Region of Recife in Northeast Brazil landslides of occupied hillsides are closely related to the occurrence of concentrated rainfall in 72 h or less and associated with long-term cumulative rainfall. The parameters for an early warning system proposed in this study for civil defense actions is presented in Tables 2, 3 and 4 and in Fig. 13 (parameter follow-up graph). The majority of landslides occurred with parameters recommended for Alert. In Camaragibe, for example, 67% of the landslides occurred at that level, 29% with parameters suggested for the Warning level, and 4% with parameters recommended for the Observation level. Tables 2, 3 and 4 and Fig. 13 show that when the critical rainfall values suggested for $I_{72\,h}$ and R_{crit} were considerably higher, there was a sharp increase in the consequences. This fact suggests the need for future studies to determine different levels of Alert. The assessment of the performance of Alerts using the ROC analysis has proven very satisfactory in the Areas of Camaragibe. Although the proposal has been studied for only one year, assessments of landslide events a year later in the three municipalities studied were correlated to the parameters recommended in the study herein, confirming the validity of the suggested proposal. In short, considering the data, it has been possible to propose rainfall parameters for actions in the Metropolitan Region of Recife and, especially, for operating states of Warning and Alert.

References

Alheiros, M.M.; Lima Filho, M.F.; Monteiro, F.A.J. & Oliveira Filho, J.S. (1988) Depositional systems in the Barreiras Formation in the eastern northeast. Proc. Brazilian Congress of Geology, 35. Belém, 6 v. il. v. 2 pp. 753-760.

Alheiros, M.M.; Souza, M.A.A.; Bitoun, J.; Medeiros, S.M.G.M. & Amorim Junior, W.M.A. (2003) Manual of Hillside Occupation of the Metropolitan Region of Recife. Municipality of Recife, Pernambuco, Brazil (CD-ROM).

Bandeira, A.P. (2010) Technical Parameters for Landslide Risk Management of Hillside Areas in the Metropolitan Region of Recife. PhD Thesis. Department of Civil Engineering, University Federal of Pernambuco, Recife.

Bandeira, A.P. (2003) Landslides and Erosion Risk Map of the Hillsides of the Municipality of Camaragibe-PE. Master's Dissertation, Department of Civil Engineering, University Federal of Pernambuco, Recife.

Bandeira A.P.; Coutinho, R.C. & Alheiros, M.M. (2009) The importance of geological-geotechnical characterization and of rainfall for risk area management. Proc. V Brazilian Conference Slopes Stability. São Paulo, November, (CD-ROM).

Bandeira A.P.; Coutinho, R.C. & Alheiros, M.M. (2011) Landslides on hillsides in the municipality of Camaragibe, Pernambuco. Proc. 3rd Brazilian Symposium on Natural and Technological Disasters. São Paulo, November, (CD-ROM).

Bezerra, F.H.R.; Mello, C.L. & Suguio, K. (2006) The Barreiras Formation: recent knowledge and old questions. USP geology. Scientific series [online]. v. 6(2):III-VI.

Calvello, M. (2014) Landslide warning systems. Proc. Workshop Landslide History, Mechanisms & Controlling Variable: Scientific Basic for Risk Assessment. INCT-REAGEO, UFRJ, Rio de Janeiro - Brazil, pp. 18-24.

Coutinho, R.Q. (coord. & org. 2013) Parameters for geotechnical map and intervention measures of areas submitted to natural disasters. Technical Document, Ministry of Cities and GEP/UFPE Cooperation. Forthcoming Publication (in press).

Coutinho, R.Q.; Bandeira, A.P. & Silva, R.R. (2010) Technical report CNPq universal project: actions for risk reduction in hillsides of the Metropolitan Region of Recife. CNPq Universal Project - Process 472384 / 2007-4.

Coutinho, R.Q. & Bandeira, A.P.N. (2012a) Processes of hillside instability and landslide risk evaluation: case study in the municipalities of Recife and Camaragibe. Willy A. Lacerda; Ennio M. Palmeira; Ana Luiza Coelho Netto & Mauricio Ehrlich. (orgs.). Natural Disasters: Susceptibility and isk, Mitigation and Prevention, Management and Emergency Actions. COPPE/UFRJ, Rio de Janeiro, v. 1, pp. 41-61.

Coutinho, R.Q. & Bandeira, A.P.N. (2012b) Landslide risk area management: structural and nonstructural actions. Willy Alvarenga Lacerda; Ennio Marques Palmeira; Ana Luiza Coelho Netto & Mauricio Ehrlich. (Org.). Natural Disasters: Susceptibility and Risk, Mitigation and Prevention, Management and Emergency Actions. COPPE/UFRJ, Rio de Janeiro, v. 1, pp. 163-178.

Coutinho, R.Q. & Severo, R.N.F. (2009) Conference: Geotechnical investigation for hillside stability project. Proc. V Brazilian Conference Slopes Stability. São Paulo (CD-ROM).

EM-DAT - Emergency Events Database (2013) Available at: http://www.em-dat.net/. Accessed: March 17, 2013.

EM-DAT - Emergency Events Database (2012) Proc. The OFDA/CRED International Disaster Database. Available at: http://www.em-dat.net/. Accessed: Oct 10, 2012.

Fawcett, T. (2006) An introduction to ROC analysis. Pattern Recognition Letters, v. 27, p. 861-874.

Fell, R. & Hartford, D. (1997) Landslide risk management. Proc. Int. Workshop on Landslide Risk Assessment - Edited by Cruden & Fell, Published by Balkema, pp. 51-110.

Fell, R.; Corominas, J.; Bonard, C.; Cascini, L.; Leroi, E. & Savage, W. (2008) Guidelines for landslide susceptibility, hazard and risk zoning for land use planning. JTC-1 Joint Technical Committee on Landslides and Engineered Slopes. Engineering Geology, v. 102:83-111.

Fell, R.; Ho, K.K.S.; Lacasse, S. & Leroi, E. (2005) A Framework for Landslide Risk Assessment and Management. Proc. Int. Conf. on Landslide Risk Management - Edited by Hungr, Fell, Couture & Eberhardt, pp. 3-26.

FIDEM (1987) Development Foundation of the Metropolitan Region of Recife. Metropolitan Region of Recife: Basemap.

FIDEM (2006) Available at: http://www.cidades.gov.br. Accessed: Feb 3, 2010.

Girão, O. (2007) Analysis of the Erosion Process in Hillsides of the Southeast Zone of the Recife City. PhD thesis. Federal University of Rio de Janeiro, Rio de Janeiro, 305 p.

Gonçalves, N.M.S. (2003) Rainfall impacts and disorganization of the urban area in Salvador. In: Urban Climate. Monteiro, C.A.F. & Mendonça, F. (orgs), São Paulo, p. 192.

Gusmão Filho, J.A. (2001) The Historical Olinda City: Problems and Engineering Solutions. UFPE University Publisher, Recife, 193 p.

Gusmão Filho, J.A.; Jucá, J.M.T. & Justino da Silva, J.M. (1987) Groundwater effects on moving mechanisms in the hills of Olinda. Proc. 9th European Conference on Soil Mechanics and Foundation Engineering, Dublin, Ireland, v. l, pp. 431-434.

http://www.sistemaalerta-rio.com.br. Accessed March 27, 2013.

Intrieri, E.; Gigli, G.; Casagli, N. & Nadim, F. (2013) Landslide early warning system: toolbox and general concepts. Nat. Hazards Earth Syst. Sci., 13:85-90.

Macedo, E.S.; Santoro, J. & Araújo, R.E. (2004) Preventive plan of civil defense (PPCD) for landslides, state of São Paulo, Brazil. Proc. Brazilian Symposium of Natural Disasters. Florianopolis. pp. 908-919 (CD-ROM).

Macedo, E.S.; Ogura, A.T. & Santoro, J (1999) Civil defense and landslides: the preventive plan for São Paulo coastline. Proc. 9th Brazilian Congress of Engineering Geology. São Paulo. ABGE.

UNISDR (2009) ISDR: Terminology. http://www.unisdr.org/eng/library/lib-terminology-eng%20home.htm.

Tavares, R.; Sant'anna Neto, J.L.; Tommaselli, J.T.G.; Pressinotti, M.M.N. & Santoro, J. (2004) Analysis of the temporal and spatial variability of the rainfall associated with landslides in the North coastline of São Paulo. Proc. Brazilian Symposium of Natural Disasters. Florianopolis. GEDN/UFSC, pp. 680-696 (CD-ROM).

Influence of Soil Cracking on the Soil-Water Characteristic Curve of Clay Soil

M.M. Abbaszadeh, S.L. Houston, C.E. Zapata

Abstract. The hydraulic conductivity for unsaturated soil conditions is more difficult to estimate than for the saturated condition. In addition, as the soil transitions from intact to cracked, the difficulty in estimating the unsaturated hydraulic conductivity increases. One critical step in the determination of unsaturated flow hydraulic conductivity is the evaluation of the Soil-Water Characteristic Curve (SWCC). In this paper, a series of laboratory studies of direct measurements of cracked soil SWCCs is presented, including challenges associated with the control of very low suction levels associated with crack dewatering. An oedometer-type SWCC apparatus, capable of suction and net normal stress control, and volume change measurement, was used in these experimental studies. It is common that SWCCs are comprised of matric suction values below about 1500 kPa, and total suction values for suctions higher than about 1500 kPa (Fredlund *et al.*, 2012). In this study, all measured or controlled suction values were less than 1500 kPa and obtained using the axis translation method, and the curve in the higher suction range was projected by forcing the SWCC through 10^6 kPa for completely dried conditions (Fredlund *et al.*, 2012). Volume change corrections were made to the reported volumetric water contents, which is of particular importance when the soil under consideration undergoes volume change in response to wetting or drying. A technique for the determination of the SWCC for cracked clay soils is presented. Test results validated the fact that the SWCC of a cracked soil can be represented by a bimodal function due to the Air Entry Value (AEV) of the cracks being much lower than the AEV of the soil matrix. It was also found that differences between the SWCC for cracked and intact soil appears only in the very low suction range.

Keywords: SWCC, cracked soil, unsaturated soil mechanics, air entry value, bimodal behavior, laboratory testing.

1. Inroduction

The problem of estimating ground surface flux is one of great interdisciplinary interest, and the literature is replete with related articles from disciplines including soil science, geotechnical engineering, environmental ecology, hydrology, water resources, forestry, landscape architecture, geology, and environmental engineering. Surface flux is related to complex interrelationships between the soil and atmosphere, and soil anomalies such as cracks must be appropriately considered in any surface flux modeling process. However, there is little data available for the assessment of the effect of cracks on unsaturated flow related properties, such as the Soil-Water Characteristic Curve (SWCC) and the hydraulic conductivity function.

The properties and behavior of unsaturated cracked soil are potentially different from those of intact soil, and the absence of direct test data on cracked soil properties leads to uncertainty in the evaluation of surface flux conditions. It is important to develop an improved understanding of cracked soil properties because seasonal cracking of soil results in poor estimates of runoff and infiltration due to the changing soil storage conditions (Arnold *et al.*, 2005).

The primary focus of this paper is to present laboratory data for cracked and intact clay SWCCs. An oedometer pressure plate device was used so that the overall volume change of the soil specimens could be tracked during the experiment. The laboratory SWCC data presented in this paper also contributes to the previously proposed idea of use of bimodal characteristic of fractured soils and gap graded granular soils (Zhang & Fredlund, 2004; Zhang & Chen, 2005; Fredlund *et al.*, 2010a; Booth *et al.*, 2013). In this study, a bimodal SWCC is obtained for a cracked expansive clay. Previously developed models for bimodal SWCCs were for gap-graded granular soils and for fractured rock (Zhang & Fredlund, 2004; Zhang & Chen, 2005). For gap graded granular soils the assumption in modeling is that the volume of the soil (including the relative porosity of both the finer and coarser fractions) does not change. Similarly, in the study of fractured rock, the volume of the fractures and the volume of the intact rock matrix can reasonably be assumed to remain constant. Booth *et al.*, 2013, applied similar no-volume-change assumptions to London clay and showed promising results. However, the laboratory results of this study are for a moderately expansive clay, and provide much needed data for consideration of the effect of soil cracks on unsaturated soil property models for the case where the volume change in the cracks, and the soil matrix itself, may not be negligible.

Mohammad M. Abbaszadeh, Ph.D., Senior Geotechnical Engineer, MWH Americas, Tempe, AZ, USA. e-mail: sam.abbaszadeh@mwhglobal.com.
Sandra L. Houston, Ph.D., Professor, Arizona State University, Tempe, AZ, USA. e-mail: sandra.houston@asu.edu.
Claudia E. Zapata, Ph.D., Associate Professor, Arizona State University, Tempe, AZ, USA. e-mail: claudia.zapata@asu.edu.
Submitted on November 11, 2013; Final Acceptance on April 2, 2015; Discussion open until December 31, 2015.

2. Background

A soil water characteristic curve (SWCC), also known as water retention curve, represents the relationship between soil suction and the amount of water that the soil can hold at that particular suction, which can be expressed in terms of moisture content or degree of saturation. Relationships for estimating the hydraulic conductivity function for unsaturated soils based on the SWCC are commonly used, but have not been thoroughly evaluated for cracked soils through laboratory testing. The measurement of the hydraulic conductivity for an unsaturated soil is extremely difficult, and the existence of cracks further complicates the measurement. For this reason, the SWCC has been used to predict the hydraulic conductivity of a cracked material (Peters & Klavetter, 1988; Mallant *et al.*, 1997; Köhne *et al.*, 2002; Liu *et al.*, 2004; Zhang & Fredlund, 2004; Li *et al.*, 2011). Thus, one challenge for predicting the hydraulic conductivity of cracked soil is determining the SWCC for such soils. Once the SWCC is established, it is likely that one of several existing predictive models can be used to estimate the unsaturated hydraulic conductivity function for a cracked soil.

Few researchers have attempted to directly measure the SWCC for cracked materials, although some researchers have studied cracked clay SWCCs. Among those, Chertkov & Ravina (2000) studied the shrinking-swelling behavior of clay including a network of capillaries to represent cracks in the soil. The SWCC for the cracked soil was determined by modeling, rather than through laboratory testing; the models used incorporated the total crack volume and the volume of water-filled cracks, and the van Genuchten-Mualem model for estimating the unsaturated hydraulic conductivity function (van Genuchten, 1980). In other modeling efforts, Liu & Bodvarsson (2001) studied the use of the van Genuchten (1980) and Brooks & Cory (1964) SWCC models for the hydraulic conductivity of a fractured rock.

Zhang & Fredlund (2004) discussed that a fractured rock will produce a bimodal SWCC with a matrix phase and a fracture phase. The Soil-Water Characteristic Curve of the fractured rock was presented as the sum of the effects of the two phases, weighted according to their respective porosities. The combined matrix and fracture medium was treated as a continuum, with the same suction applied to the combined material and to the individual fracture and matrix phases. A computed Soil-Water Characteristic Curve for the rock matrix, the fractures, and the entire fractured rock mass is shown in Fig. 1 (Modified from Zhang & Fredlund, 2004). The first AEV belongs to the fractured media and the second AEV belongs to the intact (non-fractured) media. Taking a similar continuum approach to cracked soils, the Soil-Water Characteristic Curve of a cracked clay might be expected to take on a bimodal character. Several mathematical models for the SWCC are available that allow for a bimodal SWCC representation of the SWCC (Durner, 1994; Burger & Shackelford, 2001; Gitirana & Fredlund, 2004; Zhang & Chen, 2005), however none of these take into consideration volume change of the cracks and the intact matrix.

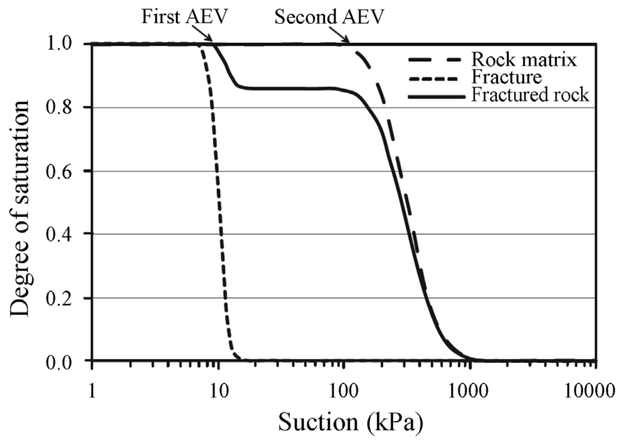

Figure 1 - Typical Bimodal SWCC for Cracked Soil (Modified from Zhang & Fredlund, 2004).

Fredlund *et al.* (2010b) provided numerical modeling results for a slab on ground foundation on expansive soils, with the cracked clays near the ground surface modeled using a bimodal SWCC, such as that shown in Fig. 1. Booth *et al.* (2013) showed that using bimodal SWCC and hydraulic conductivity function in numerical modeling of the hydrology of a cracked soil results in more accurate predictions of the matric suction. However, no supporting laboratory data was available for validation of the bimodal SWCC models used, and as previously discussed, available bimodal models do not consider volume change, either quantitatively or through direct measurement.

A capillary model, based on crack geometry, has been used to determine the air-entry value corresponding to the desaturation of the cracks in clays, along with supporting laboratory data (Abbaszadeh *et al.*, 2010). Li *et al.* (2011) employed the same theoretical capillary-model based relationship proposed by Abbaszadeh *et al.* (2010), and reported 11.8-millimeters (mm) as the maximum crack size for which the capillary model is applicable. Li *et al.* (2011) also suggested a method to predict the SWCC and permeability function for cracked soil considering crack volume change during drying-wetting cycles. The authors argued that the crack development can be explained by a relationship between the matric suction and crack porosity differences, Li *et al.* (2011) present a three-dimensional SWCC model wherein the bimodal behavior of the cracked soil appears as the crack porosity increases. The method used by Li et al. requires that the relationship between the crack porosity and suction be established. The authors suggest the use of a linear relationship, which has not been demonstrated across a wide range of soil types and suction values or through direct measurement. Clearly, there is a need for further research on the behavior of cracked clays for which the matrix and the crack volume change with change in soil suction. The data presented in this paper represents a start on development of a database required for refinement of SWCC models for cracked expansive clays.

3. Material and Laboratory Testing Program

Five SWCC tests were conducted for intact soil entailing both drying (3 tests) and wetting (2 tests) paths. Replicate tests were performed so that average curves could be developed for comparison of cracked to intact soils. The averaging of data helps to remove some of the effects of natural sample variability. In addition, six SWCC tests were conducted for cracked soil, four of which followed the drying path and two followed the wetting path. These experiments were conducted under two confining stress levels: (1) essentially zero, and (2) 20 kPa net normal stresses. When zero normal stress was desired, a token load of about 1 to 3 kPa was applied in order to maintain the specimen in contact with the ceramic stone. The net normal stress was varied to simulate very near-surface soils and soils of depth of approximately 1-meter which is a common depth of mitigation for expansive clay profiles. An oedometer-type pressure plate device (Perez-Garcia *et al.*, 2008) was used to obtain the SWCC and the hanging manometer technique was used to apply very low matric suctions required to capture the AEV of the crack. The oedometer-type pressure plate device is essentially a pressure plate cell that is outfitted with a loading piston to apply a net normal stress to a specimen that is restrained from radial deformation by a confining ring. A Linear Variable Displacement Transducer (LVDT) can be attached to the loading piston so that vertical deformations are measured as suction is changed. Suction values are controlled by the axis translation method. The hanging manometer was required to apply a very low suction value to the specimen because pressures lower than about 5 kPa cannot be consistently maintained with traditional pressure regulators.

3.1. Soil characteristics

The soil used in this study was obtained from a site near San Diego, California, and is named San Diego Soil in this paper. The index properties of the test soil are presented in Table 1.

3.2. Sample preparation

Identical companion specimens were compacted in three equal layers inside brass rings of 25-mm in height and 61-mm in diameter. The compaction condition corresponded to 98% of Standard Proctor maximum dry density (1.74 g/cm^3) and optimum water content (18%). Prior to sample preparation, the soil was first passed through a U.S. #4 sieve (4.76-mm), and then enough water was added to reach to the optimum water content of 18%. The soil was then sealed in plastic bags for at least 48 h before starting the sample compaction. This process allowed the water to equilibrate throughout the soil so that the moisture would be distributed more uniformly in the test specimen. After compaction of each layer was completed and just before compacting the next layer, the top surface of the preceding layer was scarified using a sharp tool. The scarification created a better contact between the two layers and produced a more uniform compacted specimen. During the compaction of the last (third) layer, care was taken not to over-compact the specimen. Any minor adjustments required in the computation of specimen dry density were made. In spite of careful control of the method of specimen preparation, some sample variability will exist. For this reason, duplicate tests were performed so that average SWCC curves of cracked and intact specimens could be compared.

To manufacture the cracked specimens, after the sample was compacted inside the brass ring, soil cracks were introduced into the soil matrix using an aluminum shim.

Table 1 - Characteristics for San Diego soil.

Specific Gravity (ASTM D854-06)		2.72
Particle Size Analysis (ASTM D422-63 (Reapproved 2007))	% Sand	63
	% Silt	30
	% Clay	7
Unified Soil Classification System (ASTM D2487-06)		SC
Atterberg Limits (ASTM D4318-05)	LL	41
	PL	17
	PI	24
Standard Proctor Test (ASTM D698-07)	Optimum water content	18%
	Maximum Dry Density (g/cm^3)	1.74
Expansion Index (ASTM D4829-08)		114

The cracks were approximately 1-mm wide and 10-mm deep. The total volume of cracks was measured, as a percentage of the overall specimen volume, to be about 3 to 5%. The volume of cracks was decided based on the results of a companion study that was conducted with the same soil to evaluate the extent of natural crack formation due the drying and wetting cycles. From this study, it was concluded that the total volume of cracks in the field was about 3-5% of the overall volume of the clay (Abbaszadeh, 2011).

Based on a thorough literature review, a crack pattern consistent with field crack observations was selected. Due to the extremely complex process of soil cracking, it is almost impossible to generalize or choose one crack pattern which forms in all desiccated soils. However, it was concluded that a hexagon pattern was the most appropriate pattern because it was relatively consistent with actual crack patterns observed in near-surface clays. This finding is also consistent with the conclusion of Konrad & Ayad (1997), who suggested a polygon crack pattern develops during different stages of cracking (Fig. 2), as well as the observed field cracks reported by Longwell (1928) as shown in Fig. 3.

There are several uncertainties associated with crack behavior in response to wetting and drying (*i.e.* suction change). For example, the extent of crack healing during wetting and the opening of cracks during drying are not entirely predictable. To exhibit the SWCC bimodal behavior, the cracks must be initially fully saturated, but must be wide enough so they will not heal completely, due to swelling of the soil, upon saturation. Further, the cracks must be small enough in width to prevent desaturation by gravity drainage. The size of cracks selected for laboratory study must also be consistent with cracks that form in the field. Based on laboratory observations on the test soil of this study, and also based on literature review related to the size of cracks in the field, an appropriate crack width for this study was determined to be about 1 to 1.5-mm. This range of crack width falls within the range of crack widths observed in the field (Ruy *et al.*, 1999), and corresponds to a crack size that does not drain under gravity alone or fully close due to swelling upon wetting. For the test soil, cracks of 1.1 to 1.3-mm width were observed to shrink to about 0.7 to 0.8-mm width after specimen saturation. Figure 4 shows an example of a cracked sample at the end of the specimen preparation process. The crack widths varied from 1.1 to 1.3-mm in this study due to difficulties in making exactly identical cracks in the soil specimens.

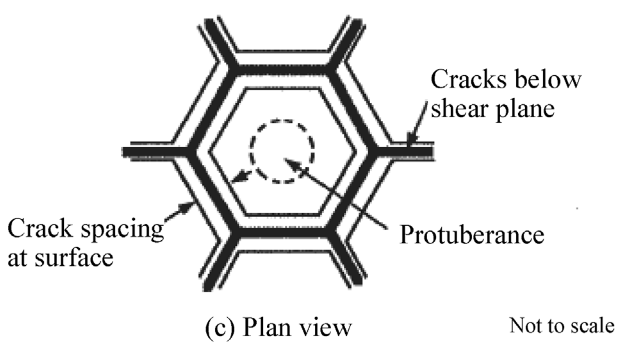

Figure 2 - Potential crack polygon (from Konrad & Ayad, 1997).

Figure 3 - Potential crack polygon (from Konrad & Ayad, 1997, after Longwell, 1928).

3.3. Test procedure

To obtain the drying path SWCC, the sample was saturated by submerging the specimen inside a water tray, and both ends of the soil sample were covered by one filter paper directly in contact with the soil surface, followed by a porous stone in contact with the filter paper. This process prevented loss of soil during the swelling and saturation phase and also facilitated the infiltration of water through the porous stones. For the wetting path SWCC, the specimen was air-dried until it reached the water content range corresponding to the desired initial suction for the test; equilibration time was allowed after the specimen reached the initial (starting) value of soil suction for the test.

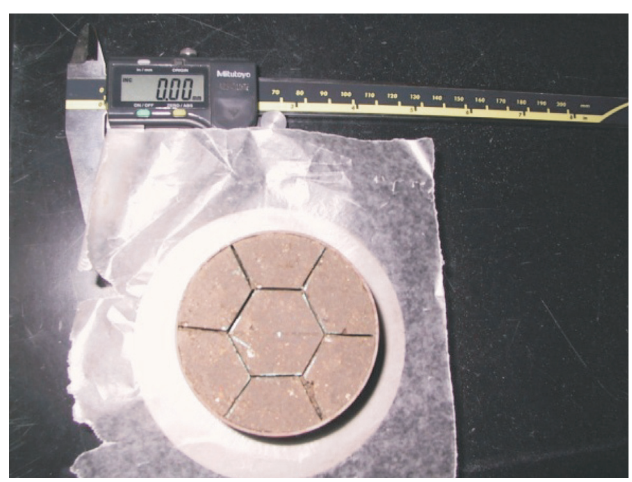

Figure 4 - Artificially cracked specimen with hexagonal pattern used for SWCC determination in the laboratory.

The axis translation technique was used to apply various levels of matric suction for SWCC determination. The hanging manometer technique was used, in accordance with ASTM D6836-02, to apply very low suction pressures. The hanging manometer technique involves creating a negative pore water pressure (u_w) at the base of the specimen, while keeping the pore air pressure (u_a) constant and equal to atmospheric pressure inside of the oedometer pressure plate device. This will result in an applied matric suction equal to the value of the negative pore water pressure imposed by the hanging manometer by positioning the water level in the tube at a lower elevation than the based on the specimen. For example, to apply 0.1 kPa matric suction, the elevation difference between the water level in the tubes and the cell base (where the sample rests) should be equal to 1.0 cm. Figure 5 schematically illustrates the hanging manometer technique.

One of the major difficulties associated with setting a fixed low suction value is the continuous elevation change of the water that occurs inside the tube as the specimen seeks equilibration with the target applied suction. Thus, the applied suction changes as the water elevation in the tube is allowed to change. To maintain the small target applied suction constant, close monitoring is required (if overflow of excess water from the tube is not allowed or is water tends to move into the specimen). This monitoring can be tedious in consideration of the lengthy test times required for equilibration for highly plastic soils.

Another issue which makes testing at very low suctions challenging is that it is not possible to fully saturate the intact portion of the specimen because back-pressure saturation techniques are not easily employed in pressure plate testing. In the laboratory tests of this study, it was observed that although initial crack dewatering typically occurred rather quickly, under very low suctions some samples started to absorb water after the initial crack dewatering process. It is believed that water uptake by the specimen at very low suctions and after crack dewatering, is a result of the incomplete saturation of the intact matrix of the soil, in spite of the cracks having been filled with water and the specimen having been submerged for an extensive time during the pre-test saturation of the specimen. In other words, at early stages of the test under very low applied matric suction, when the cracks are still full of water, the cracks in the soil dominate the behavior; however, at values of suction greater than that required for crack dewatering, the intact soil matrix (not 100% saturated, and having some remaining matric suction) dominates the response. Table 2 summarizes conditions for the SWCC tests that were conducted for cracked specimens.

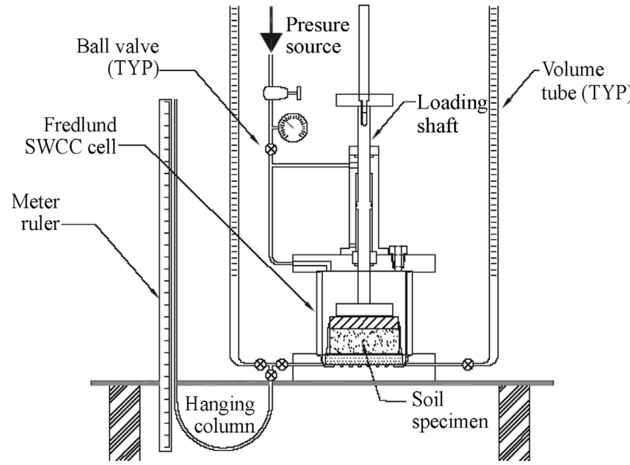

Figure 5 - Hanging manometer technique used to obtain the SWCC at very low suction values (from GCTS, Inc.).

Although volume change measurements were made in the course of SWCC measurements for this study, the volume change behavior of the soil was not explicitly ad-

Table 2 - Test characteristics for cracked and intact specimens – San Diego soil.

Test ID	Test type	Applied suction* (kPa)	Applied normal stress (kPa)
Intact-01	Drying	10, 90, 200, 450, 1240	0
Intact-02	Drying	25, 100, 200, 450, 1240	0
Intact-03	Drying	8, 50, 265, 480, 1240	0
Intact-04	Wetting	1320, 320, 140, 35	0
Intact-05	Wetting	1320, 320, 140, 35	20
Cracked-01	Drying	0.1, 1.0, 25, 90, 200, 485, 1240	0
Cracked-02	Drying	0.075, 1.035, 8.0, 30, 90, 345, 1240	0
Cracked-03	Drying	0.075, 0.555, 1.46, 10, 25, 90, 565, 1240	0
Cracked-04	Drying	0.09, 0.78, 10, 45, 100, 200, 425, 1260	0
Cracked-05	Wetting	1255, 290, 100, 35	0
Cracked-06	Wetting	1255, 290, 100, 36	20

* Suction values less than 5 kPa were obtained using a hanging manometer device

dressed here; nonetheless, volume change of the cracks did occur during both wetting and drying, and volume change of the clay matrix also occurred, and the impact of volume change was captured phenomenologically in the test data. Hence, the cracks did not have a constant porosity throughout the test and the soil matrix did not have a constant porosity, but the volume changes of the specimen matrix and cracks are reflected in the directly measured SWCC data (and associated directly measured AEV). In general, volume change should be expected when soil suction is changed, particularly for swelling, high plasticity soils. In expansive clays, the presence of cracks provides a cavity for expansion that reduces vertical heave and swell pressure. Abbaszadeh (2011), provides data, including data on the clay of this present study, showing that cracks decrease swell pressure and heave of expansive clays.

4. Results

A total of five SWCC experiments were conducted for intact specimens. Three of these tests followed drying paths and the other two followed wetting paths. The SWCC results for the drying and wetting tests on intact specimens of San Diego soil are presented in Fig. 6. The values of volumetric water content at the lowest plotted suction value (0.01 kPa) were estimated to be equal to the directly calculated values for the specimens at zero suction. This was done due to the necessity of plotting suction on a log scale.

A total of six SWCC tests were conducted on cracked specimens prepared by compaction of San Diego soil. Four of these tests followed drying paths and the other two followed wetting paths. The SWCC test results of the cracked specimens are presented in Fig. 7, including both wetting and drying paths. Although it is difficult to draw a single curve representing the entire data set, the data shown in Fig. 7 demonstrates the bimodal behavior of the SWCC for the cracked samples.

Quantification of a bimodal SWCC for cracked soil is difficult to accomplish for a variety of reasons, not the least of which is the difficulty in controlling the required extremely small suctions for observing the AEV associated with crack dewatering. Nevertheless, it was possible to bracket the AEV on a test specimen. The specimen was prepared with cracks of an initial width, w_c, of about 1.1 to 1.3-mm and a depth, h_c, of about 10-mm. After wetting the specimen to essentially saturation, a slight closing of the cracks to a width of about 0.75-mm was observed. A value of $u_a - u_w$ of 0.075 kPa was applied in the oedometer-type SWCC cell and the specimen was allowed to equilibrate. It was directly observed, by disassembly of the pressure plate cell, that a few of the cracks showed signs of starting to

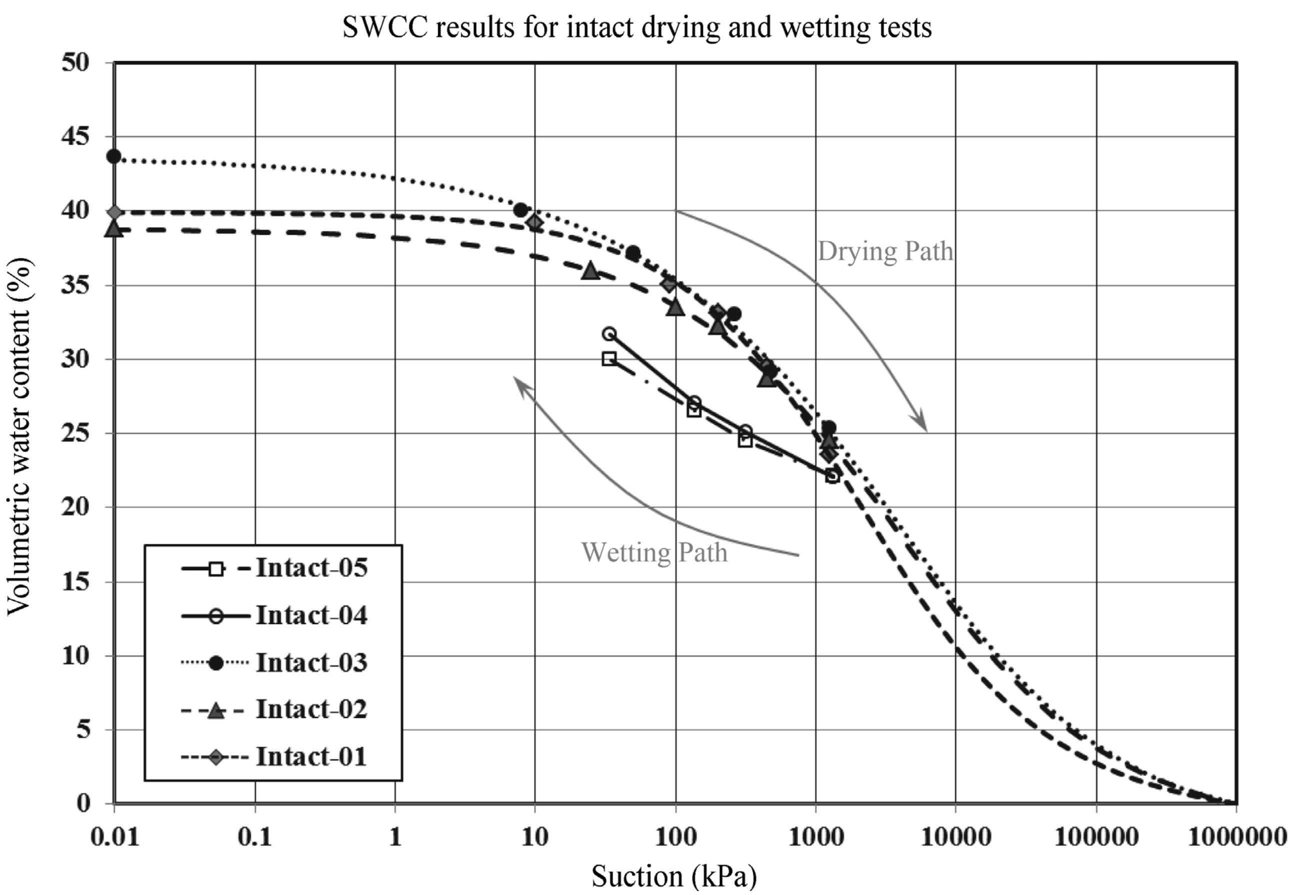

Figure 6 - Summary of SWCC test results for intact drying and wetting tests - San Diego soil.

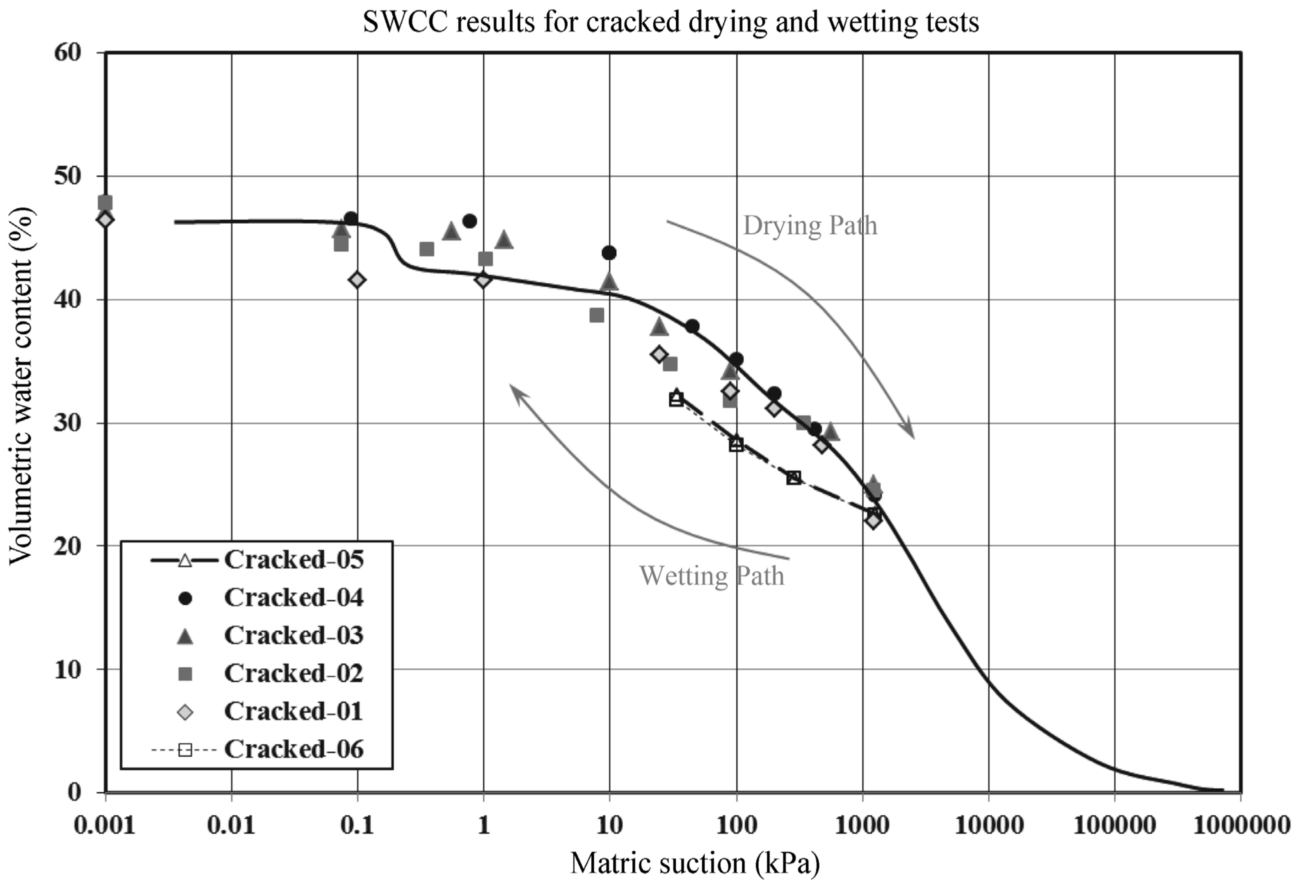

Figure 7 - Summary of SWCC test results for intact drying and wetting tests-San Diego soil.

dewater at 0.075 kPa suction (Cracked-02 and Cracked-03 specimens). Direct examination of the cracks was also performed after equilibration at 0.09 to 0.1 kPa suction (Cracked-01 and Cracked-04 specimens), and the cracks were found to be more or less completely dewatered. Thus, the u_a - u_w causing initiation of dewatering was somewhere between 0.075 kPa and 0.1 kPa, experimentally, and perhaps closer to 0.07 kPa. This is consistent with the theoretical calculations of Abbaszadeh *et al.* (2010) wherein a capillary model was used to estimate the air entry value of cracks, and cracks of 0.75-mm width were found to dewater at a value of u_a-u_w of about 0.07 kPa.

4.1. Effect of overburden pressure

The effect of overburden stress, for the limited stress range considered in this study, was negligible. An overburden stress of 20 kPa, the highest stress considered in this study, corresponds to approximately 1-meter depth. Many field cracks are observed to be of limited depth, such that an overburden stress of 20 kPa is reasonable for the SC soil of this study. However, field cracking and weathering of high plasticity clays has been observed to depths of approximately 10-meter. The tests in this study were performed using hanging dead weights to achieve net normal stress, and therefore higher values of net normal stress were not practical. Therefore, further testing at higher overburden stress is required to make definitive statements concerning the impact of net normal stress on the SWCC of cracked clay.

4.2. Comparing SWCCs for intact and cracked specimens

The purpose of performing SWCC tests for intact and cracked specimens was to evaluate the effect of soil cracking on the water retention properties of the expansive soil of this study. Figure 8 compares the best-fit (using all test results) SWCCs for intact and cracked specimens for the drying path. Averaged curves (*i.e.* curves obtained using all test specimen data) were used for making a better comparison between intact and cracked specimens due to the inevitable sample variability that occurs in specimen compaction and crack creation, as well as all other variables associated with the SWCC test procedure itself.

From Fig. 8, it can be concluded that the significant difference between the SWCC for cracked and intact soil is only at very low suction range. The cracked soil exhibits bimodal behavior which can be explained by the pore space disparity that the cracks create in the matrix structure of the soil. In other words, at very low suctions the cracks will dewater, but the much smaller voids in the intact soil matrix will not dewater. However, at higher suctions the SWCC of

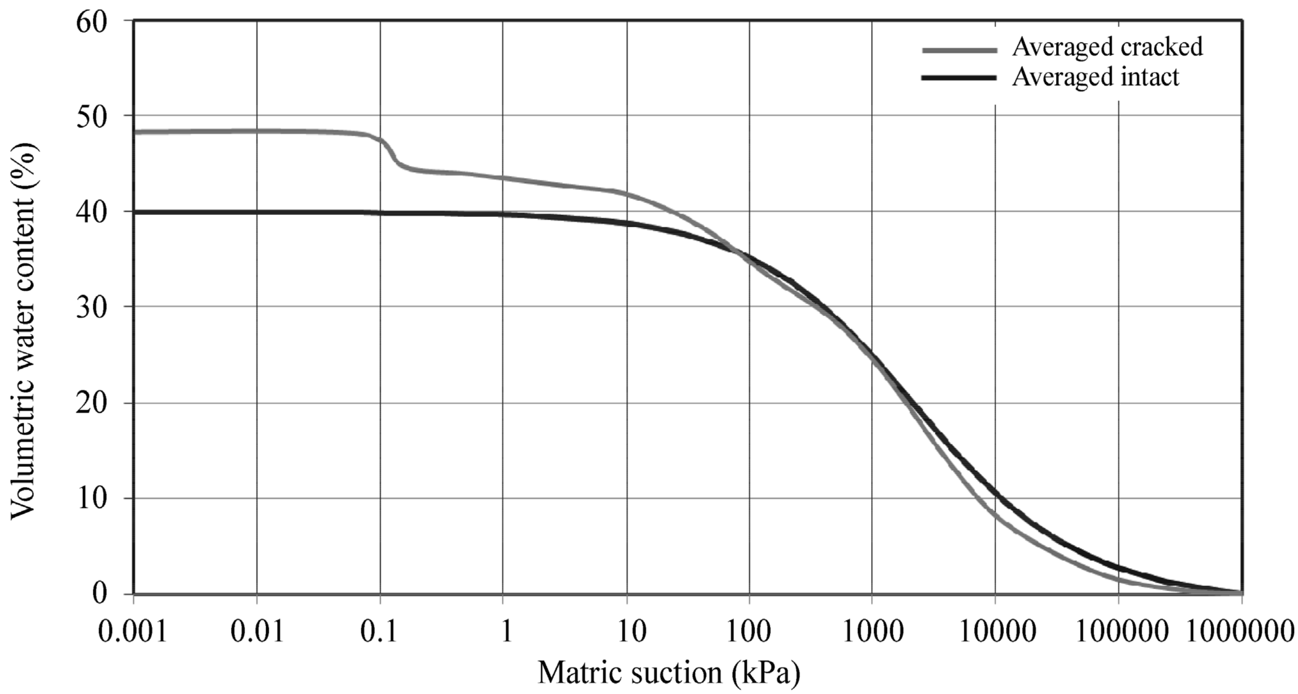

Figure 8 - Comparison between cracked and intact averaged SWCCs for San Diego soils.

the cracked soil is controlled by the intact matrix. Thus, after a certain matric suction range, the water storage capacity of the intact and cracked soils tend to merge.

The suction range at which the cracked and intact SWCC curves merge depends entirely on the crack dimensions. The fact that the cracked and intact clay SWCCs merge at very low values of matric suction (associated with the width of the crack), represents a significant finding for geotechnical engineering field applications because many unsaturated soils problems of a practical nature involve unsaturated conditions where the soil suction is much higher than the AEV of cracks typical of field conditions.

5. Summary and Conclusion

The effect of soil cracking on the SWCC of soil was investigated through laboratory testing. Both wetting and drying paths were studied. The effect of net normal stress on the SWCC test results was also considered. A hexagonal crack pattern was adopted for the cracked clay specimens as being a reasonable pattern for field conditions based on literature review.

The hanging manometer technique was implemented in order to apply and maintain very low matric suctions required for capturing the AEV of the cracked samples. Experimental results showed that the SWCC for a cracked soil can be represented by a bimodal curve. However, the AEV of the cracks is very low, even for the relatively small crack widths considered in this laboratory study. Dewatering of larger field cracks would be expected to occur at extremely low suction values, and larger cracks may dewater under gravity alone. Because cracks dewatered at a very low AEV, the SWCCs of intact and cracked clays at suctions greater than the AEV of the cracks were found to be very similar (*i.e.* were found to essentially merge).

The net normal stress values applied during the measurement of SWCCs in this study corresponded to soil depths of 0 to 1-meter, and some additional testing at higher net normal stress values is recommended for future study. Further, the crack sizes studied in this research represent the lower range of crack width dimensions found in the field. Consequently, for field applications where the soil remains unsaturated, a cracked soil could rationally be modeled using the properties of the intact matrix, and ignoring the bimodal behavior at very low suction values. However, for field applications where the ground surface becomes saturated and extremely low suction to positive pore water pressures develop, the impact of cracks can, of course, be dramatic with regard to the amount of water entering the subsurface. Thus, it is critical to keep in mind that although the unsaturated soil SWCC for cracked and intact specimens is essentially the same over a wide range of suction values of interest for unsaturated soil mechanics problems, saturated flow properties of cracked and intact specimens are quite different.

The findings of this study provide support treating cracked soil as a continuum for unsaturated flow conditions, using lumped parameters for the cracked soil mass. This is because when the soil remains in an unsaturated state, the dominant flow of water is through the soil matrix, rather than through the cracks, which have been shown to dewater at very low suction values. However, for saturated-unsaturated flow problems, such as when the ground surface becomes saturated and positive pore water pressures develop, it is possible that the cracks within the soil are best modeled as discrete elements to avoid sharp discontinuities in the unsaturated soil property functions at the AEV of the cracks. Additional research on numerical modeling of flow through cracked soils is needed.

Acknowledgments

This study was supported by the National Science Foundation (NSF) under grant number CMMI-0825089. The opinions, conclusions, and interpretations expressed in this paper are those of the authors, and not necessarily of NSF.

References

Abbaszadeh, M.M.; Houston, S.; Zapata, C.; Houston, W.; Welfert, B. & Walsh, K. (2010). Laboratory determination of soil water characteristic curves for cracked soil. Unsaturated Soils. Alonso and Gens (eds) Proceedings of the International Conference for Unsaturated Soils, Barcelona, Spain, pp. 409-415.

Abbaszadeh, M.M. (2011). The Effect of Cracks on Unsaturated Flow and Volume Change Properties of Expansive Clays and Impacts on Foundation Performance. Ph.D. Dissertation, Department of Civil and Environmental Engineering, School of Sustainable Engineering and Built Environment, Arizona State University, Tempe, 256 p.

Arnold, J.G.; Potter, K.N.; King, K.W. & Allen, P.M. (2005). Estimation of soil cracking and the effect on surface runoff in a Texas Blackland Prairie Watershed. Hydrol Process, 19(3):589-603.

ASTM (2006). Standard Practice for Classification of Soils for Engineering Purposes (Unified Soil Classification System) - D2487. ASTM International, West Conshohocken, Pennsylvania, USA. DOI: 10.1520/D2487-00.

ASTM (2007). Standard Test Methods for Particle-Size Analysis of Soils - D422. ASTM International, West Conshohocken, Pennsylvania, USA. DOI: 10.1520/D0422-63R07.

ASTM (2005). Standard Test Methods for Liquid Limit, Plastic Limit and Plasticity Index of Soils - D4318. ASTM International, West Conshohocken, Pennsylvania, USA. DOI: 10.1520/D4318-00.

ASTM (2011). Standard Test Method for Expansion Index of Soils - D4829. ASTM International, West Conshohocken, Pennsylvania, USA. DOI: 10.1520/D4829-11.

ASTM (2002). Standard Test Methods for Determination of the Soil Water Characteristic Curve for Desorption Using Hanging Column, Pressure Extractor, Chilled Mirror Hygrometer, or Centrifuge - D6836. ASTM International, West Conshohocken, Pennsylvania, USA. DOI: 10.1520/D6836-02R08E02.

ASTM (2000). Standard Test Methods for Laboratory Compaction Characteristics of Soil Using Standard Effort (12,400 ft-lbf/ft3) - D698. ASTM International, West Conshohocken, Pennsylvania, USA. DOI: 10.1520/D698-00a.

ASTM (2006). Standard Test Methods for Specific Gravity of Soil Solids by Water Psychrometer - D854. ASTM International, West Conshohocken, Pennsylvania, USA. DOI: 10.1520/D854-06.

Booth, A.J.; El-Hamalawi, A. & Dixon, N. (2013). Modeling suctions in a cutting with a bimodal soil water characteristic curve and hydraulic conductivity function. Proceedings of Geo-Congress 2013, ASCE, San Diego, pp. 402-412.

Brooks, R.H. & Corey, A.T. (1964). Hydraulic properties of porous media. Colorado State University, Fort Collins, Hydrology Paper No. 3, 24 p.

Burger, C.A. & Shackelford, C.D. (2001). Soil-water characteristic curves and dual porosity of sand-diatomaceous earth mixtures. J. of Geotechnical and Geoenvironmental Engineering, ASCE, 127(9):790-800.

Chertkov, V.Y. & I. Ravina. (2000). Shrinking-swelling phenomenon of clay soils attributed to capillary-crack network. Theoretical and Applied Fracture Mechanic, 34(1):61-71.

Durner, W. 1994. Hydraulic conductivity estimation for soil with heterogeneous pore structure. Water Resources Research, 30(2):211-223.

Fredlund, D.G.; Vu, H.Q. & Stianson, J. (2010a). Engineering Protocols for the Assessment of the Net Moisture Flux at the Ground Surface. Geotechnical Engineering Journal of the SEAGS and AGSSEA, 41(4):1-11.

Fredlund, D.; Houston, S.; Nguyen, Q. & Fredlund, M. (2010b). Moisture Movement Through Cracked Clay Soil Profiles. Geotech. Geol. Eng., 28(6):865-888.

Fredlund, D.; Rahardjo, H. & Fredlund, M. (2012). Unsaturated Soil Mechanics in Engineering Practice. John Wiley & Sons, New York, 944 p.

GCTS, http://www.gcts.com/pdf/productos/soil-water_spec_211112_073936.pdf.

Gitirana, Jr. G. & Fredlund, D.G. (2004). Equations for the soil-water characteristic curve based on meaningful and mathematically independent parameters. ASCE J. of Geotechnical and Environmental Engineering, 130(2):209-212.

Köhne, J.M.; Köhne, S. & Gerke H.H. (2002). Estimating the hydraulic functions of dual-permeability models from bulk soil data. Water Resources Research, 38(7):1121-1132.

Konrad, J.M. & Ayad R. (1997). Desiccation of a sensitive clay: field experimental observations. Can. Geotech. J., 34(6):929-942.

Li, J.H.; Zhang, L.M. & Li, X. (2011). Soil-water characteristic curve and permeability function for unsaturated cracked soil. Can. Geotech. J., 48(7):1010-1031.

Liu, H.H. & Bodvarsson, G.S. (2001). Constitutive relations for unsaturated flow in a fracture network. J. of Hydrology, 252(1):16-25.

Liu, H.H.; Bodvarsson, G.S. & Finsterle, S. (2004). A note on unsaturated flow in two-dimensional fracture networks. Technical Note. Earth Sciences Division. Lawrence Berkeley National Laboratory. Univ. of Calif., Berkeley.

Longwell, C.R. (1928). Three common types of desert mud cracks. America Journal of Soil Science, 5th Series, XV:136-145.

Mallant, D.; Tseng, P.H.; Torde, N.; Timmerman, A & Feyen, J. (1997). Evaluation of multimodal hydraulic function in characterizing a heterogeneous field soil. J. of Hydrology, 195(1):172-199.

Perez-Garcia, N.; Houston, S.; Houston, W. & Padilla, J.M. (2008). An Odometer-Type Pressure Plate SWCC Apparatus. ASTM Geotech. Testing Journal, 31(2):115-123.

Peters, R.R. & Klavetter, E.A. (1988). A continuum model for water movement in unsaturated fractured rock mass. Water Resources Research, 24(3):416-430.

Ruy, S.; Di Pietro, L. & Cabidoche, Y.M. (1999). Numerical modelling of water infiltration into the three components of porosity of a vertisol from Guadeloupe. Journal of Hydrology, 221(1-2):1-19.

van Genuchten, M.Th. (1980). A closed form equation for predicting the hydraulic conductivity of unsaturated soils. Soil Sci. Soc. Am. J., 44(5):892-898.

Zhang, L. & Fredlund, D.G. (2004). Characteristics of water characteristic curves for unsaturated fractured rocks. The Second Asian Conference on Unsaturated Soils, Unsat-Asia, Osaka, Japan, pp. 425-428.

Zhang, L. & Chen, Q. (2005). Predicting bimodal soil-water characteristic curves. Journal of Geotechnical and Geoenvironmental Engineering, 13(5):666-670.

Feasibility of Laser Scanning to Determine Volumetric Properties of Fine Grained Soils

I. Falcon-Suarez, F. Sanchez-Tembleque, J.M. Rivera-Sar, R. Juncosa-Rivera, J. Delgado-Martin

Abstract. This study analyses the real applicability of laser scanning techniques to determine bulk densities of fine grained soils. The method, fast and accurate, can be employed both in the field and laboratory. The technique was calibrated with benchmarks and then applied to measure volumes of small samples of a specific silty soil of well-known properties (granite sawdust); next transformed into bulk densities from the sample-weights. The results are compared against those obtained from their precursor specimens, made using the Standard Proctor test. Before calculating soil sample volumes, optimum conditions for data acquisition, exportation and post-processing were assessed. The laser scanning provides highly consistent results when compared with those obtained from Standard Proctor compaction tests. However, the study shows a limiting value of moisture content below which the laser scan provides inaccurate results. Likely, this limit varies from soil to soil and therefore the technique must be calibrated before being used to determine bulk densities and derived volumetric properties (*i.e.*, porosity or void ratio). Accordingly, this work presents a helpful procedure to evaluate the applicability of the laser scanning based on the detection of the limiting water content, which considers as well anomalies derived from compositional heterogeneities or external electromagnetic interferences.
Keywords: laser scanning, standard proctor test, bulk density, granite fines.

1. Introduction

The degree of compaction is key parameter on geotechnical works since the permeability and coefficient of consolidation decrease with the reduction of void ratio for a given soil. Hence, when considering final applications in large scale contexts, the materials are subjected to adequate compaction procedures. The aim is to achieve the optimal conditions of the soil, in correspondence to those identified in the laboratory by the use of either standards or widely accepted tests - normal and modified Proctor tests (ASTM D698-07; ASTM D1557-09); moisture condition value (MTV) test (Murray *et al.*, 1992).

In soils, the degree of compaction is defined by two parameters: dry density and water content. Far from trivial, the determination of index volumetric properties (bulk density, void ratio, porosity) is addressed with special techniques which aim at characterizing bulk density and derived properties both in the field and in the laboratory. Such techniques show advantages but also inconveniences (Grossman & Reinsch 2002): the radiation method (Al-Raoush & Papadopoulos 2010; Timm *et al.*, 2005) requires special safety procedures to ensure that undue exposure to gamma radiation is avoided; the soil clod and volume excavation methods (sand or water replacement) are cumbersome; the core-cutter method, although straightforward, depends upon the skills of the operator and on the suitability of the equipment and facilities (*i.e.*, possible over-compaction effects due to the penetration of the corer); other emergent techniques include the use of Thermo-TDR (Liu *et al.*, 2014) or FDR sensors (Al-Asadi & Mouazen 2014) for calculating soil bulk densities indirectly from the dielectric response of the soil, although the results are mainly representative of the piece of soil located in the needle spacing of the probe.

Sander *et al.* (2007) and Rossi *et al.* (2008) propose a method to determine bulk density of grained soils based on the application of high precision laser scanning techniques to irregularly shaped soil samples. Their results show excellent agreement to other conventional methods. Furthermore, the technique is clean and easily reproducible. The main inconvenience is that the method limits its applicability at the laboratory scale, although this is only dependent on the laser scan model used.

So far, the laser scanning technique has been assessed on soil samples at controlled conditions of water content and compaction. In this contribution, the influence of moisture content and degree of compaction on the results obtained is

Ismael Falcon-Suarez, PhD, Postdoc Researcher, Marine Geosciences, National Oceanography Centre, University of Southampton Waterfront Campus, SO143ZH, Southampton, United Kindom. e-mail: isfalc@noc.ac.uk.
Felix Sanchez-Tembleque, PhD, Professor Assistant, Departament of Mathematics and Representation Methods, Civil Engineering School, University of A Coruna, Campus Elvina, A Coruna, Spain, and CITEEC, University of A Coruna, Campus Elvina, A Coruna, Spain. e-mail: fsanchez@udc.es
Jose Maria Rivera-Sar, MSc, Department of Construction Technology, Civil Engineering School, University of A Coruna, Campus Elvina s/n, 15071, A Coruna, Spain. e-mail: riverasar@gmail.com.
Ricardo Juncosa-Rivera, PhD, Associate Professor, Department of Construction Technology, Civil Engineering School, University of A Coruna, Campus Elvina, A Coruna, Spain. e-mail: rjuncosa@udc.es.
Jordi Delgado-Martin, Professor, Associate Professor, Department of Construction Technology, Civil Engineering School, University of A Coruna, Campus Elvina, A Coruna, Spain. e-mail: jdelgado@udc.es.
Submitted on March 19, 2014; Final Acceptance on February 6, 2015; Discussion open until December 31, 2015.

evaluated when applying the laser scanning technique for determining bulk densities on fines. The soil used consisted of two varieties of a particular grain fined material of well-known properties (*i.e.*, granite sawdust or granite fines). Mixing soil and water at different ratios, a trial of Standard Proctor tests were performed towards achieving homogenous soil specimens (*i.e.*, well-distributed moisture and degree of compaction); next, from each specimen a smaller sample was cut to scan. The study assesses the influence of soil composition and moisture on the quality of results, but also how the laser scanning signal could be affected by the presence of metallic particles within the soil matrix.

2. Materials and Methods

The so called granite sawdust or granite fines is the fine grained material used in this study. Granite fines cover the particular waste generated by the dimension stone industry of Galicia (Spain). There, the rock blocks quarried or arrived from other countries, are typically transported to the workshops where they are elaborated before being sold. The elaboration processes involve mechanical activities of abrasive nature (cutting and polishing). Consequently, a wide amount of dusty material is produced every year (*i.e.* granite fines).

After an initial geotechnical characterization, different research lines derived toward applying granite fines in real civil engineering contexts. A comprehensive characterization of the granite fines is given in Delgado *et al.* (2006) and Barrientos *et al.* (2010), while a number of its different applications are described in Vázquez *et al.* (2007), Navarro *et al.* (2008) and Falcon (2011). As a result, granite fines has become into a material of well-known properties, which can be used as reference soil. Accordingly, it is worth mentioning the recent work presented by Falcon *et al.* (2014) in which the granite saw dust is used to test a new technique to determine the permeability of unsaturated soils.

In short, granite fines is a silty material (10-15% clay; 70-75% silt; 10-15% fine sand) with low plasticity (class ML in the USCS classification scheme) and specific surface (6 to 10 $m^2 g^{-1}$). The mineralogy, consistently with its origin, is dominated by silicates (quartz, microcline, plagioclase, biotite, muscovite, chlorite) plus other accessory minerals associated with the manufacturing processes (calcite and steel grit; 3 and up to 16 wt%, respectively). Compositionally, two main types of granite fines (GF) can be distinguished according to the practices applied on the workshop of provenance: steel grit-bearing (GF1) or not (GF2). The relatively high content of steel grit particles raises the solid density of the GF1 to an average value of ~3190 kg m^{-3}, while GF2 present a common granite value of ~2600 kg m^{-3}.

2.1. Sample performance

To test the laser scanning technique described next, compacted specimens of granite fines plus water at different soil/water ratios were performed applying standard effort energy as described in the ASTM D698-07e1 reference standard (*i.e.*, Standard Proctor test), using a stiff steel mould of known capacity (see Fig. 1). Since granite fines originally present water content ~38% (*i.e.*, when generated in the elaboration workshops), as a first step, the material was oven-dried. Next, granite fines were dampened at different soil/water ratios to obtain specimens which cover the whole range of moistures.

Granite fines and water were mixed to perform 32 Standard Proctor tests (19 of GF1 and 13 of GF2), according to the ASTM D698-07. Bulk and dry densities were computed after the careful differential weighting of the empty/filled mould and the precise knowledge of the moisture content through oven-drying at 105 °C (ASTM D2216-10el). The accuracy of the density determination according to the equipment used (*i.e.*, commercial weight balance and digital Vernier caliper) was ~1%.

Each Proctor specimen (circa 1 dm^3) was halved: one half for laser scanning; the other for determining moisture content. The halves for scanning were carved with the aid of a sharp blade (a wire sculpting tool would also perform well). The flat surface at both ends of the specimen, resulting from the compaction procedure, was used to make hilly polyhedrons with flat base (see Fig. 1 and Fig. 2). This shape makes easier the calculation of sample volumes by integrating the upper surface over a constant base level. Prior to scanning, the sample is weighted directly after being cut in order to avoid moisture changes because exposure to the atmospheric conditions in the laboratory. Finally, dry density is computed with the dry-weight and the calculated volume. Keeping bearing the different measurement techniques employed in the density determination with a laser scanner (*i.e.* volume uncertainty and weighting error), the overall relative error of this technique has been evaluated in less than 0.1%.

Figure 1 - Typical elements of the sample performance: (1) Standard Proctor test mould; (2) Standard Proctor test specimen; (3) small samples, cut from the specimen; (4) the cut tool.

Figure 2 - Carved samples of granite saw dust with (GF1) and without (GF2) steel grit particles.

2.2. The 3D scanning technique

The Polhemus FastSCANTM system is a lightweight, portable line scanner that captures accurate 3D contours of opaque subjects using a built-in diode laser (λ = 670 nm; power = 1 mW) and two miniature digital cameras. It is worth mentioning that the equipment consists of class 2 laser product which means it is safe because the blink reflex will limit the exposure to no more than 0.25 s, as is specified by the IEC 60825-1 standard. The laser and the digital cameras are mounted in a special bracket (transmitter) that holds three orthogonal magnetic coils that pulse an electromagnetic field that allows its accurate tracking with respect to a receiver reference table. FastSCANTM projects a fan of laser light on the object of interest while the cameras view the laser to record cross-sectional depth profiles and render a real-time 3D reconstruction of the object.

The system uses a constant line scanning rate of 50 Hz while the resolution along the laser line is related to the object-scanner distance (0.1 to 0.5 mm at 200 mm distance). The resolution between scanned lines depends on the speed of the sweep of the laser system over the surface of the object while being scanned (1 mm at 50 mm s^{-1}). In this context, Rousseau *et al.* (2012) studied the problems that can be found during scanning mineral surfaces at very high resolutions, pointed out that scanning speed is a crucial aspect to keep bearing. They argued that the faster the speed, the more likely the scanning process remain incomplete; unlike, if it is too low, although the number of measured points makes the data processing complicated, it leads to a better mapping (*i.e.*, resolution is greatly improved when sweeping is slow). Accordingly, the distance to the object was set in 200-250 mm, and 10-20 mm s^{-1} for scanning rate. Fig. 3 shows a typical scanning procedure over a sample of granite fines.

The 3D data generated in the scanning process is stored in a computer: scatter plots or a mesh of triangular facets suitable for exporting to a number of file formats used for late post-processing (González *et al.*, 2007). In the present case, post-processing focused on the quantification of volumes was carried out with Surfer® 10.4 (Golden Software, Inc).

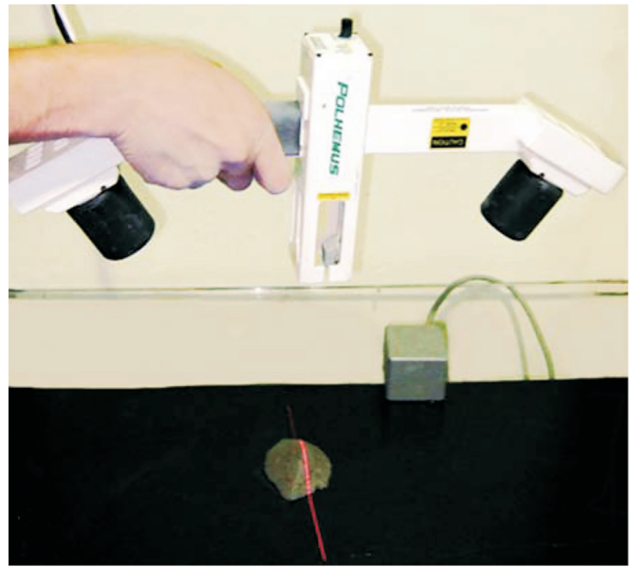

Figure 3 - Typical laser scanning procedure over a sample of granite fines.

2.3. Instrument calibration

Nixon *et al.* (1998) cautioned on the negative influence of local electromagnetic fields and their potential effect in distorting the tracking signal. To evaluate this effect within the workspace, a calibration process was carried out using two benchmarks consisting of polyhedrons made of plastic polymer and machined in a workshop with a precision lathe. The polyhedrons presented pyramidal shapes (*i.e.*, P1 and P2; see Fig. 4), differing in the finish: P1 is a common pyramid, while P2 makes a bent in the middle, resulting in a double-pyramid shape. The corresponding volumes (167.4 and 209.7 cm^3 for P1 and P2, respectively) were computed from fundamental geometric relationships, according to the nominal dimensions reported by the fabricant and verified with a digital Vernier caliper.

2.4. Optimum conditions for data acquisition

Surfer® implements a wide number of interpolation algorithms able to generate regular grids from unevenly spaced scatter data; next, the software allows the user to

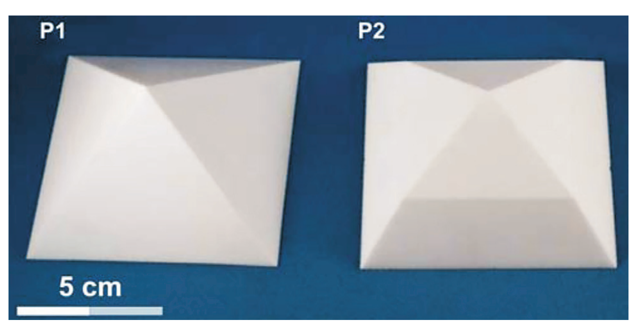

Figure 4 - Polyhedrons of reference employed in the calibration of the 3D laser scanner.

compute the surface-constrained volume from the regular grid. The accuracy of the volume calculation depends on the density of the grid and the method used for interpolation. The first grid is interpolated from the raw data recorded with the laser scanner. So that, it is expected to improve the accuracy of results with a regular grid of points equally distributed (*i.e.*, interpolating points between original raw data).

In this study, it has been considered the performance of twelve gridding algorithms in Surfer® to address with the study of the optimum conditions for post-processing: inverse-distance-to-a-power (IDP); kriging (KG); minimum curvature (MC); modified Shepard's method (MSM); natural neighbour (NN); nearest neighbour (NeN); polynomial regression (PR); radial basis function (RBF); triangulation with linear interpolation (TLI); moving average (MA); data metrics (DM); and local polynomial (LP). From each one of them it is obtained an inferred volume (V_{inf}) that, for the purpose of calibration, can be compared with theoretic volume (V_{the}). The relative volume difference (ΔV_{rel}, in %) can be computed from the following equation:

$$\Delta V_{rel} = \frac{|V_{inf} - V_{the}|}{V_{inf}} \times 100 \qquad (1)$$

3. Results and Discussion

3.1. Optimum tuning settings and gridding

Fig. 5 to Fig. 8 illustrates the results of the settings and gridding calibration process. The two benchmark pyramidal shapes (P1 and P2) are scanned using four smoothness/resolution pair (Sm/Res in mm/mm) corresponding with each figure (*i.e.*, Sm/Res = 0.5/0.5, Fig. 5; Sm/Res = 0.5/1, Fig. 6; Sm/Res = 1/1, Fig. 7; Sm/Res = 1/1.5, Fig. 8). Then, the raw data file is converted into volume by the twelve gridding algorithms of Surfer described in the previous section, independently for both P1 and P2, and the results expressed in terms of relative volume difference against the theoretical volume (Eq. 1).

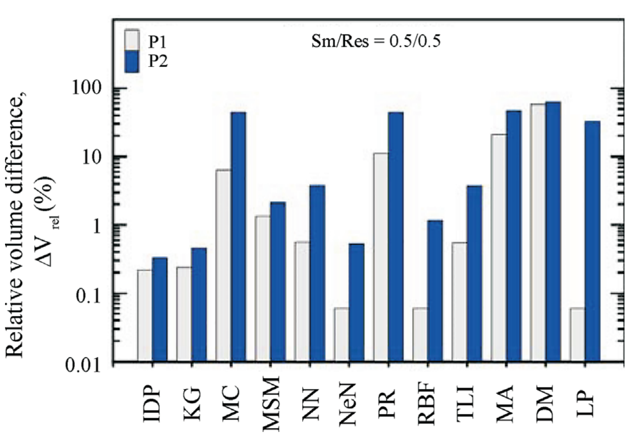

Figure 5 - Twelve methods gridding at Sm/Res = 0.5/0.5.

The results shown in Fig. 5 to Fig. 8 lead to point out some interesting observations. First, according to the experimental settings (*i.e.*, distance to the object and scanning rate), ΔV_{rel} presents minimums when the raw data is exported with a smoothing factor of 0.5 mm; however, resolution ranges between 0.5 and 1 mm without significant

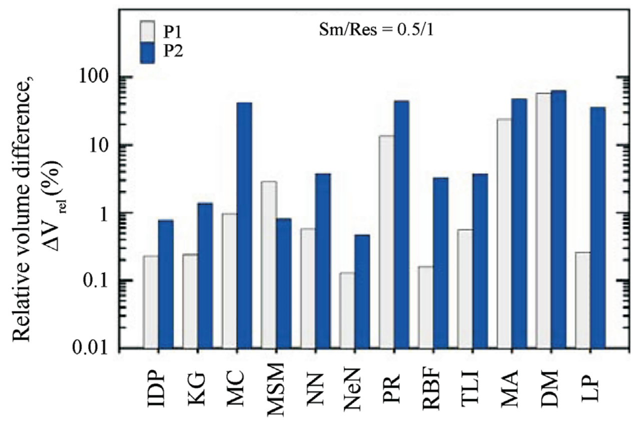

Figure 6 - Twelve methods gridding at Sm/Res = 0.5/1.

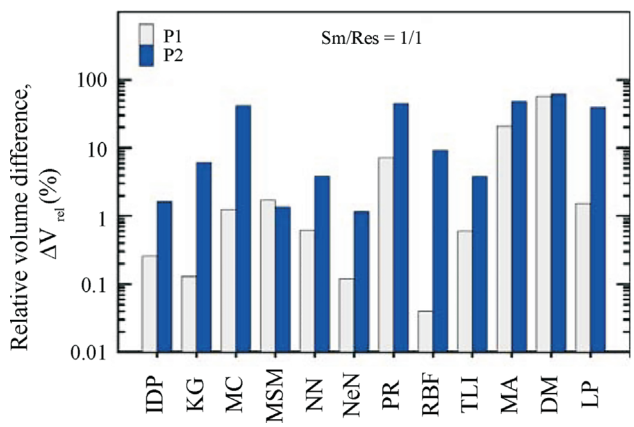

Figure 7 - Twelve methods gridding at Sm/Res = 1/1.

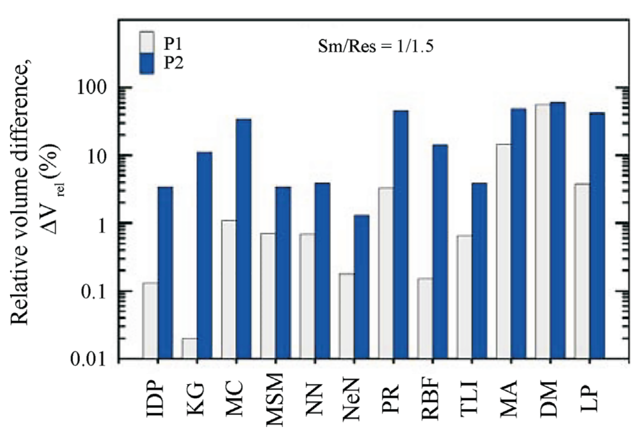

Figure 8 - Twelve methods gridding at Sm/Res = 1/1.5.

differences. Second, some methods show great differences between P1 and P2, which means that they clearly depend on the shape of the scanned surface, being P2 the most affected. Third, it can be observed that calculated volumes greatly vary depending on the considered gridding algorithm. Furthermore, in connection with the work of Yilmaz (2007), the best results are given by the minimum curvature radial basis function, kriging, natural neighbour, triangulation with linear interpolation, nearest neighbour and inverse distance to a power; while the poorest are obtained by MC, PR, DM, and MA.

Among best set of methods mentioned above, the inverse-distance-to-a-power (IDP) and nearest neighbour (NeN) interpolation lead to minima ΔV_{rel}. Although either IDP or NeN is expected to provide good results, this study has been conducted applying the former and using a par-setting smoothing/resolution of 0.5/0.5 mm to the raw data.

3.2. Scanning technique on granite fines

From the Standard Proctor bulk specimens it is obtained a value of dry density and water content. This pair is adopted as the reference values for the sample that is posteriorly cut and scanned from the specimen. The approximation shown in Eq. 1 can be modified in order to study the relative difference of dry densities ($\Delta\rho_{d,REL}$) between the Standard Proctor specimen ($\rho_{d,ASTM}$) and that of the sample cut and scanned from the specimen ($\rho_{d,LS}$). Thus, the expression becomes into the following:

$$\Delta\rho_{d,REL} = \frac{|\rho_{d,ASTM} - \rho_{d,LS}|}{\rho_{d,ASTM}} \times 100 \quad (2)$$

Figure 9 compares the relative dry density difference and the corresponding water content (constant for a given Standard Proctor specimen). It shows that the higher the water content, the smaller the relative dry density difference. A closer look reveals that, when the water content drops below 20%, $\Delta\rho_{d,REL}$ sharply increases (up to 40% if moisture ranges 5 to 10%; see the grey area on Fig. 9). For water contents higher than 20%, $\Delta\rho_{d,REL}$ reduces to a range between 0.1 to 2%.

Figure 10 illustrates the same fact by the direct comparison of dry densities. Those samples of water content higher than 20% show good correlation. Moreover, $\rho_{d,LS}$ is lower than $\rho_{d,ASTM}$ when the water content is below 20%. Figure 10 is therefore suggesting that the consistence of the Proctor specimen decreases after being extracted from the mould and shaped to scanning when the water content is lower than 20%. It can be interpreted as a bulking effect connected with the reduced adhesion of small solid particles, when capillary bridges become less effective and, consequently, the sample losses cohesiveness (Paajanen *et al.*, 2006; Zhang *et al.*, 2008).

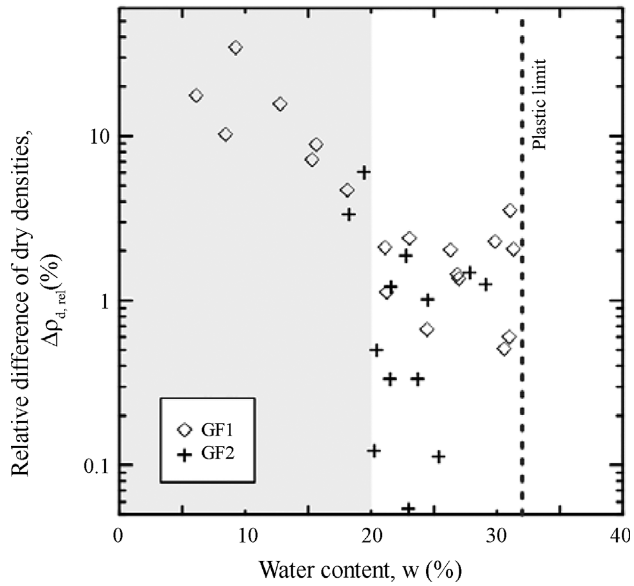

Figure 9 - Dry density difference ($\Delta\rho_{d,REL}$, in %) *vs.* water content, from granite fines samples with (GF1) and without (GF2) steel grit particles.

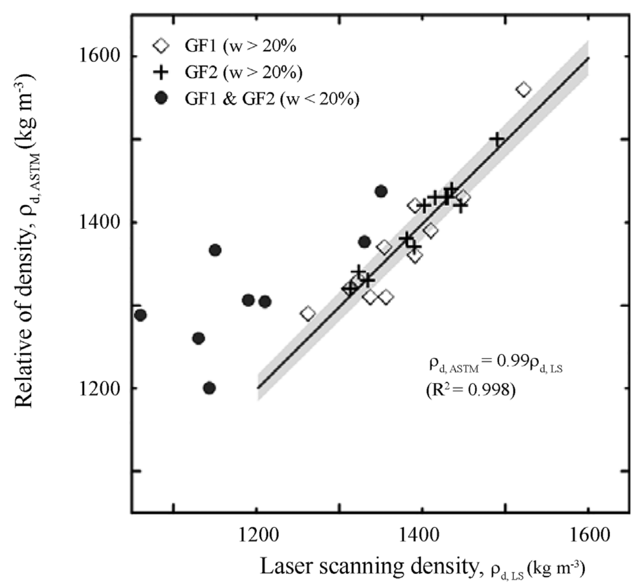

Figure 10 - Dry density from scanner ($\rho_{d,LS}$) *vs.* those from the Standard Proctor tests ($\rho_{d,ASTM}$), of granite saw dust samples with (GF1) and without (GF2) steel grit. Solid line is a linear fit (95% confidence, grey band).

3.3. Heterogeneities in the soil matrix

GF1 samples display slightly higher dispersion than GF2, according to the relative density differences observed (Fig. 9). This effect is likely related to the presence (GF1) or absence (GF2) of steel grit particles in the sample. The proportion of heavy fine grained steel particles within the granite fines matrix is random, independently of the scale. Moreover, steel grit preferentially forms local aggregates within the granite fines matrix (Vazquez *et al.*, 2007; Barrientos *et al.*, 2010; Falcon, 2011).

The effect of heterogeneous steel grit distribution on the dry density is analysed through Fig. 11, that shows the Proctor test results in a common soil-compaction graph (*i.e.*, dry density *vs.* water content), on which polynomial fits for both types of granite fines are also provided. The zero air voids (ZAV, *i.e.*, the theoretic saturation line) differs from GF1 to GF2. However, Proctor tests result on similar values either the type of granite fines. It can be interpreted that, although a low percentage of steel substantially increases the mean value of the density of solid particles (used to theoretically calculate the ZAV of a given soil), the effect on the final bulk weight is scale-dependent: the smaller the sample size, the more sensitive it is to lead unexpected high weights as a result of local high steel content and, consequently, anomalous high dry densities.

The presence of steel grit appears to be a rather specific issue concerning the granite fines that has been addressed from the viewpoint of the increase of the samples weights. However, there is another effect to keep bearing: steel grit may carry to anomalies in the quality of the signal. The presence of magnetic steel grit particles raises also the question of whether they can distort or not the electromagnetic field used to track the position of the scanned surface. To this respect, Nixon *et al.* (1998) indicate that ferromagnetic materials can induce variations in the scanned position but this effect reduces with the size of the ferromagnetic particle. Keeping bearing the average granulometry of GF1 (~20 μm), the results illustrated by these authors demonstrate that the distortion effect associated to the presence of steel grit particles is negligible when compared with the resolution provided by the apparatus. Therefore, the increased dispersion observed in the GF1 samples is attributable to local heterogeneities in the steel grit distribution rather than inferred instrumental errors.

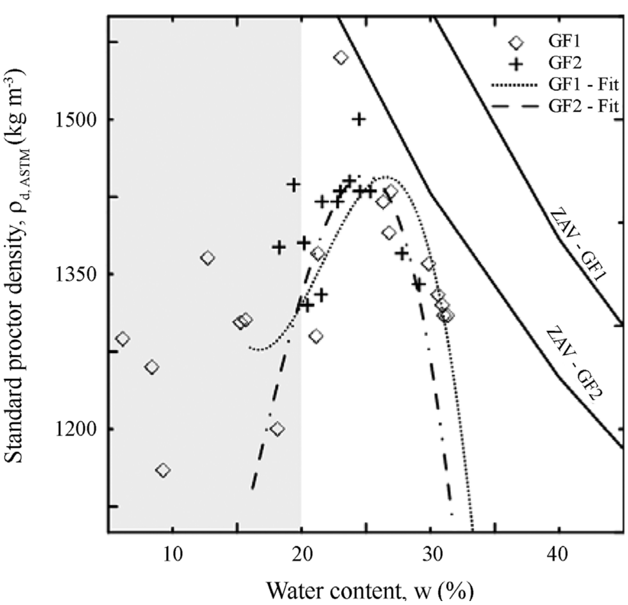

Figure 11 - Results of Standard Proctor tests performed with granite fines with (GF1) and without (GF2) steel grit. Dashed curves represent best third-degree polynomial fits; ZAV, is the Zero Air Voids line (saturation line).

3.4. Applicability of the laser scanning technique on real contexts

Although other authors present lower resolutions of work (Sander *et al.*, 2007; Rossi *et al.*, 2008), our results show how resolutions of 0.5 mm improve the accuracy of density determinations (0.1%) when comparing with the Standard Proctor procedure (1%) worldwide used to specify compaction requirements for roadway construction. Furthermore, the methodology applied in this study (including the sharping, pre-process, and the scanning), last no more than 2 min per sample, which significantly differs from the 40 min proposed by Rossi *et al.* (2008) whom use a similar technique at higher resolutions of about 0.13 mm. In addition, Rousseau *et al.* (2012) argued that scanning under very high resolutions may lead to record some atypical points associated either with the orientation of some minerals or their own optical properties.

In relation with the performance of the laser scanning technique it has been identified a strong dependence respect to the water content of the soil: those samples with lower water content give higher deviations. Such a behaviour, that it is likely to vary from soil to soil, appears to be related with a bulking effect associated to the reduction in the adhesion of solid particles when the attraction force of capillary water becomes small. Although this effect could be reduced by increasing the size of the samples, the uncertainty of the measurement could lead to inaccurate results. Rather, more appropriated is to calibrate the laser scanning technique for a given soil to identify the water content that represents the limit of applicability, and any other anomalies that might affect the measurements.

4. Conclusions

This study has assessed the feasibility of the laser scanning technique to measure bulk densities of fine grained soils. The technique has been studied with samples of granite sawdust as reference material because of their well-known properties. This work presents a singular methodology to address the determination of bulk density of soils which covers, first, the cutting and shaping of granite fines samples performed using the Standard Proctor test procedure and, next, the 3D scanning of the samples and the integration of the scanned surfaces into volumes.

The laser scanning technique provides a fast and accurate method to monitor bulk density but also derived volumetric properties of soils, plausible to be used either in the laboratory or in the field. However, a limiting water content below which the technique is unappropriated was identified. This limit factor is likely related with the cohesiveness of the granite sawdust below moistures of ~20%. This value is specific of the tested material, which suggests the technique must be calibrated from soil to soil. To this respect, the use of Standard Proctor specimens as benchmarks ensures homogenized soil samples to calibration while covering the entire range of moisture content. The simplicity and fastness of the methodology applied in this work (reshaping samples from Proctor benchmarks) make it suitable to address with the calibration of the laser scanning on fine grained soils.

Acknowledgments

Funds for this work have been provided by the Ministry of Science and Innovation (BIA2005-07916-C02-01), Xunta de Galicia (10REM003CT & 10MDS007CT) and the European Regional Development Funds 2007/2013.

References

Al-Raoush, R. & Papadopoulos, A. (2010). Representative elementary volume analysis of porous media using X-Ray computed tomography. Powder Technology, 200(1-2):69-77.

Al-Asadi R.A. & Mouazen A.M. (2014). Combining frequency domain reflectometry and visible and near infrared spectroscopy for assessment of soil bulk density. Soil and Tillage Research, 135:60-70.

ASTM (2007). Standard Test Methods for Laboratory Compaction Characteristics of Soil Using Standard Effort (12 400 ft-lbf/ft (600 kN-m/m)) - D698-07. ASTM International, West Conshohocken, Pennsylvania, USA, 13 p.

ASTM (2009). Standard Test Methods for Laboratory Compaction Characteristics of Soil Using Modified Effort (56,000 ft-lbf/ft3 (2,700 kN-m/m3)) - D1557. ASTM International, West Conshohocken, Pennsylvania, USA, 10 p.

ASTM (2010). Standard Test Methods for Laboratory Determination of Water (Moisture) Content of Soil and Rock by Mass - D22160-10. ASTM International, West Conshohocken, Pennsylvania, USA, 7 p.

Barrientos, V.; Delgado, J.; Navarro, V.; Juncosa, R.; Falcon, I. & Vazquez, A. (2010). Characterization and geochemical-geotechnical properties of granite sawdust produced by the dimension stone industry of O Porrino (Pontevedra, Spain), Quarterly Journal of Engineering Geology and Hydrogeology, 43(2):141-155.

Delgado, J.; Vázquez, A.; Juncosa, R. & Barrientos, V. (2006). Geochemical assessment of the contaminant potential of granite fines produced during sawing and related processes associated to the dimension stone industry, Journal of Geochemical Exploration, 88(1-3):24-27.

IEC (2007). Safety of laser products - Part 1: Equipment classification and requirements - IEC 60825-1 Edition 2.0. International Electrotechnical Commission, p. 199.

Falcón, I. (2011). Los serrines de granito como barrera de impermeabilización para su uso en vertederos. PhD Dissertation, Department of Civil Engineering, University of A Coruña, A Coruña, 245 p.

Falcon-Suarez, I.; Rammlmair, D.; Juncosa-Rivera, R. & Delgado-Martin, J. (2014). Application of Rhizon SMS for the assessment of the hydrodynamic properties of unconsolidated fine grained materials. Engineering Geology, 172(0):69-76.

González, E.P.; Díaz-Pache, F.S.-T.; Mosquera, L.P. & Agudo, J.P. (2007). Bidimensional measurement of an underwater sediment surface using a 3D-Scanner. Optical and Laser Technology, 39(3):481-489.

Grossman, R.B. & Reinsch, T.G. (2002). The solid phase. Bulk density and linear extensibility. J.H. Dane & G. Clarke (eds), Methods of Soil Analysis, Part 4, SSSA, Madison, Wisconsin, p. 201-228.

Liu X.; Lu S.; Horton R. & Ren T. (2014). In Situ Monitoring of Soil Bulk Density with a Thermo-TDR Sensor. Soil Sciences Society of America Journal, 78(2):400-407.

Murray, E.J.; Rix, D.W. & Humphrey, R.D. (1992). Clay linings to landfill sites. Quarterly Journal of Engineering Geology and Hydrogeology, 25(4):371-376.

Navarro, V.; Barrientos, V.; Yustres, A. & Delgado J. (2008) Settlement of embankment fills constructed of granite fines. Computers and Geosciences, 34(8):978-992.

Nixon, M.; McCallum, B.; Fright, W. & Price, N. (1998). The effects of metals and interfering fields on electromagnetic trackers. Presence: Teleoperators Virtual Environments, 7(2):204-218.

Paajanen, M.; Katainen, J.; Pakarinen, O.H.; Foster, A.S. & Lahtinen J. (2006). Experimental humidity dependency of small particle adhesion on silica and titania. Journal of Colloid and Interface Science, 304(2):518-523.

Rossi, A. M.; Hirmas, D. R.; Graham, R. C. & Sternberg, P. D. (2008). Bulk density determination by automated three-dimensional laser scanning. Soil Science Society of America Journal, 72(6):1591-1593.

Rousseau, B.; Rivard, P.; Marache, A.; Ballivy, G. & Riss, J. (2012). Limitations of laser profilometry in measuring surface topography of polycrystalline rocks, International Journal of Rock Mechanics and Mining Sciences, 52(0):56-60.

Sander, T. & Gerke, H.H. (2007). Noncontact shrinkage curve determination for soil clods and aggregates by three-dimensional optical scanning. Soil Science Society of America Journal, 71(5):1448-1454.

Timm, L.C.; Pires, L.F.; Reichardt, K.; Roveratti, R.; Oliveira, J.C.M. & Bacchi, O.O.S. (2005). Soil bulk density evaluation by conventional and nuclear methods. Australian Journal of Soil Research, 43(1):97-103.

Vazquez, A.; Juncosa, R.; Barrientos, V.; Falcon, I.; Delgado, J. & Navarro, V. (2007). Hydrodynamic and reactive transport modeling of the behavior of compacted granite saw dust for landfill liners and covers. Proceedings of the 12th International Symposium on Water/Rock Interaction, Rotterdam, v. 1, pp. 653-659.

Yilmaz, H. M. (2007). The effect of interpolation methods in surface definition: an experimental study. Earth Surface Processes and Landforms, 32(9):1346-1361.

Zhang, T.; Zeng, Q.; Li, Y. & Xiang, Y. (2008). Study on relation between InSAR coherence and soil moisture. Proceedings of The International Archives of the Photogrammetry, Remote Sensing and Spatial Information Sciences, Beijing, v. 37 Part B7, pp. 131-134.

A Case of 3-D Small Pile Group Modeling in Stiff Clay Under Vertical Loading

A.C. Freitas, B.R. Danziger, M.P. Pacheco

Abstract. The behavior of experimental pile groups is simulated by 3-D finite element modeling in this paper. The modeled results are compared to small-scale tests in a row of three closely spaced piles in the London clay. The tests aimed at investigating soil-pile-cap interaction and pile-group effect. It is shown that 3-D FE modeling can be regarded as an appropriate tool to predict settlements and load-transfer mechanisms in pile groups under working conditions, with a satisfactory match between simulated and measured results.

Keywords: pile group effect, 3-D modeling, load transfer, settlement prediction.

1. Introduction

3-D finite element modeling is an effective tool to simulate soil-pile-cap interaction since pile elements with prescribed ultimate values of tip resistances and nearly any type of shaft distribution can be assigned to individual piles, applicable boundary conditions can be easily simulated, efficient constitutive soil models can be selected, and plate elements can be used to simulate the structural response of the pile cap. In this paper the simulations have been performed by the program Plaxis 3-D Foundation version 2.1.

The results of tests on three closely spaced and aligned piles tested by Cooke *et al.* (1980) in the London Clay are used for comparison with the present 3-D FEM analysis. The piles were tested under equal pile loading, equal pile displacements and also with the piles connected by a rigid concrete cap on the clay surface. The settlements in each pile were measured by loading the piles individually and simultaneously. In each case, predictions of settlements and load transfer are presented and compared to the experimental results.

The tests were performed in 5 m long, 168 mm diameter steel pipe piles with 6.4 mm wall thickness, embedded 4.5 m in the soil. The tests were performed in Hendon, Northern London. The soil parameters for the numerical analyses were obtained from a comprehensive literature review (Freitas, 2010) which also included the instrumentation and the field investigation conceived by Cooke *et al.* (1980).

2. Test Lay Out and Soil Parameters

Figure 1 shows a sketch of the test comprising three aligned piles A, B and C installed by jacking in this order. The distance *s* between the pile axes was 3 pile diameters. Piles A and B had settlement gauges near the top and load cells at the top and at other three locations in the shaft. Pile C was not instrumented since it was expected to behave similarly to pile B under assumption of symmetry.

The three piles were monitored with horizontal inclinometers whose readings were obtained with aid of the observation trenches shown in Fig. 1. The trenches were installed sufficiently far from the testing piles (Cooke *et al.*, 1980). The main trench was set six months before installation of pile A. The trench was 5.2 m deep, with the working face 2.1 m away from the pile alignment. The secondary trench had the working face 2.7 m away from the axis of pile A, to install the inclinometers. The secondary trench was set after the tests on piles A and B, but before installing pile C. Cooke *et al.* (1980) reported that although the effects of drilling, instrumentation, and installation of the observational trenches on the pile-soil stiffness are not strictly known, evidence suggests that such effects are small and therefore have been neglected in the numerical analyses.

A concrete pile cap 1.5 m long, 0.5 m wide and 0.3 m thick was cast around the pile heads and rigidly connected to them, in order to produce identical settlements in the three piles. The base of the cap was 0.2 m below ground level with no contact between the vertical sides of the cap and the surrounding soil.

The piles were loaded incrementally with each increment maintained for a period of nearly 3 minutes, up to settlement stabilization. Due to the low loading applied, an elastic behavior has been observed. The test rarely surpassed one hour, Cooke *et al.* (1980).

The piles were loaded according to the sequence shown in Fig. 2. The tests designation is the same adopted by Cooke *et al.* (1980).

Alessandra Conde de Freitas, PhD, Associate Professor, Departamento de Construção Civil, Setor de Geotecnia, Universidade Federal do Rio de Janeiro, 21941-909 Rio de Janeiro, RJ, Brazil. e-mail: alessandracfreitas@poli.ufrj.br.
Bernadete Ragoni Danziger, PhD, Associate Professor, Departamento de Estruturas e Fundações, Universidade do Estado do Rio de Janeiro, 20550-013 Rio de Janeiro, RJ, Brazil. e-mail: bernadeterd@hotmail.com.
Marcus Peigas Pacheco, PhD, Full Professor, Departamento de Estruturas e Fundações, Universidade do Estado do Rio de Janeiro 20550-013, Rio de Janeiro, RJ, Brazil. e-mail: marcus_pacheco@terra.com.br.
Submitted on June 9, 2014; Final Acceptance on April 21, 2015; Discussion open until December 31, 2015.

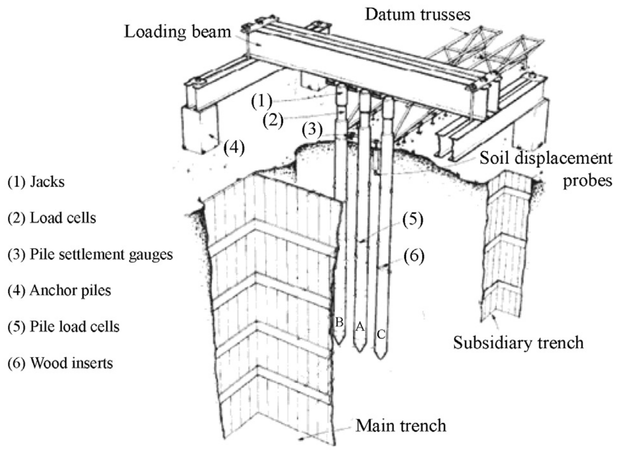

Figure 1 - Main features of the test set-up (adapted from Cooke *et al.*, 1980).

Test 1: Pile A loaded alone to 57.5 kN (about 60% of the estimated ultimate load of the isolated pile estimated by Cooke *et al.*, 1980) to compare to piles A and B loaded simultaneously (to the same value). Test 1 occurred 16 weeks after the test in Pile A and 1 week after the installation of pile B.

Test 2: Piles A and B loaded separately to 40 kN (about 40% of the ultimate load) to compare to piles A and B loaded simultaneously. Test 2 occurred 4 weeks after the installation of pile B.

Test 4: Piles A, B and C loaded simultaneously up to 40 kN to measure the shaft distribution and the soil displacements in piles A and B. Test 4 occurred 13 months after installation of pile B and 6 months after the installation of pile C.

Test 5: Piles A, B and C loaded separately and in increments up to 40 kN to measure the shaft distribution and the soil displacements in piles A and B. Test 5 occurred 13 months after pile B and 6 months after the installation of pile C.

Test 7: Piles A, B and C loaded simultaneously by the rigid pile cap to 120 kN keeping the bottom cap surface in contact with the clay, preventing however the soil contact with the side faces. Some adjustments on the loading pattern were needed to ensure as much as possible uniform settlement of the cap. Test 7 occurred 8 months after the installation of pile C and 2 weeks after the cap was finished.

Considering the low permeability of the soil and the short time interval between tests 2 and 3 (only 6 weeks), the corresponding results are nearly equivalent and Test 3 has been discarded. Test 3 occurred 10 weeks after installation of pile B and aimed at the investigation of the time effect on piles A and B and also the effect in load settlement curve. Test 6 was also discarded as some adjustments in the measuring equipment reported by Cooke *et al.* (1980) could bring additional difficulties in the numerical analysis, in addition to the fact that Test 6 was also similar to Test 4, whose analyses are illustrated in the present paper. Test 6 occurred 13 months after installation of pile B and 6 months after the installation of pile C.

A summary of the parameters assigned to the numerical analyses is shown next, based on a comprehensive literature review presented by Freitas (2010) for the London clay comprising experimental research by Skempton (1944), Ward *et al.* (1959, 1965), Skempton (1961), Webb (1964), Bishop *et al.* (1965), Skempton & La Rochelle (1965), Bishop (1966), Skempton *et al.* (1969), Marsland (1971, 1974), Butterfield & Banerjee's (1971), Wroth (1971), Atkinson (1973), St John (1975), Sandroni (1977), Skempton (1977), Windle & Wroth (1977), Cooke *et al.* (1979), Cooke *et al.* (1980), Burland (1990), Fleming *et al.* (1992), Hight & Jardine (1993), Addenbrooke *et al.* (1997), Hight *et al.* (1997), Jovicic & Coop (1998), Kovacevic *et al.* (2001), Hight *et al.* (2003), Wongsaroj *et al.* (2004), Standing & Burland (2006), Gasparre (2005), Gasparre *et al.* (2007), Hight *et al.* (2007) and Davies *et al.* (2008).

The London clay specific weight ranges from 18.1 to 18.8 kN/m^3 (Kovacevic *et al.*, 2001; Davies *et al.*, 2008). The value γ = 18 kN/m^3 was assigned to the present analysis.

The high overconsolidation of the London Clay gives rise to K_0 values greater than unity. Skempton (1961) and

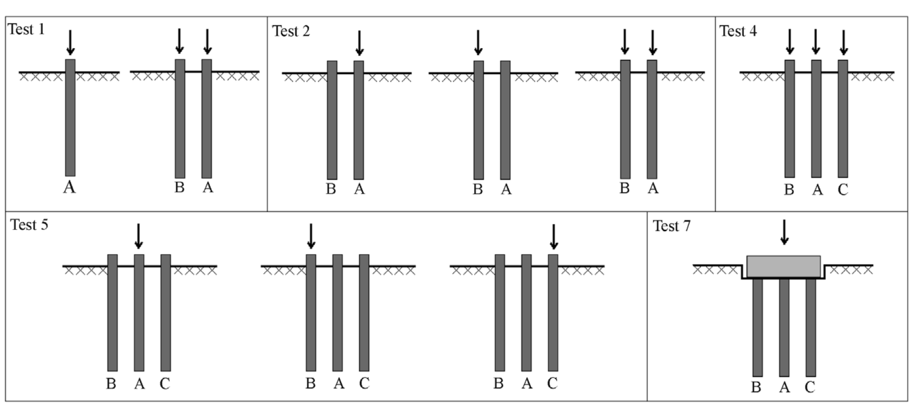

Figure 2 - Loading sequences for the tests.

Skempton & La Rochelle (1965) reported K_0 values between 2.0 and 2.5 in the upper clay layer (upper 10 m), decreasing to $K_0 = 1.5$ down to 30 m. Freitas (2010) summarized K_0 profiles proposed by Bishop *et al.* (1965) and Hight *et al.* (2003) in Fig. 3, which support the value $K_0 = 2$ assigned to the present numerical analyses.

Cooke *et al.* (1979) summarized the values of undrained shear strength and undrained elastic modulus reported by Marsland (1971, 1974). Gasparre *et al.* (2007) compared the stiffness parameters obtained by bender-element aided triaxial tests and HCA tests (instrumented hollow cylinder apparatus) for depths ranging from 0.8 m to 7.9 m. Accordingly, those authors reported E_u values for the London clay in the range 122 ± 3 MN/m^2 for the bender-element tests, and E_u values (inferred from G_u) in the range 112 ± 14 MN/m^2 for the static HCA tests, with good agreement to the band indicated in Fig. 4. Finally, Marsland (1974) recommended a linear E_u profile ranging from 35 kN/m^2 at the ground surface to 78 kN/m^2 at the depth of 4.6 m, which is very close to the E_u profile proposed in this paper. By combining the results of undrained elastic modulus by Marsland (1971) to several other results reported in the literature for the London clay (references above), Freitas (2010) assigned E_u = 33 MN/m^2 at the ground surface, increasing linearly to 177 MN/m^2 at 4.5 m below the ground, which is very close to the profile recommended by Marsland (1974). The full line in Fig. 4 shows the E_u profile selected for calculation. It falls within the shaded area, which is limited according to the references listed in the figure. The selected E_u profile was adjusted to fit the results of Test 1 and to satisfy equation 1 below:

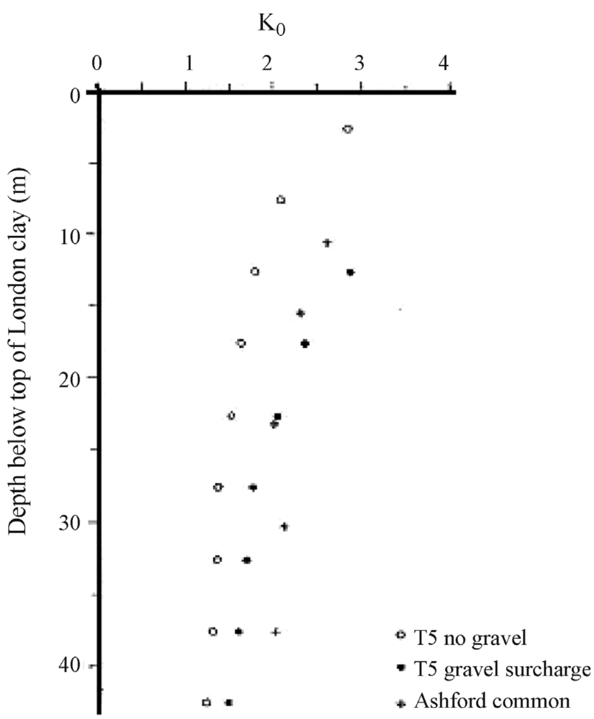

Figure 3 - K_0 profile for London clay. (adapted from Hight *et al.*, 2003).

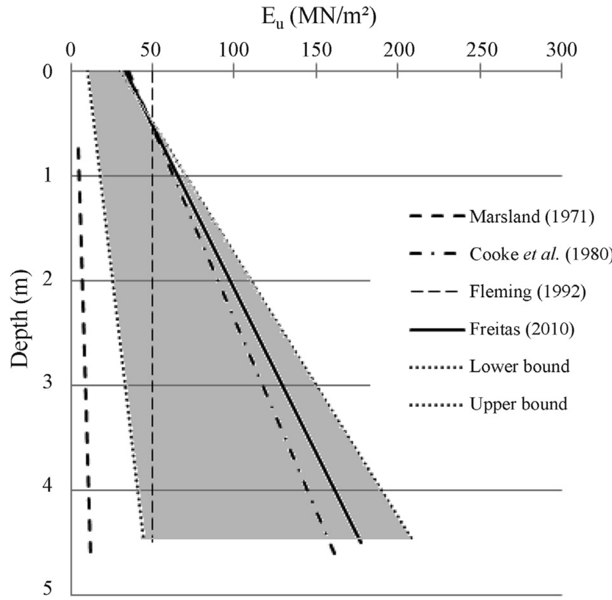

Figure 4 - Variation of secant undrained elastic modulus.

$$R_s = 1 + \Omega_s \qquad (1)$$

where Ω_s is the interaction factor, s is the pile spacing and R_s is the settlement ratio defined by the ratio of the average group settlement to the settlement of an isolated pile under the average load on the piles of the group.

Table 1 shows a summary of the soil parameters assigned to the FEM modeling. The Young modulus $E = 2.1 \times 10^8$ kN/m^2 and the Poisson's ratio $\nu = 0.2$ were assigned to the hollow steel piles and to the steel plate on top of the cap (a composite cap consisting of a 25 mm thick steel plate on top of the 0.3 m high concrete cap was used in the tests). $E = 2.1 \times 10^7$ kN/m^2 and $\nu = 0.2$ were assigned to the concrete portion of the cap. According to data obtained from instrumentation, Cooke *et al.* (1979) obtained maximum skin friction resistances of 66.7 kN/m^2 and 107.1 N/m^2 (at the top and at the tip, respectively) and maximum unit base bearing of 9.2 MPa. These values were selected as ultimate resistances to model the piles in the numerical analyses. Freitas (2010) present further details of the modeling.

3. Model Definition

The external boundaries on the horizontal (XZ) plane are fully restrained and the discretization of the FE mesh is shown in Fig. 5. The ground level was set at the elevation $Y = 0$ m, from which a single layer of the London clay was simulated down to $Y = -30$ m. The simulation extended to the same depth as the investigation carried out in Hendron, North London. The water table was assumed to coincide with the ground level. As the tested pipe piles had closed

Table 1 - Geotechnical parameters for numerical analyses - London Clay (Freitas, 2010).

Parameter		Value	Unity
Natural unity weigth	γ_{unsat}	16	kN/m^3
Total unity weigth	γ_{sat}	18	kN/m^3
Young modulus at surface (Y = 0)	E_{ref}	33 000	kN/m^2
Young Incremental modulus	E_{inc}	32 000	kN/m^2/m
Undrained cohesion at surface (Y = 0)	c_{ref}	35	kN/m^2
Increase of the above with depth	c_{inc}	9.25	kN/m^2/m
Poisson ratio	ν	0.499	-
Friction angle	ϕ	0	(°)
Coefficient of earth pressure at rest	K_0	2	-
Interface factor	R_{inter}	0.75	-
Soil permeability	k	5.10^{-9}	m/day

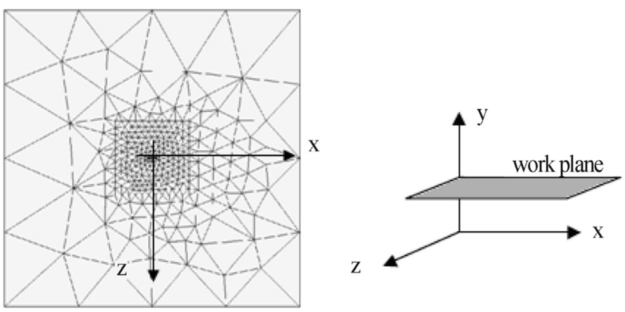

Figure 5 - System of axes in a horizontal plane X-Z.

conical tips, they were modeled as massive piles with equivalent specific weight.

The numerical modeling was based on undrained analyses. According to Brinkgreve & Swolfs (2007) $\psi = 0$ was assigned to the dilatancy angle. The Mohr Coulomb failure criterion was selected for simplicity, considering that the piles were loaded to about 60% of the ultimate loading capacity. For the analyses of the tests without the pile cap the FEM mesh had 15,450 elements and 40,561 nodes, whereas the tests with the pile cap the mesh comprised 17,496 elements and 47,752 nodes.

Mandolini (1999) and de Sanctis & Mandolini (2006) pointed out that even when the load-settlement response of a single loaded pile is markedly non-linear, adjacent unloaded piles usually exhibit a linearly increasing settlement. Referring to the tests performed by Cooke *et al.* (1980) and by Caputo & Viggiani (1984), Mandolini (1999) stated that when the soil surrounding the pile shaft is highly stressed, the rapid decrease of the shear stresses within short distances from the loaded shaft makes elastic conditions prevail. Mandolini (1999) also pointed out that the interaction factor defined by Cooke *et al.* (1980) is constant and independent on the load level. The findings above support the validity of the linear approach to model the mutual interaction among piles.

4. Results

In the following the results of the numerical analyses are presented for tests 1, 2, 4, 5 and 7 (Freitas, 2010). As already explained in session 2, considering the low permeability of the soil and the short time interval between tests 2 and 3 (only 6 weeks), the corresponding results are nearly equivalent and Test 3 has been discarded. Test 6 has also been discarded as some adjustments in the measuring equipment reported by Cooke *et al.* (1980) could bring additional difficulties in the numerical analysis.

4.1. Test 1 - Two piles (B and A) in a row and Pile (A) Isolated

The load settlement curve of pile A and B loaded simultaneously is shown in Fig. 6 and compared with the corresponding curve at the end of the test on pile A (loaded alone) before the installation of pile B. Figure 6 presents the corresponding numerical and experimental results and also illustrates that the load applied in each pile is the same when only pile A is loaded and when pile A and B are loaded simultaneously.

Poulos (1968) introduced the interaction factor (α) to evaluate the interaction between two piles loaded simultaneously:

$$\alpha = \rho_{12} / \rho_{11} \qquad (2)$$

where (ρ_{12}) is the additional settlement on pile (1) due to the loading of the adjacent pile (2), whereas (ρ_{11}) is the settlement of pile (1) due to its own load. For a more convenient data interpretation the interaction factor (Eq. 1) was redefined by Cooke *et al.* (1980) as:

$$\Omega = \bar{\rho}_{12} / \rho_{22} \qquad (3)$$

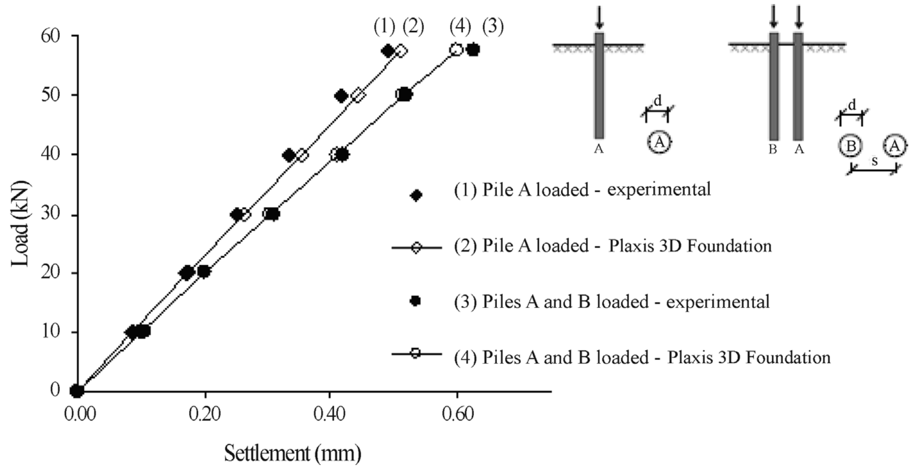

Figure 6 - Load versus settlement curve for pile A and piles A and B, test 1 (adapted from Freitas, 2010).

where ($\bar{\rho}_{12}$) is the induced settlement in pile (1) due to loading of pile (2) and (ρ_{22}) is the settlement of the loaded pile (2). Another useful definition is the settlement ratio (R_s) previously defined as Eq. 1. In the particular case of two equal piles equally loaded the additional settlements due to the interaction are equal.

Cooke *et al.* (1980) observed that for three pile diameters spacing the settlements of the two piles loaded simultaneously were nearly identical for all loading levels and about 25% higher than the settlement of the isolated pile, that is, $R_s = 1.25$. Numerical analysis using Plaxis 3D Foundation showed good agreement with the results shown in Fig. 6. The value of interaction factor obtained from the numerical analysis was $\Omega_3 = 0.20$, or $R_s = 1.20$.

Figure 7 presents the contours of vertical displacements obtained in a vertical plane passing through the piles axis. It also shows the respective view for both analyses.

Cooke *et al.* (1980) pointed out that the load-settlement curves were expected to depart from linearity for axial loads higher than 40 kN, and for this reason the loads on each pile in all tests were limited to this value. This limit may not be noticed when using a simple model such as Mohr-Coulomb. However, considering that all tests have been limited to the linear range and the linear approach is well supported in the literature for mutual pile interaction, the Authors considered that the use of more complex constitutive models would not be justifiable for the present application.

4.2. Test 2 - Row With Two Piles (B and A)

In test 2 the settlements of pile A loaded separately and the effect on pile A by loading pile B are compared with those obtained with piles A and B loaded simultaneously, as shown in Fig. 8.

Settlement predictions of pile A are close to the experimental value. When the load is applied at the neighbor pile B, the experimental settlements in pile A are slightly higher than the numerical results for loads higher than 30 kN, and converge to the experimental values in the case where both piles are loaded simultaneously.

Cooke *et al.* (1980) present the load transfer for piles A and B. The load transfers are nearly equal in the numerical analysis due to the symmetry of the piling, which makes it unnecessary to represent the load transfer produced by pile B. It is worth noting that the minor differences on the transfer curve are attributed not only to small numerical errors, but also to the fact that the finite element mesh becomes slightly asymmetric in the automatic generation of

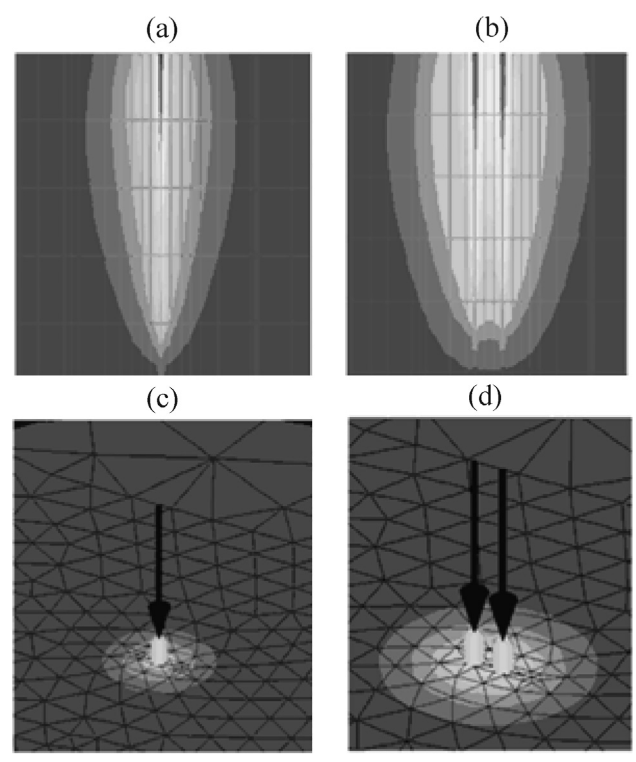

Figure 7 - Settlements for the pile loaded alone ((a) and (c)), and piles A and B loaded simultaneously ((b) and (d)), for the pile load of 50 kN (Freitas, 2010).

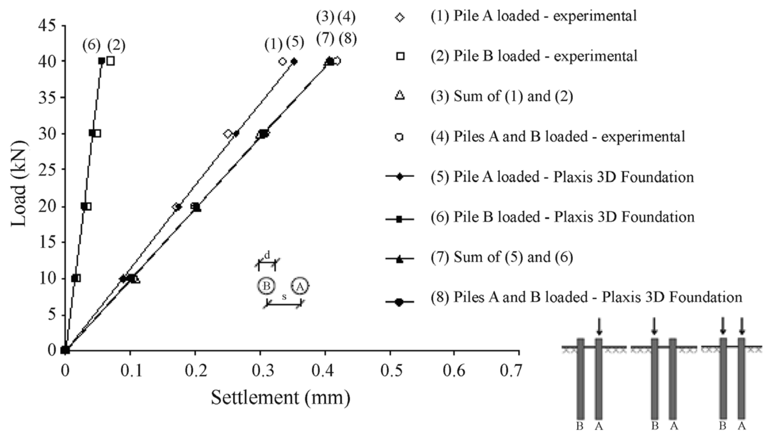

Figure 8 - Results of Test 2 - settlements in pile A (adapted from Freitas, 2010).

the tetrahedral elements. The results obtained for pile A are shown in Fig. 9.

Santana (2008) observed that for a pile group a larger proportion of the load is transferred to the pile tips when compared to isolated piles under the same loading, as also confirmed in the present numerical analysis (Fig. 9). According to Cooke *et al.* (1980) the displacement produced by the source pile generates negative friction on the adjacent piles and therefore a higher load is transferred to the tip, as shown in Fig. 9.

The load transferred by the group to the pile tips is usually less pronounced in clays than in sands. However, Fig. 9 shows that even for clays the higher the loading level, the higher the load transferred by the two-piled group comparably to the isolated pile, as indicated by the higher slopes of the higher load curves.

Figures 10-a (pile A loaded separately) and 10-b (piles A and B loaded simultaneously) show that the displacements at the ground surface are negligible for dis-

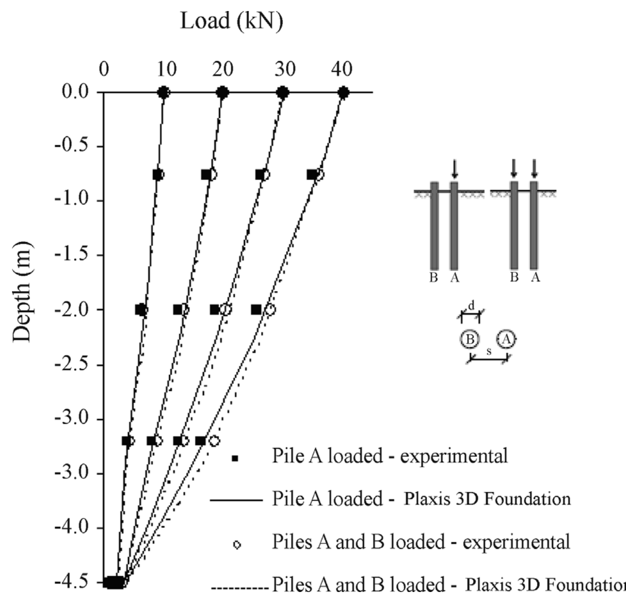

Figure 9 - Load Transfer - Pile A - Test 2 (Freitas, 2010).

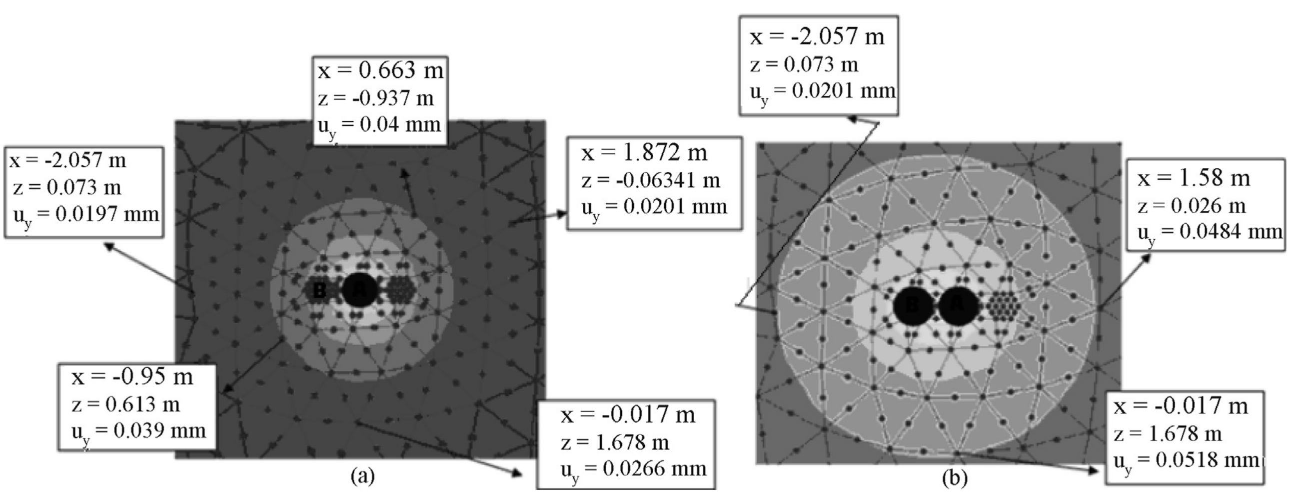

Figure 10 - Vertical displacement (u_y) at the ground surface for loads of (a) 40 kN at pile A (central pile) and (b) 40 kN in piles A and B (Freitas, 2010).

tances higher than 12.5 diameters (2.1 m) from the loaded piles, as also confirmed by Cooke *et al.* (1980).

4.3. Tests 4 and 5 - Row With Three Piles (B, A and C)

Tests 4 and 5 are shown in Fig. 11 according to the following scenarios: i- pile A is loaded alone; ii- pile B is loaded and its effect on pile A (or C) is observed: iii- pile C is loaded and its effect on pile A (or B) is observed; iv- piles A, B and C are loaded simultaneously.

According to Fig. 11, the numerical results for the settlements of pile A (6) are slightly higher than those obtained experimentally (1). On the other hand, the modeled influence on pile A when pile B is loaded (or pile C, by symmetry) practically coincided with the experimental results (2, 3, 7 and 8). The results obtained from the sum of the effects of loads on each pile in pile A (4) are lower than the results obtained when the three piles are loaded simultaneously (5). The settlements in A when the piles in the group are loaded simultaneously are nearly identical to those obtained experimentally (5 and 10).

The numerical results for loading pile B provided values of settlement in pile B a little higher than those obtained experimentally. The numerical values for pile B considering the three piles loaded simultaneously were also a little higher than the experimental results, as shown in Fig. 12.

According to Fig. 13, the numerical results for loading pile C, denoted as (8), provided settlement in C slightly higher than those obtained experimentally (3). However, the effect on pile C for loading pile B, denoted as (7), practically coincided with the experimental data (2), whereas the effect on pile C for loading pile A (6) was slightly lower than the experimental results (1).

The experimental results obtained from the sum of the effects of the loadings on each pile on pile C, denoted as (4) in Fig. 13, were lower than those obtained when the three piles were loaded simultaneously (5). The numerical analysis produced similar results in both cases. The settlements obtained by the numerical analysis in C when the pile group was loaded simultaneously (10) were similar to those obtained experimentally (5).

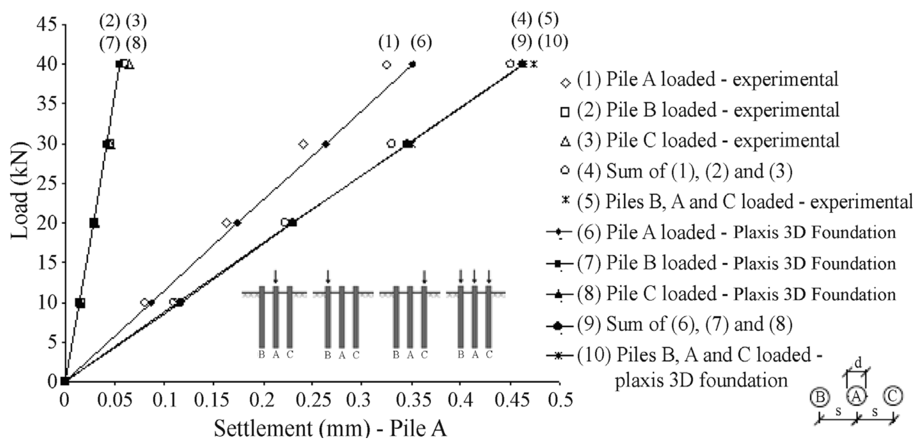

Figure 11 - Results from Tests 4 and 5 - Settlements on pile A (adapted from Freitas, 2010).

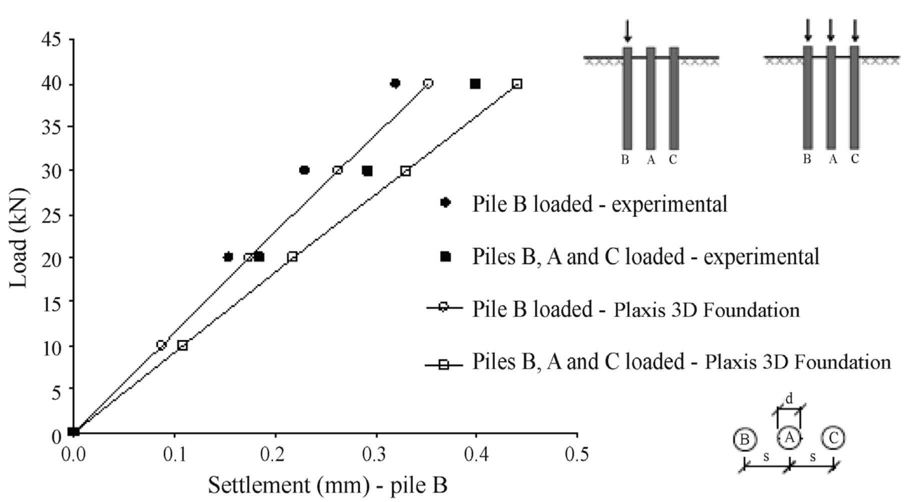

Figure 12 - Results obtained from Tests 4 and 5 - Settlements on pile B (adapted from Freitas, 2010).

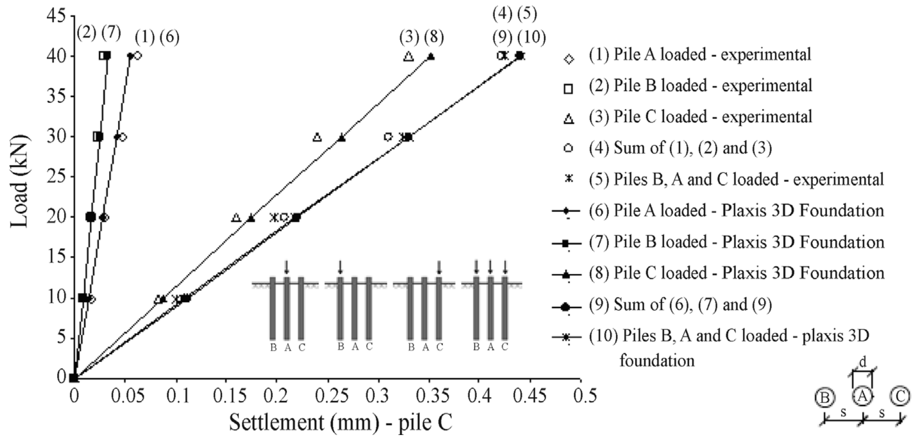

Figure 13 - Results from Tests 4 and 5 - Settlements on pile C (adapted from Freitas, 2010).

Although by symmetry the response of piles B and C should be similar, the experimental settlements on pile B were smaller than those on pile C in the tests with three piles. Clearly such response cannot be reproduced in the numerical results by the simple Mohr-Coulomb model. In fact, pile B has been tested previously in the two-pile array, what most likely caused some overconsolidation in the soil around the pile, in addition to possible soil natural inhomogeneity.

The load transfer obtained experimentally and numerically for pile A is shown in Fig. 14. It is seen that the numerical response is closer to the experimental behavior of the pile A in the group than the same pile loaded alone.

Figure 15 shows the response of pile B, which by symmetry is similar to the response of pile C.

Figure 16 presents the vertical displacements field for the case where the three piles are installed and simultaneously loaded with the same load of 40 kN.

Figure 17, similarly to Fig. 10, also illustrates that for piles B, A and C loaded simultaneously the displacements at the ground surface are negligible for distances larger than 12.5 diameters (2.1 m).

4.4. Test 7 - Row with Three Piles (B, A and C) and Pile Cap

Test 7 compares the settlements obtained when piles A, B and C were loaded simultaneously by the rigid pile cap with the settlements obtained by the three piles loaded simultaneously without the pile cap. Figure 18 illustrates the pile arrangement in the numerical model.

Cooke *et al.* (1980) reported that for the group of three piles with the pile cap loaded incrementally up to the

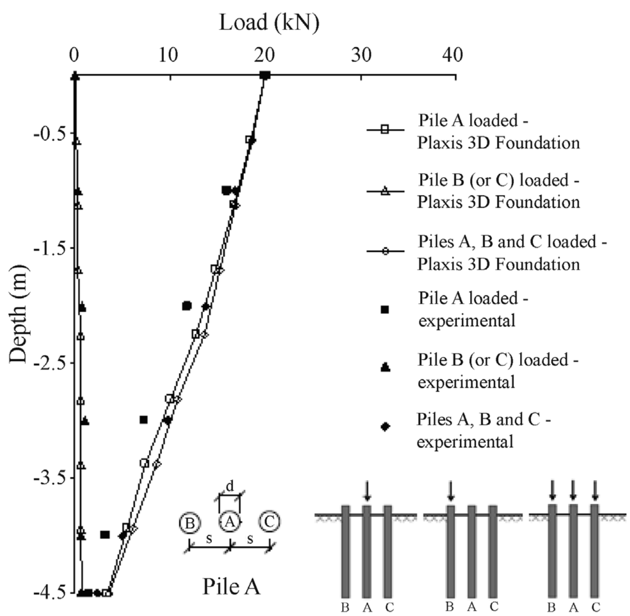

Figure 14 - Results of the Tests 4 and 5 - Load Transfer for pile A (adapted from Freitas, 2010).

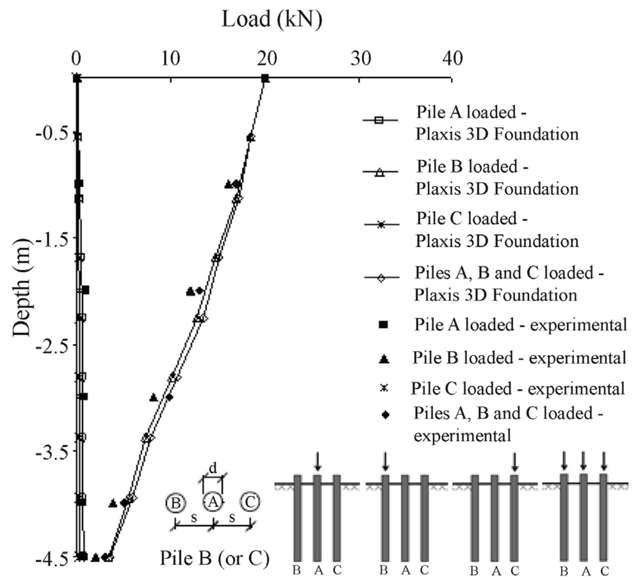

Figure 15 - Results of the Tests 4 and 5 - Load transfer for pile B (Similar to pile C) (adapted from Freitas, 2010).

load of 118.7 kN successive adjustments were needed in the loading as an attempt to ensure as much as possible uniform settlements on the pile cap. These adjustments were not entirely successful, as illustrated in Fig. 19. Clearly, these trial adjustments were not possible to be reproduced in the numerical analysis. As a result, a more rigid behavior of the cap was obtained in the simulated results, as shown in Fig. 19. Therefore the difference between the modeled and the experimental results are attributed to the uncertainty in the application of the loads. Nevertheless, a good agreement was obtained on the average settlements, as illustrated in Fig. 20. Figure 21 illustrates the load transfer for test 7.

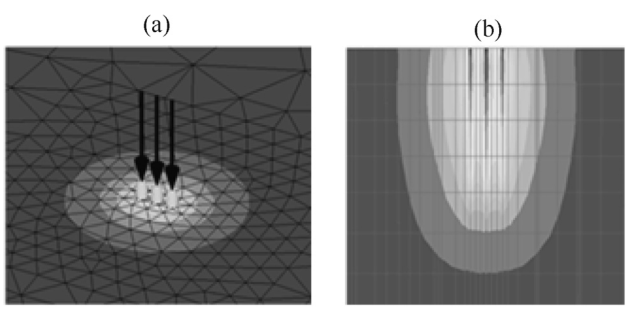

Figure 16 - Vertical displacement in perspective (a) and a section through the axis of the piles (b) for the simultaneous loading of 40 kN at the piles B, A and C (Freitas, 2010).

The load in Fig. 20 is that for the whole group in test 7, while only the central pile is represented in test 4 (considering the three piles loaded simultaneously).

For the case the pile group is loaded through the cap, greater loads were observed experimentally for higher load levels, both for central pile (A) and also for the corner one (B).

For test 7, it is observed on Fig. 22, through both sections A'A (a) and B'B (b), the field of vertical displace-

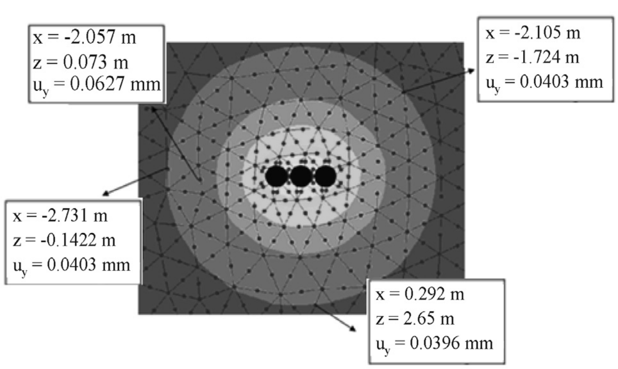

Figure 17 - Vertical displacements at the top of the ground for the loading of 40 kN in each of the piles B, A and C (Freitas, 2010).

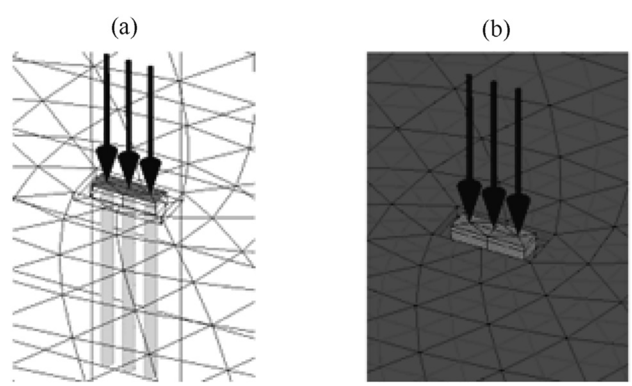

Figure 18 - Test 7: (a) the pile arrangement and (b) the pile cap loading (Freitas, 2010).

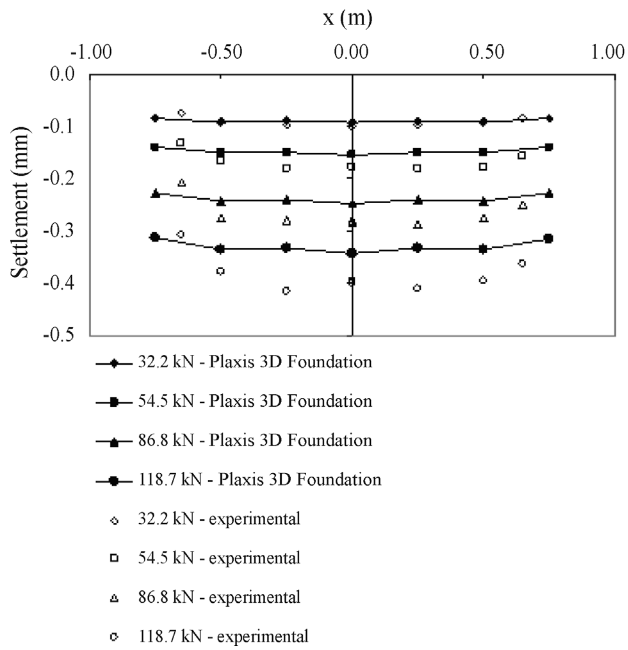

Figure 19 - Settlements measurements in various points of the pile cap (Freitas, 2010).

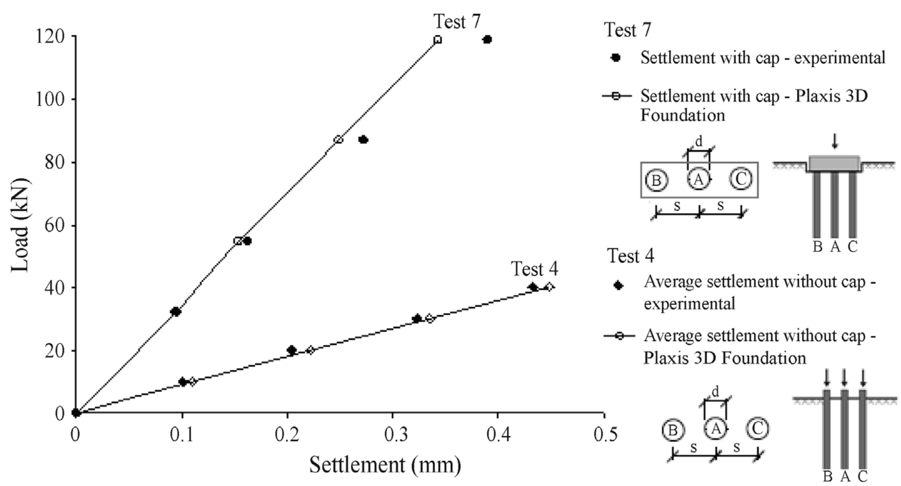

Figure 20 - Results from Tests 4 and 7 - Average settlements (adapted from Freitas, 2010).

ments, numerically obtained in 3-D finite element modeling, when all piles were carried out under 39.6 kN.

5. Conclusions

The paper summarizes some results from Freitas (2010) who extensively examined different arrangements of pile groups through 3-D FEM modeling. The back analysis of Test 1 (isolated pile) enabled the Authors to successfully predict other pile interaction schemes tested by Cooke *et al.* (1980) and to validate the numerical analyses of the tested piles.

The numerical analyses of test 2 showed that the superposition effect of loading two piles separately was very close to the results obtained when both piles were loaded simultaneously. The small differences observed in the load transfer in both piles are attributed to minor differences due to the asymmetric pattern of the automatically generated meshes.

In tests 4 and 5 the effect on pile A when loading pile B (or C by symmetry) coincided fairly well with the experimental data. However, in the tests with three piles, the measured settlements of pile B were lower than the settlements of pile C, a trend not observed numerically. This is probably because pile B had been previously loaded in the sequence with only two piles, causing some over-consolidation in the nearby soil.

The difference between experimental and numerical results in test 7 was mainly attributed to the testing defi-

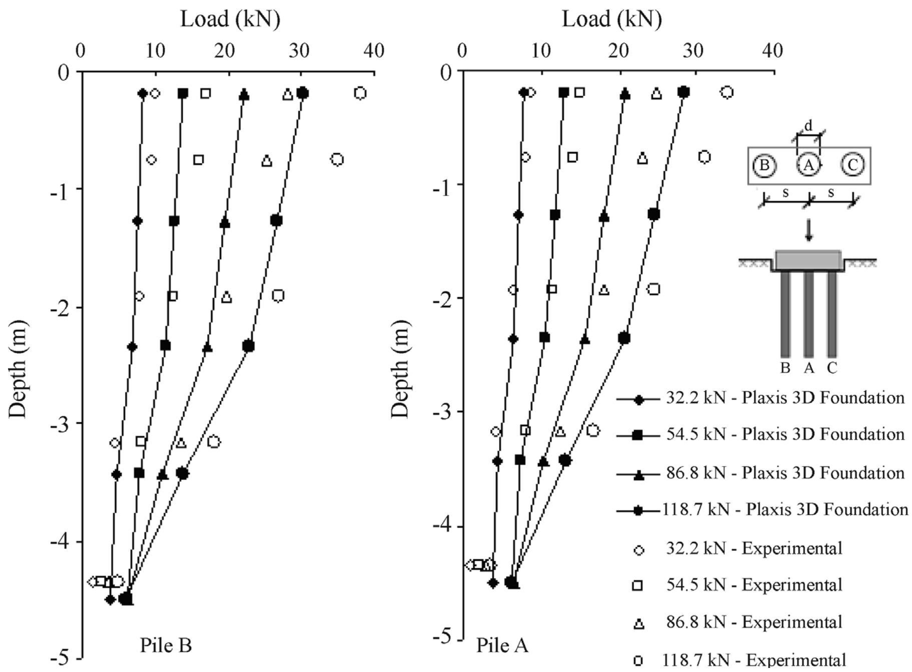

Figure 21 - Results from Test 7 - Load transfer on piles B and A (adapted from Freitas, 2010).

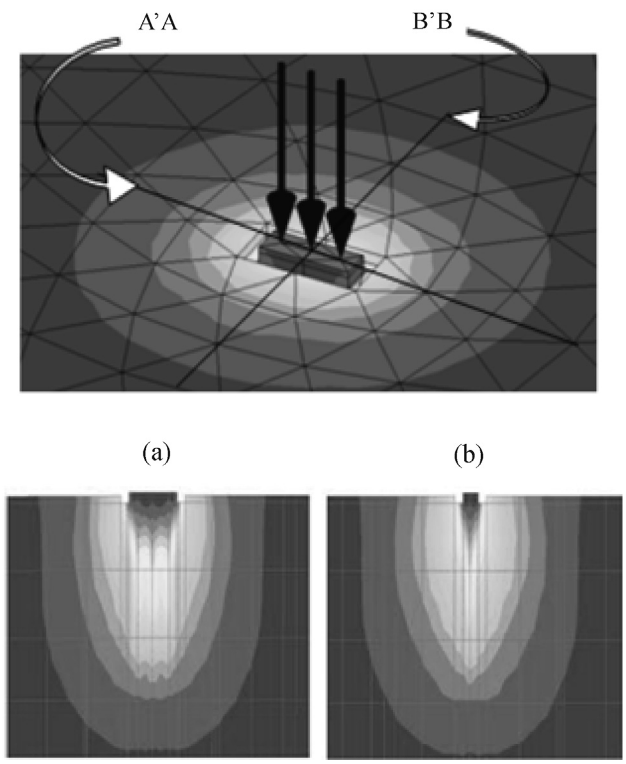

Figure 22 - Vertical displacements of the piles under 39.6 kN for section A'A (a) and vertical displacement for the section B'B (b) (Freitas, 2010).

ciencies reported by Cooke *et al.* (1980) to reproduce the effect of a rigid cap response. The model realistically captured the influence of a nearly rigid cap, with small differential settlements of the three piles, as expected.

It was shown that 3-D FEM analysis is an effective tool to predict pile group settlements and load transfer mechanisms in pile groups. The differences between modeled and experimental results were generally very small in all tests.

References

Addenbrooke, T.I.; Potts, D.M. & Puzrim, A.M. (1997). The influence of pre-failure soil stiffness on the numerical analysis of tunnel construction. Géotechnique, 47(3):693-717.

Atkinson, J.H. (1973). The Deformation of Undisturbed London Clay. PhD Thesis, Imperial College of Science, Technology and Medicine, University of London, London.

Bishop, A.W.; Webb, D.L. & Lewin, P.I. (1965). Undisturbed samples of London Clay from the Ashford Common Shaft: strength-effective stress relationships. Géotechnique, 15(1):1-31.

Bishop, A.W. (1966). Soils and Soft Rocks as Engineering Materials. Inaugural Lecture, Imperial College, University of London.

Brinkgreve, R.B.J. & Swolfs, W.M. (2007). Plaxis 3D Foundation. Version 2. Plaxis BV, 5 v.

Burland, J.B. (1990). On the compressibility and shear strength of natural soils. Géotechnique, 40(3):329-378.

Butterfield, R. & Banerjee, P.K. (1971). The elastic analysis of compressible piles and pile groups. Géotechnique, 21(1):43-60.

Caputo, V. & Viggiani, C. (1984). Pile foundation analysis: a simple approach to non-linearity effects. Rivista Italiana di Geotecnia, 18(2):32-51.

Cooke, R.W.; Price, G. & Tarr, K. (1980). Interaction and group behaviour under working conditions. Géotechnique, 30(2):97-136.

Cooke, R.W.; Price, G. & Tarr, K. (1979). Jacked piles in London clay: a study of load transfer and settlement under working conditions. Géotechnique, 29(2):113-147.

Davies, O.; Rouainia, M.; Glendinning, S. & Birkinshaw, S.J. (2008). Assessing the influence of climate change on the progressive failure of a railway embankment. Proc. International Conference of International Association for Computer Methods and Advances in Geomechanics, Goa, India, v. 6, pp. 4478-4487.

De Santis, L. & Mandolini, A. (2006). Bearing capacity of piled rafts on soft clay soils. Journal of Geotechnical and Geoenvironmental Engineers, ASCE, 132(12):1600-1610.

Fleming, W.G.K.; Weltman, A.J.; Randolph, M.F. & Elson, W.K. (1992). Piling engineering. 2nd ed. Surrey University Press, London.

Freitas, A.C. (2010). Contribuição ao Estudo do Efeito Tridimensional de Instalação e de Grupo em Estacas Cravadas em Areias. M.Sc. Thesis, Universidade do Estado do Rio de Janeiro, 231 p.

Gasparre, A. (2005). Advanced Laboratory Characterization of London Clay. PhD Thesis, Department of Civil and Environmental Engineering, University of London, Imperial College, London, 598 p.

Gasparre, A.; Nishimura, S.; Minh, N.A.; Coop, M.R. & Jardine, R.J. (2007). The stiffness of natural London Clay. Géotechnique, 57(1):33-47.

Hight, D.W.; Bennell, J.D.; Chana, B.; Davis, P.D.; Jardine, R.J. & Porovic, E. (1997). Wave velocity and stiffness measurements of the Crag and Lower London Tertiaries at sizewell. Géotechnique, 47(3):451-474.

Hight, D.W.; Gasparre, A.; Nishimura, S.; Minh, N.A.; Jardine, R.J.& Coop, M.R. (2007). Characteristics of the London Clay from the Terminal 5 site at Heathrow Airport. Géotechnique, 57(1):3-18.

Hight, D.W.; McMillan, F.; Powell, J.J.M.; Jardine, R.J. & Allenou, C.P. (2003). Some characteristics of London Clay. Proc. Conference on Characterization and Engineering, Singapore, v. 2, pp. 851-907.

Hight, D.J. & Jardine, R.J. (1993). Small strain stiffness and strength characteristics of hard London Tertiary clays. Proc. International Symposium on Hard Soils-Soft Rocks, Athens, v. 1, pp. 533-522.

Jovicic, V. & Coop, M.R. (1998). The measurement of stiffness anisotropy in clays with bender element tests in the triaxial apparatus. Geotechnical Testing Journal, 21(1):3-10.

Kovacevic, K.; Potts, D.M. & Vaughan, P.R. (2001). Progressive failure in clay embankments due to seasonal climate changes. Proc. International Conference on Soil Mechanics and Geotechnical Engineering, Istanbul, v. 5, pp. 2127-2130.

Mandolini, A. (1999). Small-strain stiffness and settlement prediction for piled foundations. Panel Report, Proc. of the 2nd International Symposium on Pre-failure deformation characteristics of geomaterials, Torino. M. Jamiolkowski, R. Lancellotta & D. Lo Pres (eds) Balkema Publishes, Netherlands, v. 2, pp. 1397-1404.

Marsland, A. (1971). Laboratory and in situ measurements of the deformation moduli of London Clay. Proc. Symposium on Interaction of Structure and Foundation, London, pp. 7-17.

Marsland, A, (1974). Comparisons of the results from static penetration tests and large in situ plate tests in London Clay. Proc. European Symposium of Penetration Testing, Stockholm, pp. 245-252.

Poulos, H.G. (1968). Analysis of the settlement of pile groups. Geotechnique,18(4):449-471.

Sandroni, S.S. (1977). The Strength of London Clay in Total and Effective Stress Terms. PhD Thesis, University of London, London.

Santana, C.M. (2008). Comparação entre metodologias de análise de efeito de grupo de estacas. MSc Thesis, COPPE, Universidade Federal, Rio de Janeiro, 160 p.

Skempton, A.W. (1944). Notes on the compressibility of clays. Quarterly Journal of the Geological Society of London, 100:119-135.

Skempton, A.W. (1961). Horizontal stresses in an overconsolidated Eocene clay. Proc. International Conference in Soil Mechanics and Foundation Engineering, Paris, v. 5, pp. 351-357.

Skempton, A.W. & La Rochelle, P. (1965). The Bradwell slip: a short-term failure in London Clay. Géotechnique, 15(3):221-242.

Skempton, A.W.; Schuster, F.R.S. & Petley, D.J. (1969). Joints and fissures in the London Clay at Wraysbury and Edgware. Géotechnique, 19(2):205-217.

Skempton, A.W. (1977). Slope stability of cutting in brown London clay. Proc. International Conference in Soil Mechanics and Foundation Engineering, Tokyo, v. 9, pp. 261-270.

Standing, J.R. & Burland, J.B. (2006). Investigation on variations in tunneling volume loss: a case study. Proc. 5th International Conference on Geotechnical Aspects of Underground Construction in Soft Ground, Amsterdam, pp. 305-311.

St. John, H.D. (1975). Field and Theoretical Studies of the Behaviour of Ground Around Deep Excavations in London Clay. PhD Thesis, University of Cambridge, Cambridge.

Ward, W.H.; Samuels, S.G. & Butler, M.E. (1959). Further studies of the properties of London Clay. Géotechnique, 9(2):33-58.

Ward, W.H.; Marsland, A. & Samuels, S.G. (1965). Properties of the London Clay at the Ashford Common shaft: in-situ and undrained strength tests. Géotechnique, 15(4):321-344.

Webb, D.L. (1964). The Mechanical Properties of Undisturbed Samples of London Clay and Pierre Shale. PhD Thesis, University of London, London.

Windle, D. & Wroth, C.P. (1977). Ln situ measurements of the properties of stiff clays. Proc. International Conference on Soil Mechanics and Foundation Engineering, Tokyo, v. 9, pp. 347-352.

Wongsaroj, J.; Soga, K.; Yimsiri, S. & Mair, R.J. (2004). Stiffness anisotropy of London Clay and its modelling: laboratory and field. Proc. The Skempton Memorial Conference on Advances in Geotechnical Engineering, London, v. 3, pp. 1205-1216.

Wroth, C.P. (1971). Some aspects of the elastic behaviour of overconsolidated clay. Proc. Roscoe Memorial Symposium, Foulis, pp. 347-361.

Precipitation Influence on the Distribution of Pore Pressure and Suction on a Coastal Hillside

L.P. Sestrem, A.C.M. Kormann, J.H.F. Pretto, F.A.M. Marinho

Abstract. The frequent interruption of roads in some freeways in Brazil due to slope failure has caused economic losses and potential harm to users. The paper presents data from a monitoring system installed at Serra do Mar in Santa Catarina State, Brazil. The slope monitored is called Morro do Boi and is located on BR-101 south, near the municipality of Itapema. It was stabilised using anchor and flexible metal mesh. Hence, all the pore water pressure measured is due to environmental changes. After approximately sixteen months of readings, it was possible to observe that the suction variation in the unsaturated layers presents a time delay in relation to the rainfall observed in the area. The ground water table presented a variation of about 1.5 m. The analyses of the data allowed establishing a trigger accumulated rainfall that reduces the negative pore water pressure to values below 10 kPa. So far, no significant positive pore water pressure has been observed above the ground water table.

Keywords: coastal slopes, geotechnical instrumentation, mass movements.

1. Introduction

The implementation and operation of highways as well as the management of potential risks through their life cycle represent a major engineering challenge which involve multidisciplinary knowledge (geological, geotechnical and environmental). These operations become even more complex when structures are located along regions such as Serra do Mar (Tavares, 2010). Soil masses at this location, mainly composed of colluvial and residual soils, are characterized by a weathering profile as a result of physical, chemical and biological processes. Such formations are shaped by the strong influence of environment and geomorphology dynamic agents (climate, topography, rock matrix, etc.). The data obtained by an instrumentation system deployed in a stabilized slope are presented and discussed herein, aiming to correlate pore water pressure readings with rainfall events. The instrumentation system measured the pore pressure variations in order to better understand the mechanisms which promote slope instability.

2. Study Area Description

The instrumentation was installed at a slope located at km 140+70 m of freeway BR-101 south track between the cities of Balneário Camboriú and Itapema, in Santa Catarina. Figure 1 presents a satellite view of the area. The slope monitored is at an elevation of 160 m above sea level, with inclinations between 1.0V:1.5H and 1.0V:2.0H. Site history shows scars of instability created after a heavy rainfall (1005 mm accumulated that month) occurred in November 2008, which caused partial highway interruption. After these occurrences, the slope was stabilized with a passive anchors system combined to a specific metal mesh to retain the slipped masses in their remaining position (Kormann *et al.*, 2011).

The region of Morro do Boi is characterized by the occurrence of two types of rock: intrusive Nova Trento granites and Morro do Boi migmatites. Such lithologies are lightly fractured and have relatively high strength when they remain unexposed to considerable climate changes. Morro do Boi is affected by NE-SW and NW-SE shear surfaces, and by sub-horizontal fractures that divide the rock mass into blocks, considerably reducing the mechanical strength of the slope. It is worth noting that the presence of colluvial/talus soils results in a very heterogeneous structure with a high weathering degree and an extremely low cohesion (Fiori, 2011).

Another key aspect is the occurrence of localized underground water flow through the slope, resulting from connections between discontinuity families. Therefore, translational or wedge slides occur involving rock block movements along planar surfaces and rock block motions along two intersecting joint surfaces. The occurrence of shallow landslides in the soil-rock contacts or in adjacent planes of discontinuities is normally associated with cuts that result in soil layers with irregularly distributed thicknesses. Moreover, the phreatic level is not constant along the slope, being the rock permeability controlled by the fractures, particularly by the ones which experienced pressure relief, usually disposed in a parallel direction to the slope (Sestrem & Kormann, 2013).

Liamara Paglia Sestrem, PhD. Student, Researcher, Universidade Federal do Paraná, Curitiba, PR, Brazil, e-mail: liamarasestrem@gmail.com.
Alessander Christopher Morales Kormann, PhD, Associate Professor, Universidade Federal do Paraná and Director, Fugro In Situ Geotecnia Ltda, Curitiba, PR, Brazil, e-mail: alessander@ufpr.br.
José Henrique Ferronato Pretto, MSc, Researcher, Universidade Federal do Paraná, Curitiba, PR, Brazil, e-mail: jose.fpretto@gmail.com.
Fernando Antônio Medeiros Marinho, PhD, Associate Professor, Universidade de São Paulo, São Paulo, SP, Brazil, e-mail: fmarinho@usp.br.
Submitted on December 21, 2014; Final Acceptance on April 21, 2015; Discussion open until December 31, 2015.

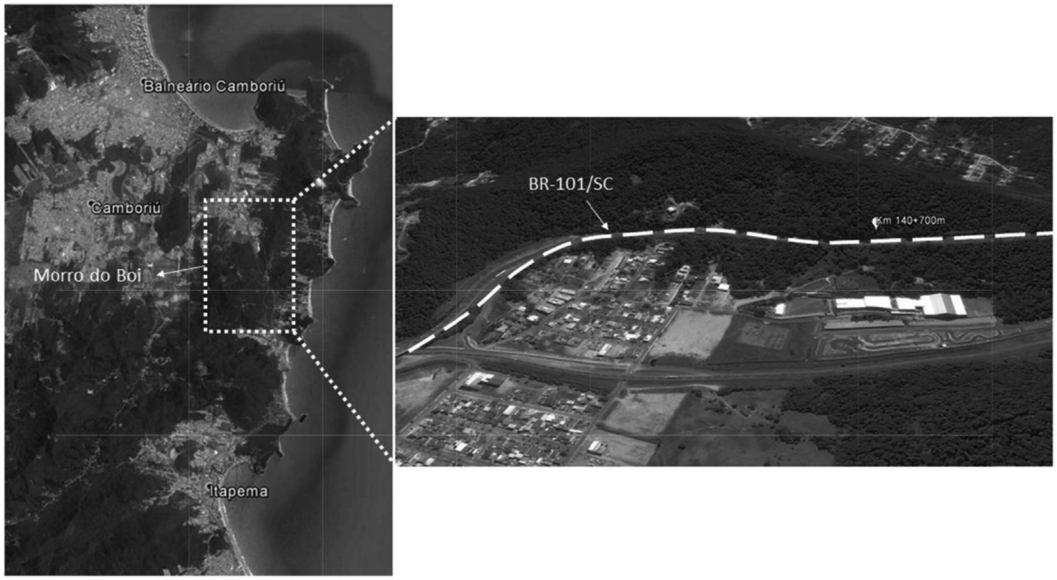

Figure 1 - Study area location.

In order to obtain more precise information about the local stratigraphy, prior to the instrument system installation, two boreholes were carried out at the site as can be observed in Fig. 2. The boreholes stopped at 3 m below the bedrock and its perforations were subsequently used for installing inclinometers. Figure 2 also indicates the three groups of instrumentation of the slope. The range of ground water table variation is indicated in Fig. 2. Based on the results, a layer of soil and weathered rock with total thickness varying between 8 and 10 m was identified. The following layers were observed: colluvial soil with thicknesses up to 3 m, highly weathered rock (residual soil) with thicknesses between 2 and 3 m and moderately weathered rock with thicknesses between 3 and 4 m. Underneath these layers, there is a bedrock of migmatite.

Further characterization and shear strength laboratory tests were performed by Lazarim (2012). Based on these tests, the results showed an average unit weight of 2.66 g/cm^3, average liquid limit of 32% and average plastic limit of 27%, representing materials of low plasticity and compressibility. Particle size distribution indicated predominantly sandy soils (60.4%) with 27.0% of silt,

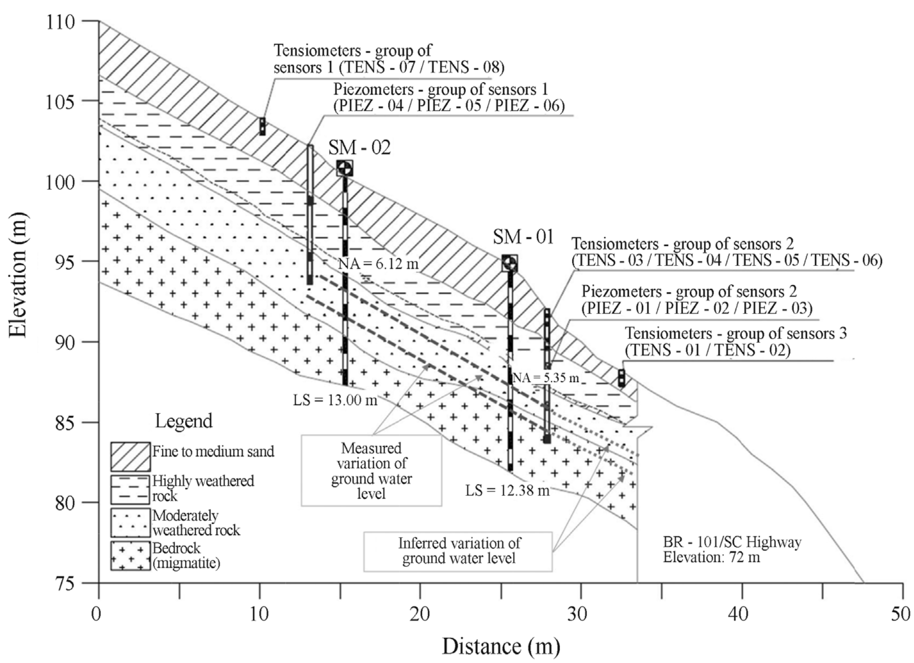

Figure 2 - Geological and geotechnical profile of the studied slope.

8.3% of gravel and only 4.3% of clay. Based on direct shear tests performed in four different block samples, effective friction angles between 28° and 39° and cohesion intercepts between 1 and 17 kPa were obtained. The collection depth ranged between 0.25 and 1.27 m, the water content between 3 and 10% and saturation degree ranged between 2 and 8%.

3. Instrumentation and Geotechinical Monitoring Plan

The monitoring system used was conceived aiming to increase the understanding of the water movement and pressure variation along the soil profile studied. For that purpose, an instrumentation plan with an automated data collection system was designed to evaluate the pore pressure variations due to rainfall. Figure 3 presents a topographic plan of the studied area indicating the groups of instrumentation.

The monitoring system began with the installation of 2 conventional inclinometers embedded 3 m in the bedrock (recovery above 95%). Based on the description of materials found in these borings (Fig. 2), it was possible to define the depth for the installation of the vibrating wire piezometers (Geokon, 2014b), with the initial objective of monitoring the ground water table. The piezometers were installed at the residual soil layer center, at the interface soil - weathered rock, and at the contact between the weathered rock and bedrock. This configuration was used in two sections of the slope, being one uphill of the stabilized area (group of sensors 1) and the other inside it (group of sensors 2), enabling a comparative analysis between both places.

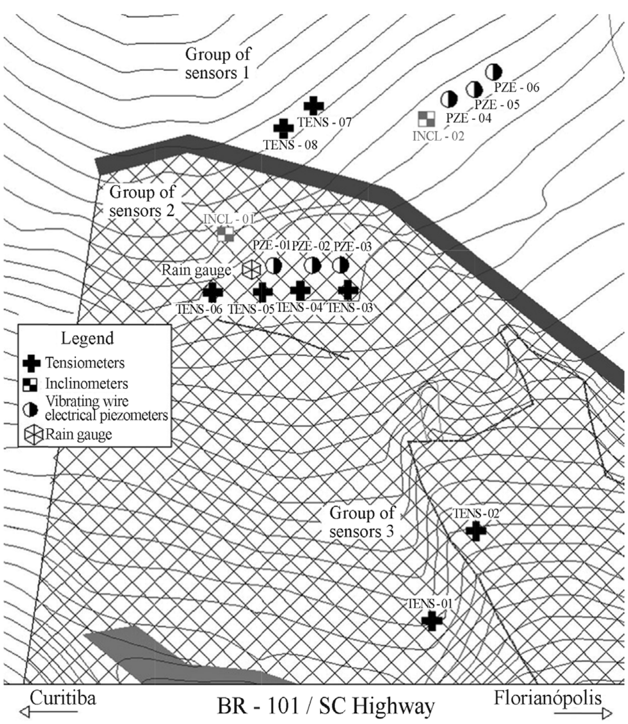

Figure 3 - Instruments location.

Regarding suction measurements, eight ordinary tensiometers using a pressure transducer with capability of reading between -100 to +75 kPa (Soilmoisture, 2014a; 2014b). The position of each sensor is shown in Table 1 and in Table 2.

For rainfall monitoring, a pluviometer of the tipping bucket type was installed, able to register events at each 0.25 mm of precipitation. Data were stored in a proper data logger with a maximum reading capacity of 700 mm/h and able to register date and time of each event (Hydrological Services, 2014a, 2014b).

The monitoring of all sensors began in May 2012 in an automated way through a data logger (Geokon, 2014a) with time intervals initially set to 8 h . During the period between 11/08/2012 and 12/12/2012, it was not possible to collect data due to technical problems.

4. Results and Discussions

In the following items, based on the monitoring system installed and on additional data related to the rainfall in the studied area, the results are presented and discussed. The main focus is to correlate the pore pressure readings with rainfall and with the geometric, geologic and geotechnical characteristics of the slope.

Table 1 - Installation depths of piezometers.

Group of sensors	Instrument	Installation elevation (m)	Depth (m)
1	PIEZ-01	92.4	8.65
	PIEZ-02	92.4	6.40
	PIEZ-03	92.4	3.90
2	PIEZ-04	101.5	8.60
	PIEZ-05	101.5	7.20
	PIEZ-06	101.5	3.70

Table 2 - Installation depths of tensiometers.

Group of sensors	Instrument	Installation elevation (m)	Depth (m)
1	TENS-01	86.0	1.00
	TENS-02	88.0	2.00
2	TENS-03	92.4	0.50
	TENS-04	92.4	3.00
	TENS-05	92.4	1.00
	TENS-06	92.4	2.00
3	TENS-07	103.7	1.00
	TENS-08	103.9	2.00

4.1. Rainfall

Figure 4 shows the total monthly precipitation during the monitoring period. It can be observed that the monthly precipitation presented an extremely variable pattern. Dividing the monitoring period in seasons, between the Summer and Autumn of 2015 the highest precipitation was observed. However, the Autumn of 2012 and the beginning of the Winter of 2012 presented a high level of precipitation as well. The extremely variable distribution of rain during the period of the study makes the use of monthly precipitation less useful from a geotechnical point of view.

To emphasize the great variability observed, Fig. 5 presents a comparison between the months of the different years monitored. The use of precipitation data for geotechnical purposes requires a detailed analysis.

A summary of some characteristics of rainfall events recorded by the rain gauge is shown in Fig. 6, listing the maximum daily volumes and respective occurrence schedules. The data for Nov/2012 and Jun/2013 include partial acquisition periods. From the results, March 2013 was verified to have the highest rainfall so far (382.50 mm) and the lowest ones occurred in June 2013 (55.75 mm), representing a variation of almost 700%. Regarding the distribution of these events, it is possible to observe periods whose cumulative monthly volumes are similar in spite of having very different average intensities, such as the months of February 2013 and July 2013. In the first one, rains were spread over 28 days (occurrence of daily events) and in the second one only over 16. Sestrem (2012) and Acevedo (2013) compared the precipitations measured by the rain gauge of Morro do Boi with the ones acquired in nearby cities (Navegantes and Itajaí), respectively. The authors report significant variations that show the importance of sensor installation in areas of specific interest.

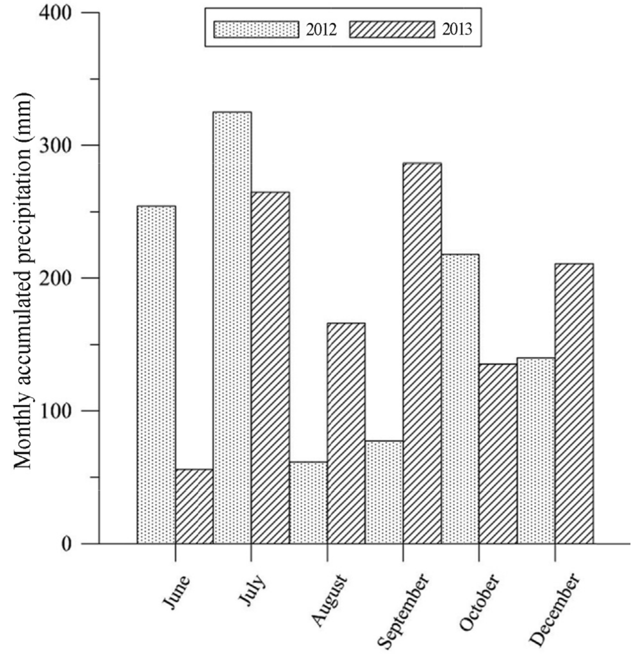

Figure 5 - Comparison between similar periods - monthly accumulated precipitation (mm).

Readings can also be assembled according to seasons, as displayed in Table 3. There are large differences between the values obtained in the same period for the first two years of monitoring, reinforcing the importance of precipitation

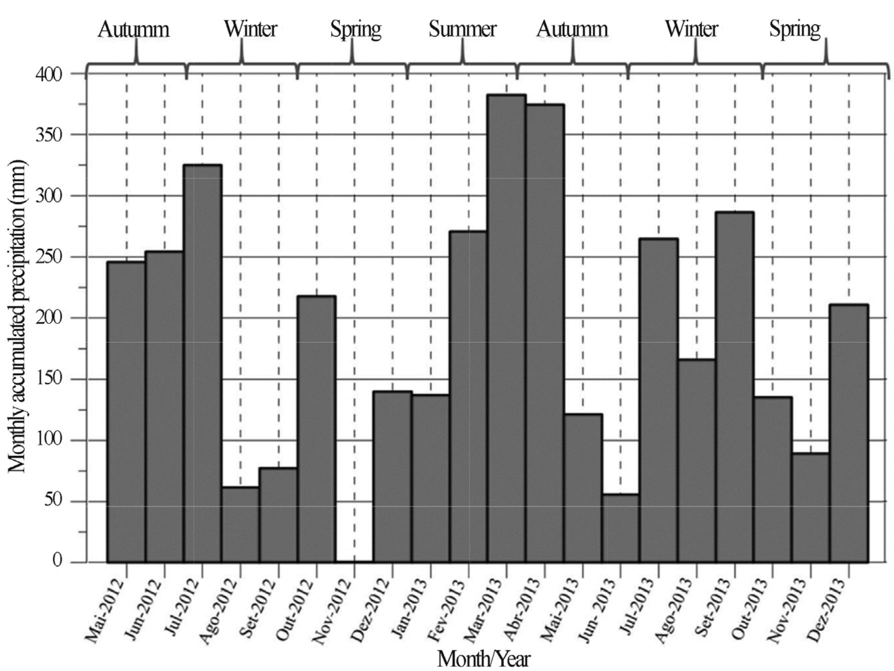

Figure 4 - Monthly accumulated rainfall (mm).

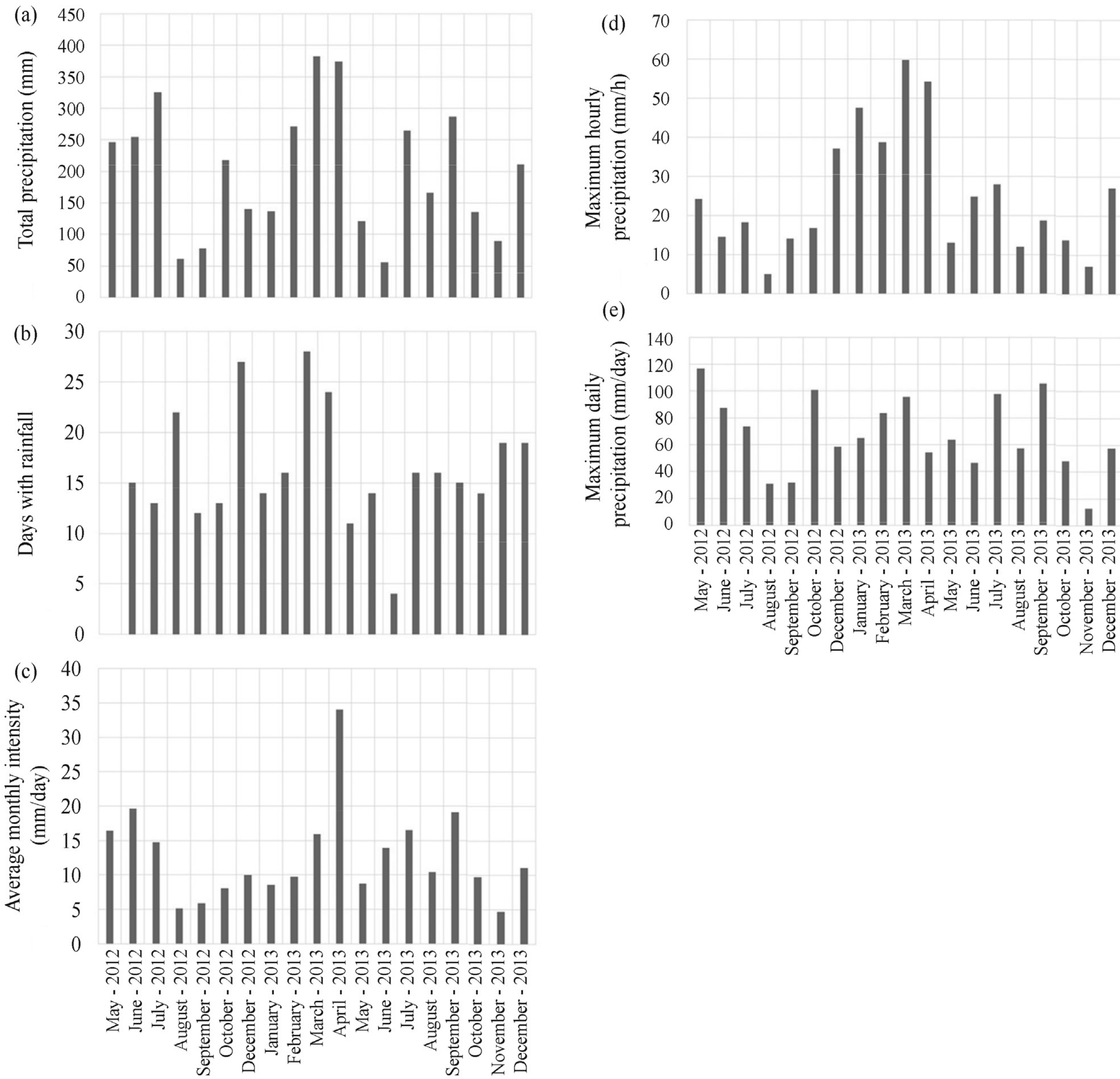

Figure 6 - Rainfall events during the monitoring period - (a) Total precipitation, (b) Days with rainfall, (c) Average monthly intensity (mm/day), (d) Maximum hourly precipitation (mm/h) and (e) Average monthly intensity (mm/day).

Table 3 - Precipitation according to seasons.

Number	Period	Precipitation (mm)		
		Daily maximum	Mean	Total
1	Autumn - 2012	116.75	8.69	451.75
2	Winter - 2012	73.75	5.35	502.50
3	Spring - 2012	100.75	3.56	317.00
4	Summer - 2012	95.75	9.14	822.75
5	Autumn - 2013	194.00	6.19	569.75
6	Winter - 2013	105.50	7.54	708.50
7	Spring - 2013	57.75	4.54	408.25

monitoring in areas of specific interest. However, the importance of continued monitoring is emphasized which is essential for a better interpretation as well as for developing reading forecasts and alert criteria.

4.2. Changes in pore pressure

The six vibrating wire piezometer installed aimed to monitor the water table, but they were also capable of measuring negative pore water pressure. According to Geokon (2014b, 2014c) those sensors can record pore water pressure between - 100 kPa and 350 kPa In Fig. 7a, the one-day accumulated rainfall with time is presented. Figure 7b presents the data from piezometers 04, 05 and 06 with time and Fig. 7c presents the results from piezometers 01, 02 and 03 with the daily accumulated precipitation. All of them are associated to the period of monitoring between May 2012 and December 2013. It seems that there is a correspondence between the piezometer readings and the rainfall, particularly for the piezometers with positive readings.

The most significant changes were observed at events with precipitations in excess of 20 mm. A clear correspondence is observed at the beginning of the Winter of 2012, beginning of Autumm of 2013 and the same occurred at the beginning of the Winter and Spring of 2013. The data from three-day accumulated rainfall shown in Fig. 6a show a clear trend.

Note that both absolute values and the maximum variations obtained so far (about 11 kPa) are consistent with the local stratigraphy, which is characterized by the occurrence of layers with irregular thicknesses of colluvial and

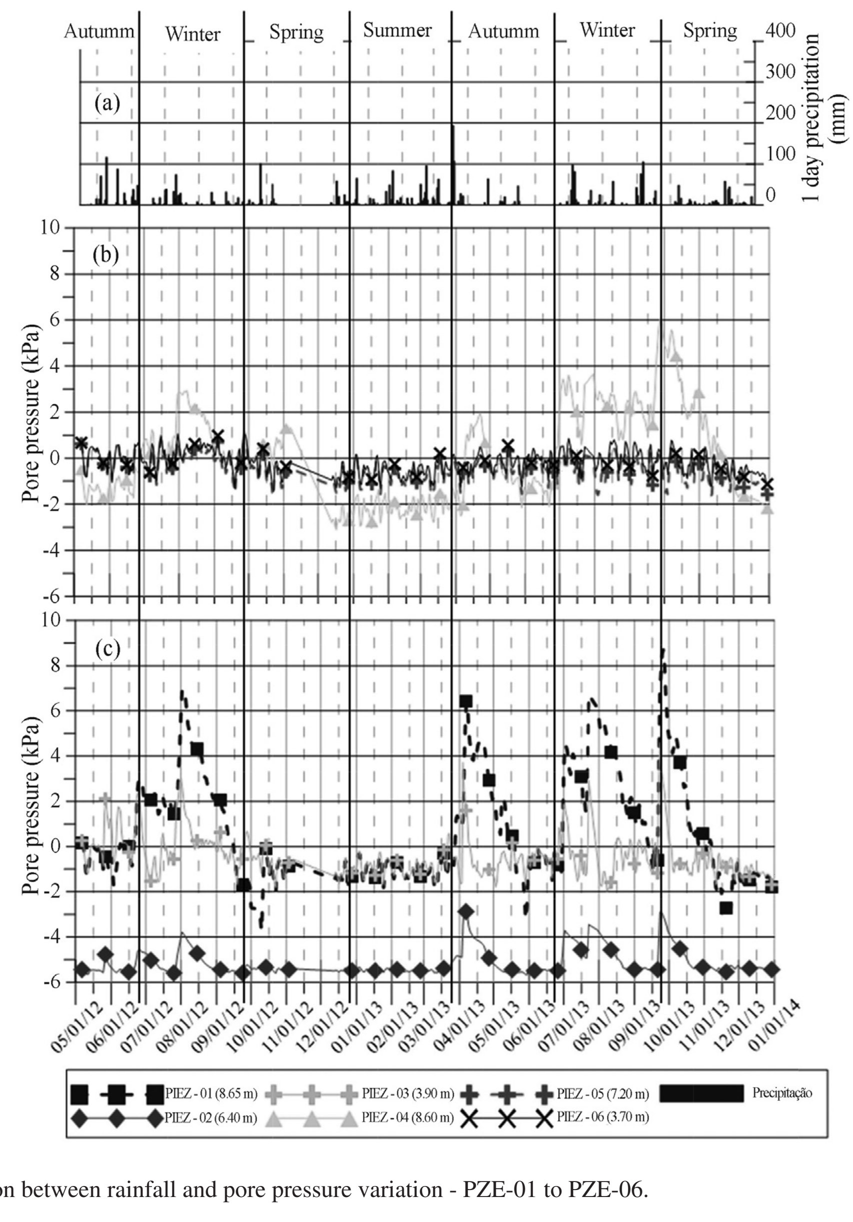

Figure 7 - Comparison between rainfall and pore pressure variation - PZE-01 to PZE-06.

residual soils. In addition, the occurrence of the families of fractures mentioned previously, responsible for the secondary order permeability of the slope, may act to control the ground water table. Figure 8 presents the maximum variations according to the depth of the piezometer and related to the season. Based on these analyses, it is possible to identify larger variations for deeper sensors (8.60 and 8.65 m), mainly during the Winters of 2012 and 2013. Some piezometers seem to be always above the ground water table.

The lack of coherence observed between rainfall events and pore pressure changes in the group of sensors 1 and 2 may be justified by the data presented in Fig. 9. The ground water level can be seen to be below the piezometers elevations for most of the time.

4.3. Suction variations

Readings obtained with the eight installed tensiometers are shown in Figs. 10 to 12, according to the instrumentation groups of sensors shown in Fig. 3. The results are shown with the daily precipitation data obtained from the rain gauge. The response of the tensiometers to the rainfall did not show the same behavior observed for the piezometers measuring the ground water table. This was clearly true for piezometers installed below the ground water table which showed an increase in level immediately after a daily rain fall higher than about 60 mm.

Although the response of the tensiometers was not directly related to the rainfall in the monitoring area, a systematic delay for the response can be observed both in terms of suction increases and reductions. One of the factors for the time delay for the response may be associated to the vegetation, as mentioned by Sestrem & Kormann

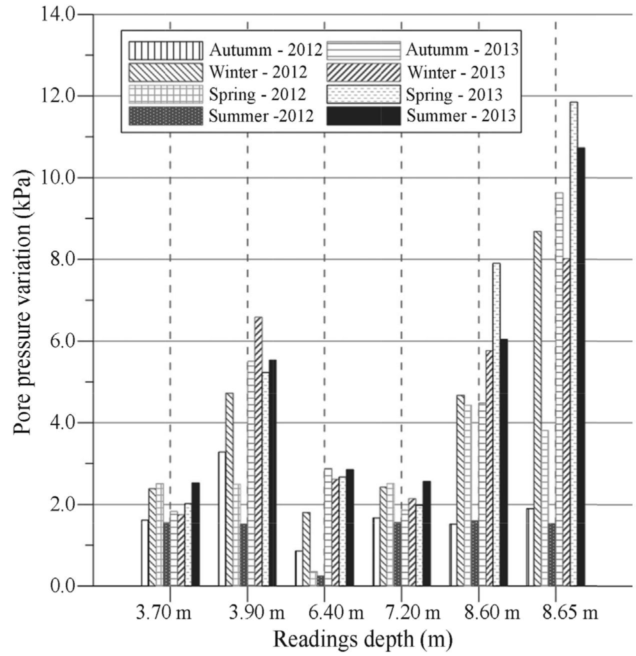

Figure 8 - Maximum pore pressure variations according seasons - data grouped by sensor.

(2013). Figure 13 presents two photos, one taken at the beginning of the monitoring (Fig. 13a) and the other four months later (Fig. 13a). It can be observed that the growth of vegetation in the area may contribute not only to the evaporation increase but also to a delay in the rainfall infiltration rate. Attention should be called to the difference in behavior observed for the tensiometers installed at group 3. The level of suction was most of the time below 10 kPa. It

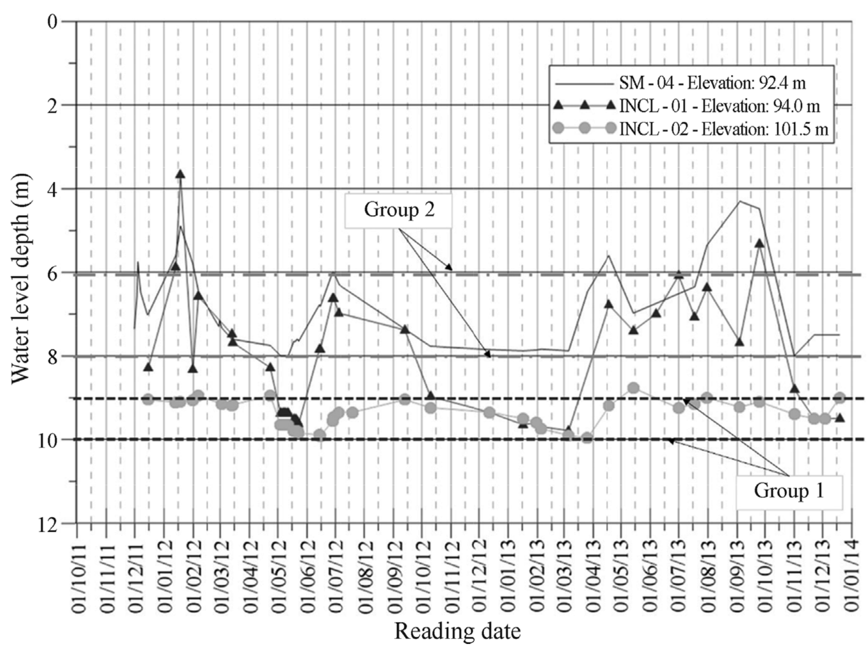

Figure 9 - Variation of water level.

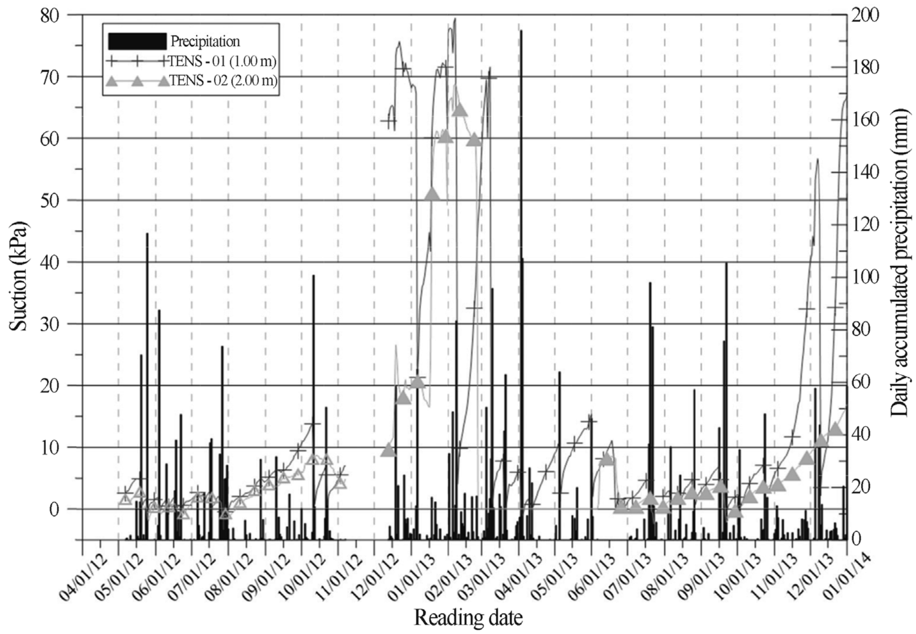

Figure 10 - Comparison between precipitation and suction variation - TENS-01 and TENS-02 (Group 1).

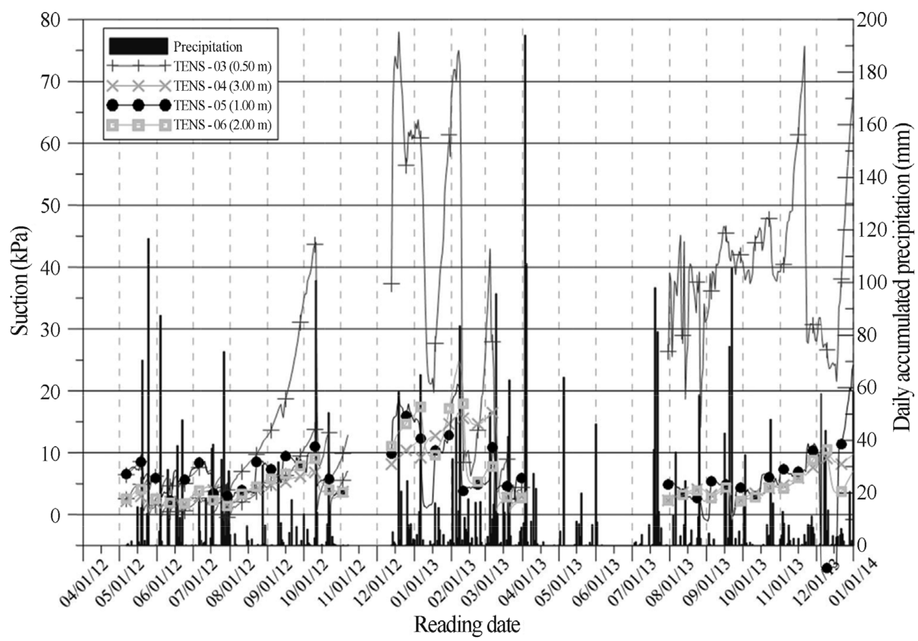

Figure 11 - Comparison between precipitation and suction variation - TENS-03 and TENS-06 (Group 2).

must be observed that the only difference between group 3 location and the others is the vegetation, which may affect superficial drainage.

In order to have a more comprehensive picture of the behavior of the suction with depth, the data were gathered by group and by months, giving the suction profile for each month. The results suggested a behavior that could be divided according to the season.

Figure 14 compares the seasonal variations of measured suction by group 2 in Spring and Winter in 2012. It should be noted the difference between these two periods. In Spring 2012, the magnitude of suction was higher, which could be associated with the low accumulated monthly precipitation in this period (317 mm). On the other hand, in Winter 2012, when the accumulated monthly precipitation was 502.5 mm (58% higher), the suction levels in the upper layers remained below 30 kPa. Based on the minimum and maximum groundwater level presented in Fig. 9, two additional lines were drawn in Fig. 14. It can be seen that the suction levels vary within the equilibrium range.

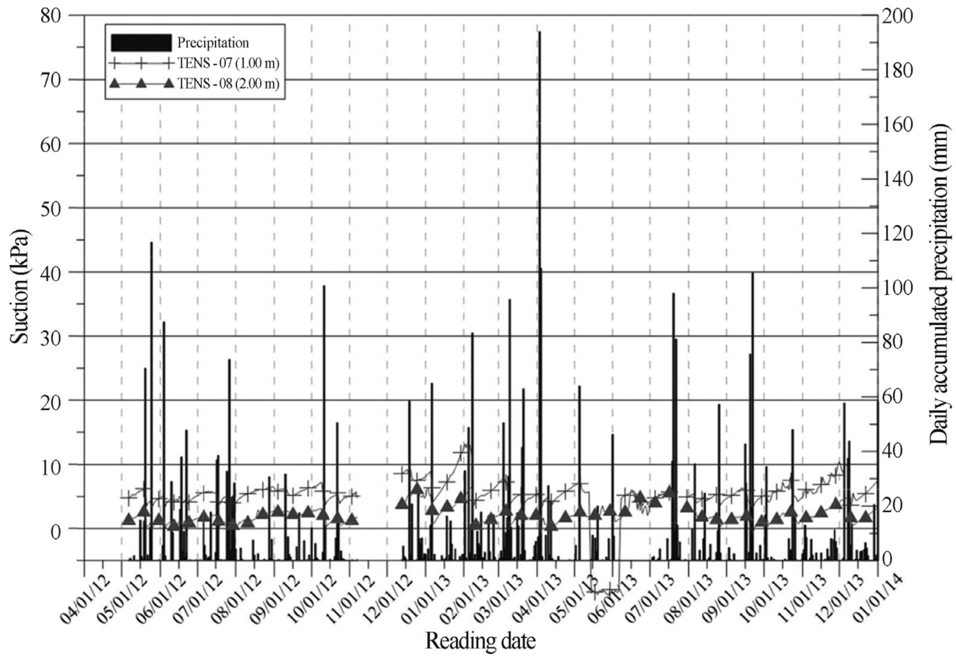

Figure 12 - Comparison between precipitation and suction variation - TENS-07 and TENS-08 (Group 3).

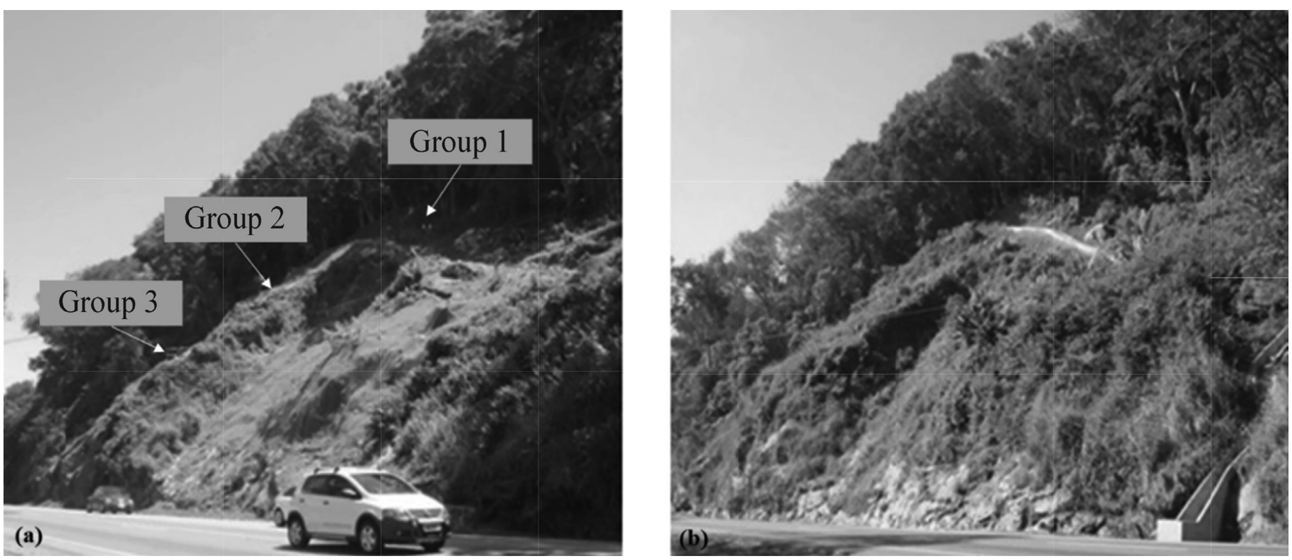

Figure 13 - Vegetation on the site the instruments were installed: (a) at the start of monitoring (b) after four-month monitoring.

Figure 15 shows the variation in the measured suction by sensors of group 2 throughout the study period. Based on these results, it appears that between 1 and 4 m suction level remains below 30 kPa. The most superficial sensor (TENS-03 at 0.5 m) reaches suction levels of about 80 kPa. These changes still seem to lie within the range of equilibrium.

Considering the lack of direct correlation between the rainfall and the suction change, it was investigated whether the accumulated rainfall for 3, 5 and 7 days could be used to justify the changes in suction. It was verified that the better correlation was associated to the three-day accumulated rainfall. The comparison between suction variation and the accumulated rainfall in three days are shown in Fig. 16 (a) and (b). Events above 150 mm of precipitation in 3 days are observed to keep the suction levels below 10 kPa. Furthermore, it is possible to conclude that the suction level is maintained above 20 kPa when 3-day accumulated precipitation is less than approximately 100 mm.

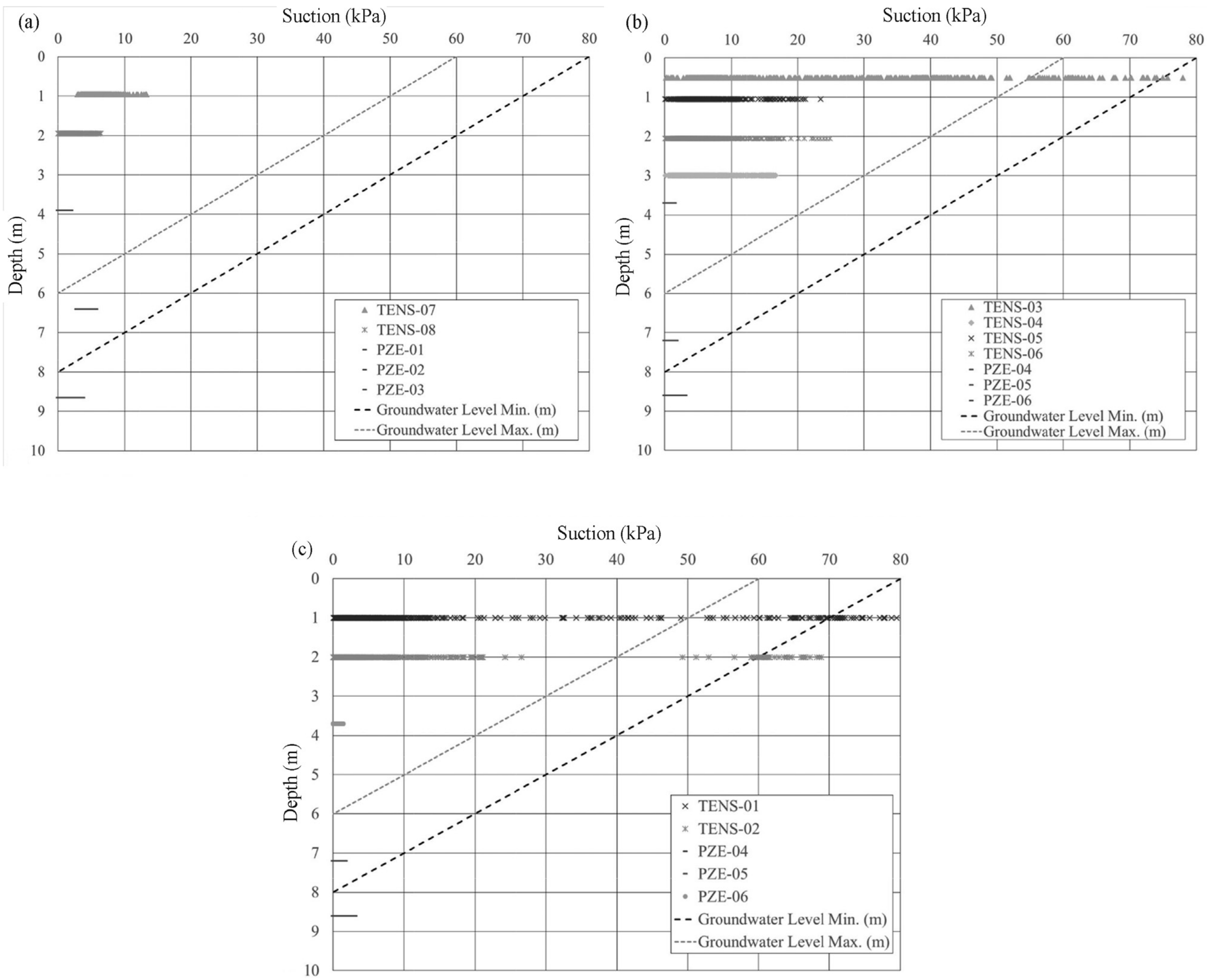

Figure 14 - Seasonal variations of measured suction by group - (a) Group 1, (b) Group 2 and (c) Group 3.

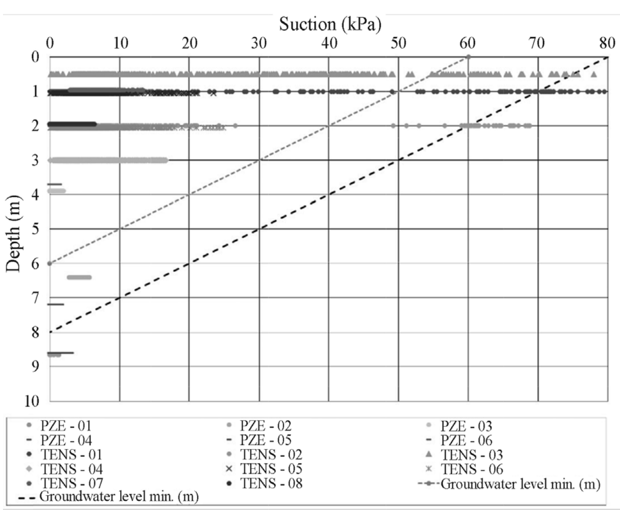

Figure 15 - Measured variations of suction by group 2 all over the monitored period.

Figure 17 presents the three-day accumulated rainfall according to time. Most 3-day rainfall events are lower than 100 mm which is important information regarding eventual reduction in the slope safety factor.

5. Conclusions

The instrumentation used for this study provided important information regarding the presence of water along nearly two years on a slope in a tropical area of the South part of the Serra do Mar in Brazil. The use of tensiometers and rain gauges associated with piezometers allowed better understanding the water movement along the soil profile during the study period. The following conclusions can be drawn from the present study:

The analyses of the rain distribution along the monitoring period could not be directly related to pore water pressure changes.

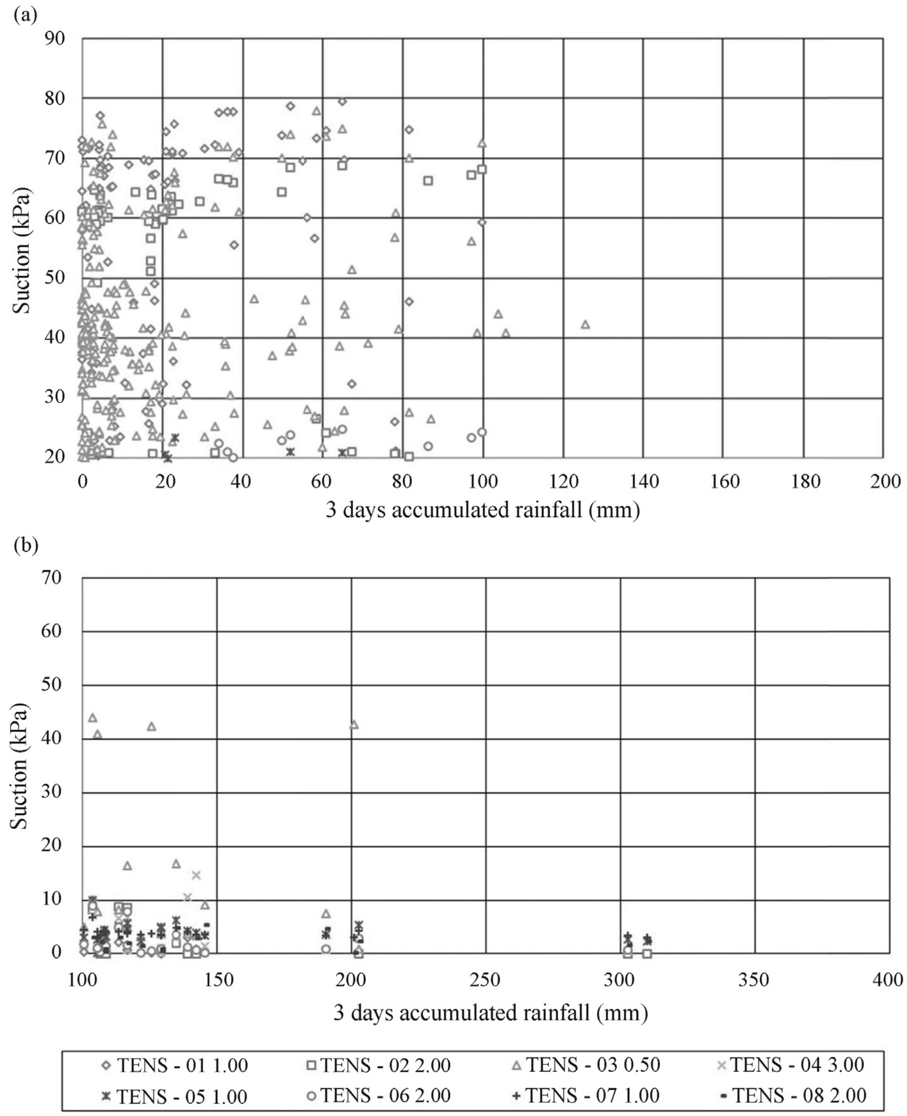

Figure 16 - Comparison between measured value of suction and 3-day accumulated precipitation.

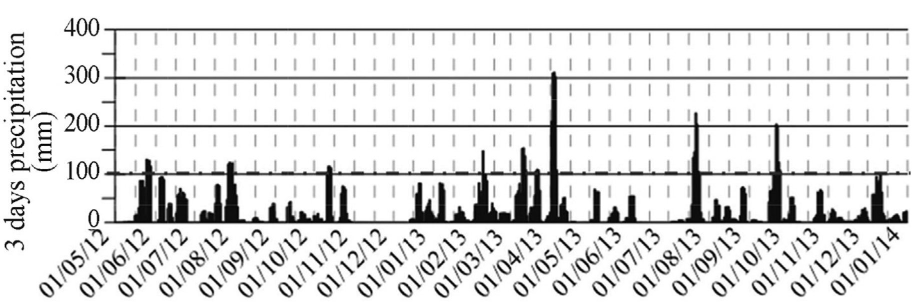

Figure 17 - Three days accumulated rainfall events.

A time delay was observed between the rainfall events. The three-day accumulated precipitation presented an interesting relation to pore water pressure variation.

When the three-day accumulated precipitation was higher than 100 mm, an important reduction in suction was observed along the soil profile.

In general, the suction level is maintained above 20 kPa when the three-day accumulated precipitation is less than approximately 100 mm.

The evaluation of the suction profile showed that only in very few occasions was the suction higher than the equilibrium value inferred from the ground water table level.

The suction profile during the monitoring period suggested that the region near the instrumentation group 1 presented the lower value of suction. The suction level was generally lower in the region where the vegetation is composed by grass. In areas with dense vegetation, higher suction levels were observed.

Continued monitoring and analysis is of utmost importance for deepening the understanding of the meteorological, geological and geotechnical factors which control the slope behavior.

Acknowledgments

The authors wish to express their gratitude to ANTT - Agência Nacional de Transportes Terrestres and to Autopista Litoral Sul - Grupo Arteris for their support to the research.

References

Acevedo, A.M.G. (2013). Estudo de Séries de Leituras Obtidas Através do Monitoramento da Instrumentação Geotécnica Implantada em uma Encosta Litorânea – Estudo de caso. M.Sc. Dissertation, Postgraduate Program in Civil Engineering Construction, Federal University of Paraná, Curitiba, 187p.

Fiori, A.P. (2011). II Internal Research Report. Resources for Technological Development. Project 03, Curitiba (In Portuguese).

Geokon (2014a). Instruction manual model 8021 (Micro-1000) Multi-Channel Datalogger. Available at http://www.geokon.com/content/manuals/8021-1_Micro-1000_Datalogger.pdf.

Geokon (2014b). Instruction manual model 4500 series Vibrating Wire Piezometers. Available at http://www.geokon.com/content/manuals/4500_Piezometer.pdf.

Geokon (2014c). Instruction manual model VW Piezometers & Pressure Transducer. Available at http://www.geokon.com/content/datasheets/4500_Series_VW_Piezometers.pdf.

Hydrological Services (2014a). Instruction manual TB4 Tipping Bucket Rain Gauge model TB4. Available at http://www.hydroserv.com.au/products/mpdf/mtb4.pdf.

Hydrological Services (2014b). Instruction manual Minilog Digital Data Logger model ML1-FL. Available at http://www.hydroserv.com.au/products/mpdf/mml1.pdf.

Kormann, A.C.M.; Sestrem, L.P. & Asakawa, S. (2011). Avaliações de estabilidade e do desempenho de sistemas de proteção de taludes rodoviários em uma encosta litorânea instrumentada. In: Anais do VI Workshop Desenvolvimento Tecnológico nas Concessões Rodoviárias, Brasília, pp. 8-9.

Lazarim, T.P. (2012). Caracterização Geotécnica e Retroanálise da Ruptura de um Talude Rodoviário - BR-101, Santa Catarina. Monograph, Department of Civil Engineering, Federal University of Paraná, Curitiba, 79 p.

Sestrem, L.P. (2012). Concepção e Implantação de um Plano de Instrumentação para Avaliação das Condicionantes Geotécnicas de uma Encosta Litorânea. M.Sc. Dissertation, Postgraduate Program in Civil Engineering Construction, Federal University of Paraná, Curitiba, 195 p.

Sestrem, L.P. & Kormann, A.C.M. (2013). Implantação de um sistema de monitoramento automatizado para monitoramento de uma encosta litorânea rodoviária. In: Proc. 8º Congresso Brasileiro de Rodovias e Concessões, Santos.

Soilmoisture (2014a). Instruction manual model 2725ARL Jet Fill Tensiometers. Available at http://www.soilmoisture.com/pdf/0898-2710_2725.pdf.

Soilmoisture (2014b). Instruction manual model 5301 Current Transducer. Available at http://www.soilmoisture.com/pdf/0898-5301.pdf.

Tavares, R. (2010). Imbricações Entre os Ritmos do Clima e os Ritmos da Urbanização na Formação de Risco e Vulnerabilidade Socioambientais a Deslizamentos de Terra na Serra do Mar - Ubatuba/SP. PhD Thesis, Post Graduate Program in Geography, Federal University of Paraná, Curitiba, 263 p.

SOILS and ROCKS
An International Journal of Geotechnical and Geoenvironmental Engineering

Publication of
ABMS - Brazilian Association for Soil Mechanics and Geotechnical Engineering
SPG - Portuguese Geotechnical Society
Volume 38, N. 1, January-April 2015

Author index

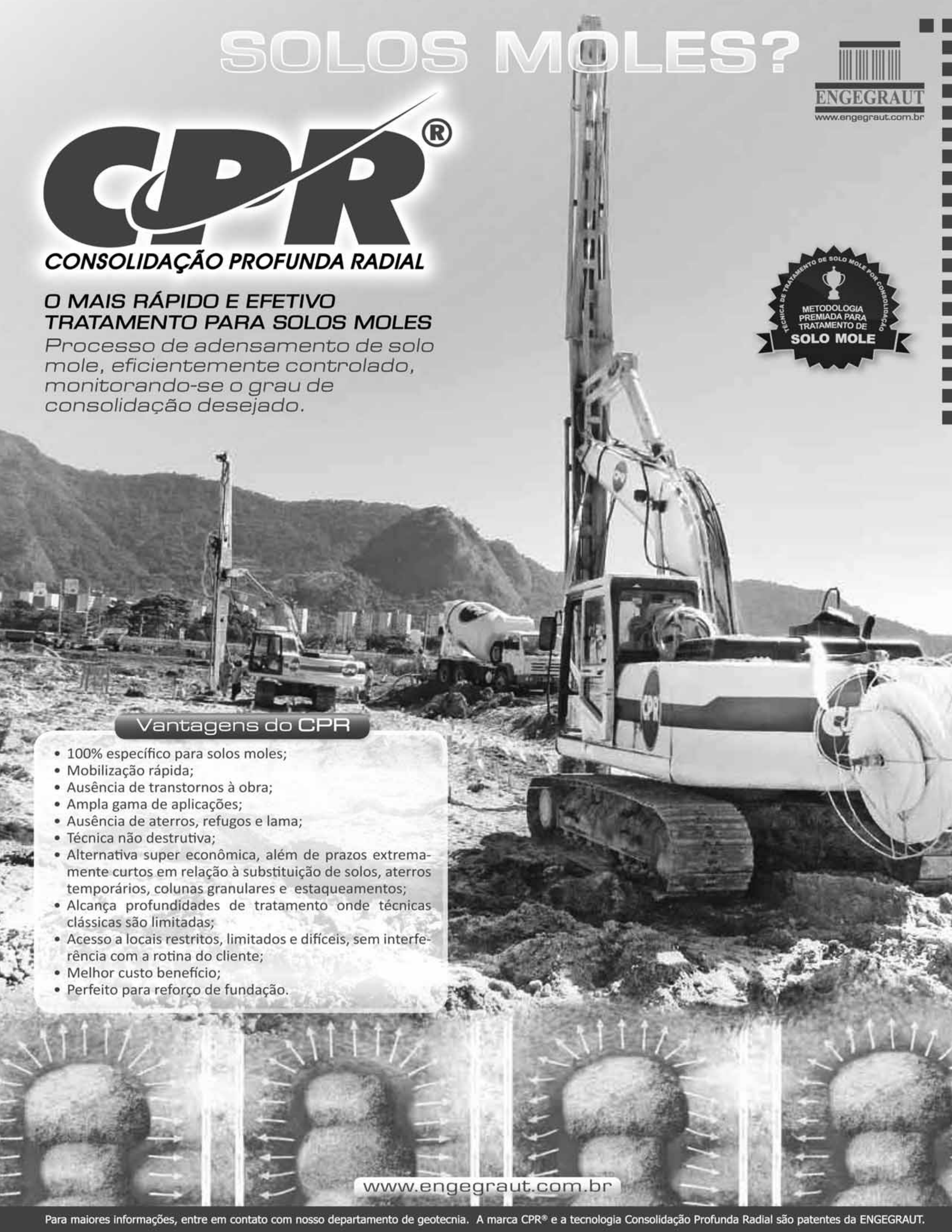

SOLOS MOLES?
ENGEGRAUT
www.engegraut.com.br
CPR®
CONSOLIDAÇÃO PROFUNDA RADIAL
O MAIS RÁPIDO E EFETIVO TRATAMENTO PARA SOLOS MOLES
Processo de adensamento de solo mole, eficientemente controlado, monitorando-se o grau de consolidação desejado.
TÉCNICA DE TRATAMENTO DE SOLO MOLE POR CONSOLIDAÇÃO
METODOLOGIA PREMIADA PARA TRATAMENTO DE SOLO MOLE
Vantagens do CPR
• 100% específico para solos moles;
• Mobilização rápida;
• Ausência de transtornos à obra;
• Ampla gama de aplicações;
• Ausência de aterros, refugos e lama;
• Técnica não destrutiva;
• Alternativa super econômica, além de prazos extremamente curtos em relação à substituição de solos, aterros temporários, colunas granulares e estaqueamentos;
• Alcança profundidades de tratamento onde técnicas clássicas são limitadas;
• Acesso a locais restritos, limitados e difíceis, sem interferência com a rotina do cliente;
• Melhor custo benefício;
• Perfeito para reforço de fundação.
www.engegraut.com.br
Para maiores informações, entre em contato com nosso departamento de geotecnia. A marca CPR® e a tecnologia Consolidação Profunda Radial são patentes da ENGEGRAUT.

Instructions for Submission of Manuscripts

Category of the Papers

Soils and Rocks is the international scientific journal edited by the Brazilian Association for Soil Mechanics and Geotechnical Engineering (ABMS) and the Portuguese Geotechnical Society (SPG). The aim of the journal is to publish (in English) original research and technical works on all geotechnical branches.

According to its content the accepted paper is classified in one of the following categories: Article paper, Technical Note, Case Study or Discussion. An article paper is an extensive and conclusive dissertation about a geotechnical topic. A paper is considered as a technical note if it gives a short description of ongoing studies, comprising partial results and/or particular aspects of the investigation. A case study is a report of unusual problems found during the design, construction or the performance of geotechnical projects. A case study is also considered as the report of an unusual solution given to an ordinary problem. The discussions about published papers, case studies and technical notes are made in the Discussions Section.

When submitting a manuscript for review, the authors should indicate the category of the manuscript, and is also understood that they:

a) assume full responsibility for the contents and accuracy of the information in the paper;

b) assure that the paper has not been previously published, and is not being submitted to any other periodical for publication.

Manuscript Instructions

Manuscripts must be written in English. The text is to be typed in a word processor (preferably MS Word), **single column**, using ISO A4 page size, left, right, top, and bottom margins of 25 mm, Times New Roman 12 font, and line spacing of 1.5. All lines and pages should be numbered. The text should be written in the third person.

The first page of the manuscript must include the title of the paper followed by the names of the authors with the abbreviation of the most relevant academic title. The affiliation, address and e-mail must appear below each author´s name. An abstract of 200 words follows after the author´s names. A list with up to six keywords at the end of the abstract is required.

Although variations on the sequence and title of each section are possible, it is suggested that the text contains the following sections: Introduction, Material and Methods, Results, Discussions, Conclusions, Acknowledgements, References and List of Symbols. A brief description of each section is given next.

Introduction: This section should indicate the state of the art of the problem under evaluation, a description of the problem and the methods undertaken. The objective of the work should be clearly presented at the end of the section.

Materials and Methods: This section should include all information needed to the reproduction of the presented work by other researchers.

Results: In this section the data of the investigation should be presented in a clear and concise way. Figures and tables should not repeat the same information.

Discussion: The analyses of the results should be described in this section.

Conclusions: The content of this section should be based on the data and on the discussions presented.

Acknowledgenments: If necessary, concise acknowledgements should be presented in this section.

References: References to other published sources must be made in the text by the last name(s) of the author(s), followed by the year of publication, similarly to one of the two possibilities below:

…while Silva and Pereira (1987) observed that resistance depended on soil density… or *It was observed that resistance depended on soil density (Silva and Pereira, 1987).*

In the case of three or more authors, the reduced format must be used, *e.g.*: Silva *et al.* (1982) or (Silva *et al.*, 1982). Two or more citations belonging to the same author(s) and published in the same year are to be distinguished with small letters, *e.g.*: (Silva, 1975a, b, c.). Standards must be cited in the text by the initials of the entity and the year of publication, *e.g.*: ABNT (1996), ASTM (2003).

Full references shall be listed alphabetically at the end of the text by the first author´s last name. Several references belonging to the same author shall be cited chronologically. Some examples are listed next:

Papers: Bishop, A.W. & Blight, G.E. (1963). Some aspects of effective stress in saturated and unsaturated soils. Geotechnique, 13(2):177-197.

Books: Lambe, T.W & Whitman, R.V. (1979). Soil Mechanics, SI Version. John Wiley & Sons, New York, 553 p.

Book with editors: Sharma, H.D.; Dukes, M.T. & Olsen, D.M. (1990). Field measurements of dynamic moduli and Poisson's ratios of refuse and underlying soils at a landfill site. Landva, A. & Knowles, G.D. (eds), Geotechnics of Waste Fills - Theory and Practice, American Society for Testing and Materials - STP 1070, Philadelphia, pp. 57-70.

Proceedings (printed matter or CD-ROM): Jamiolkowski, M.; Ladd, C.C.; Germaine, J.T. & Lancellotta, R. (1985). New developments in field and laboratory testing of soils. Proc. 11th Int. Conf. on Soil Mech. and Found. Engn., ISSMFE, San Francisco, v. 1, pp. 57-153. (specify if CD ROM).

Thesis and dissertations: Lee, K.L. (1965). Triaxial Compressive Strength of Saturated Sands Under Seismic Loading Conditions. PhD Dissertation, Department of Civil Engineering, University of California, Berkeley, 521 p.

Standards: ASTM (2003). Standard Test Method for Particle Size Analysis of Soils - D 422-63. ASTM International, West Conshohocken, Pennsylvania, USA, 8 p.

Internet references: Soils and Rocks available at http://www.abms.com.br and downloaded on August 6th 2003.

On line first publications must also bring the digital object identifier (DOI) at the end.

Figures shall be either computer generated or drawn with India ink on tracing paper. Computer generated figures must be accompanied by the corresponding digital file (.tif, .jpg, .pcx, etc.). All figures (graphs, line drawings, photographs, etc.) shall be numbered consecutively and have a caption consisting of the figure number and a brief title or description of the figure. This number should be used when referring to the figure in text. Photographs should be black and white, sharp, high contrasted and printed on glossy paper.

Tables shall be numbered consecutively in Arabic and have a caption consisting of the table number and a brief title. This number should be used when referring to the table in the text. Units should be indicated in the first line of the table, below the title of each column. Acronyms should be avoided. When applicable, the units should come right below the corresponding column heading. Additional comments can be placed as footnotes.

Equations shall appear isolated in a single line of the text. Numbers identifying equations must be flushed with the right margin. International System (SI) units must be used. The definitions of the symbols used in the equations must appear in the List of Symbols. It is recommended that the symbols used are in accordance with Lexicon in 8 Languages, ISSMFE (1981) and the ISRM List of Symbols.

The text of the submitted manuscript (including figures, tables and references) intended to be published as an article paper or a case history should not contain more than 30 pages, formatted according to the instructions mentioned above. Technical notes and discussions should have no more than 15 and 8 pages, respectively. Longer manuscripts may be exceptionally accepted if the authors provide proper explanation for the need of the required extra space in a cover letter.

Discussion

Discussions must be written in English. The first page of a discussion should contain:

The title of the paper under discussion;

Name of the author(s) of the discussion, followed by their position, affiliation, address and e-mail. The author(s) of the discussion should refer to himself (herself/themselves) as the reader(s) and to the author(s) of the paper as the author(s).

Figures, tables and equations should be numbered following the same sequence of the original paper. All instructions previously mentioned for the preparation of article papers, case studies and technical notes also apply to the preparation of discussions.

Editorial Review

Each paper will be evaluated by reviewers selected by the editors according to the subject of the paper. The authors will be informed about the results of the review process. If the paper is accepted, the authors will be required to submit a version of the revised manuscript with the suggested modifications. If the manuscript is rejected for publication, the authors will be informed about the reasons for rejection. In any situation comprising modification of the original text, classification of the manuscript in a category different from that proposed by the authors, or rejection, the authors can reply presenting their reasons for disagreeing with the reviewer comments.

Submission

The author(s) must upload a digital file of the manuscript to the Soils and Rocks website.

Follow Up

The online management system will provide a password to the corresponding author, which will enable him/her to follow the reviewing process of the submitted manuscript at the Soils and Rocks website.

Volume 38, N. 1, January-April 2015

Table of Contents